NASA TECHNICAL NOTE

NASA TN D-7194

NASA TN D-7194

WIND-TUNNEL INVESTIGATION OF EFFECTS OF VARIATIONS IN REYNOLDS NUMBER AND LEADING-EDGE TREATMENT ON THE AERODYNAMIC CHARACTERISTICS OF AN EXTERNALLY BLOWN JET-FLAP CONFIGURATION

by
Lysle P. Parlett, Charles C. Smith, Jr.,
and James L. Megrail

Langley Research Center and
Langley Directorate, U.S. Army Air Mobility R&D Laboratory
Hampton, Va. 23665

NATIONAL AERONAUTICS AND SPACE ADMINISTRATION • WASHINGTON, D. C. • AUGUST 1973

1. Report No.	2. Government Accession No.	3. Recipient's Catalog No.
NASA TN D-7194		

4. Title and Subtitle	5. Report Date
WIND-TUNNEL INVESTIGATION OF EFFECTS OF VARIATIONS IN REYNOLDS NUMBER AND LEADING-EDGE TREATMENT ON THE AERODYNAMIC CHARACTERISTICS OF AN EXTERNALLY BLOWN JET-FLAP CONFIGURATION	August 1973
	6. Performing Organization Code

7. Author(s)	8. Performing Organization Report No.
Lysle P. Parlett, Charles C. Smith, Jr., Langley Research Center; and James L. Megrail, Langley Directorate, U.S. Army Air Mobility R&D Laboratory	L-8745
	10. Work Unit No. 760-61-02-01

9. Performing Organization Name and Address	11. Contract or Grant No.
NASA Langley Research Center Hampton, Va. 23665	
	13. Type of Report and Period Covered
12. Sponsoring Agency Name and Address	Technical Note
National Aeronautics and Space Administration Washington, D.C. 20546	14. Sponsoring Agency Code

15. Supplementary Notes

16. Abstract

An investigation has been conducted in the Langley full-scale tunnel to determine the effects of variations in Reynolds number and leading-edge treatment on the aerodynamic characteristics of an externally blown jet-flap transport configuration. The model had a double-slotted trailing-edge flap and was powered by four high-bypass-ratio turbofan engines. Tests were performed by using each of three leading-edge devices (a 30-percent-chord flap and 15- and 25-percent-chord slats) at Reynolds numbers from 0.47×10^6 to 1.36×10^6 at thrust coefficients up to 3.5. The use of a 25-percent-chord slat was found to be more effective than a 15-percent-chord slat or a 30-percent-chord flap in extending the stall angle of attack and in minimizing the loss of lift after the stall. The large slat was also effective in reducing the rolling moments that occurred when the engine-out wing stalled first.

17. Key Words (Suggested by Author(s))	18. Distribution Statement
Leading-edge devices Externally blown jet flap Variations in Reynolds number	Unclassified – Unlimited

19. Security Classif. (of this report)	20. Security Classif. (of this page)	21. No. of Pages	22. Price*
Unclassified	Unclassified	154	$3.00

*For sale by the National Technical Information Service, Springfield, Virginia 22151

WIND-TUNNEL INVESTIGATION OF EFFECTS OF VARIATIONS IN REYNOLDS NUMBER AND LEADING-EDGE TREATMENT ON THE AERODYNAMIC CHARACTERISTICS OF AN EXTERNALLY BLOWN JET-FLAP CONFIGURATION

By Lysle P. Parlett, Charles C. Smith, Jr.,
Langley Research Center

and James L. Megrail
Langley Directorate, U.S. Army Air Mobility R&D Laboratory

SUMMARY

An investigation has been conducted in the Langley full-scale tunnel to determine the effects of variations in Reynolds number and leading-edge treatment on the aerodynamic characteristics of an externally blown jet-flap transport configuration. The model had a double-slotted trailing-edge flap and was powered by four high-bypass-ratio turbofan engines. Tests were performed by using each of three leading-edge devices (a 30-percent-chord flap and 15- and 25-percent-chord slats) at Reynolds numbers from 0.47×10^6 to 1.36×10^6 at thrust coefficients up to 3.5.

The results of the investigation showed that, in general, the aerodynamic characteristics of the model were not significantly affected by changes in Reynolds number through the range tested, except above the stall where the highest Reynolds number data showed the lowest rolling and yawing moments for the engine-out condition. The use of a 25-percent-chord slat was found to be more effective than a 15-percent-chord slat or a 30-percent-chord flap in extending the stall angle of attack and in minimizing the loss of lift after the stall. The large slat was also effective in reducing the rolling moments that occurred when the engine-out wing stalled first.

INTRODUCTION

The present investigation was undertaken as part of a general research program to provide some fundamental information on the aerodynamic performance and stability and control of an external-flow jet-flap STOL airplane configuration. During previous studies conducted under this program, the high-lift capabilities of the jet flap were demonstrated; also, certain problems, most notably those of longitudinal stability and engine-out lateral trim, were identified and solutions were developed. (See refs. 1 and 2.) As a result, the externally blown jet flap was shown to be an attractive means of achieving STOL performance. The models on which these investigations were performed were well adapted to

exploratory work because they were small and lightly built to permit easy modification and were low powered and inexpensive to operate. The low thrust, however, resulted in low Reynolds number data because the high thrust coefficients representative of STOL operation had to be achieved by reducing the tunnel dynamic pressure. The low velocities in combination with small model size resulted in Reynolds numbers no greater than about 0.35×10^6.

The purpose of the present investigation was to extend the range of Reynolds number for which high-lift data on the externally blown jet flap are available. An existing model, somewhat larger than the ones of references 1 and 2, was modified to be geometrically similar to the model of reference 1. The engines of the present model could produce four times the thrust of the previous engines; this higher thrust and the larger size of the model allowed testing at Reynolds numbers up to 1.36×10^6. The present model also provided a means of comparing the characteristics of three leading-edge devices on a powered-lift wing. The test program, therefore, included variations in leading-edge treatment, thrust coefficient, thrust distribution (with or without deflectors, and with one engine sometimes inoperative), angle of attack, and tunnel velocity.

SYMBOLS

The longitudinal data are referred to the stability-axis system and the lateral data are referred to the body-axis system. (See fig. 1.) The origin of the axes was at the center-of-gravity position (0.446 mean aerodynamic chord) shown in figure 2(a).

Measurements and calculations were made in U.S. Customary Units and are presented in both the International System of Units (SI) and U.S. Customary Units. Equivalent dimensions were determined by using the conversion factors given in reference 3.

b	wing span, m (ft)
C_D	drag coefficient, F_D/qS
C_L	lift coefficient, F_L/qS
C_l	rolling-moment coefficient, M_X/qSb
C_m	pitching-moment coefficient, $M_Y/qS\bar{c}$
C_n	yawing-moment coefficient, M_Z/qSb
C_Y	side-force coefficient, F_Y/qS

C_μ	engine gross-thrust coefficient, T/qS
c	local wing chord, m (ft)
$\bar{c}$	mean aerodynamic chord, m (ft)
F_A	axial force, positive rearward, N (lb)
F_D	drag force, N (lb)
F_L	lift force, N (lb)
F_N	normal force, positive upward, N (lb)
F_X	force along X-axis, positive forward, N (lb)
F_Y	side force, positive to right, N (lb)
F_Z	force along Z-axis, positive downward, N (lb)
M_X	rolling moment, m-N (ft-lb)
M_Y	pitching moment, m-N (ft-lb)
M_Z	yawing moment, m-N (ft-lb)
q	free-stream dynamic pressure, $\rho V^2/2$, N/m^2 (lb/ft^2)
R	Reynolds number based on mean aerodynamic chord
S	wing area, m^2 (ft^2)
T	static thrust, N (lb)
V	free-stream velocity, m/sec (ft/sec)
X,Y,Z	body reference axes
X_S,Y_S,Z_S	stability reference axes

x,y	wing coordinates, cm (in.)
α	angle of attack, deg
β	angle of sideslip, positive nose left, deg
δ_{f1}	deflection of forward segment of trailing-edge flap, deg
δ_{f2}	deflection of rearward segment of trailing-edge flap, deg
$(\delta_{f1}/\delta_{f2})_L$	deflection of left trailing-edge flap, deg
$(\delta_{f1}/\delta_{f2})_R$	deflection of right trailing-edge flap, deg
δ_j	jet deflection, deg
η	static flap turning efficiency, $\frac{\sqrt{F_A{}^2 + F_N{}^2}}{T}$
ρ	air density, kg/m^3 ($slugs/ft^3$)

MODEL AND APPARATUS

The investigation was conducted on the four-engine high-wing external-flow jet-flap transport model illustrated by the three-view drawing of figure 2(a). The principal dimensional characteristics of the model are given in table I, and airfoil coordinates are presented in table II. A detailed sketch of the flap assembly and engine-pylon arrangement is shown in figure 2(b). Details of the leading-edge flap and slat configurations employed during the tests are presented in figures 2(c) to 2(e). No transition strips were applied to the model. Photographs of the model mounted for static force tests in the Langley full-scale tunnel are presented in figure 3.

The model engines represented high-bypass-ratio turbofan engines and were installed at 3^o negative incidence (referred to the X-axis) to blow directly on the trailing-edge flap system. The design of the jet-exhaust deflectors used on the engines to obtain better spreading and turning efficiency of the system was the same as that used in reference 1 and is illustrated in figure 2(b). The engine turbines were driven by compressed nitrogen. Bellmouth attachments having large-radius lips were installed on the engines during static-calibration tests.

The model was mounted on a six-component strain-gage balance and was supported on a strut in the open-throat test section of the Langley full-scale tunnel, which is 9.14 by 18.3 meters (30 by 60 ft).

TESTS AND PROCEDURES

In preparation for the tests, the engines were calibrated to determine gross thrust as a function of engine rotational speed in the static condition, that is, at zero angle of attack, zero flap deflection, and with thrust deflectors off. The thrust calibrations were made through a range of engine speeds up to 35 000 revolutions per minute, at which speed the fans developed, in the static case, a thrust of approximately 378 newtons (85 lb) each. The wind-on tests were then made by setting the engine speed to give the desired thrust, or thrust coefficient, at an angle of attack of 0° and then by maintaining constant engine rotational speed as the model was tested through a range of angle of attack.

Jet-deflection angles and flap-turning efficiencies were determined from measurements of normal and axial forces made in the static thrust condition with flaps deflected and exhaust deflectors off and on. The static thrust used in computing turning efficiency was taken directly from the engine calibrations at the appropriate rotational speed.

During the wind-on tests, various changes were made to the flap geometry or to control-surface deflections with and without the jet-exhaust deflectors installed on the engines. Most tests were made for trailing-edge flap deflections δ_{f1}/δ_{f2} of $20^{\circ}/40^{\circ}$ and $30^{\circ}/60^{\circ}$ for a range of gross-thrust coefficient C_{μ} from 0 to 3.5 and a range of angle of attack α from -5° to 30°. Tests were also made over the angle-of-attack range with either an inboard or outboard engine inoperative. All tests were made without horizontal or vertical tail surfaces. The wind-on tests were made for a range of free-stream dynamic pressures of 91 to 871 N/m^2 (1.9 to 18.2 lb/ft^2) which correspond to airspeeds of 12 to 38 m/sec (40 to 124 ft/sec), respectively. The Reynolds number range covered in the tests varied from 0.47×10^6 to 1.36×10^6 (obtained by varying tunnel speed) based on the mean aerodynamic chord of the wing. An index of data figures is presented in table III.

No wind-tunnel jet-boundary corrections were applied to the data because such corrections were calculated for the most critical conditions and were found to be negligible. No corrections for sting tares were applied.

RESULTS AND DISCUSSION

Longitudinal Characteristics

Because the jet-induced lift is highly dependent on the direction and velocity of the engine slipstream as it leaves the flap system, the system must be capable of turning the slipstream efficiently through large angles. The slipstream turning angle δ_j and the static flap turning efficiency are shown in figure 4. This figure shows that a turning efficiency of about 70 percent was achieved with trailing-edge flap deflections δ_{f1}/δ_{f2}

of $20^{\circ}/40^{\circ}$ and $30^{\circ}/60^{\circ}$. The data also show that the use of jet-exhaust deflectors on the engine improved the turning angle for the $20^{\circ}/40^{\circ}$ deflection case.

Basic longitudinal wind-on data for the model in the tail-off configuration with trailing-edge flap deflections of $20^{\circ}/40^{\circ}$ and $30^{\circ}/60^{\circ}$, various leading-edge devices, and with and without jet-exhaust deflectors on the engines are presented in figures 5 to 9. The data are replotted in figures 10 to 14 to show more conveniently the effect of Reynolds number, in figure 15 to show the effect of the leading-edge devices, and in figure 16 to show the effect of the engine-exhaust deflectors. The data of figures 10 to 14 show that, in general, the longitudinal characteristics of the model were not significantly affected by changes in Reynolds number through the range tested. Figures 5 to 9 also show the usual increase in stall angle of attack and maximum lift coefficient with increasing thrust coefficient C_{μ} and that the effects of C_{μ} were more pronounced at the higher flap deflections. The higher flap deflection (fig. 7(b)) produced lift coefficients up to 8.8 (untrimmed) at a gross-thrust coefficient of 3.50. As would be expected, the high-lift coefficients are accompanied by large nose-down moments because of the rearward location of the flap loads.

The effects of varying the leading-edge treatment on the longitudinal characteristics are summarized in figure 15. This figure shows that the longitudinal characteristics are virtually the same for each of the three devices at low and moderate angles of attack; but, at the higher angles of attack and at the higher thrust coefficients (those of primary consideration in the determination of operational stall margins), the stall angle of attack was higher and the break in lift-curve slope above the stall was markedly less for the 25-percent slat than for the other two configurations. Also, the 25-percent slat was effective in controlling the unstable break in the pitching-moment curve above the stall.

The effects of thrust deflectors on the longitudinal characteristics of the model are summarized in figure 16. Static turning data (presented in fig. 4) showed that the deflectors increased the turning angle and decreased turning efficiency; these changes are reflected in the wind-on characteristics (fig. 16) as increases in both lift and drag.

Lateral Characteristics

The effects of changing Reynolds number or leading-edge treatment on the engine-out lateral characteristics of the model are presented as basic data in figures 17 to 24. Much of the data are replotted in figures 25 to 30 for a more convenient analysis of the effects of Reynolds number and in figure 31 for a more convenient comparison of the effect of the various leading-edge devices. Although the lateral moments are the prime concern during engine-out (engine inoperative) operation of a jet-flap configuration, the

loss of thrust also has a direct effect on lift. Therefore, the lateral data presented herein for the engine-out condition are accompanied by the corresponding longitudinal data.

The comparison plots presented in figures 25 to 30 show that, with either symmetric or asymmetric trailing-edge flap deflections, the effects of Reynolds number were very small at low and moderate angles of attack. In the high angle-of-attack range, where asymmetric stall in the engine-out condition caused large increases in the rolling and yawing moments, there were relatively large variations in the data with changes in Reynolds number. The variations with Reynolds number were not consistent; however, the data measured at the highest Reynolds number (1.36×10^6) generally showed the lowest values of rolling-moment and yawing-moment coefficients above the stall.

The effects of varying leading-edge treatment on the lateral characteristics of the model are summarized in figure 31. This figure shows that, at the higher Reynolds numbers, the leading-edge slats, as compared with the leading-edge flaps, tended to minimize the increase in rolling moment that occurred as the engine-out wing stalled first, starting at about 10^o angle of attack. This result appears to be consistent with the longitudinal data of figure 15, which showed that the slats tended to give a more gentle stall than the flap.

SUMMARY OF RESULTS

The results of a wind-tunnel investigation to determine the effects of variations in Reynolds number and leading-edge treatment on the aerodynamic characteristics of an externally blown jet-flap transport model may be summarized as follows:

1. In general, the aerodynamic characteristics of the model were not significantly affected by changes in Reynolds number through the range tested (0.47×10^6 to 1.36×10^6), except above the stall where the highest Reynolds number data showed the lowest rolling and yawing moments for the engine-out condition.

2. The use of a 25-percent-chord leading-edge slat was found to be more effective than a 15-percent-chord leading-edge slat or a 30-percent-chord leading-edge flap in extending the stall angle of attack and in minimizing the loss of lift after the stall. The large slat was also effective in reducing the rolling moments that occurred when the engine-out wing stalled first.

Langley Research Center,
National Aeronautics and Space Administration,
Hampton, Va., April 20, 1973.

REFERENCES

1. Parlett, Lysle P.; Freeman, Delma C., Jr.; and Smith, Charles C., Jr.: Wind-Tunnel Investigation of a Jet Transport Airplane Configuration With High Thrust-Weight Ratio and an External-Flow Jet Flap. NASA TN D-6058, 1970.

2. Parlett, Lysle P.; Greer, H. Douglas; Henderson, Robert L.; and Carter, C. Robert: Wind-Tunnel Investigation of an External-Flow Jet-Flap Transport Configuration Having Full-Span Triple-Slotted Flaps. NASA TN D-6391, 1971.

3. Mechtly, E. A.: The International System of Units – Physical Constants and Conversion Factors (Revised). NASA SP-7012, 1969.

TABLE I.- DIMENSIONS OF MODEL

Wing:		
Area, m^2 (ft^2)	1.871	(20.14)
Span (to theoretical tip), cm (in.)	386.41	(152.13)
Aspect ratio	7.75	
Length of mean aerodynamic chord, cm (in.)	53.75	(21.16)
Location of quarter chord of mean aerodynamic chord, referenced to nose of model, cm (in.)	164.77	(64.87)
Spanwise station of mean aerodynamic chord, cm (in.)	78.56	(30.93)
Root chord, cm (in.)	79.20	(31.18)
Tip chord (theoretical tip), cm (in.)	26.59	(10.47)
Break station chord, cm (in.)	49.07	(19.32)
Spanwise station of break station, cm (in.)	81.92	(32.25)
Sweep of quarter-chord line:		
Inboard panel, deg	24.08	
Outboard panel, deg	25.00	
Sweep of leading edge:		
Inboard panel, deg	28.3	
Outboard panel, deg	27.4	
Dihedral of quarter-chord line:		
Inboard panel, deg	-3.50	
Outboard panel, deg	-3.50	
Incidence of mean aerodynamic chord, deg	4.50	
Geometric twist, root to tip, deg	-3.50	
Engines:		
Spanwise location of inboard engines, cm (in.)	69.49	(27.36)
Spanwise location of outboard engines, cm (in.)	108.13	(42.57)
Incidence of all engine center lines, deg	-3.00	
Moment reference:		
Longitudinal location, referenced to nose of model, cm (in.)	175.52	(69.10)
Vertical location, referenced to top of fuselage at wing, cm (in.)	20.50	(8.09)

TABLE II.- AIRFOIL COORDINATES FOR WING

(a) Wing coordinates at buttock line 20.27 cm (7.98 in.)

x_{upper}		y_{upper}		x_{lower}		y_{lower}	
cm	in.	cm	in.	cm	in.	cm	in.
-0.018	-0.007	0.406	0.160	0.196	0.077	-0.356	-0.140
.102	.040	.729	.287	.437	.172	-.582	-.229
.251	.099	.960	.378	.645	.254	-.726	-.286
.505	.199	1.237	.487	.930	.366	-.886	-.349
1.153	.454	1.722	.678	1.537	.605	-1.163	-.458
3.581	1.410	2.664	1.049	3.594	1.415	-1.869	-.736
7.181	2.827	3.432	1.351	7.168	2.822	-2.654	-1.045
14.348	5.649	4.326	1.703	14.348	5.649	-3.576	-1.408
21.514	8.470	4.806	1.892	21.532	8.477	-4.051	-1.595
28.672	11.288	4.986	1.963	28.722	11.308	-4.181	-1.646
35.829	14.106	4.890	1.925	35.913	14.139	-3.975	-1.565
42.992	16.926	4.539	1.787	43.099	16.968	-3.454	-1.360
50.188	19.759	3.952	1.556	50.251	19.784	-2.675	-1.053
57.407	22.601	3.081	1.213	57.379	22.590	-1.748	-.688
64.623	25.442	1.842	.725	64.511	25.398	-.810	-.319
71.750	28.248	.091	.036	71.732	28.241	-.091	-.036

TABLE II.- AIRFOIL COORDINATES FOR WING – Continued

(b) Wing coordinates at buttock line 76.17 cm (29.99 in.)

x_{upper}		y_{upper}		x_{lower}		y_{lower}	
cm	in.	cm	in.	cm	in.	cm	in.
-0.013	-0.005	0.297	0.117	0.142	0.056	-0.259	-0.102
.071	.028	.528	.208	.312	.123	-.422	-.166
.178	.070	.691	.272	.462	.182	-.523	-.206
.356	.140	.886	.349	.668	.263	-.632	-.249
.808	.318	1.224	.482	1.113	.438	-.912	-.359
2.492	.981	1.900	.748	2.624	1.033	-1.440	-.567
5.055	1.990	2.314	.911	5.182	2.040	-1.605	-.632
10.178	4.007	3.124	1.230	10.292	4.052	-1.986	-.782
15.311	6.028	3.480	1.370	15.397	6.062	-2.149	-.846
20.444	8.049	3.630	1.429	20.399	8.031	-2.167	-.853
25.578	10.070	3.581	1.410	25.601	10.079	-2.050	-.807
30.709	12.090	3.345	1.317	30.706	12.089	-1.796	-.707
35.839	14.110	2.926	1.152	35.811	14.099	-1.410	-.555
40.998	16.141	2.266	.892	40.889	16.098	-.955	-.376
46.119	18.157	1.313	.517	46.004	18.112	-.498	-.196
51.184	20.151	.058	.023	51.173	20.147	-.036	-.014

TABLE II.- AIRFOIL COORDINATES FOR WING – Continued

(c) Wing coordinates at buttock line 108.13 cm (42.57 in.)

x_{upper}		y_{upper}		x_{lower}		y_{lower}	
cm	in.	cm	in.	cm	in.	cm	in.
-0.0196	-0.0077	0.264	0.104	0.127	0.050	-0.231	-0.091
.061	.024	.467	.184	.277	.109	-.373	-.147
.140	.055	.612	.241	.406	.160	-.462	-.182
.290	.114	.780	.307	.584	.230	-.554	-.218
.673	.265	1.074	.423	.963	.379	-.704	-.277
2.111	.831	1.656	.652	2.256	.888	-1.021	-.402
4.295	1.691	2.136	.841	4.435	1.746	-1.300	-.512
8.672	3.414	2.692	1.060	8.786	3.459	-1.562	-.615
13.063	5.143	2.995	1.179	13.127	5.168	-1.689	-.665
17.440	6.866	3.106	1.223	17.473	6.879	-1.720	-.677
21.8234	8.5919	3.0465	1.1994	21.8250	8.5925	-1.6325	-.6427
26.1998	10.3149	2.8186	1.1097	26.1780	10.3063	-1.4265	-.5616
30.5750	12.0374	2.4338	.9582	30.5326	12.0207	-1.1143	-.4387
34.9654	13.7659	1.8613	.7328	34.8719	13.7291	-.7475	-.2943
39.3296	15.4841	1.0671	.4201	39.2374	15.4478	-.3828	-.1507
43.6529	17.1862	.0480	.0189	43.6438	17.1826	-.0480	-.0189

TABLE II.- AIRFOIL COORDINATES FOR WING – Continued

(d) Wing coordinates at buttock line 133.30 cm (52.48 in.)

x_{upper}		y_{upper}		x_{lower}		y_{lower}	
cm	in.	cm	in.	cm	in.	cm	in.
-0.023	-0.009	0.244	0.096	0.117	0.046	-0.216	-0.085
.036	.014	.432	.170	.254	.100	-.345	-.136
.112	.044	.561	.221	.368	.145	-.424	-.167
.241	.095	.716	.282	.528	.208	-.505	-.199
.579	.228	.980	.386	.864	.340	-.632	-.249
1.849	.728	1.496	.589	1.994	.785	-.894	-.352
3.774	1.486	1.913	.753	3.914	1.541	-1.113	-.438
7.638	3.007	2.398	.944	7.742	3.048	-1.311	-.516
11.516	4.534	2.659	1.047	11.552	4.548	-1.433	-.564
15.377	6.054	2.741	1.079	15.380	6.055	-1.491	-.587
19.230	7.571	2.662	1.048	19.215	7.565	-1.422	-.560
23.084	9.088	2.431	.957	23.053	9.076	-1.234	-.486
26.937	10.605	2.062	.812	26.888	10.586	-.955	-.376
30.795	12.124	1.552	.611	30.721	12.095	-.627	-.247
34.638	13.637	.884	.348	34.567	13.609	-.305	-.120
38.451	15.138	.043	.017	38.443	15.135	-.043	-.017

TABLE II.- AIRFOIL COORDINATES FOR WING – Concluded

(e) Wing coordinates at buttock line 171.32 cm (67.45 in.)

x_{upper}		y_{upper}		x_{lower}		y_{lower}	
cm	in.	cm	in.	cm	in.	cm	in.
0.028	0.011	0.213	0.084	0.104	0.041	-0.191	-0.075
.010	.004	.376	.148	.218	.086	-.300	-.118
.069	.027	.485	.191	.315	.124	-.366	-.144
.168	.066	.617	.243	.442	.174	-.432	-.170
.437	.172	.838	.330	.709	.279	-.528	-.208
1.455	.573	1.255	.494	1.600	.630	-.704	-.277
2.987	1.176	1.572	.619	3.127	1.231	-.826	-.325
6.073	2.391	1.948	.767	6.157	2.424	-.932	-.367
9.174	3.612	2.149	.846	9.169	3.610	-1.049	-.413
12.248	4.822	2.187	.861	12.212	4.808	-1.140	-.449
15.306	6.026	2.080	.819	15.268	6.011	-1.102	-.434
18.364	7.230	1.844	.726	18.324	7.214	-.947	-.373
21.430	8.437	1.504	.592	21.372	8.414	-.714	-.281
24.478	9.637	1.085	.427	24.440	9.622	-.442	-.174
27.493	10.824	.605	.238	27.498	10.826	-.185	-.073
30.577	12.038	.033	.013	30.571	12.036	-.033	-.013

TABLE III.- INDEX OF DATA FIGURES

[Deflectors were on for all tests except where noted]

Type of data	δ_{f1}/δ_{f2}, deg/deg	Leading-edge treatment	Comment	Figure
Static turning	20/40; 30/60		Deflectors off and on	4
Wind on; longitudinal characteristics				
Basic	30/60	30% flap		5
	↓	25% slat		6
	↓	15% slat		7
	20/40	30% flap		8
	20/40	30% flap	Deflectors off	9
Summary of R effects	30/60	30% flap		10
	↓	25% slat		11
	↓	15% slat		12
	20/40	30% flap		13
	20/40	30% flap	Deflectors off	14
Effect of leading-edge devices	30/60	30% flap		15
	↓	25% slat		
	↓	15% slat		
Deflector	20/40	30% flap	Deflectors off and on	16
Wind on; lateral and longitudinal characteristics				
Basic	30/60	30% flap	Left outboard engine inoperative	17
	↓	30% flap	Left inboard engine inoperative	18
	↓	25% slat	Left outboard engine inoperative	19
	↓	15% slat	Left outboard engine inoperative	20
	20/40	30% flap	Left outboard engine inoperative	21
	20/40	30% flap	Left inboard engine inoperative	22
	Differential: 30/50 right 30/70 left	30% flap	Left outboard engine inoperative	23
	Differential: 30/50 right 30/70 left	30% flap	Left inboard engine inoperative	24
Summary of R effects	20/40	30% flap	Left outboard engine inoperative	25
	20/40	30% flap	Left inboard engine inoperative	26
	30/60	30% flap	Left outboard engine inoperative	27
	30/60	30% flap	Left inboard engine inoperative	28
	Differential: 30/50 right 30/70 left	30% flap	Left outboard engine inoperative	29
	Differential: 30/50 right 30/70 left	30% flap	Left inboard engine inoperative	30
Effect of leading-edge devices	30/60	30% flap		31
	↓	25% slat		
	↓	15% slat		

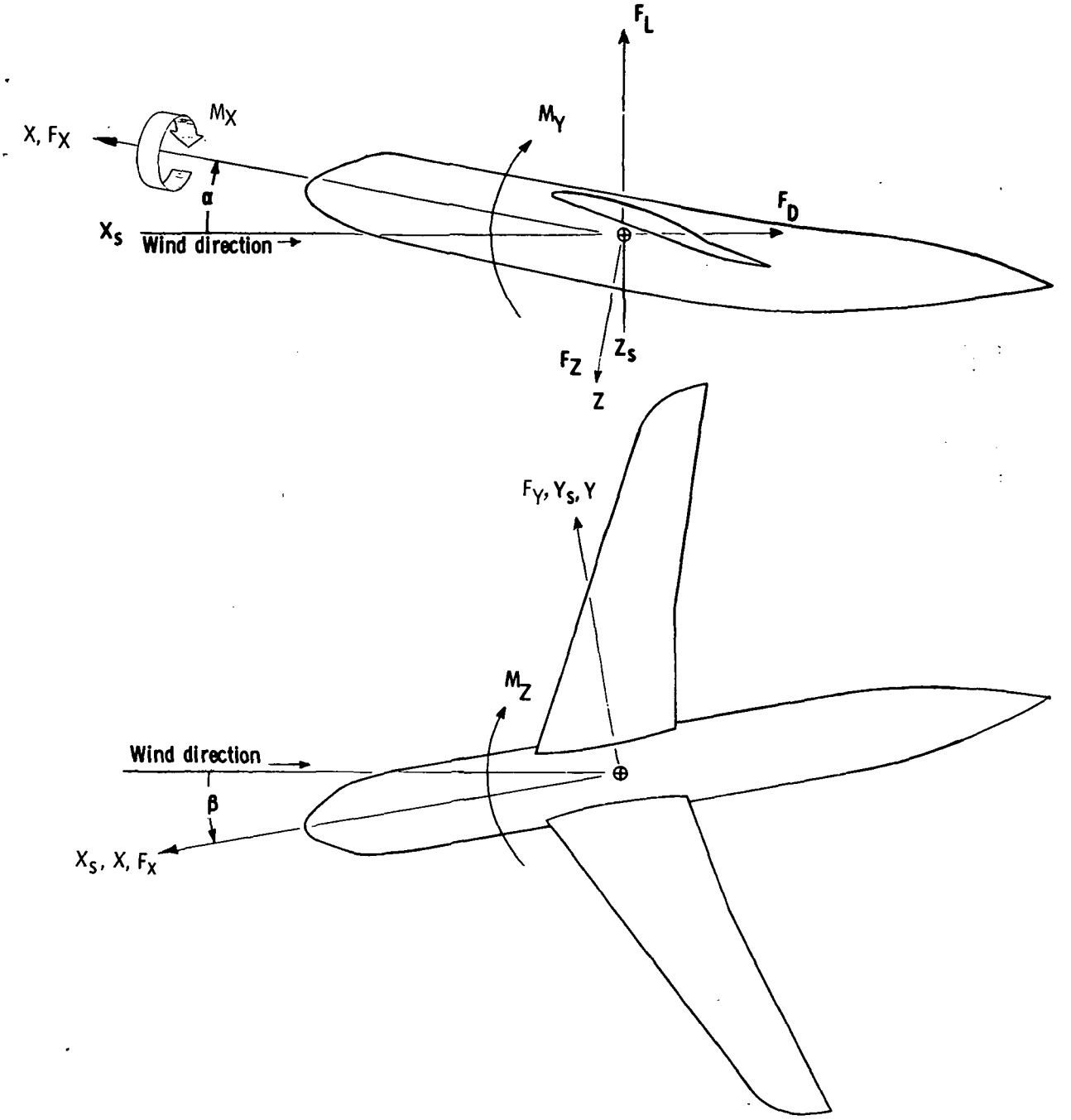

Figure 1.- Axis system used in presentation of data. Arrows indicate positive direction of moments, axis directions, and angles.

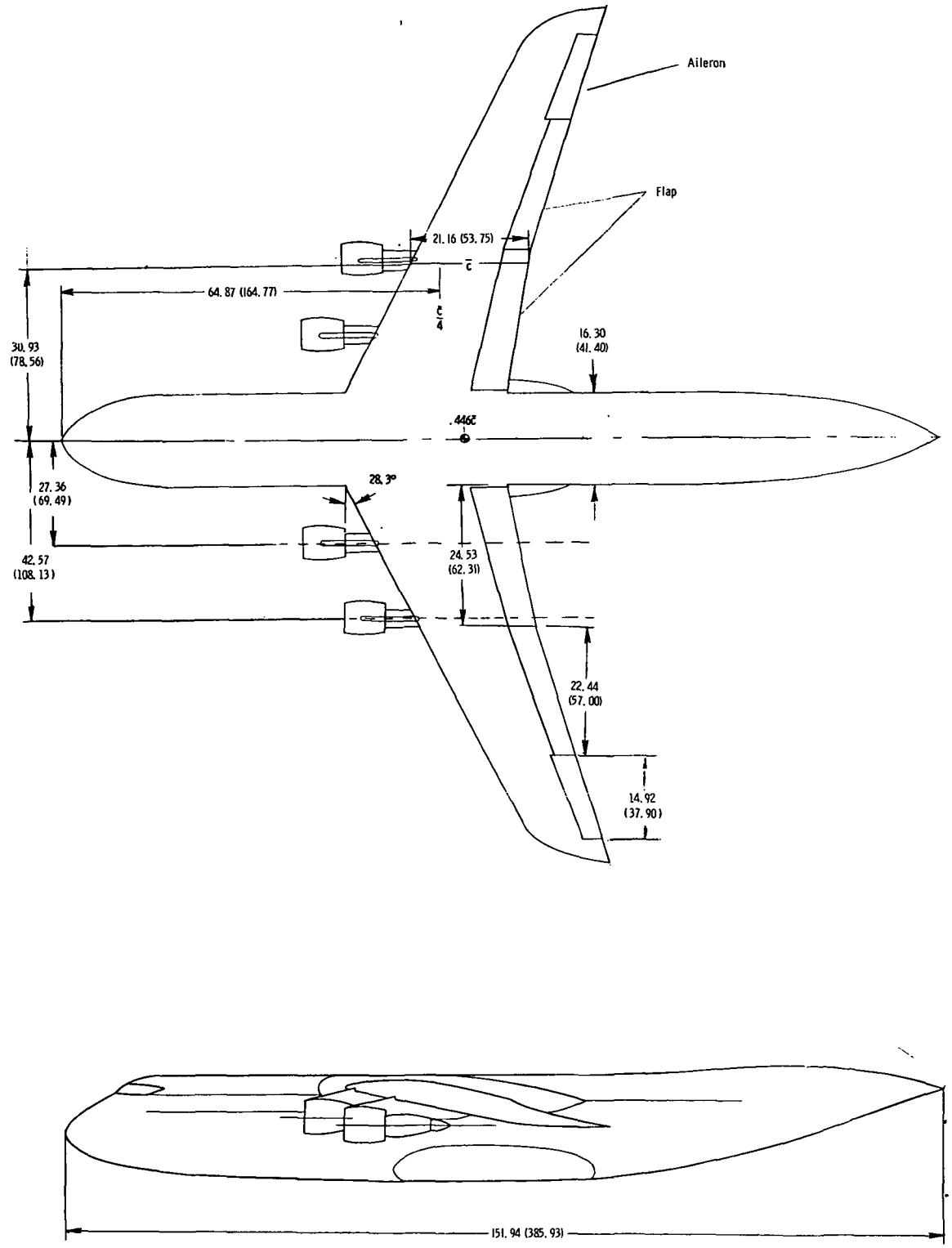

(a) Three-view drawing of complete model.

Figure 2.- Drawings of model used in investigation. All linear dimensions are in inches (centimeters).

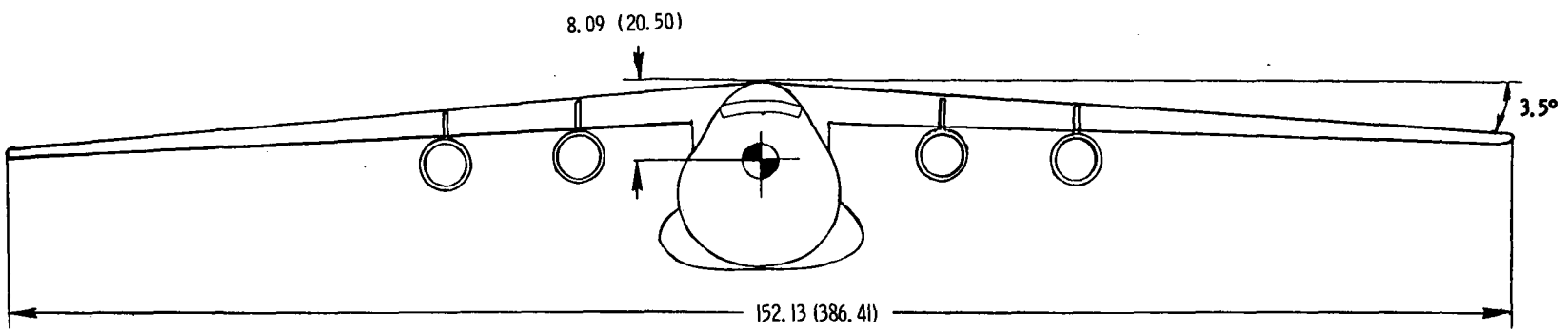

(a) Concluded.

Figure 2.- Continued.

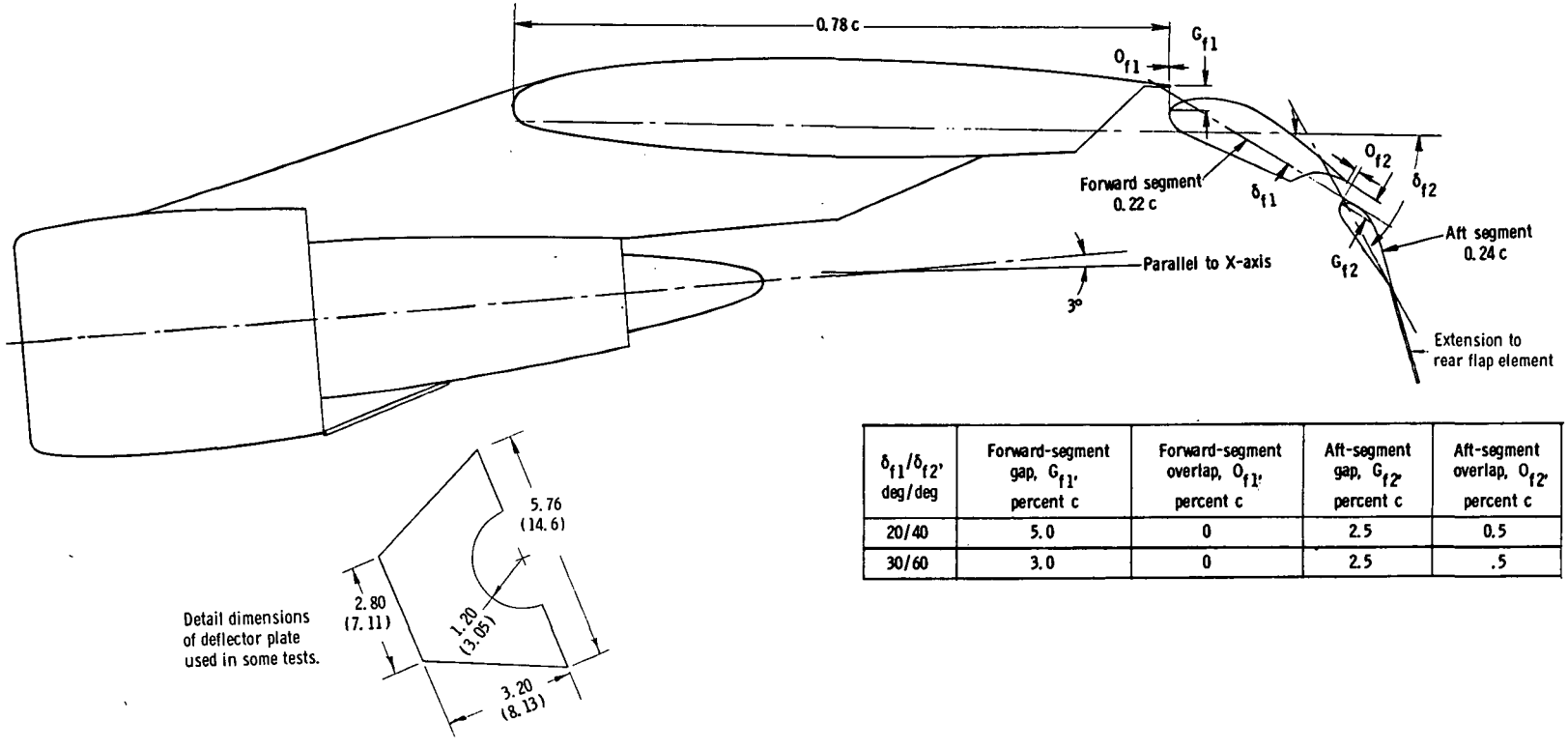

δ_{f1}/δ_{f2}, deg/deg	Forward-segment gap, G_{f1}, percent c	Forward-segment overlap, O_{f1}, percent c	Aft-segment gap, G_{f2}, percent c	Aft-segment overlap, O_{f2}, percent c
20/40	5.0	0	2.5	0.5
30/60	3.0	0	2.5	.5

(b) Flap assembly and engine-pylon details.

Figure 2.- Continued.

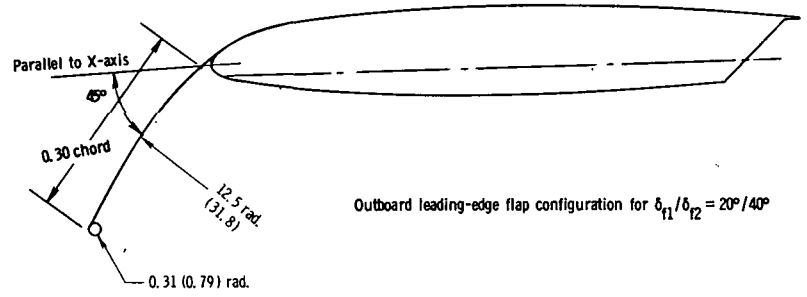

Outboard leading-edge flap configuration for $\delta_{f1}/\delta_{f2} = 20°/40°$

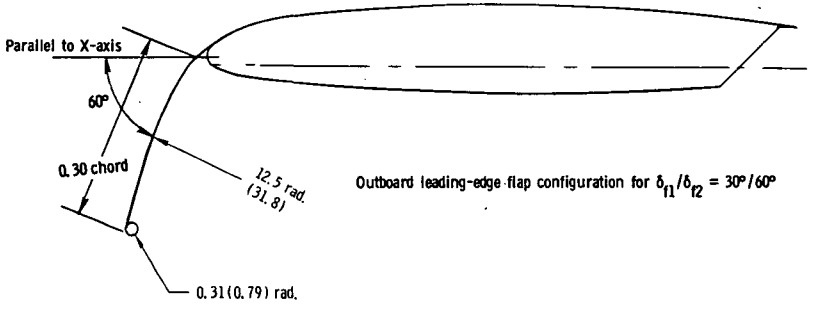

Outboard leading-edge flap configuration for $\delta_{f1}/\delta_{f2} = 30°/60°$

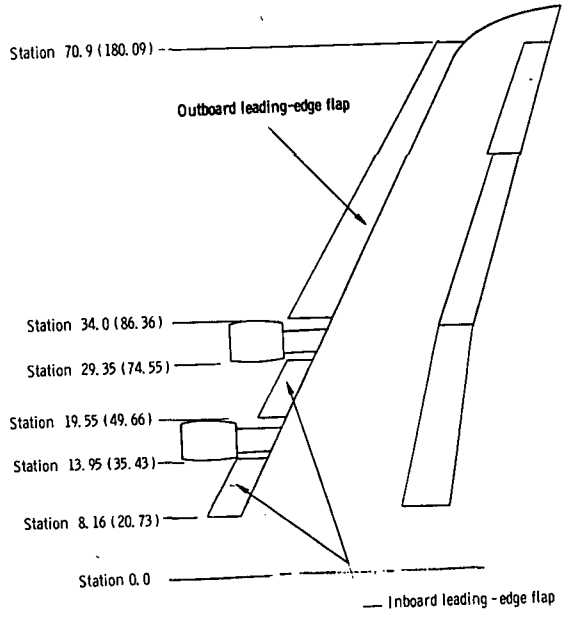

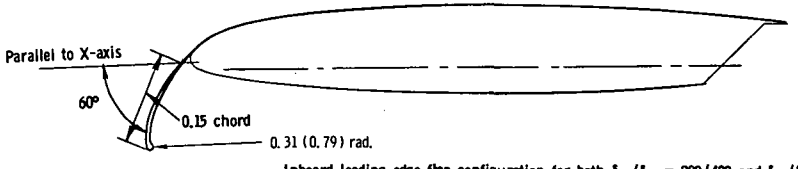

Inboard leading-edge flap configuration for both $\delta_{f1}/\delta_{f2} = 20°/40°$ and $\delta_{f1}/\delta_{f2} = 30°/60°$

(c) Flap details. All dimensions are in inches (centimeters).

Figure 2.- Continued.

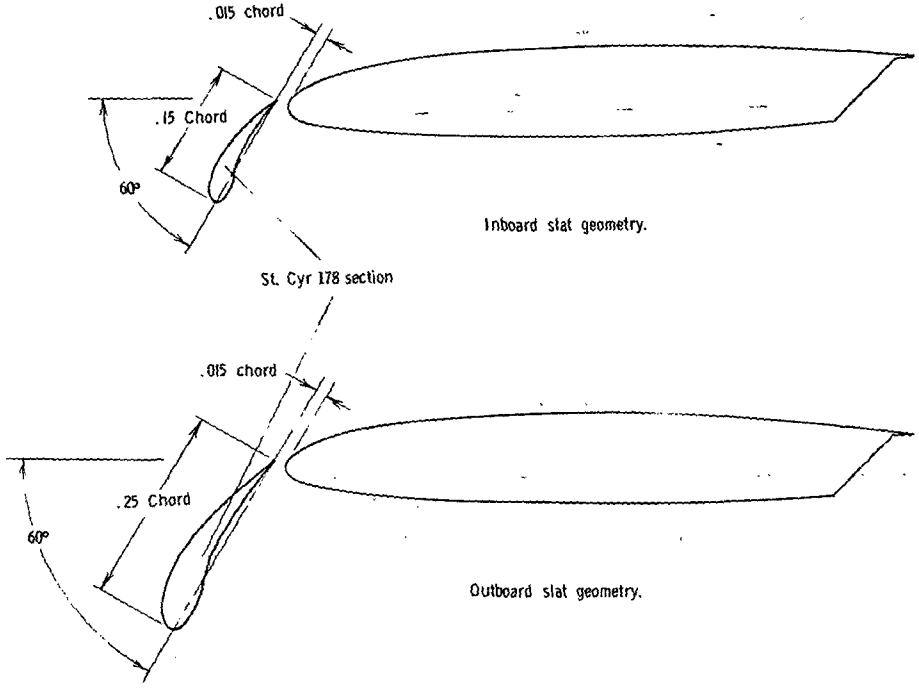

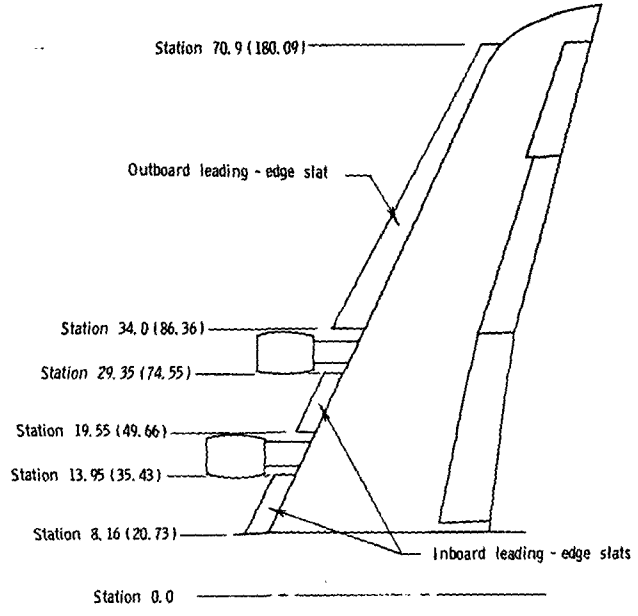

(d) Geometry of 25-percent slat.

Figure 2.- Continued.

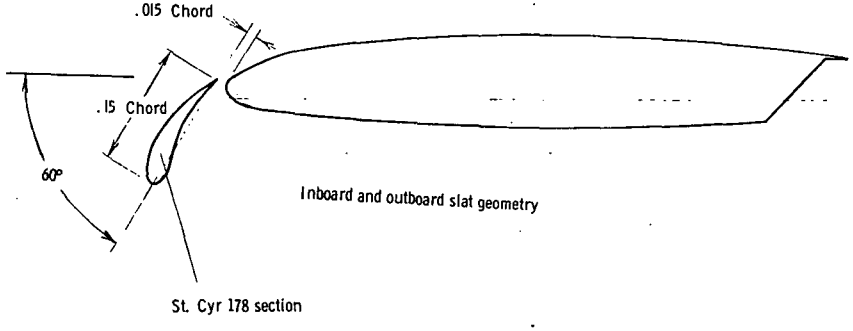

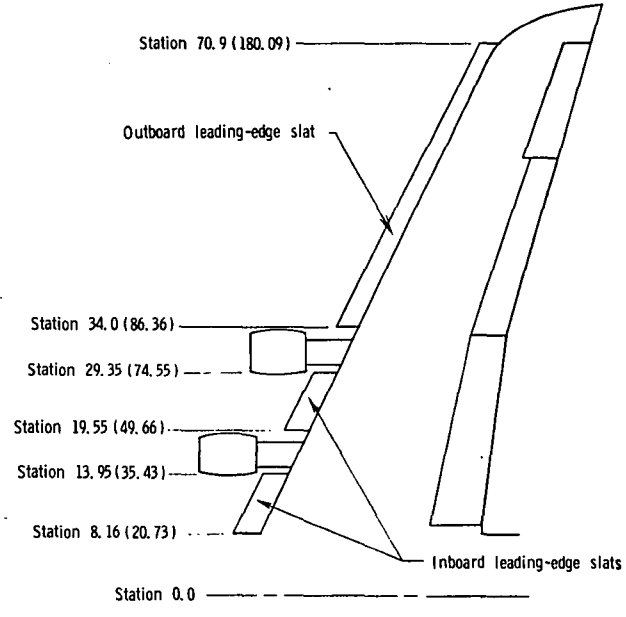

(e) Geometry of 15-percent slat.

Figure 2.- Concluded.

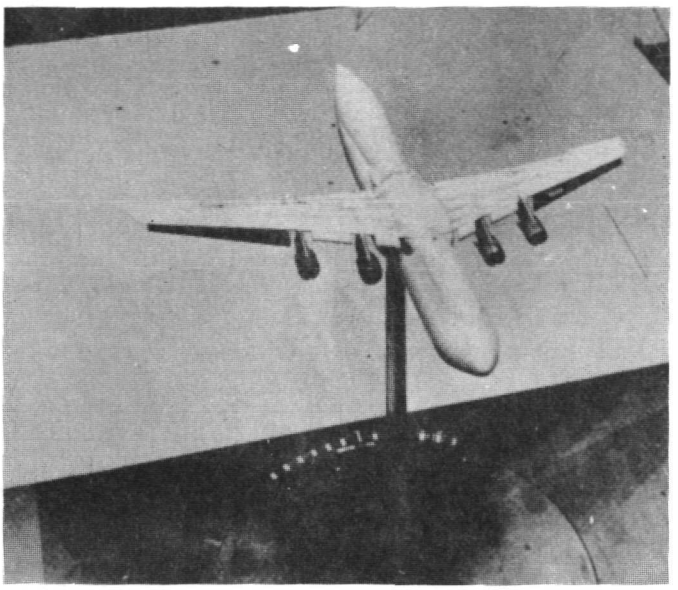

L-71-9865

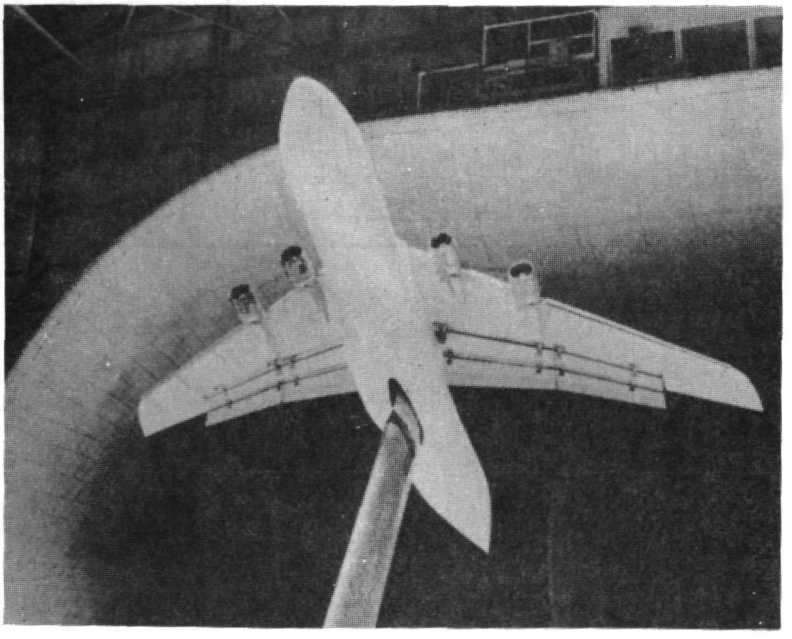

L-71-9866

Figure 3.- Photographs of model installed in tunnel.

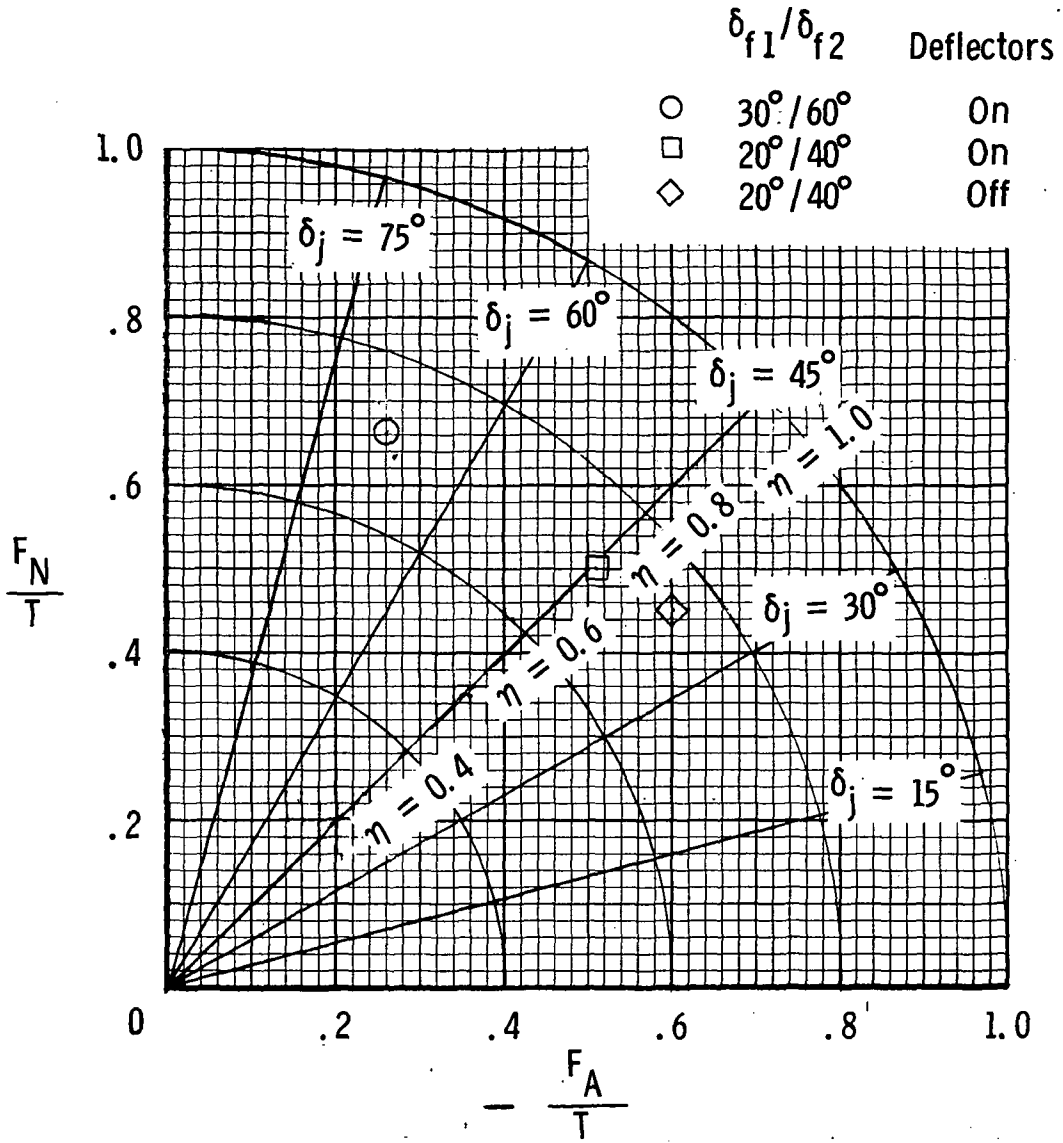

Figure 4.- Summary of static turning efficiency and turning angle.

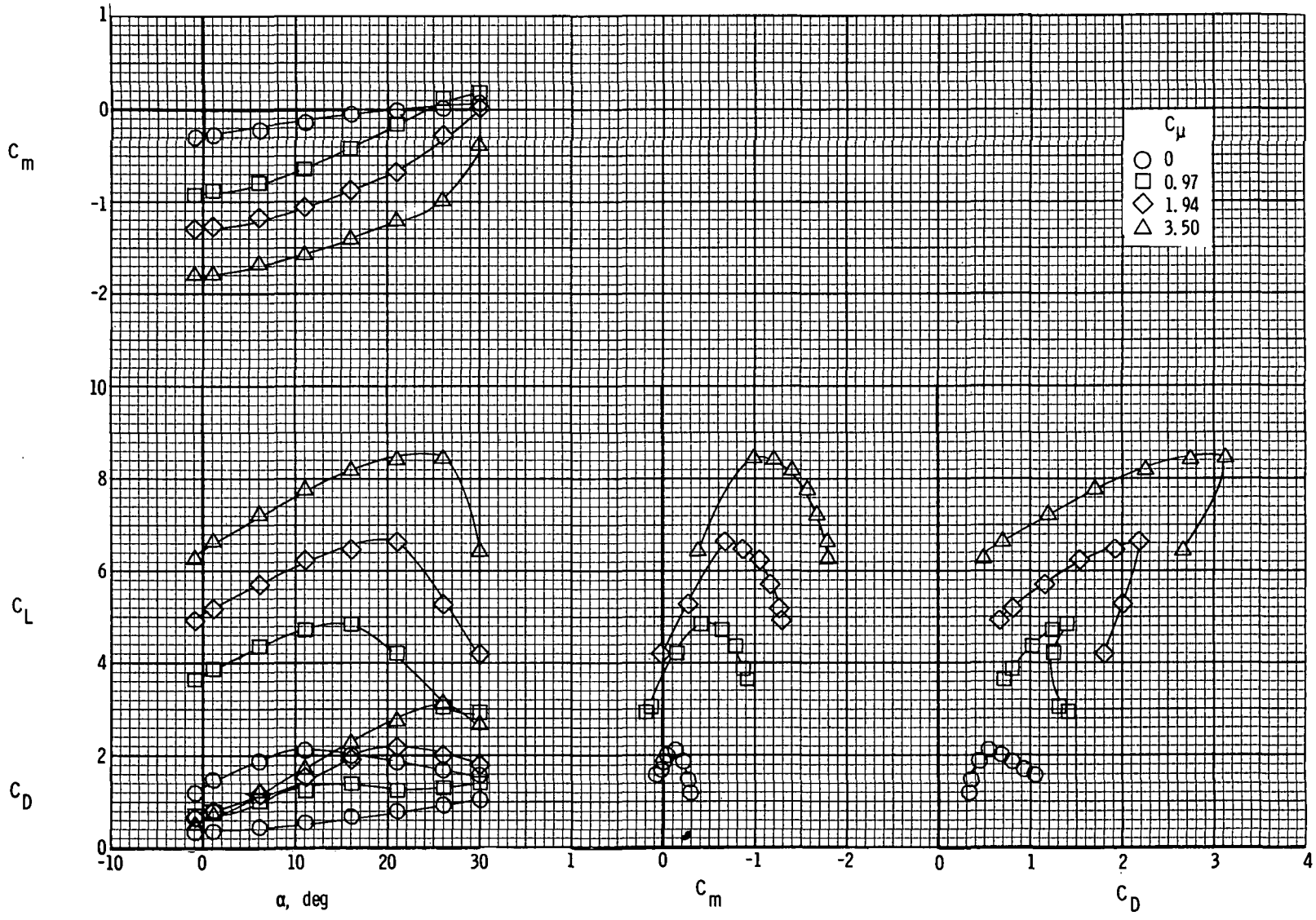

(a) $R = 0.47 \times 10^6$.

Figure 5.- Longitudinal characteristics of model with 30-percent leading-edge flap. $\delta_{f1}/\delta_{f2} = 30^o/60^o$.

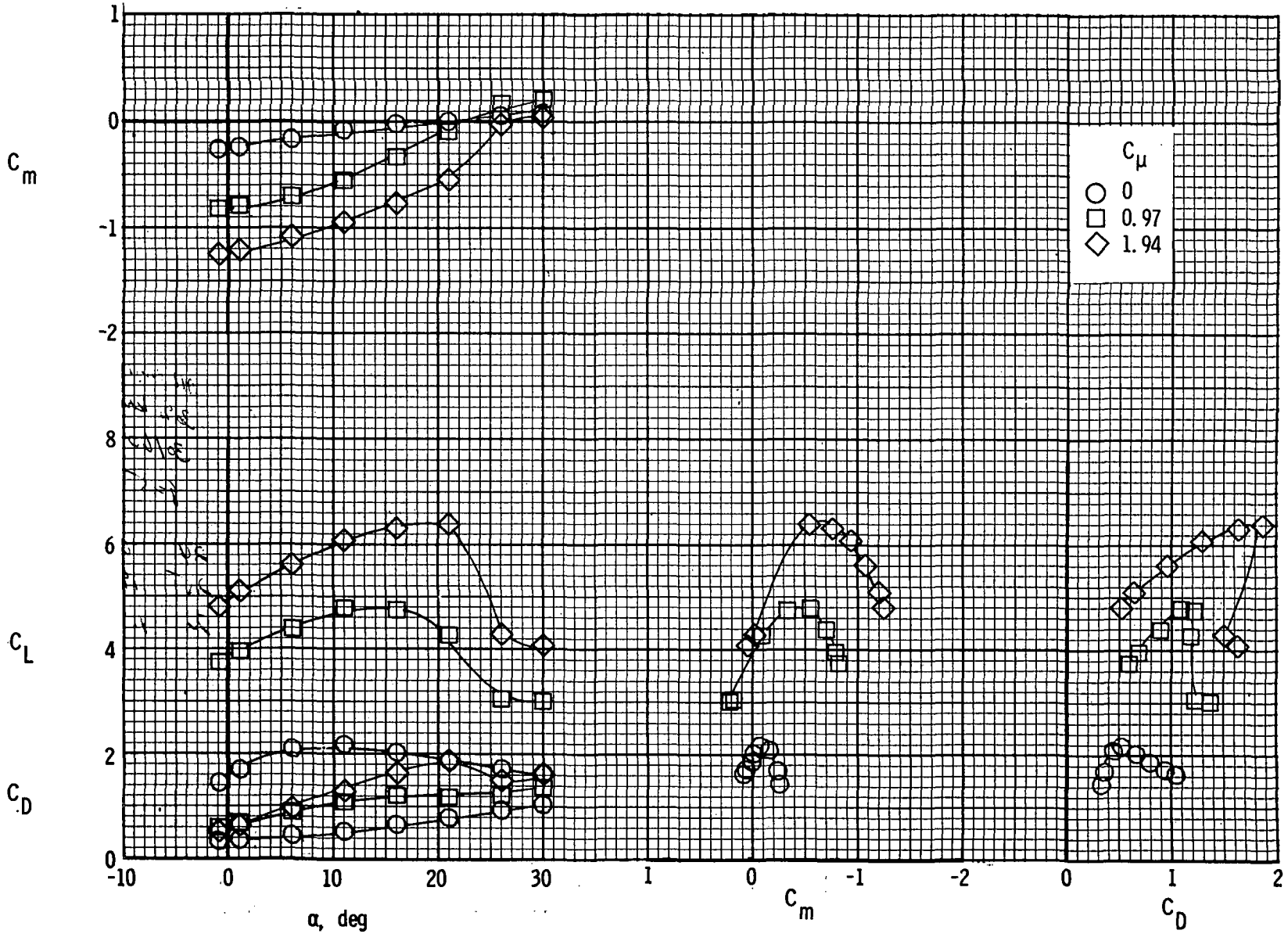

(b) $R = 0.73 \times 10^6$.

Figure 5.- Continued.

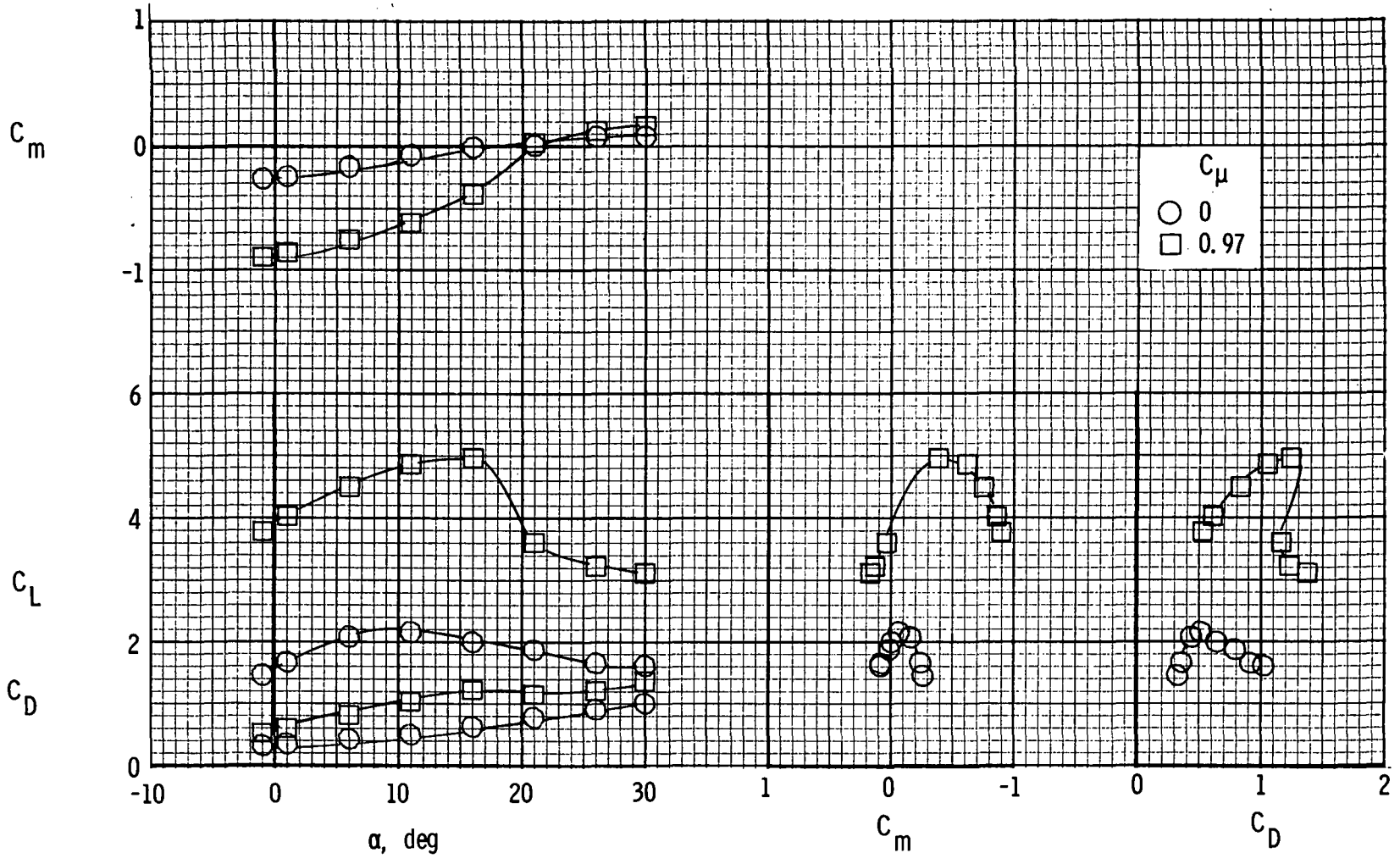

(c) $R = 1.03 \times 10^6$.

Figure 5.- Continued.

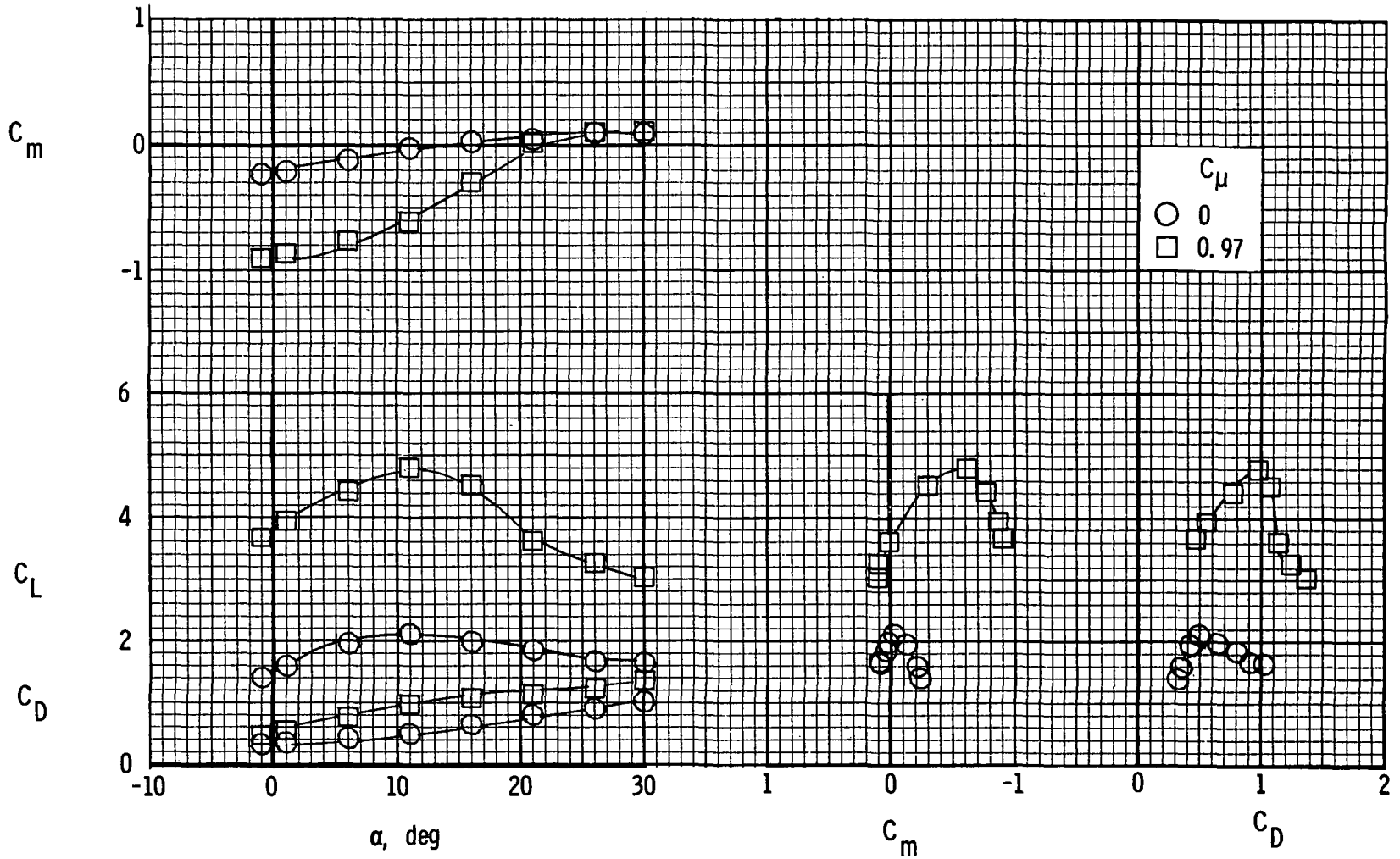

(d) $R = 1.36 \times 10^6$.

Figure 5.- Concluded.

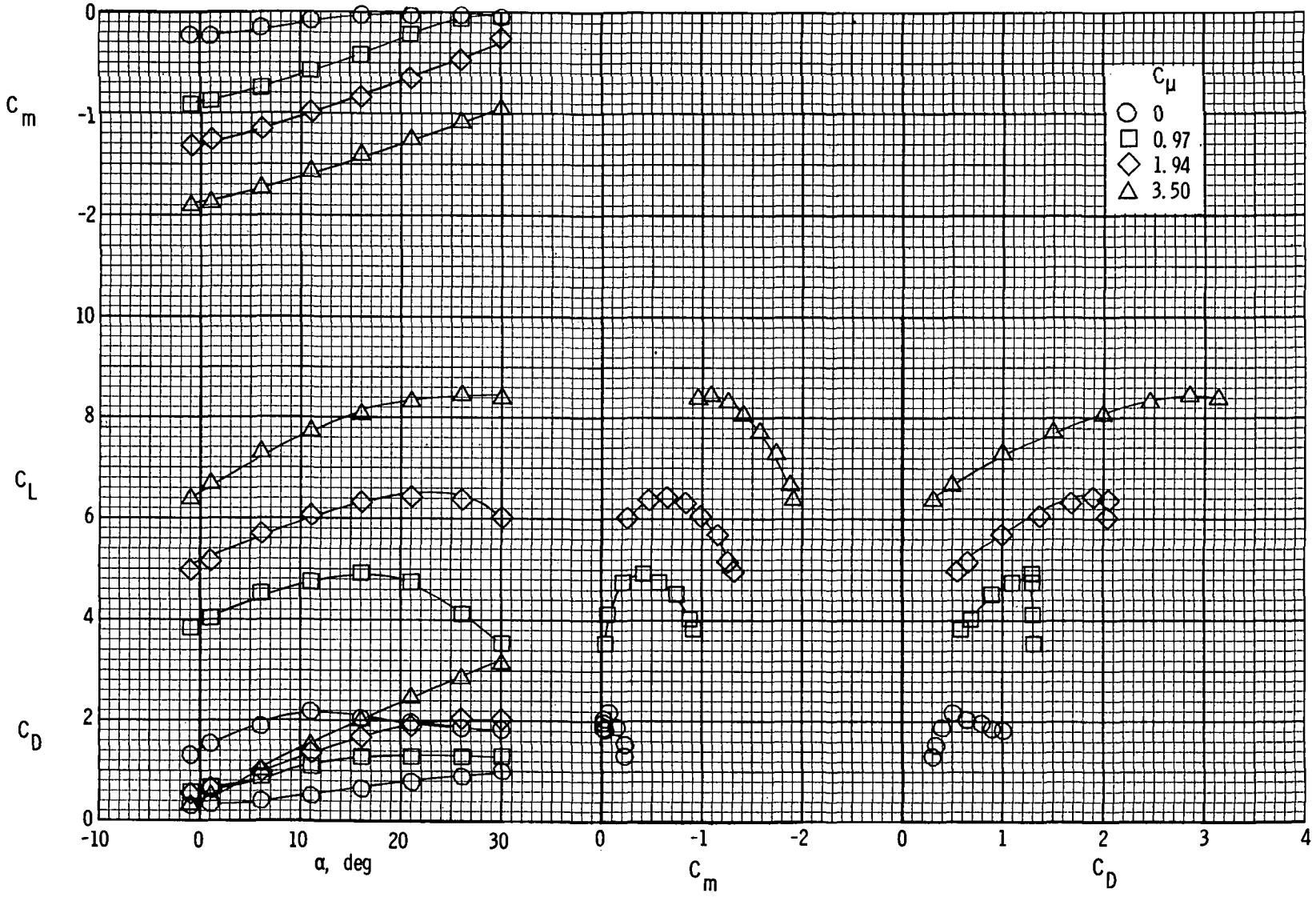

(a) $R = 0.47 \times 10^6$.

Figure 6.- Longitudinal characteristics of model with 25-percent leading-edge slats. $\delta_{f1}/\delta_{f2} = 30^o/60^o$.

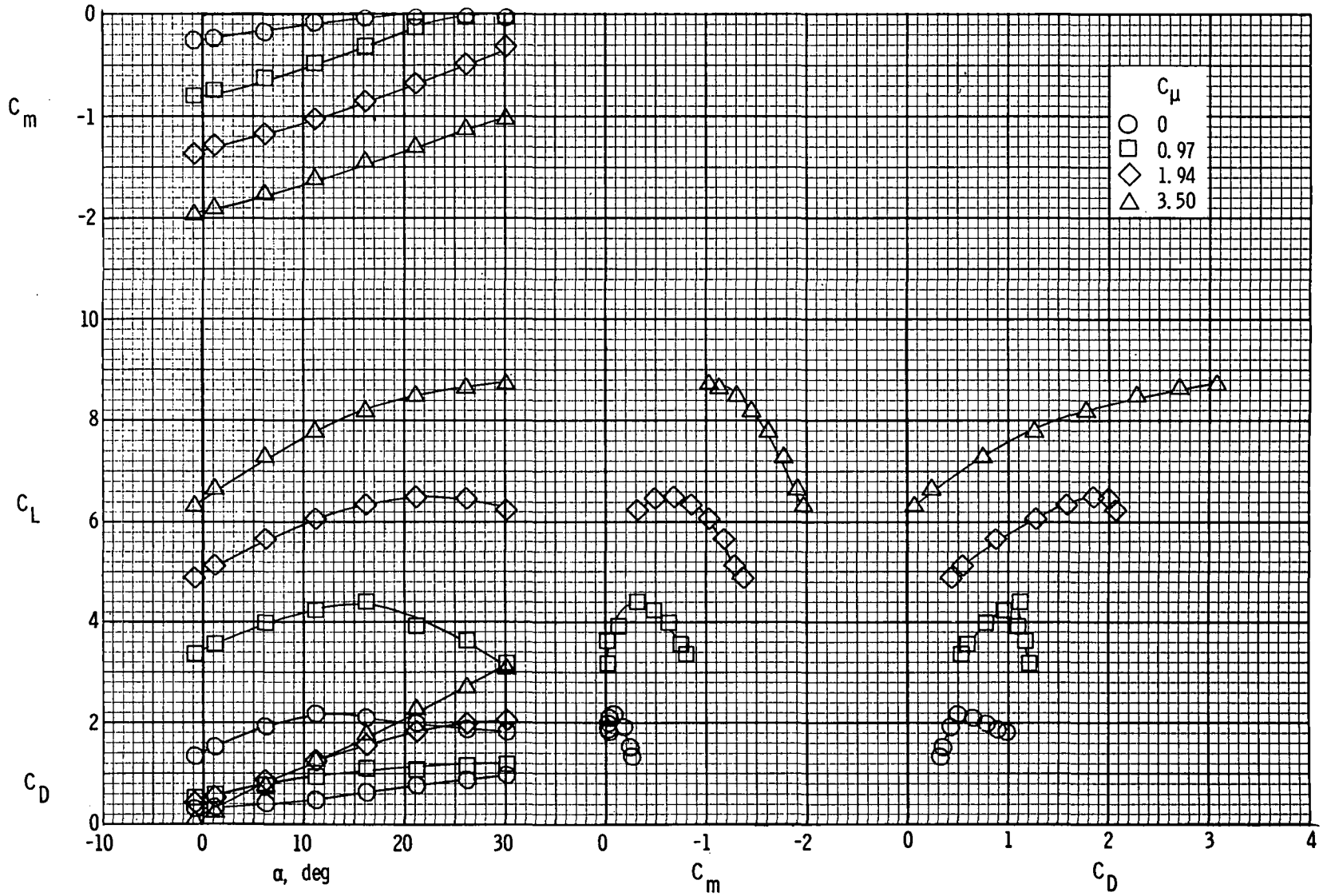

(b) $R = 0.73 \times 10^6$.

Figure 6.- Continued.

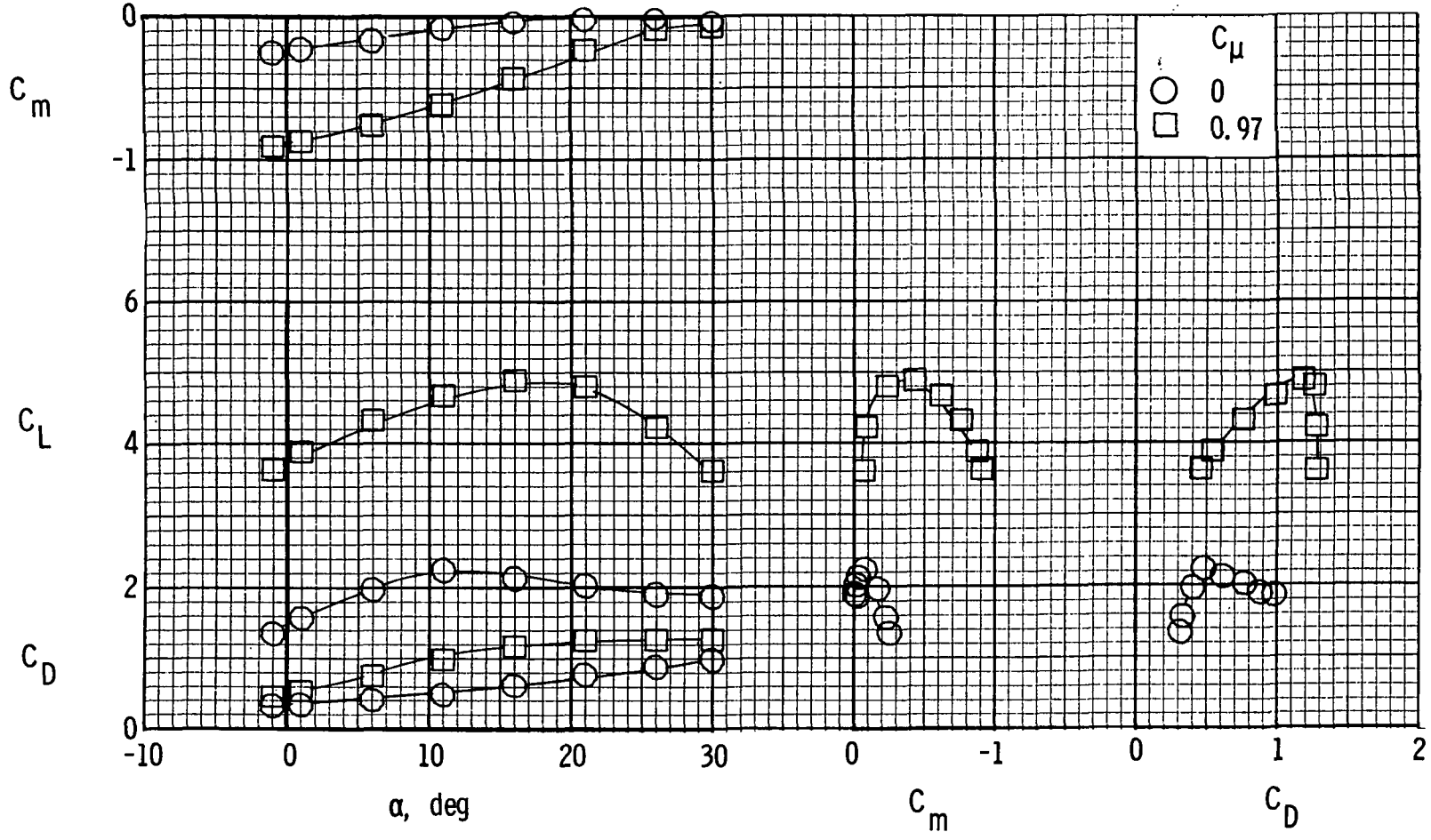

(c) $R = 1.03 \times 10^6$.

Figure 6.- Continued.

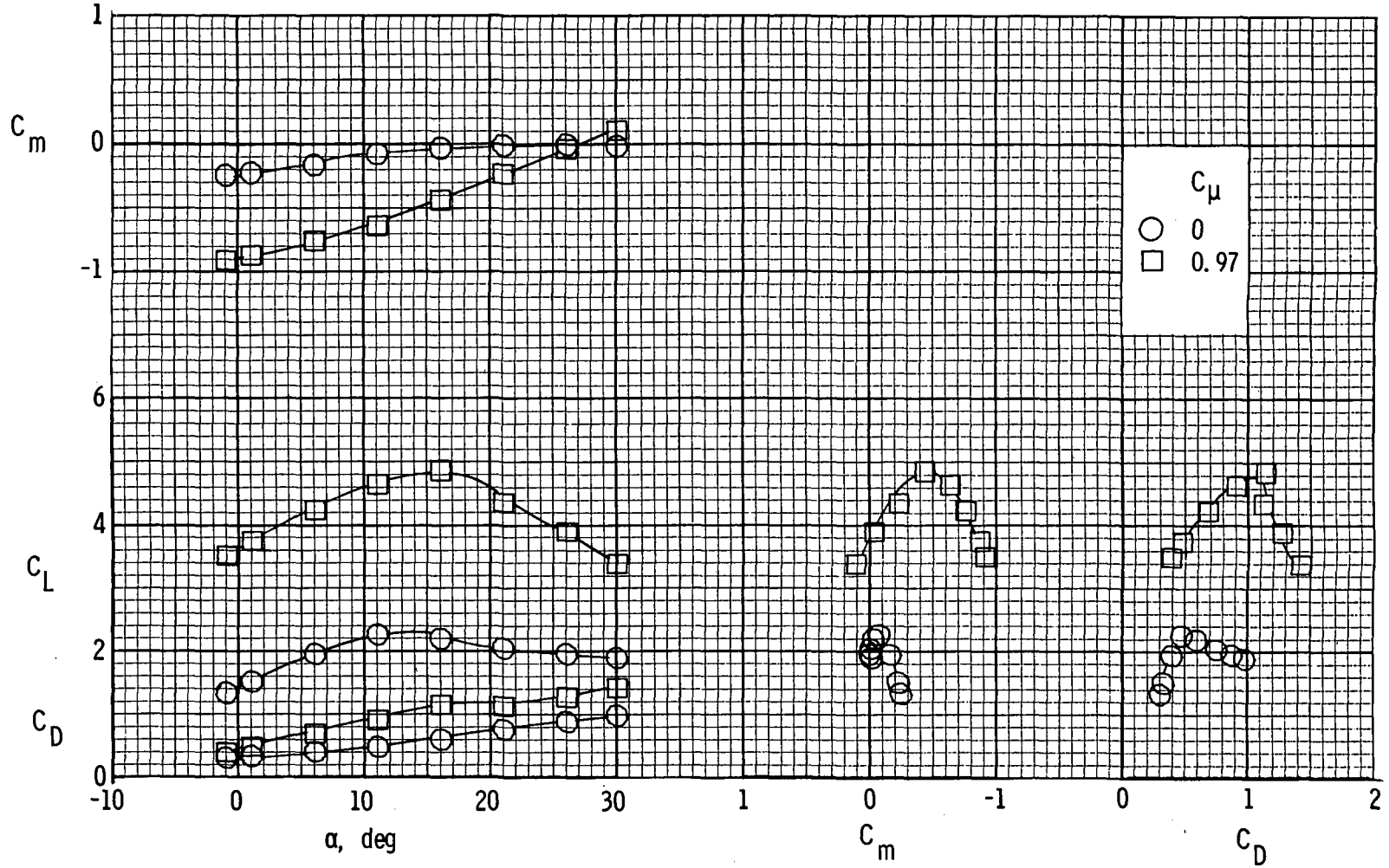

(d) $R = 1.36 \times 10^6$.

Figure 6.- Concluded.

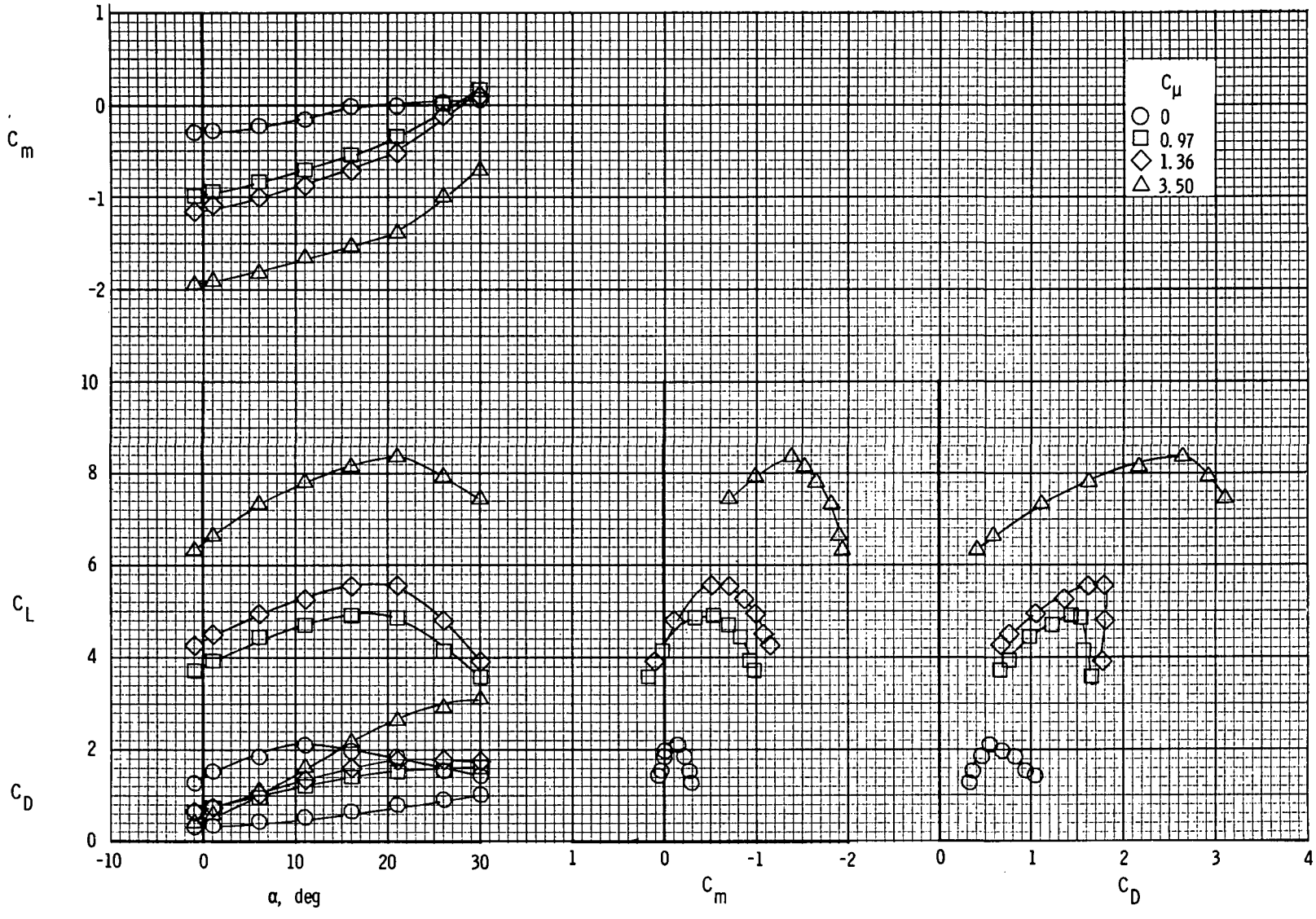

(a) $R = 0.47 \times 10^6$.

Figure 7.- Longitudinal characteristics of model with 15-percent leading-edge slats. $\delta_{f1}/\delta_{f2} = 30^o/60^o$.

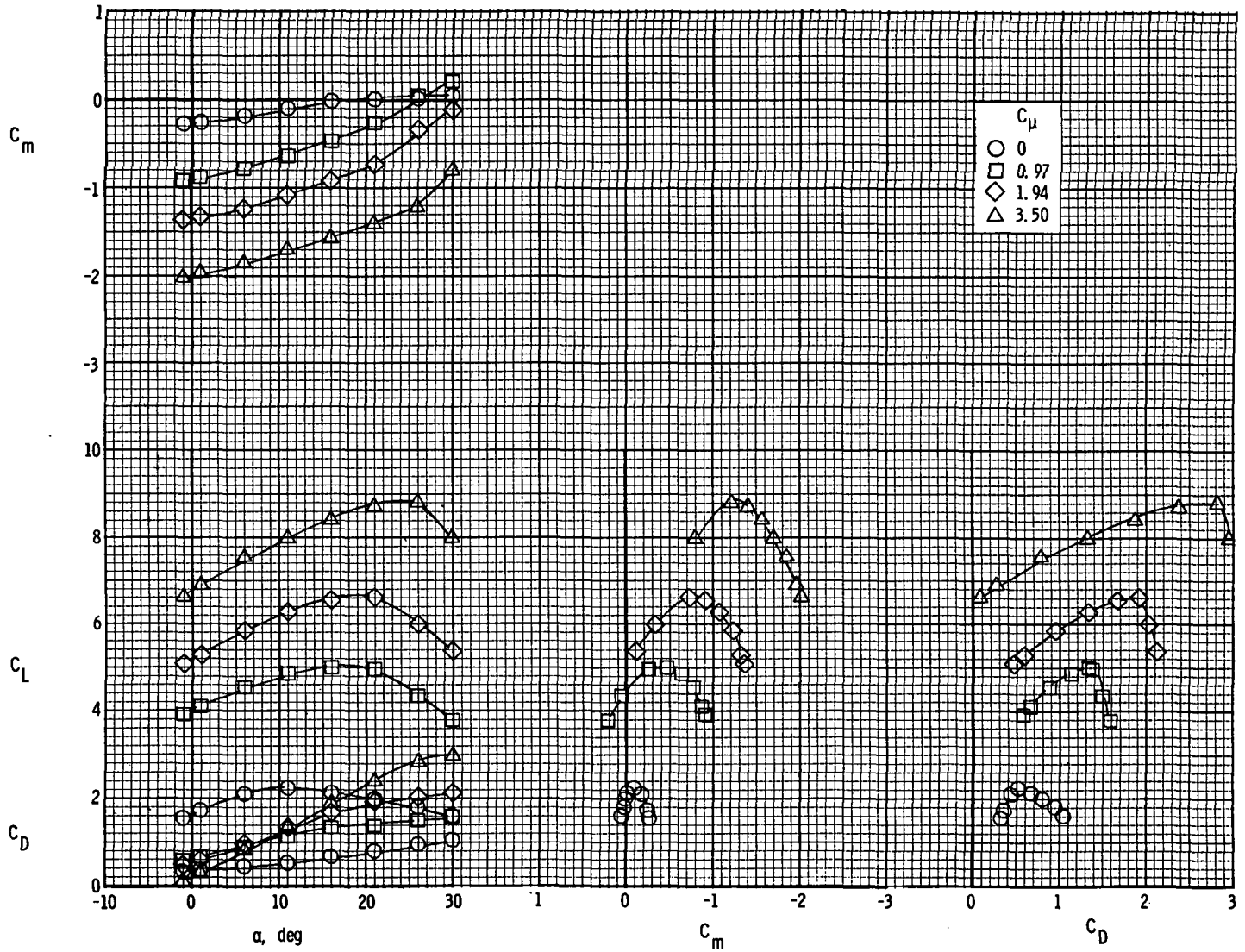

(b) $R = 0.73 \times 10^6$.

Figure 7.- Continued.

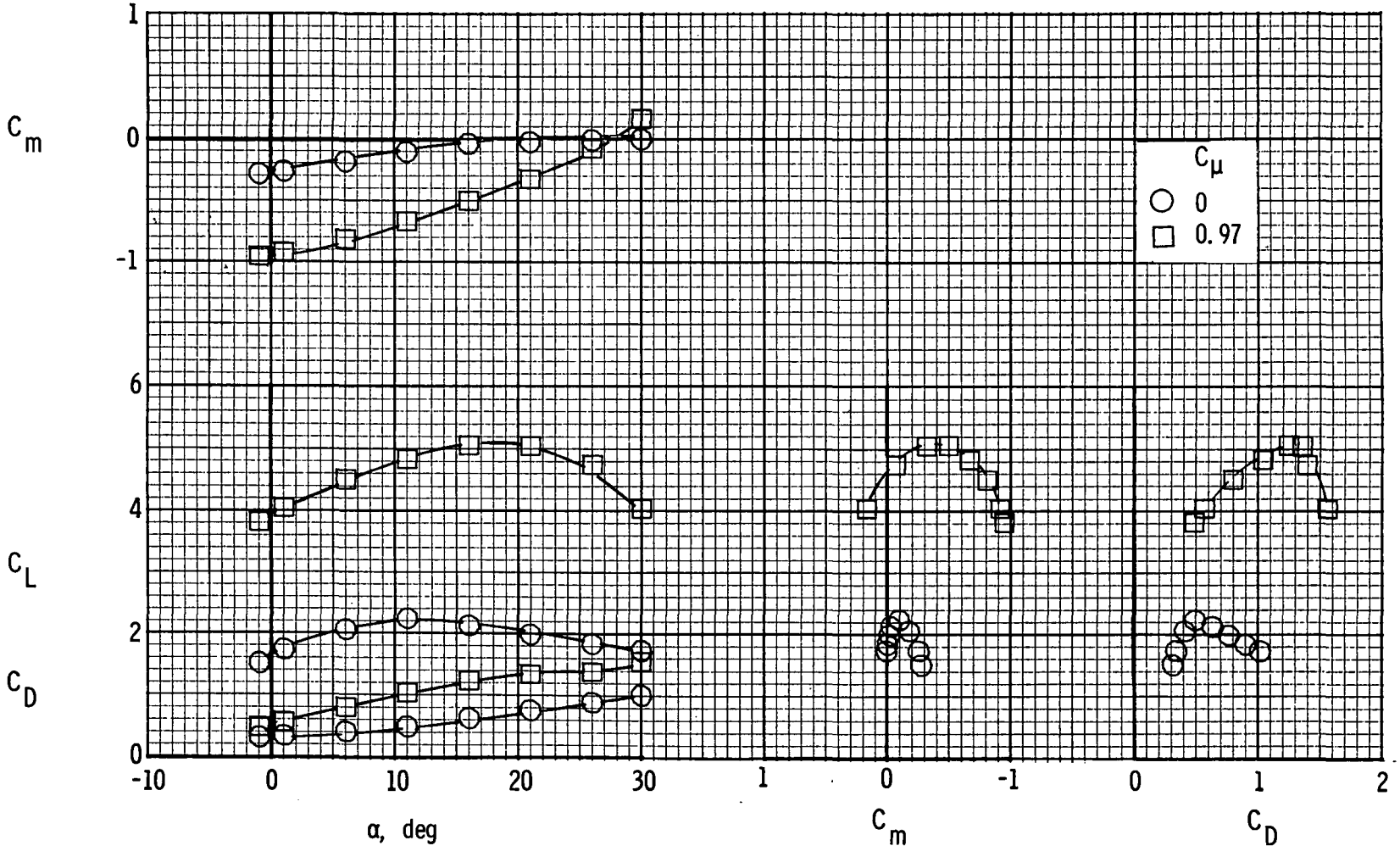

(c) $R = 1.03 \times 10^6$.

Figure 7.- Continued.

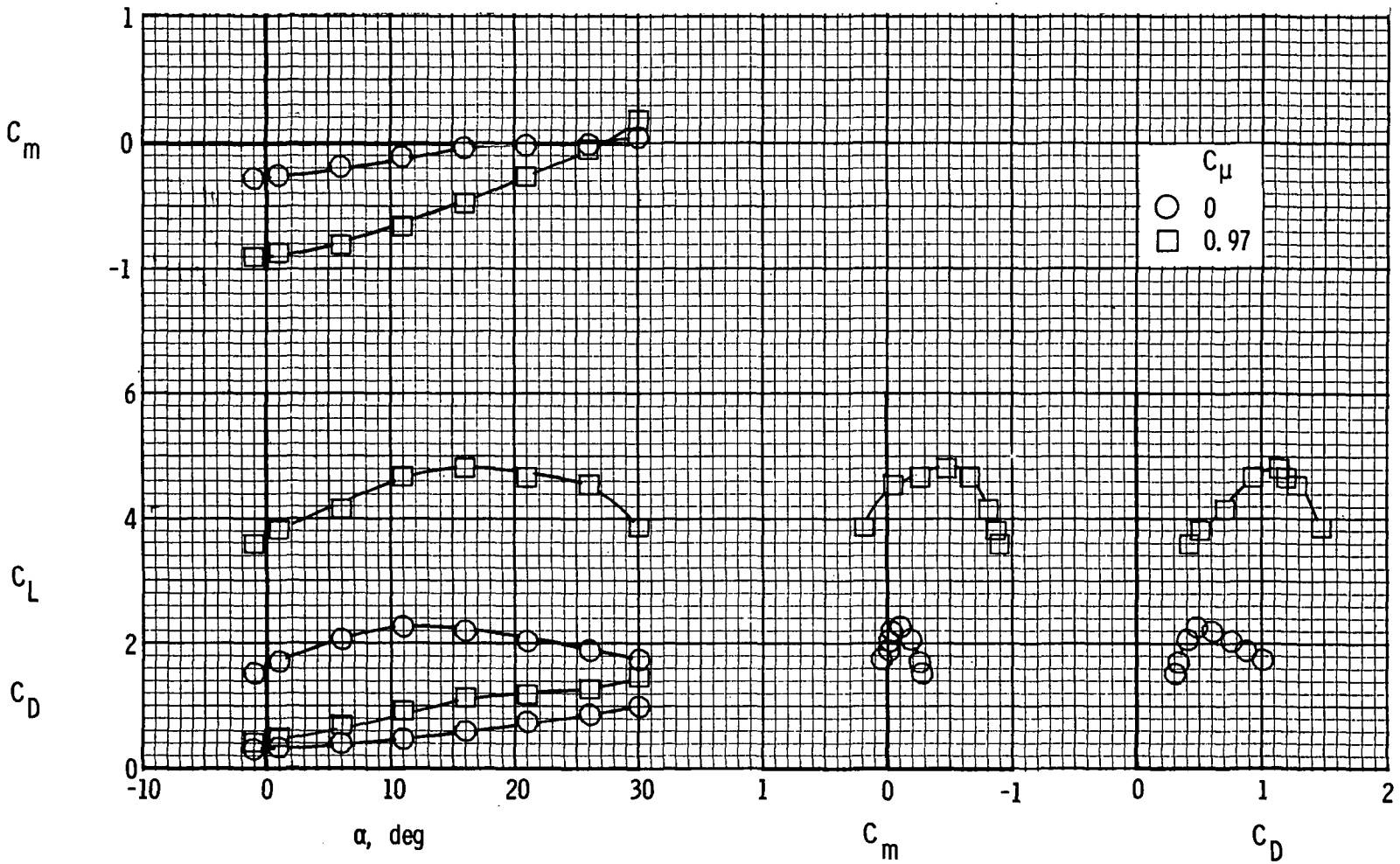

(d) $R = 1.36 \times 10^6$.

Figure 7.- Concluded.

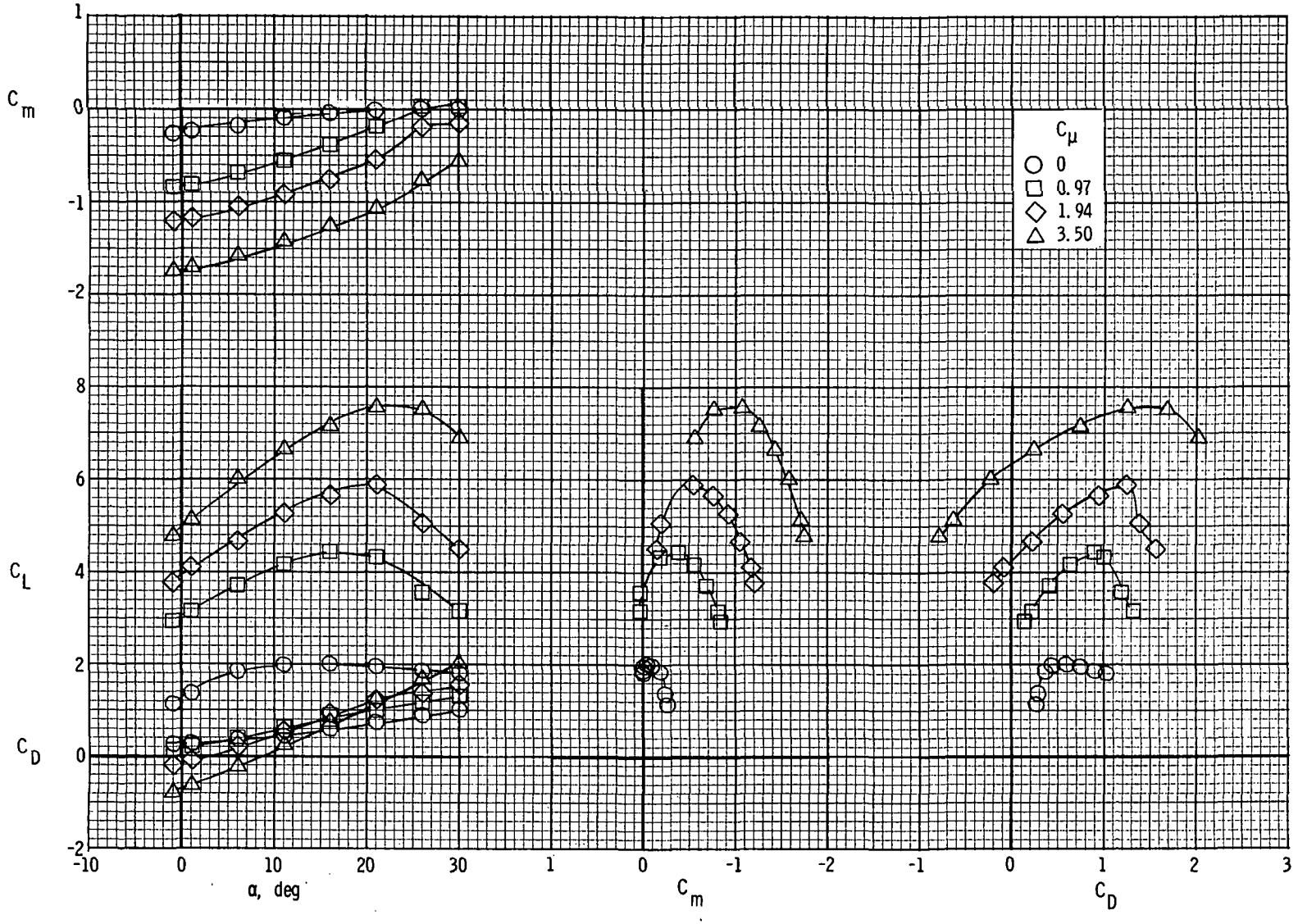

(a) $R = 0.47 \times 10^6$.

Figure 8.- Longitudinal characteristics of model with 30-percent leading-edge flap. $\delta_{f1}/\delta_{f2} = 20^o/40^o$.

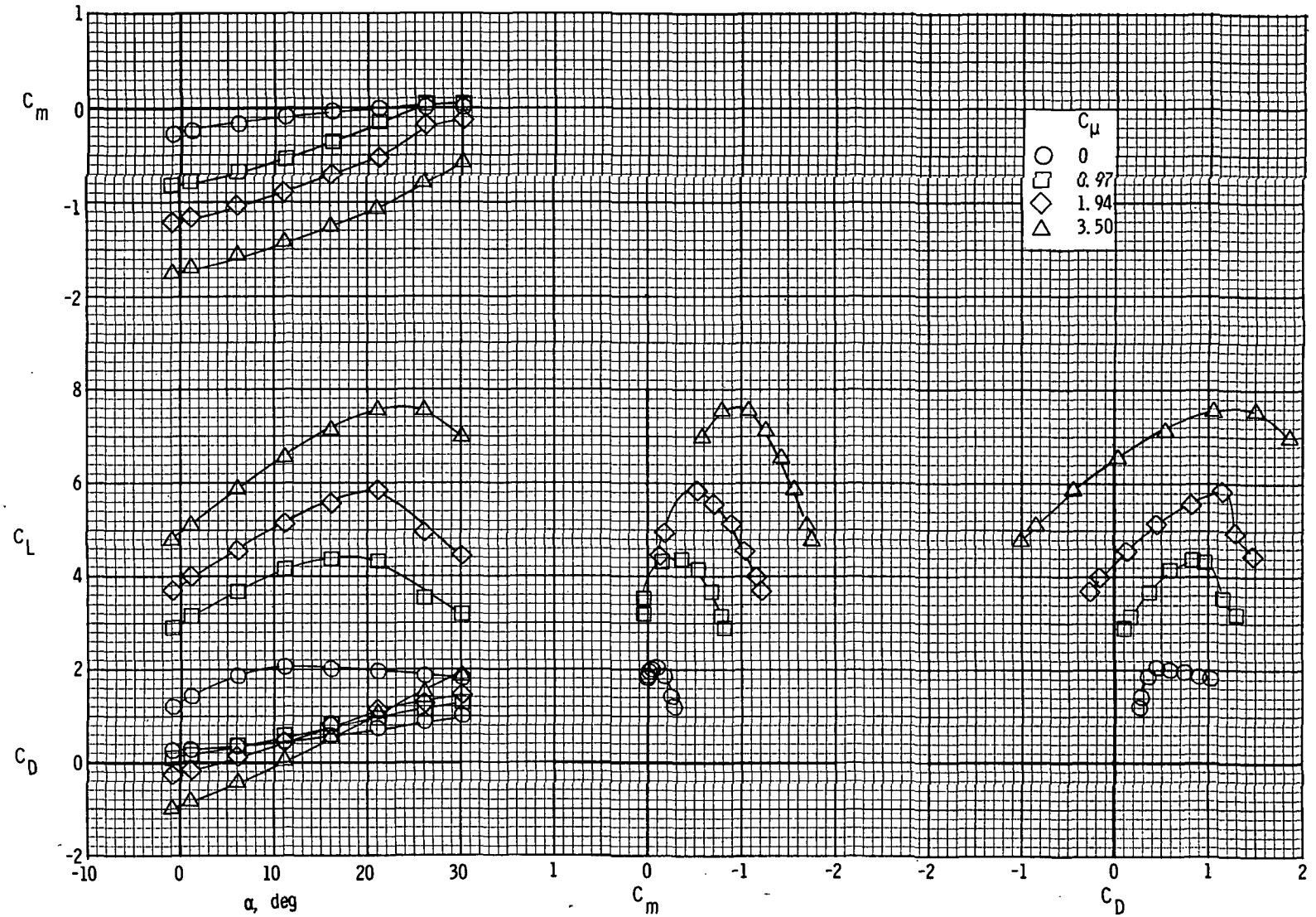

(b) $R = 0.73 \times 10^6$.

Figure 8.- Continued.

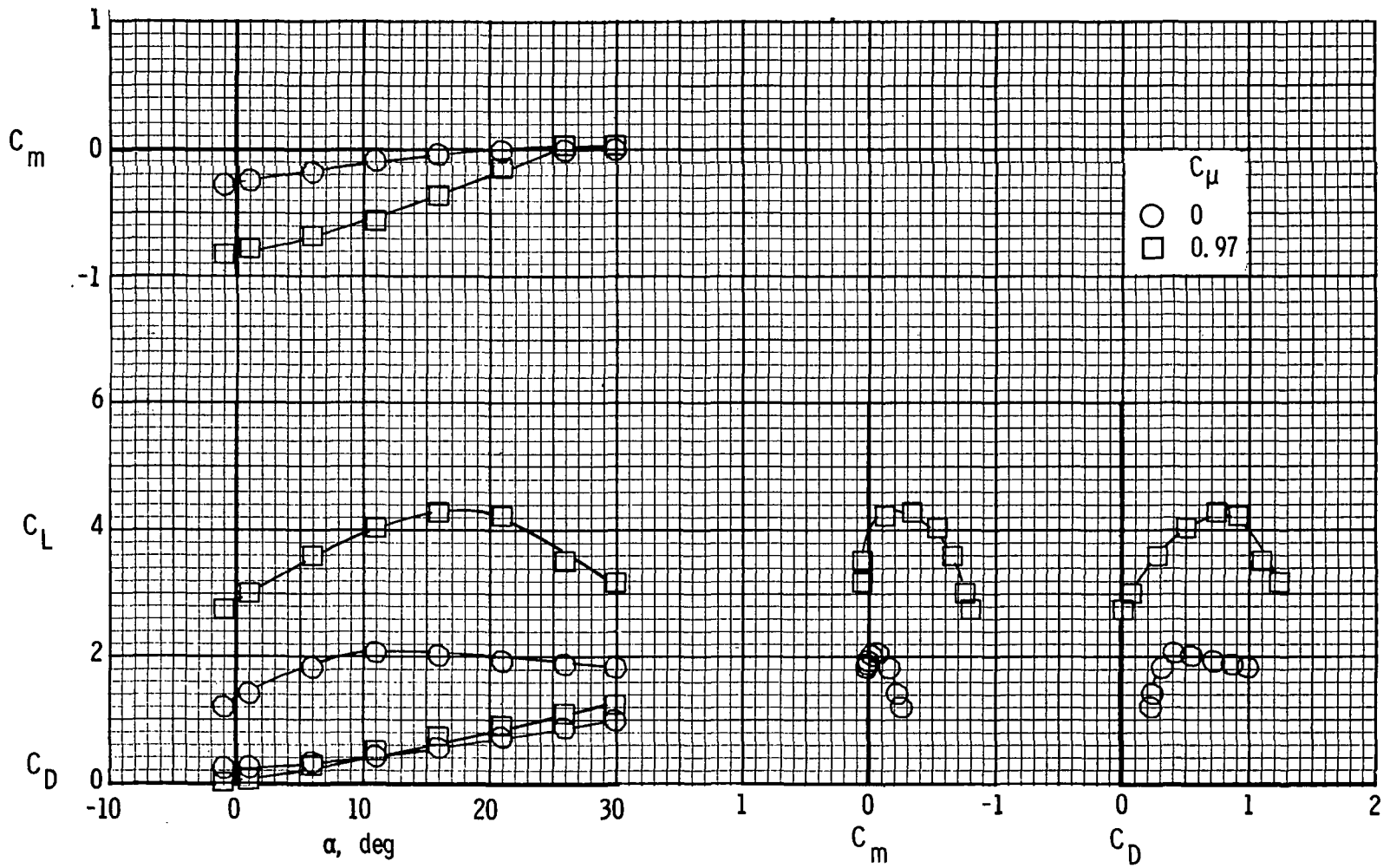

(c) $R = 1.03 \times 10^6$.

Figure 8.- Continued.

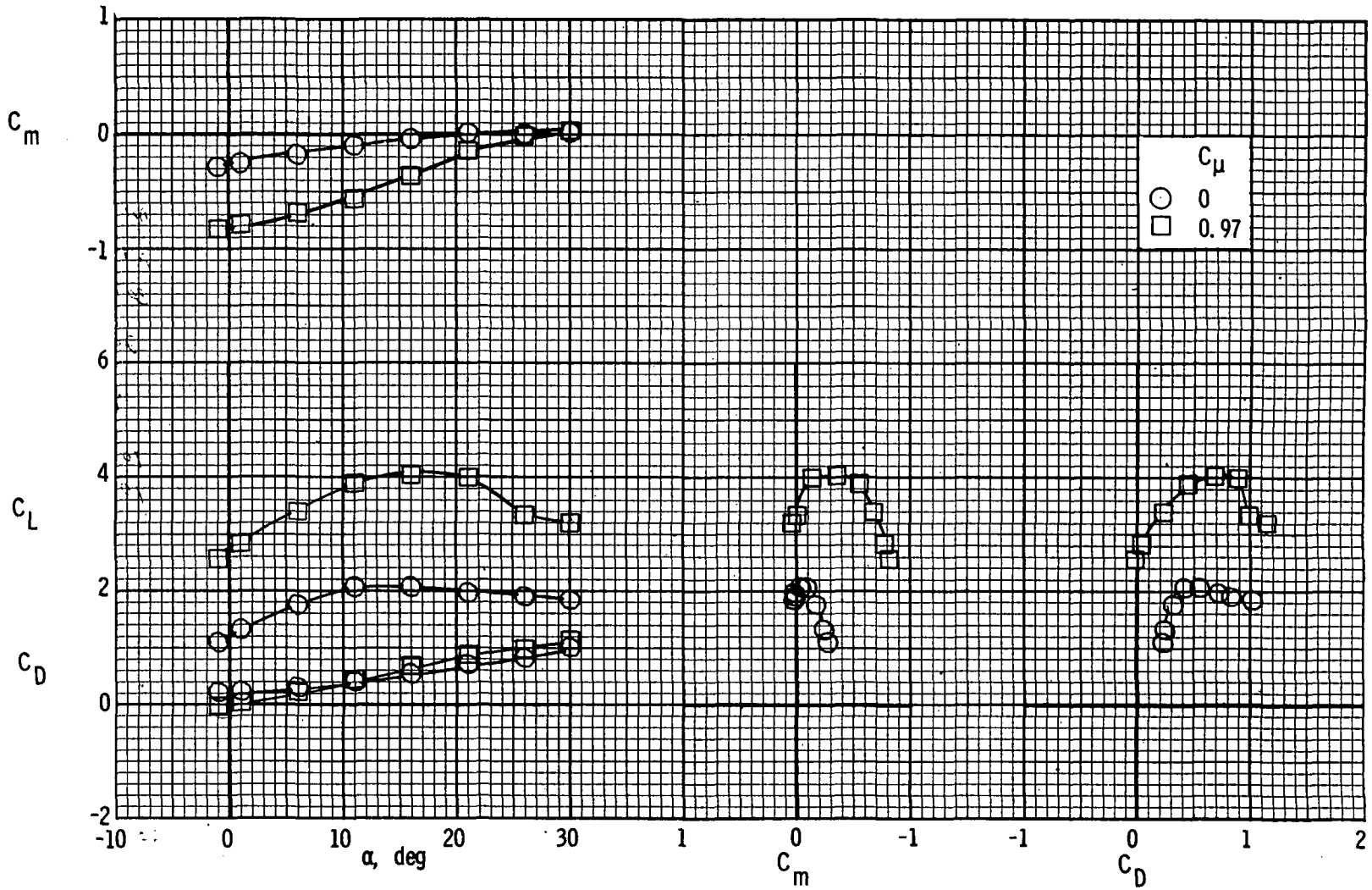

(d) $R = 1.36 \times 10^6$.

Figure 8.- Concluded.

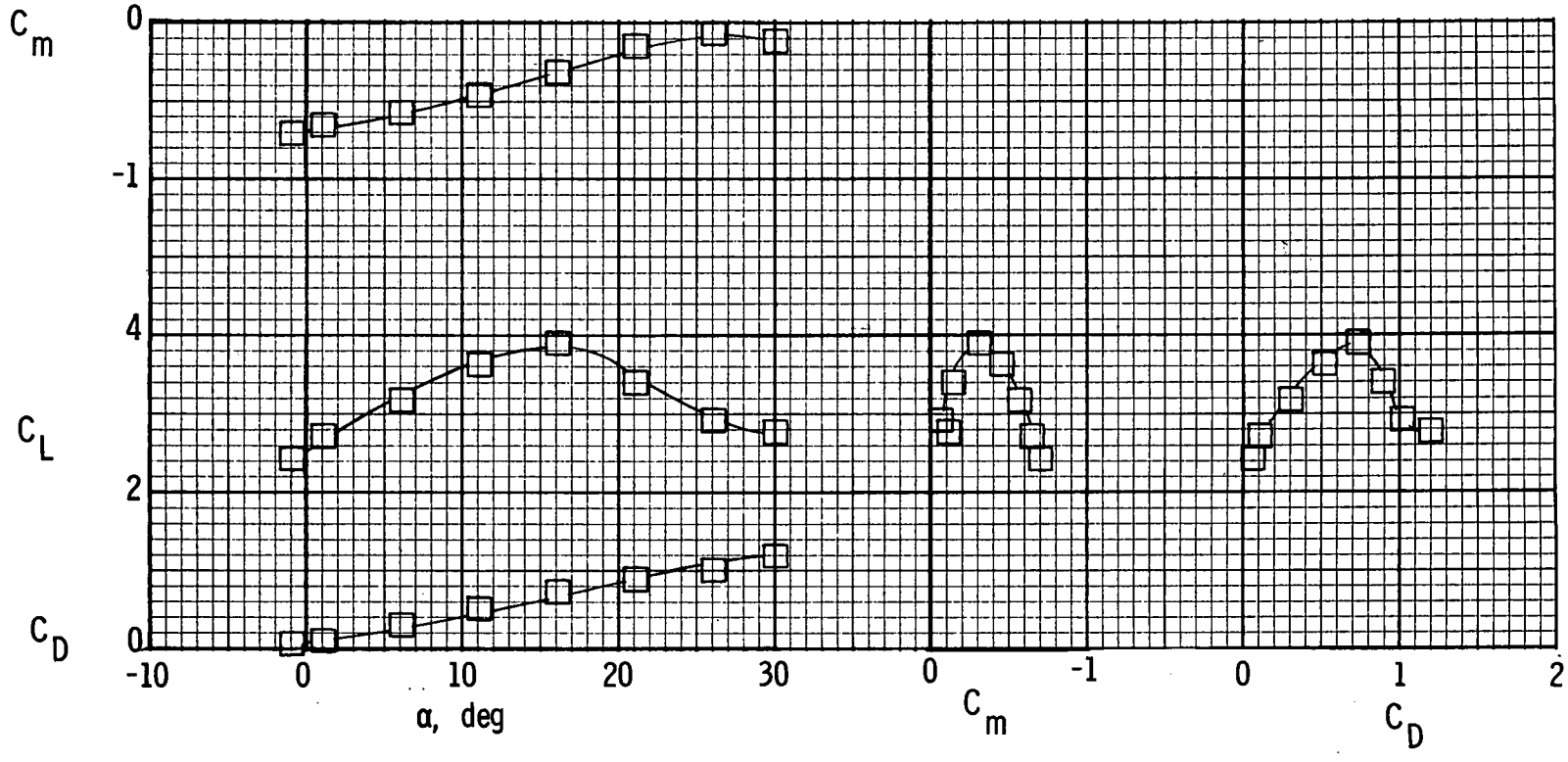

(a) $R = 0.47 \times 10^6$.

Figure 9.- Longitudinal characteristics of model with 30-percent leading-edge flap and thrust deflectors off. $C_\mu = 0.97$; $\delta_{f1}/\delta_{f2} = 20^o/40^o$.

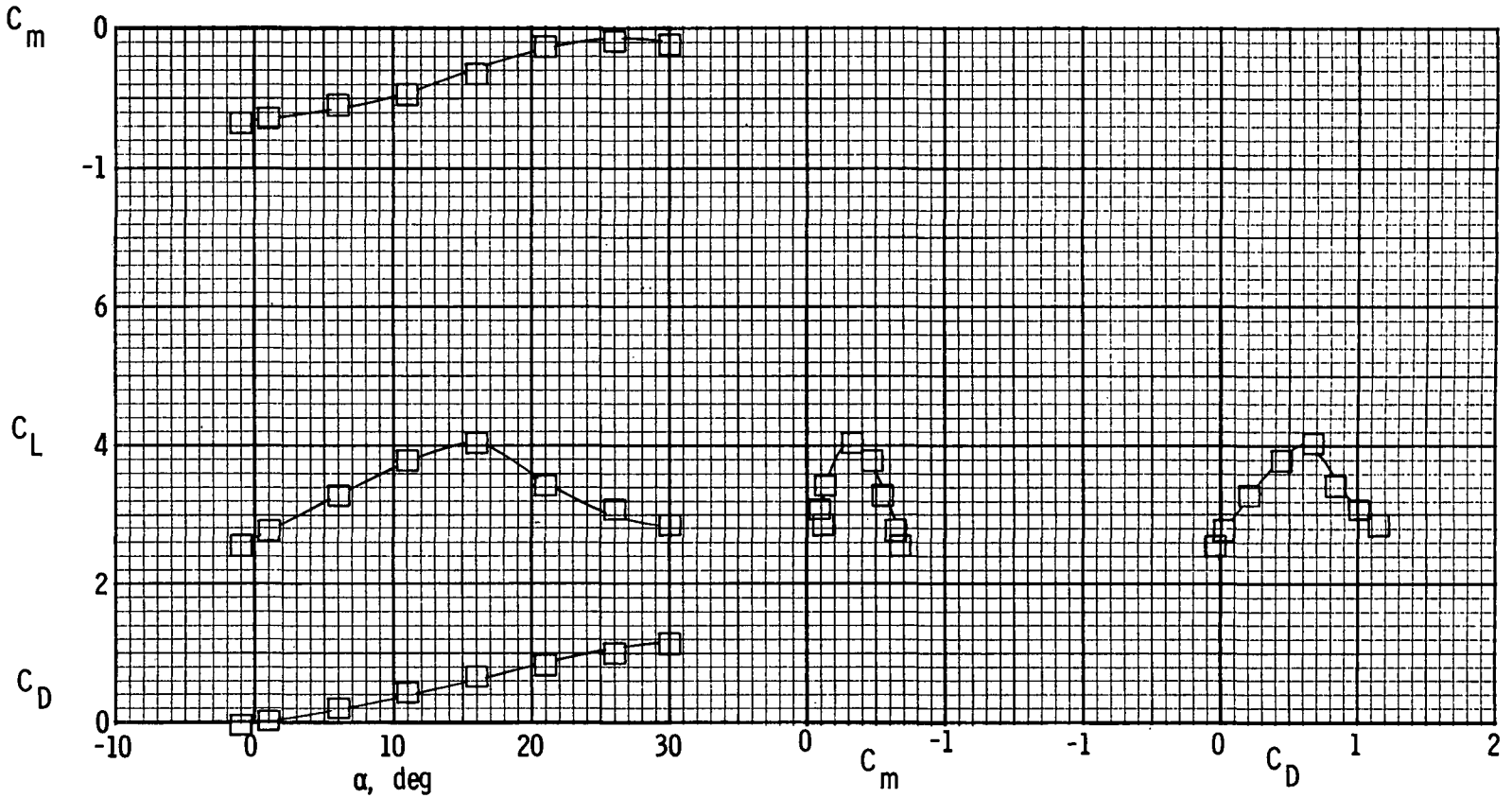

(b) $R = 0.73 \times 10^6$.

Figure 9.- Continued.

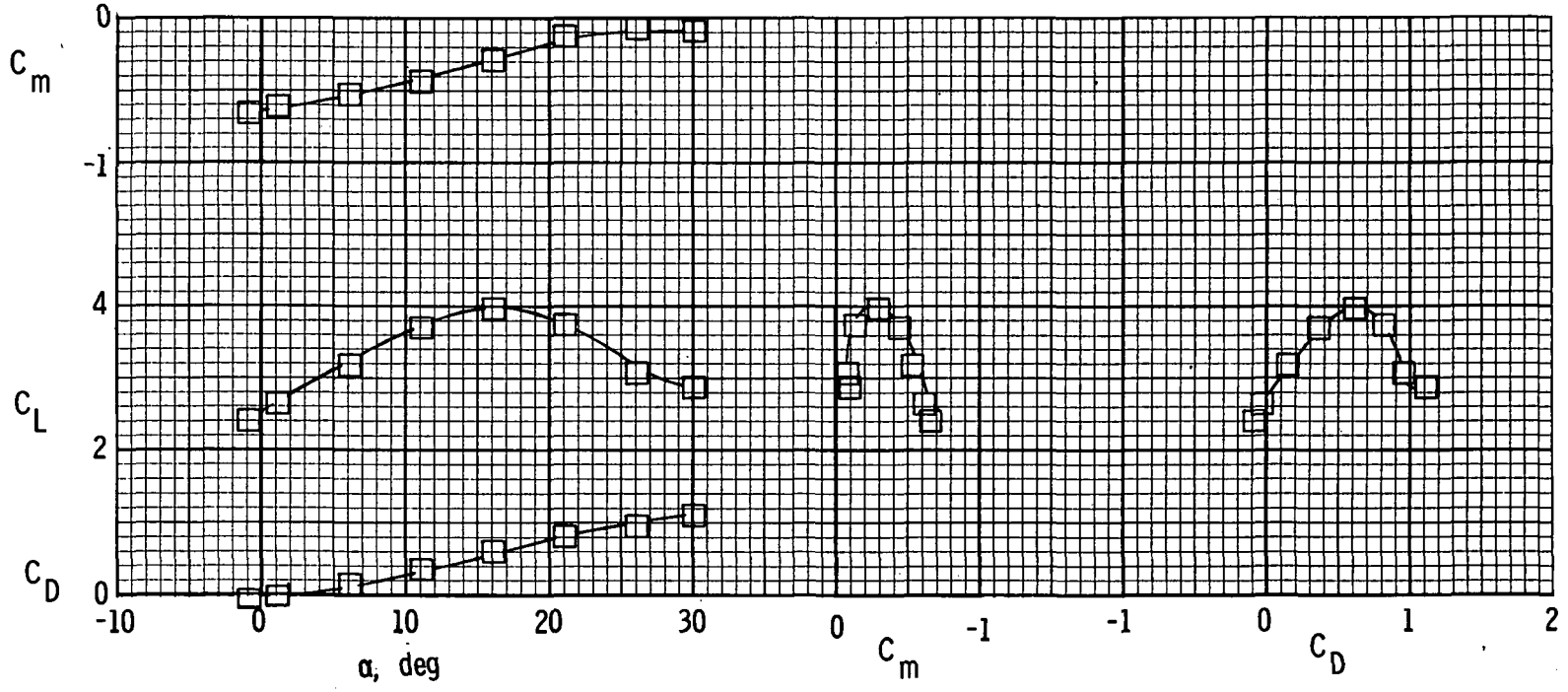

(c) $R = 1.03 \times 10^6$.

Figure 9.- Continued.

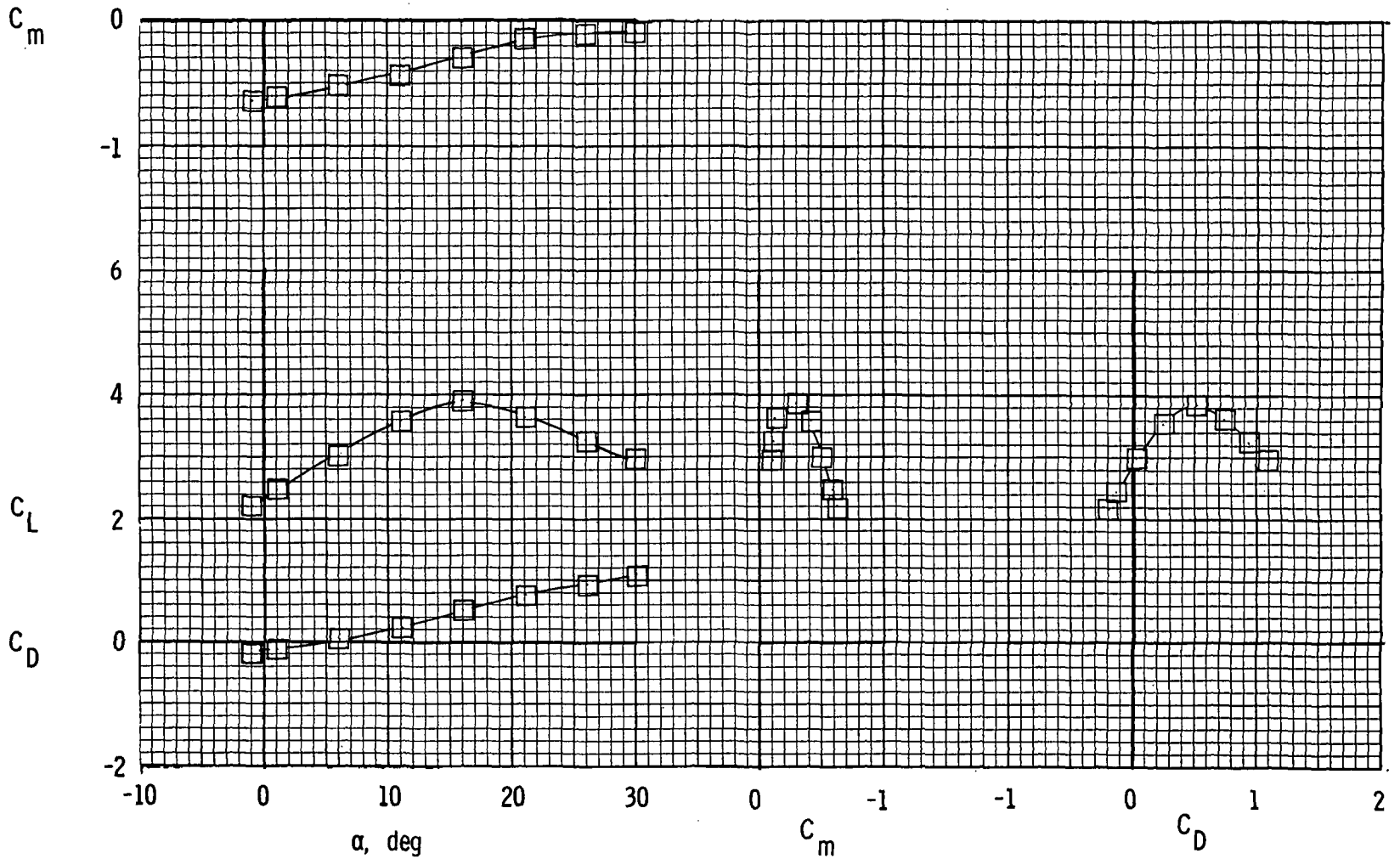

(d) $R = 1.36 \times 10^6$.

Figure 9.- Concluded.

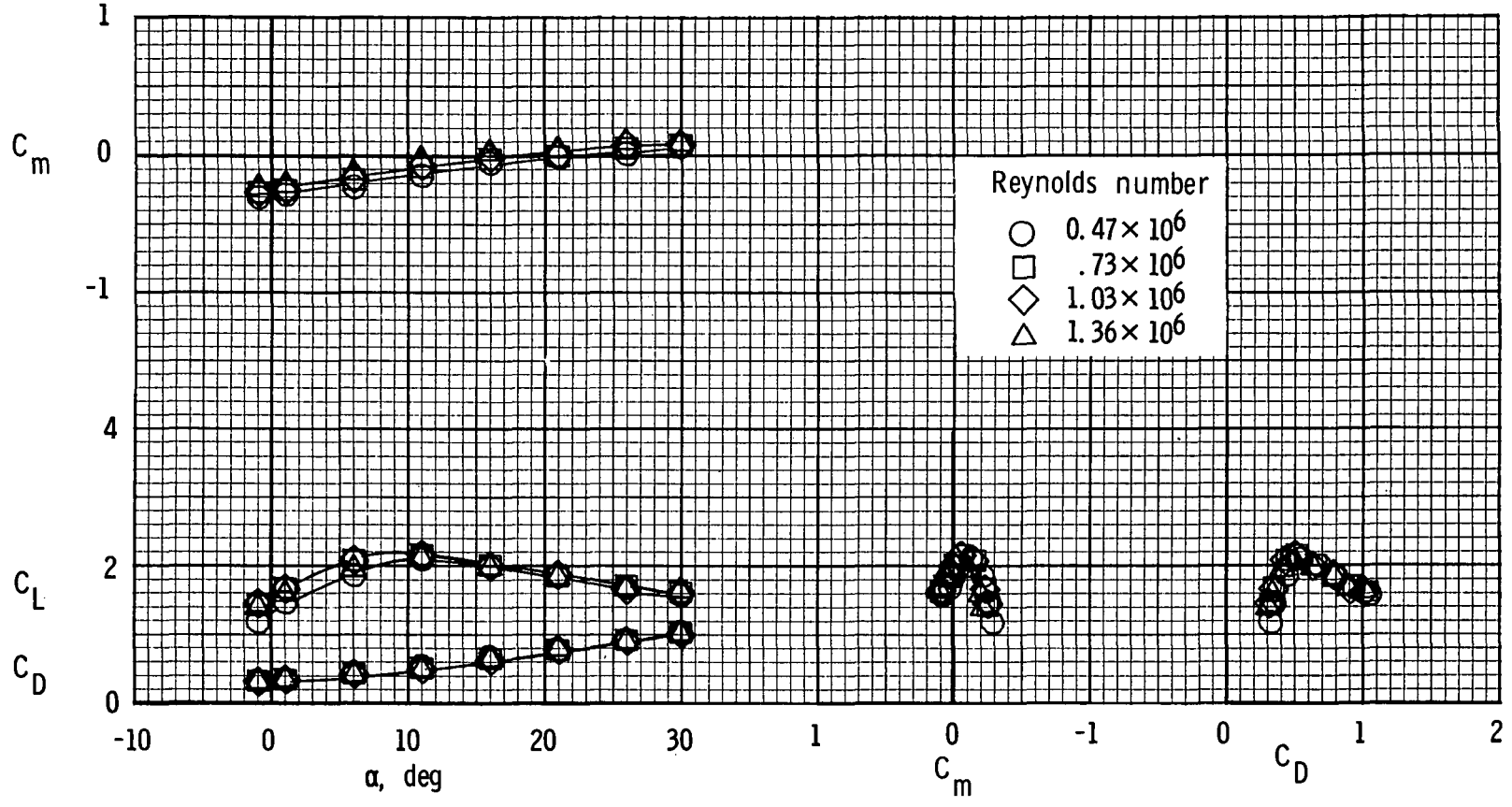

(a) $C_\mu = 0$.

Figure 10.- Effect of Reynolds number on longitudinal characteristics. $\delta_{f1}/\delta_{f2} = 30^o/60^o$; 30-percent leading-edge flap.

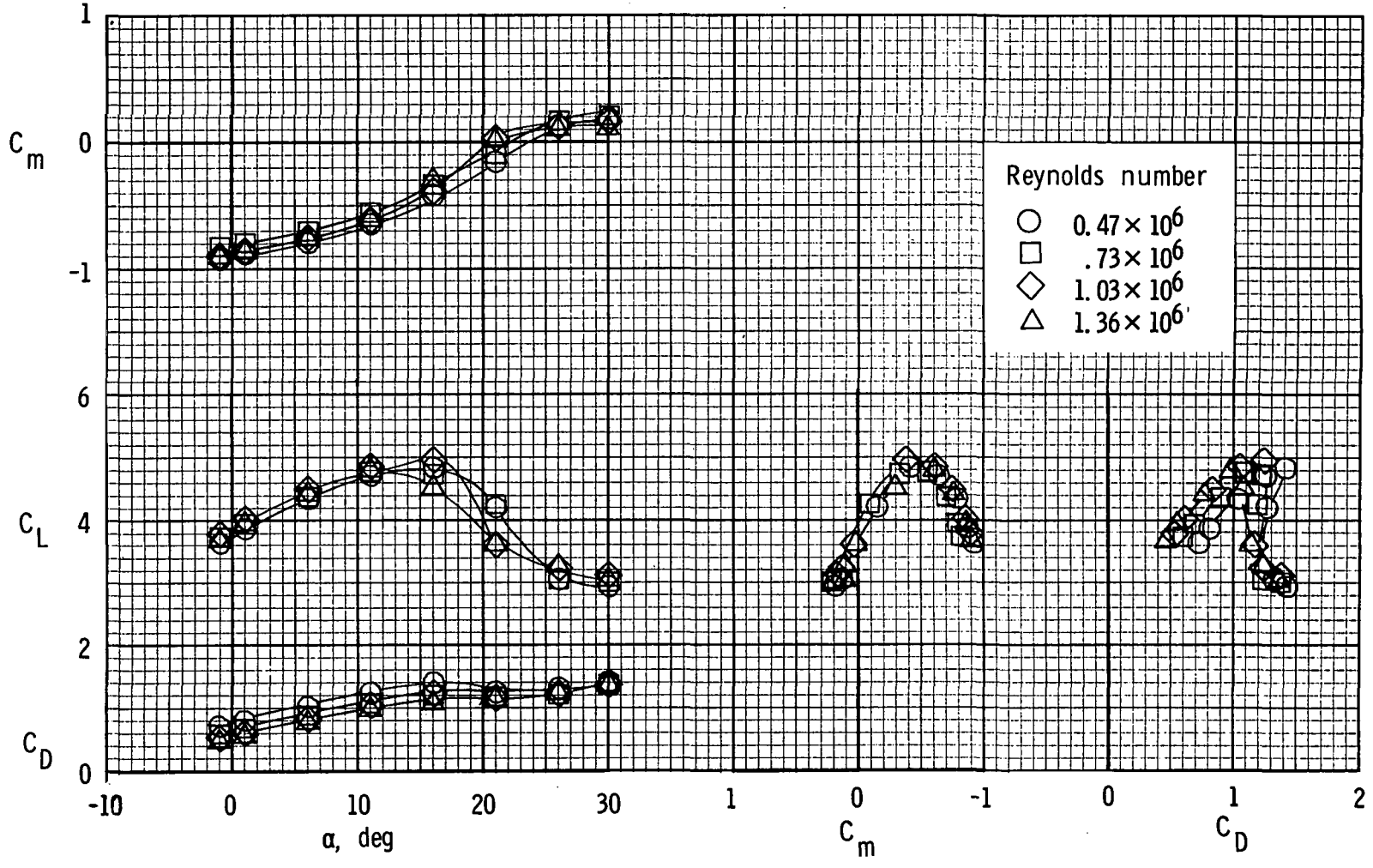

(b) $C_\mu = 0.97$.

Figure 10.- Continued.

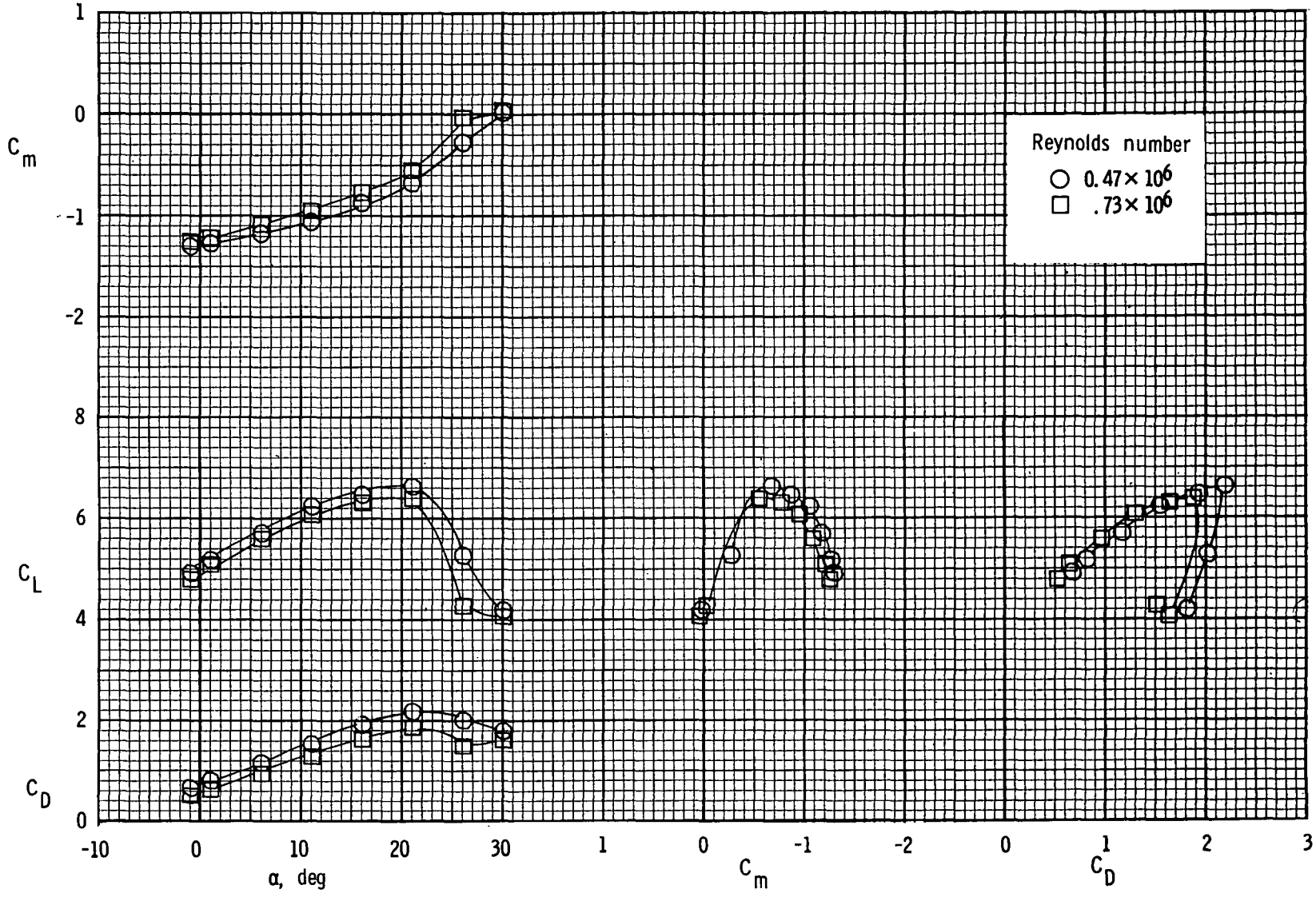

(c) $C_\mu = 1.94$.

Figure 10.- Concluded.

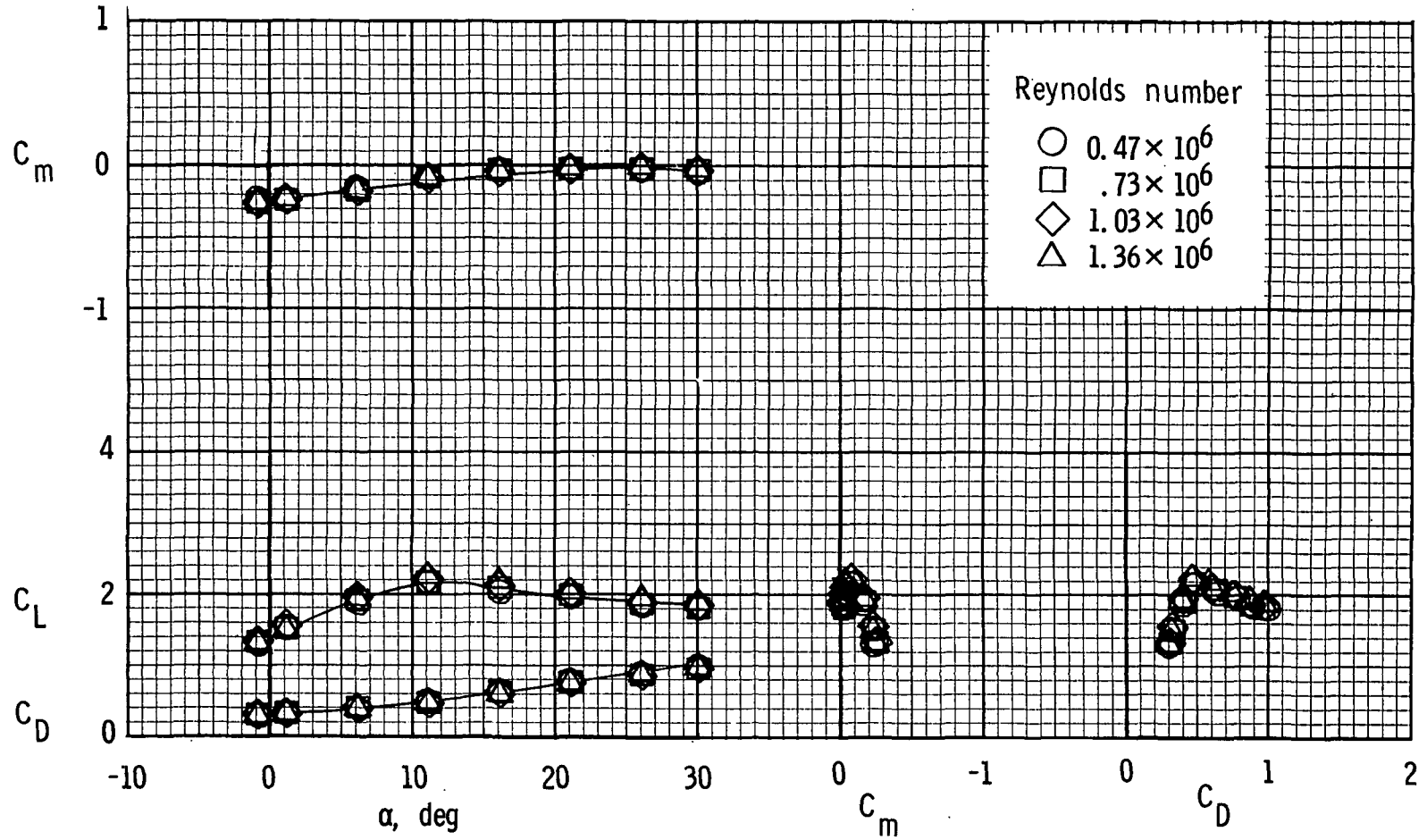

(a) $C_\mu = 0$.

Figure 11.- Effect of Reynolds number on longitudinal characteristics. $\delta_{f1}/\delta_{f2} = 30^o/60^o$; 25-percent leading-edge slat.

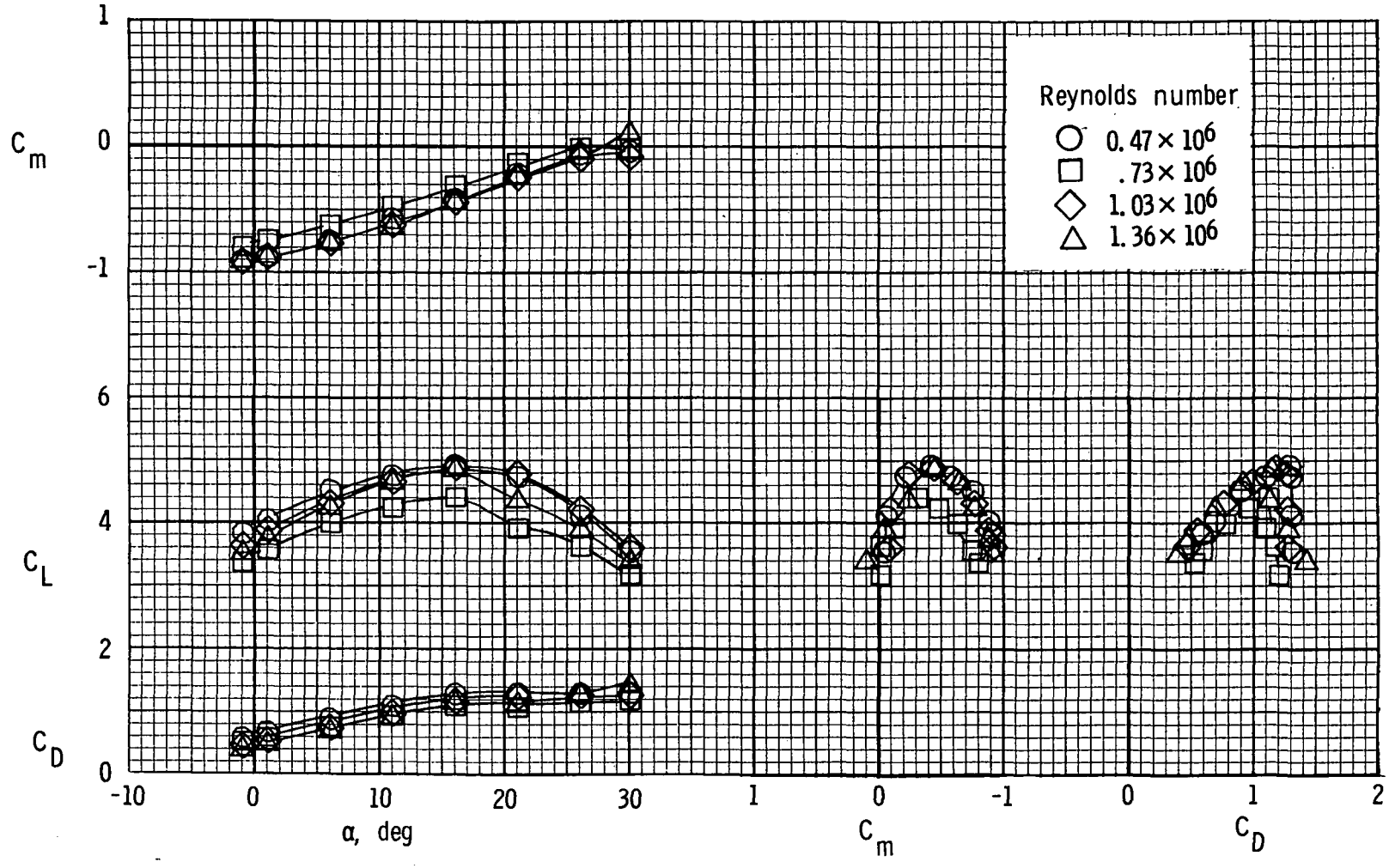

(b) $C_\mu = 0.97$.

Figure 11.- Continued.

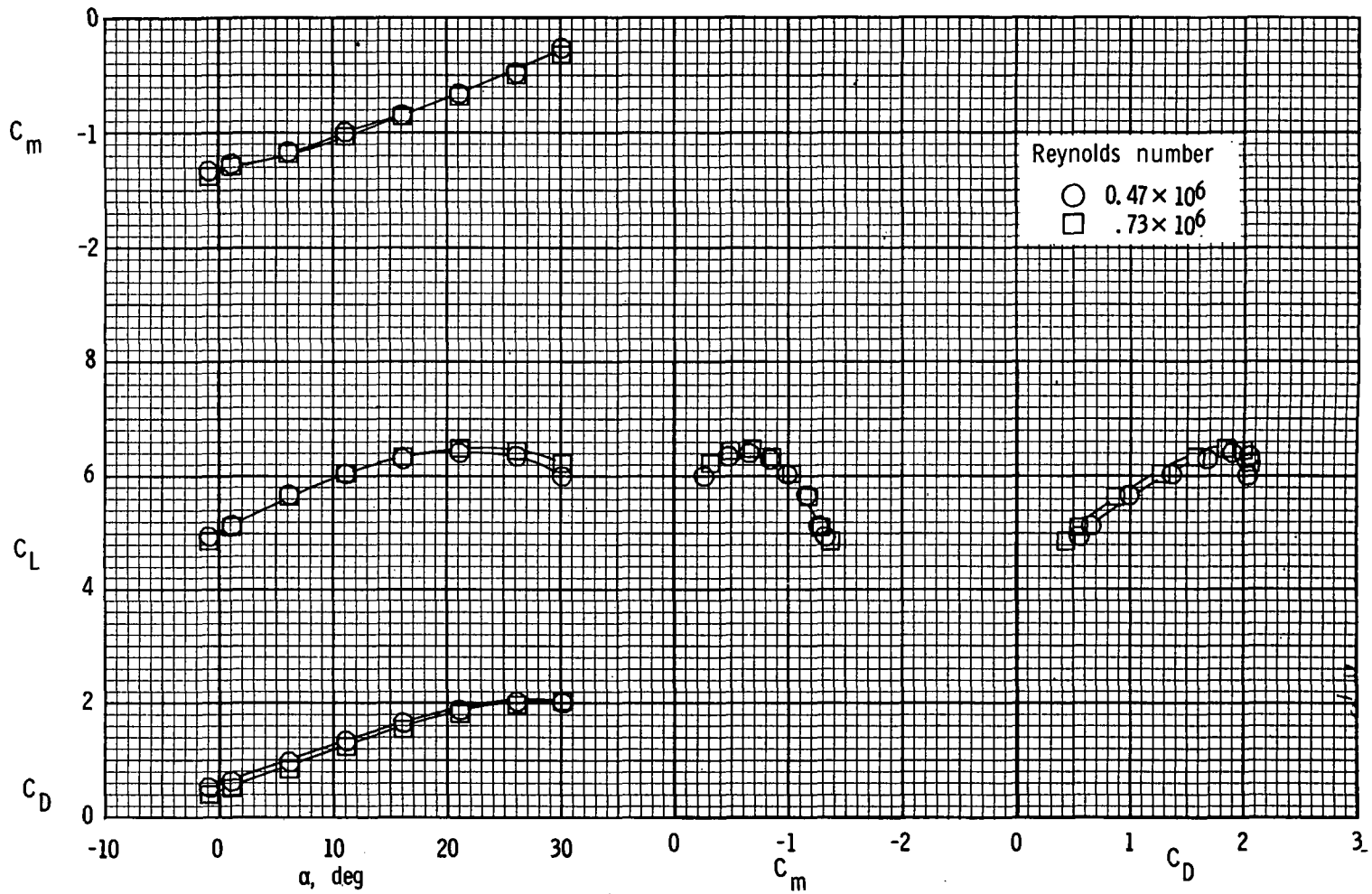

(c) C_μ = 1.94.

Figure 11.- Continued.

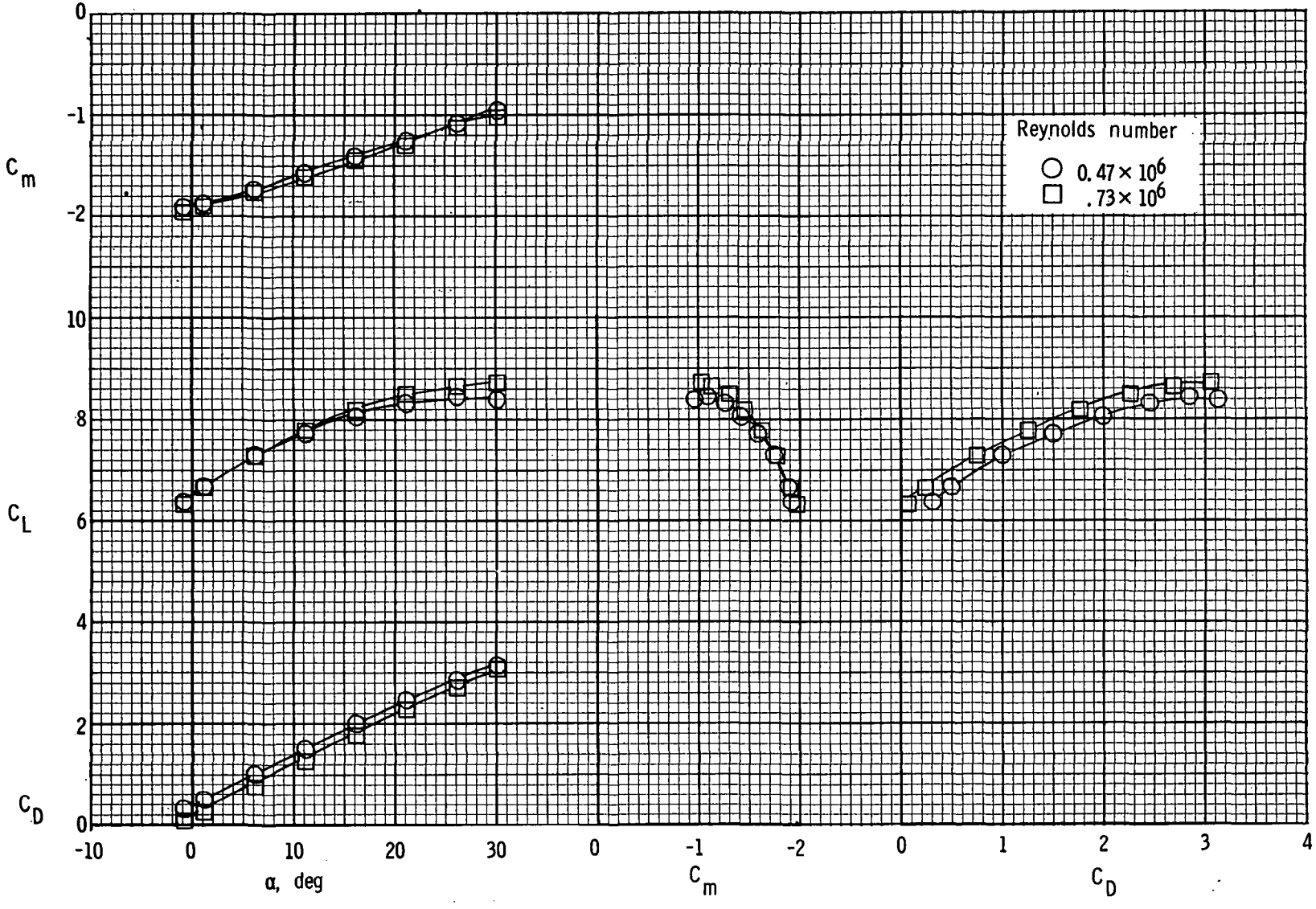

(d) C_μ = 3.50.

Figure 11.- Concluded.

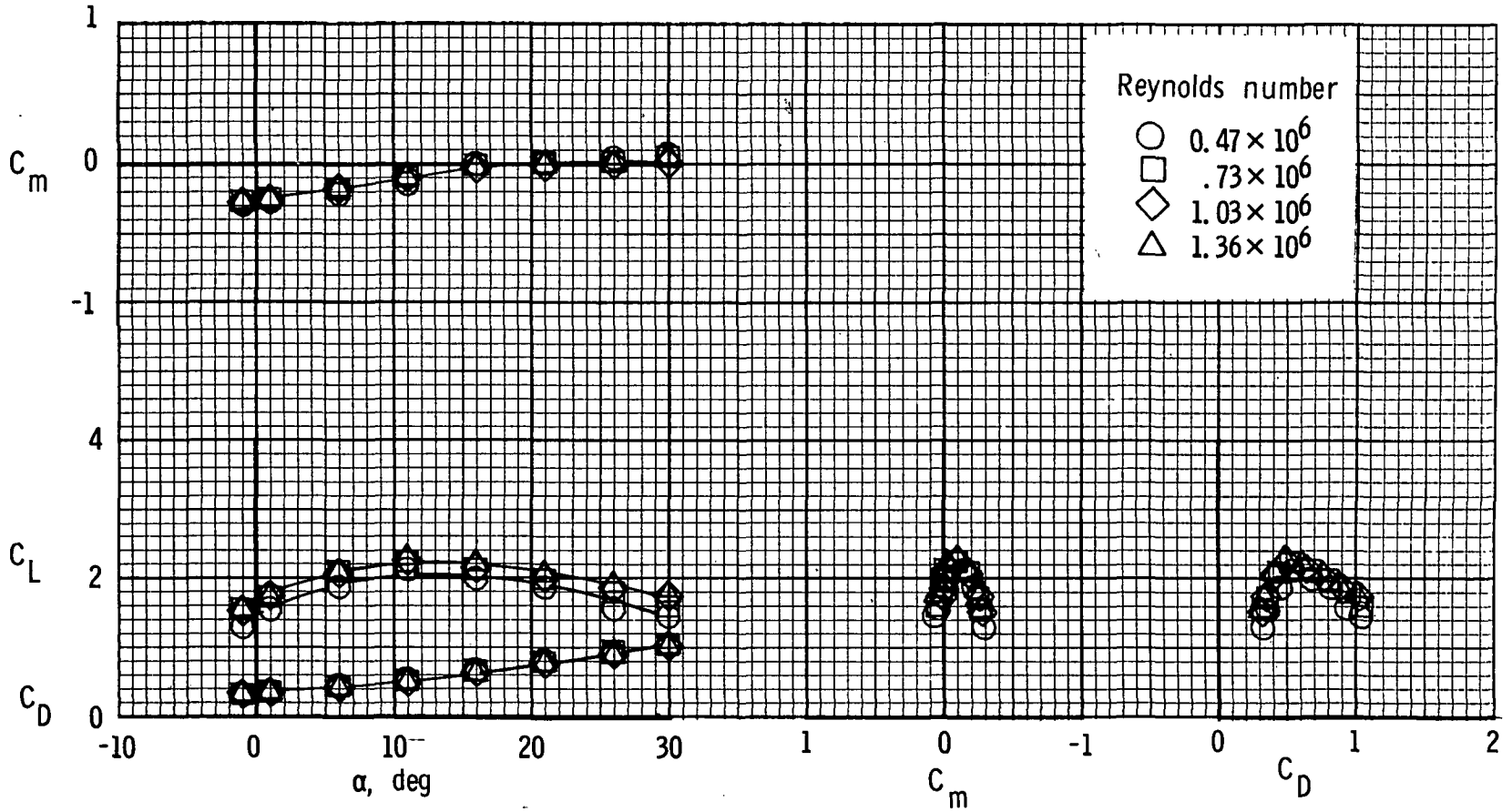

(a) $C_\mu = 0.$

Figure 12.- Effect of Reynolds number on longitudinal characteristics. $\delta_{f1}/\delta_{f2} = 30^o/60^o$; 15-percent leading-edge slat.

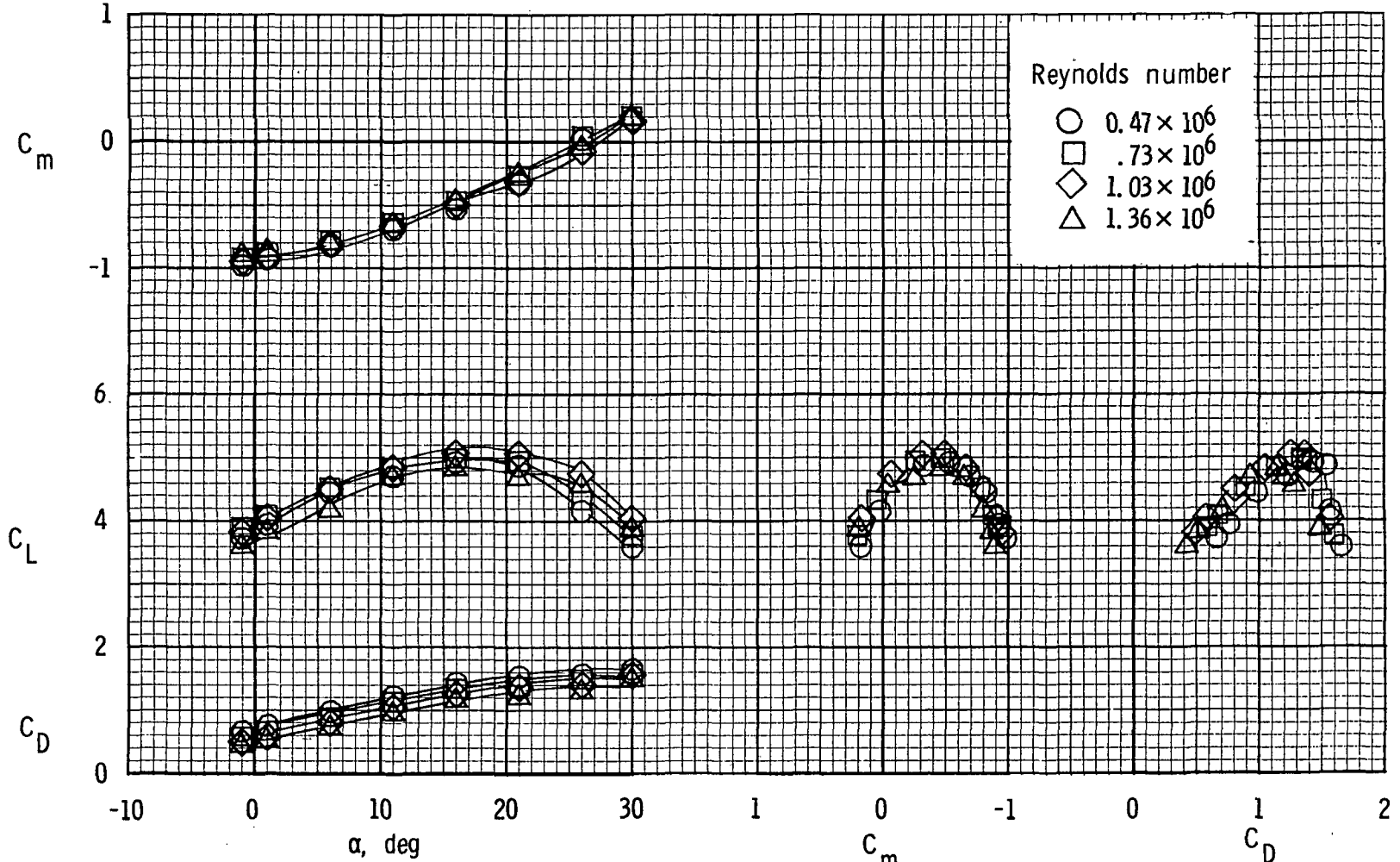

(b) $C_\mu = 0.97$.

Figure 12.- Continued.

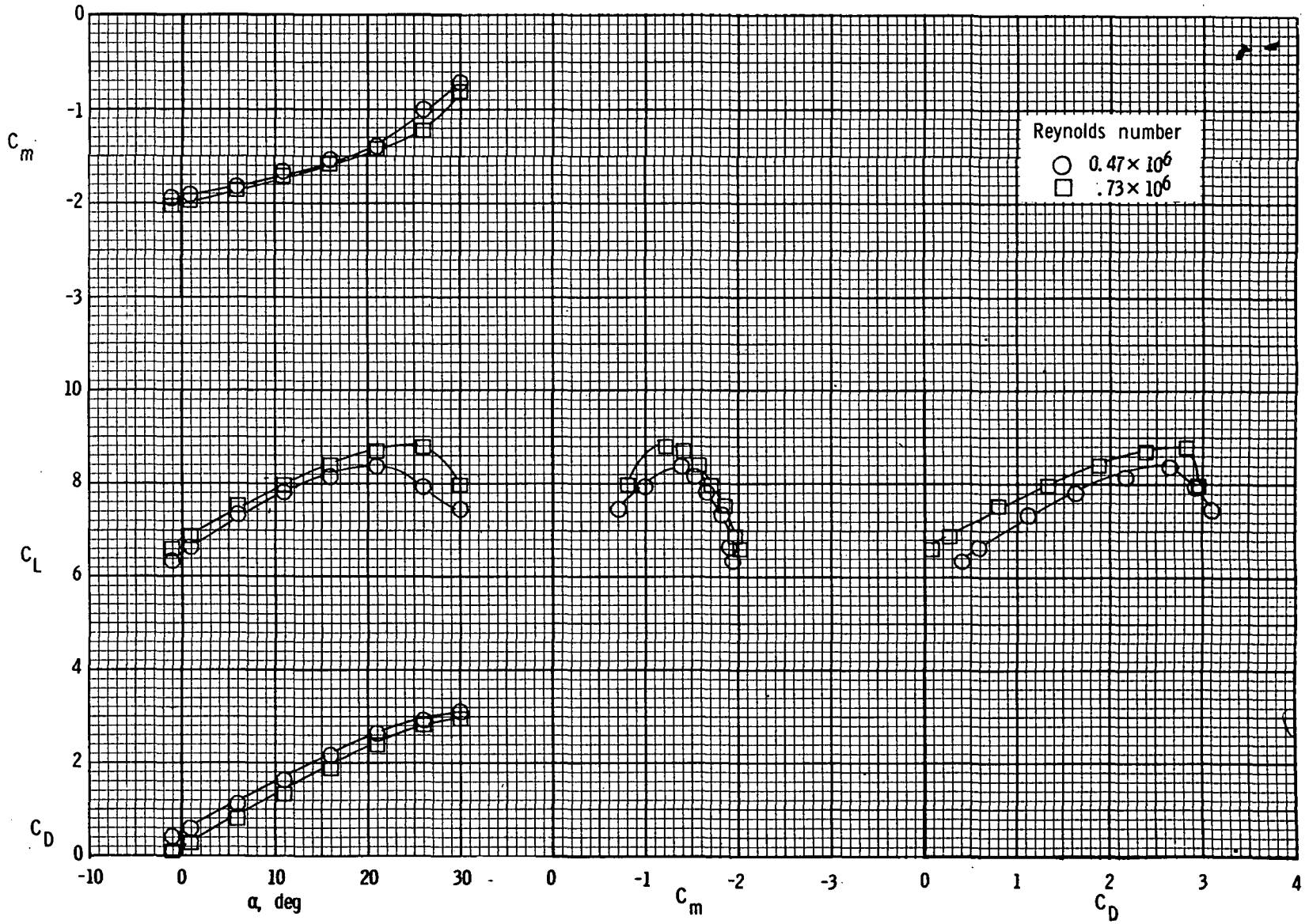

(c) C_μ = 3.50.

Figure 12.- Concluded.

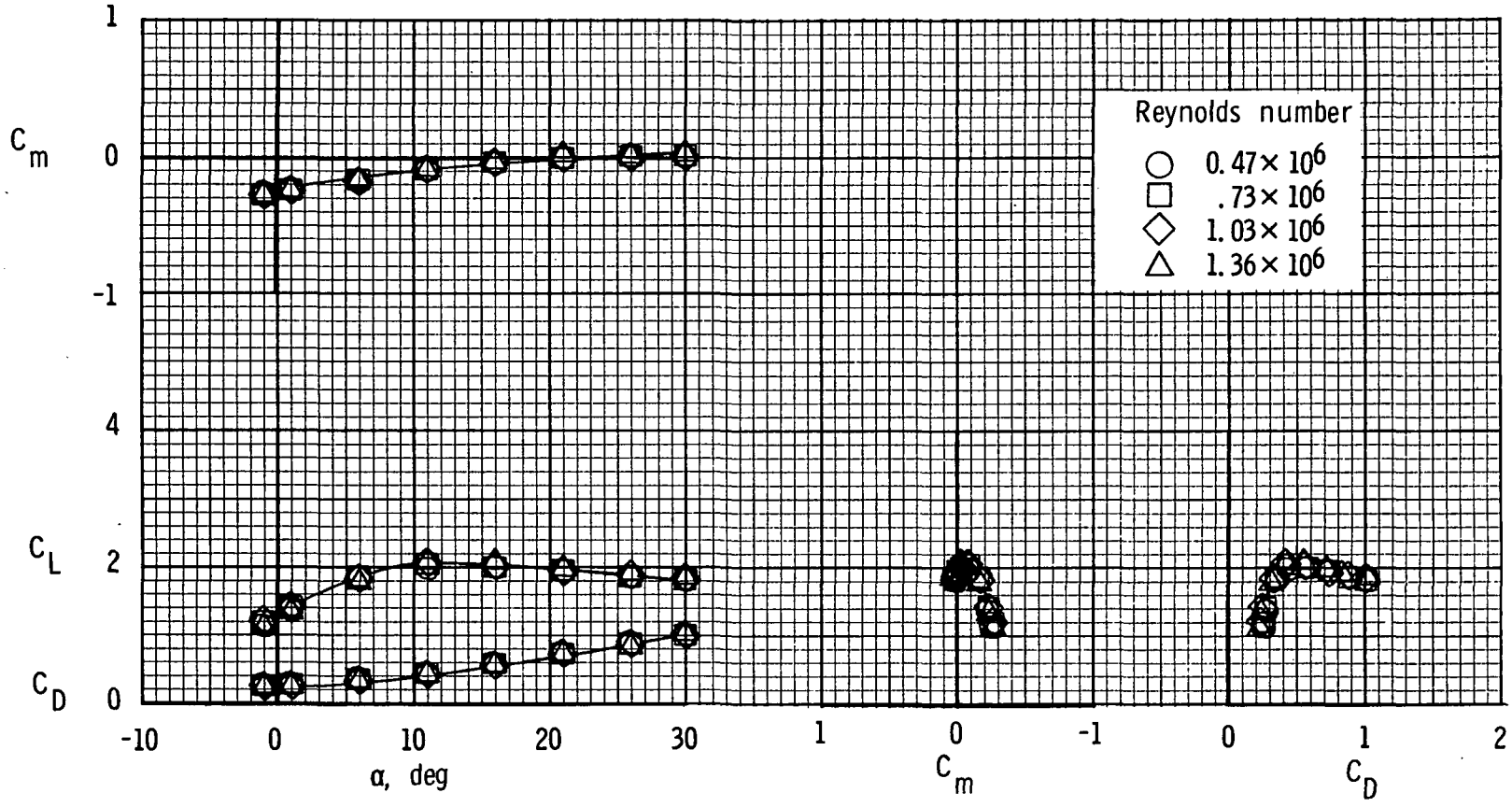

(a) $C_\mu = 0$.

Figure 13.- Effect of Reynolds number on longitudinal characteristics. $\delta_{f1}/\delta_{f2} = 20^o/40^o$; 30-percent leading-edge flap.

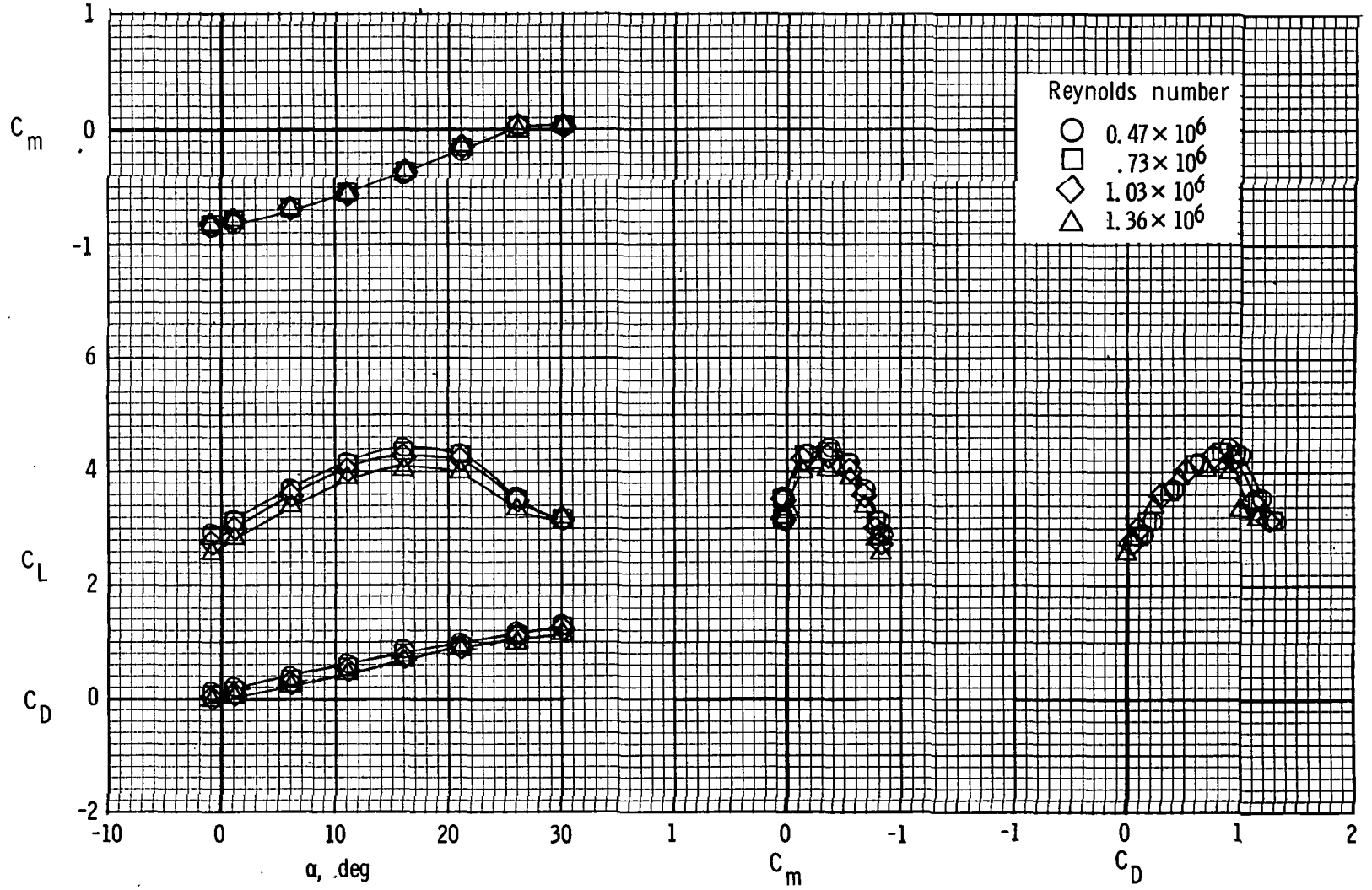

(b) $C_\mu = 0.97$.

Figure 13.- Continued.

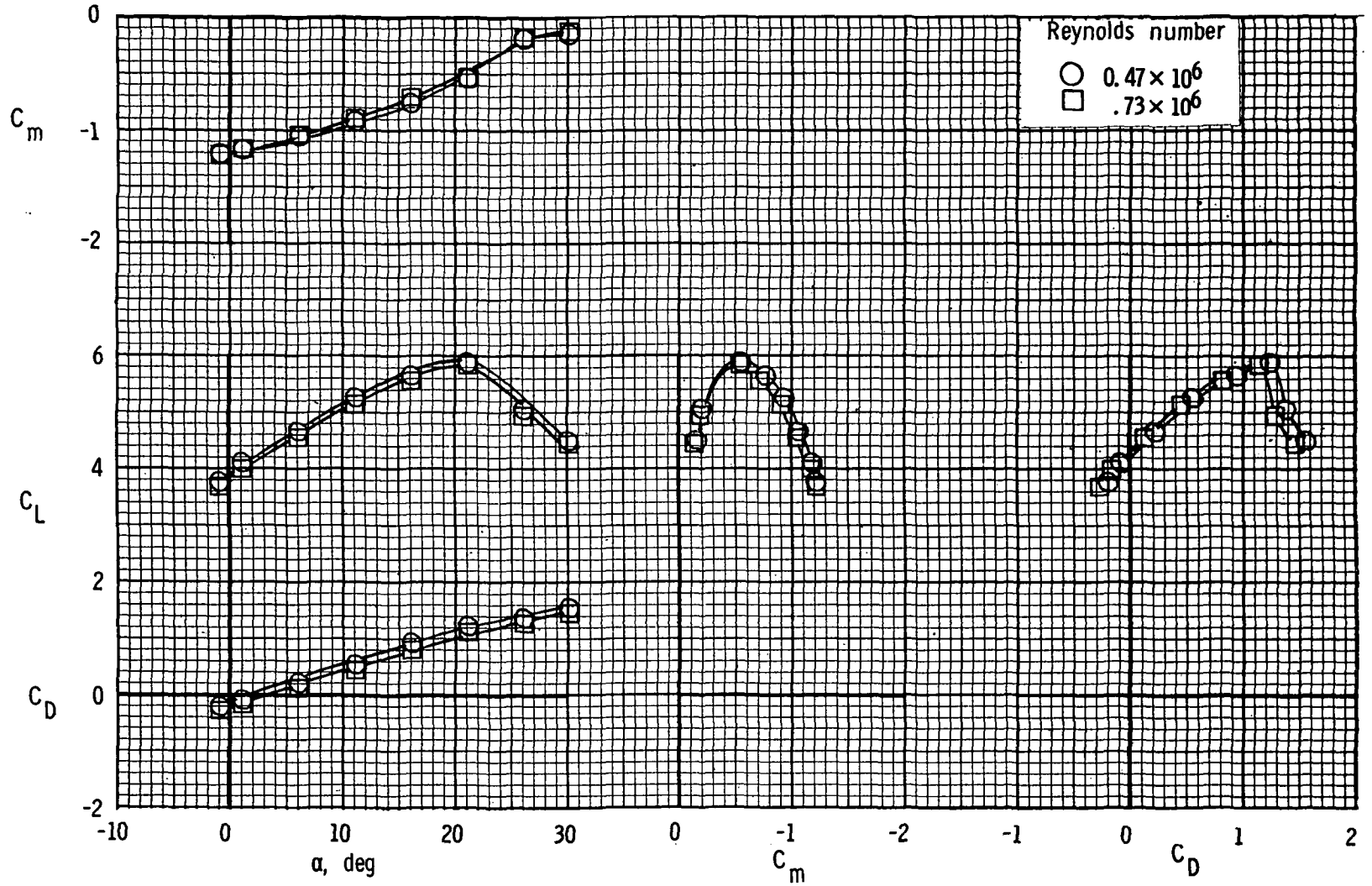

(c) C_μ = 1.94.

Figure 13.- Continued.

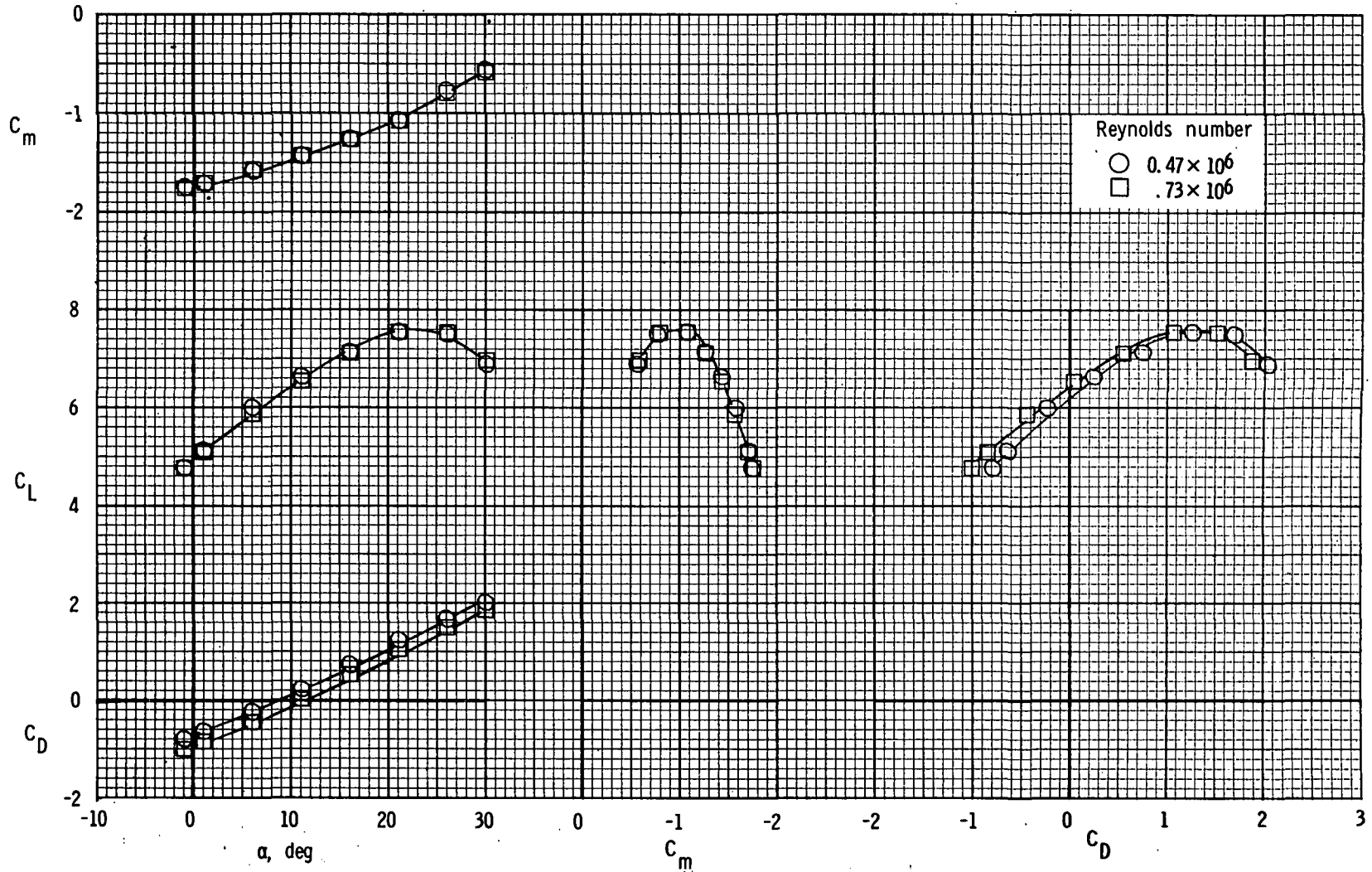

(d) C_μ = 3.50.

Figure 13.- Concluded.

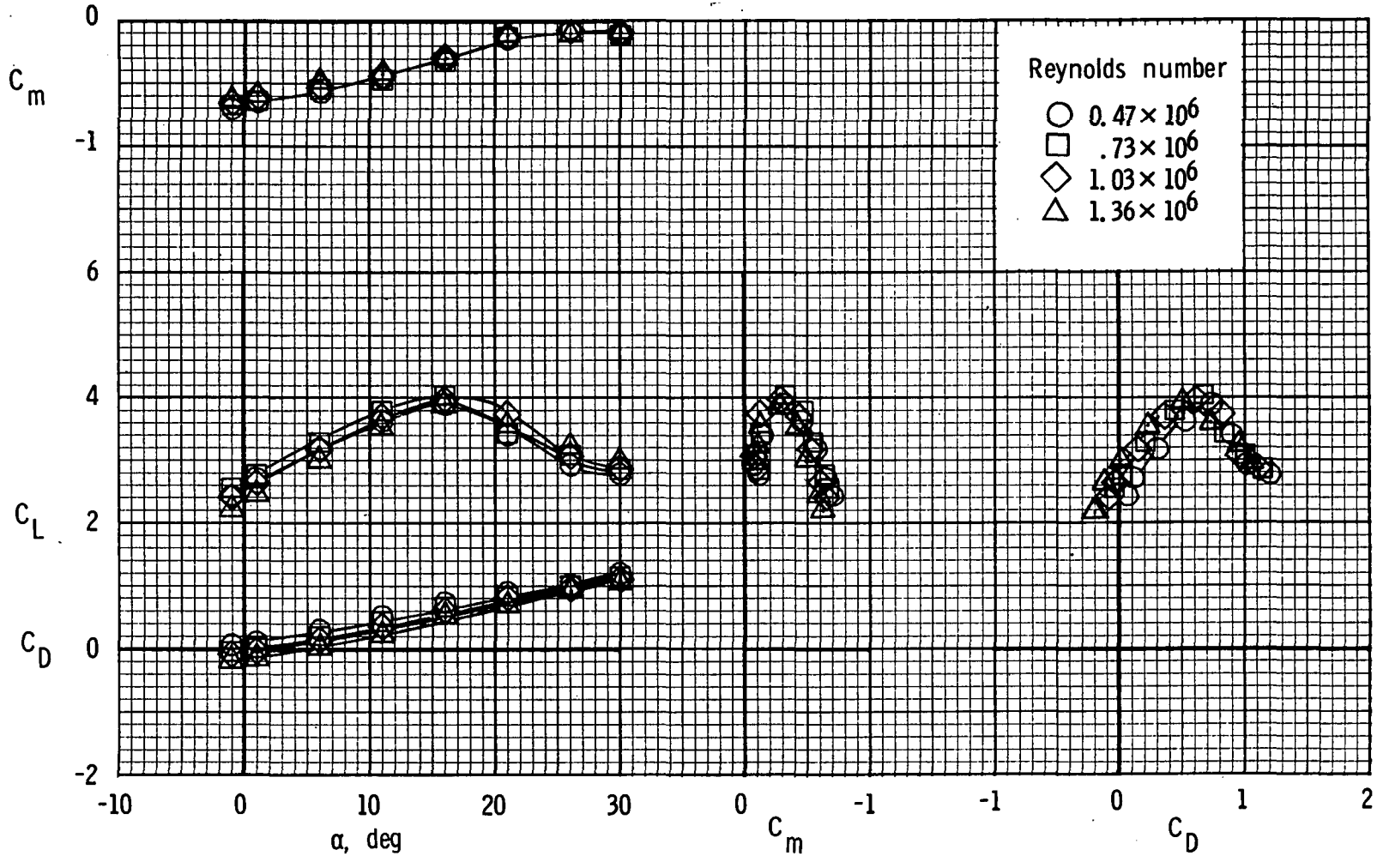

Figure 14.- Effect of Reynolds number on longitudinal characteristics. $\delta_{f1}/\delta_{f2} = 20^{\circ}/40^{\circ}$; 30-percent leading-edge flap; $C_{\mu} = 0.97$.

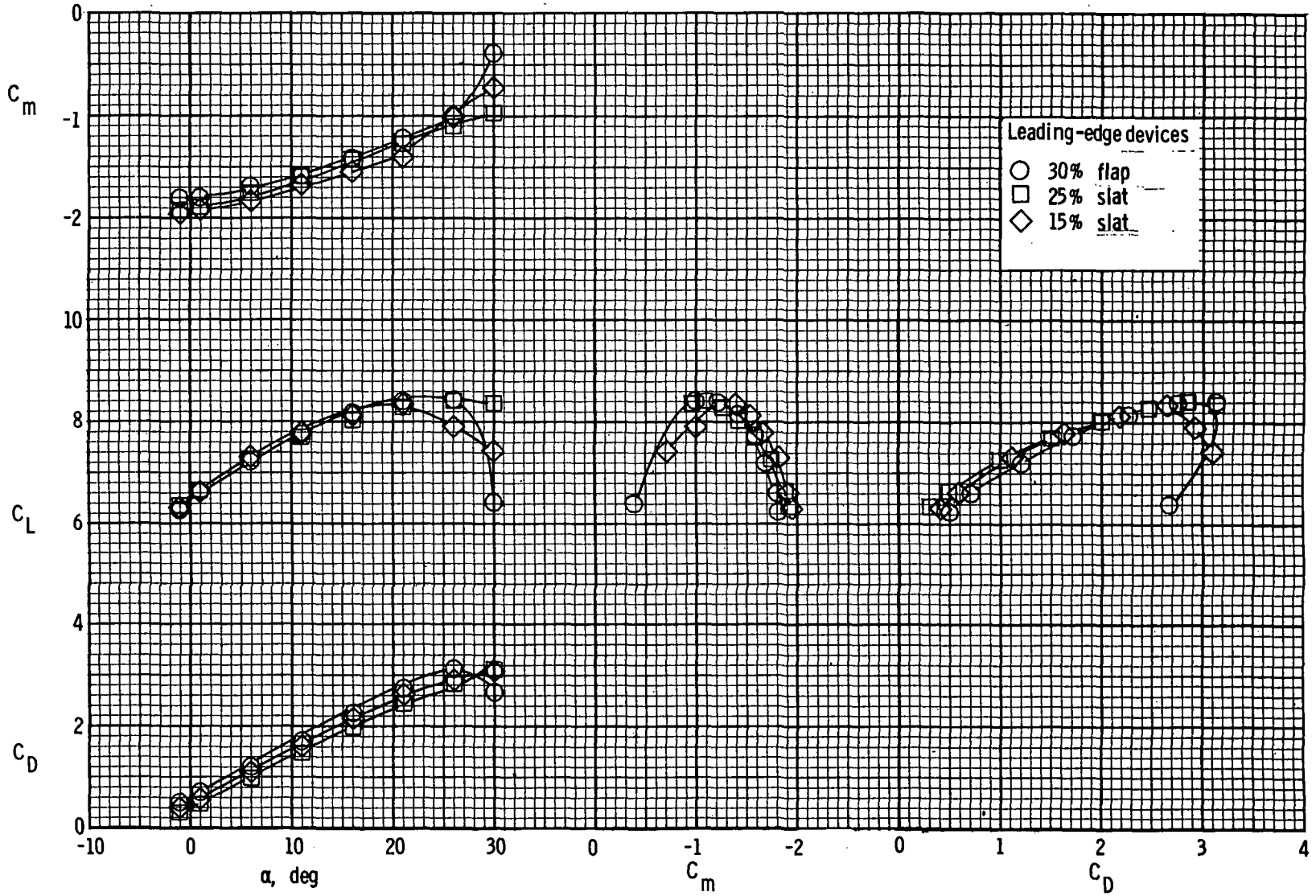

(a) $C_\mu = 3.50$; $R = 0.47 \times 10^6$.

Figure 15.- Effect of leading-edge devices on longitudinal characteristics. $\delta_{f1}/\delta_{f2} = 30^o/60^o$.

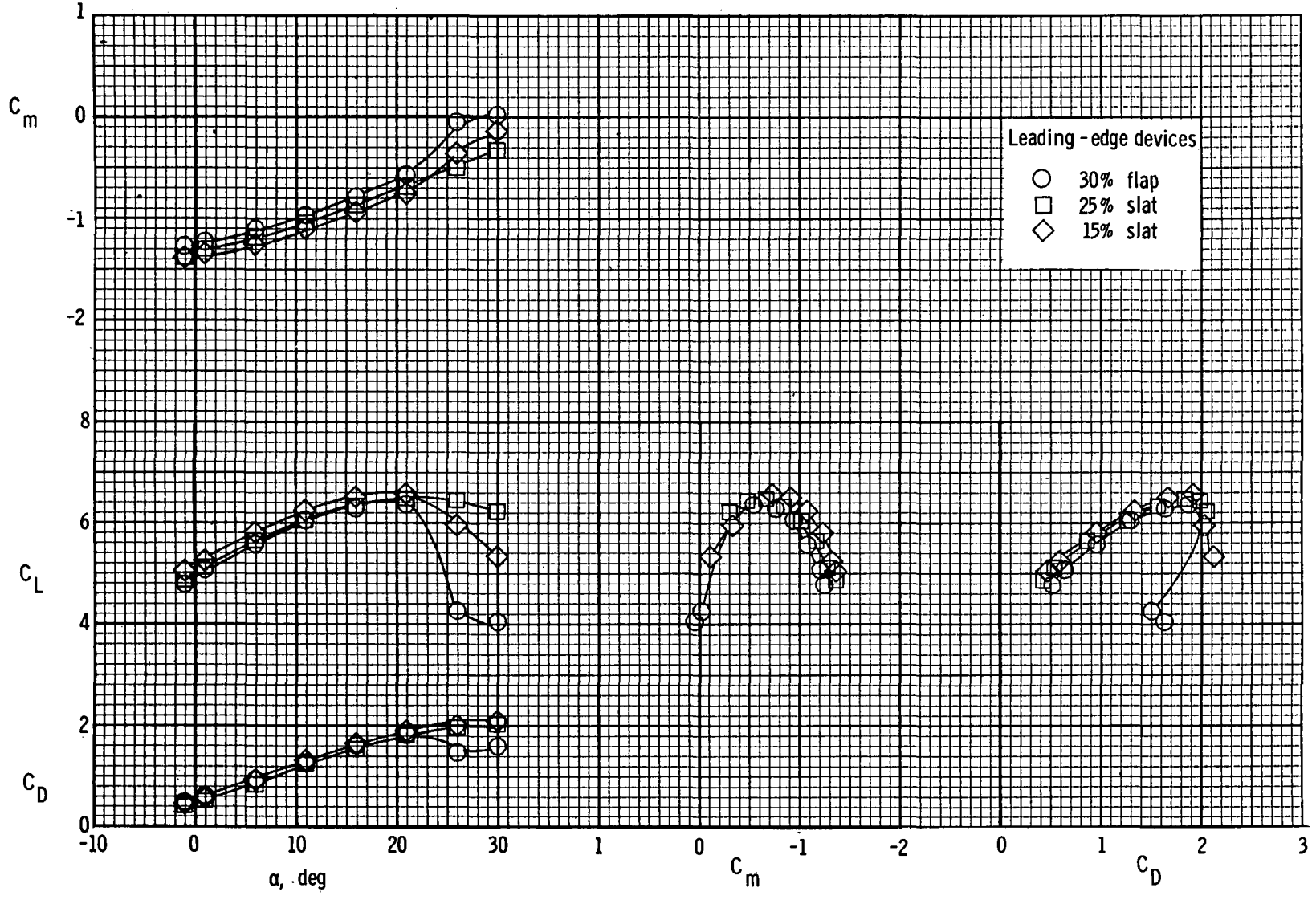

(b) $C_\mu = 1.94$; $R = 0.73 \times 10^6$.

Figure 15.- Continued.

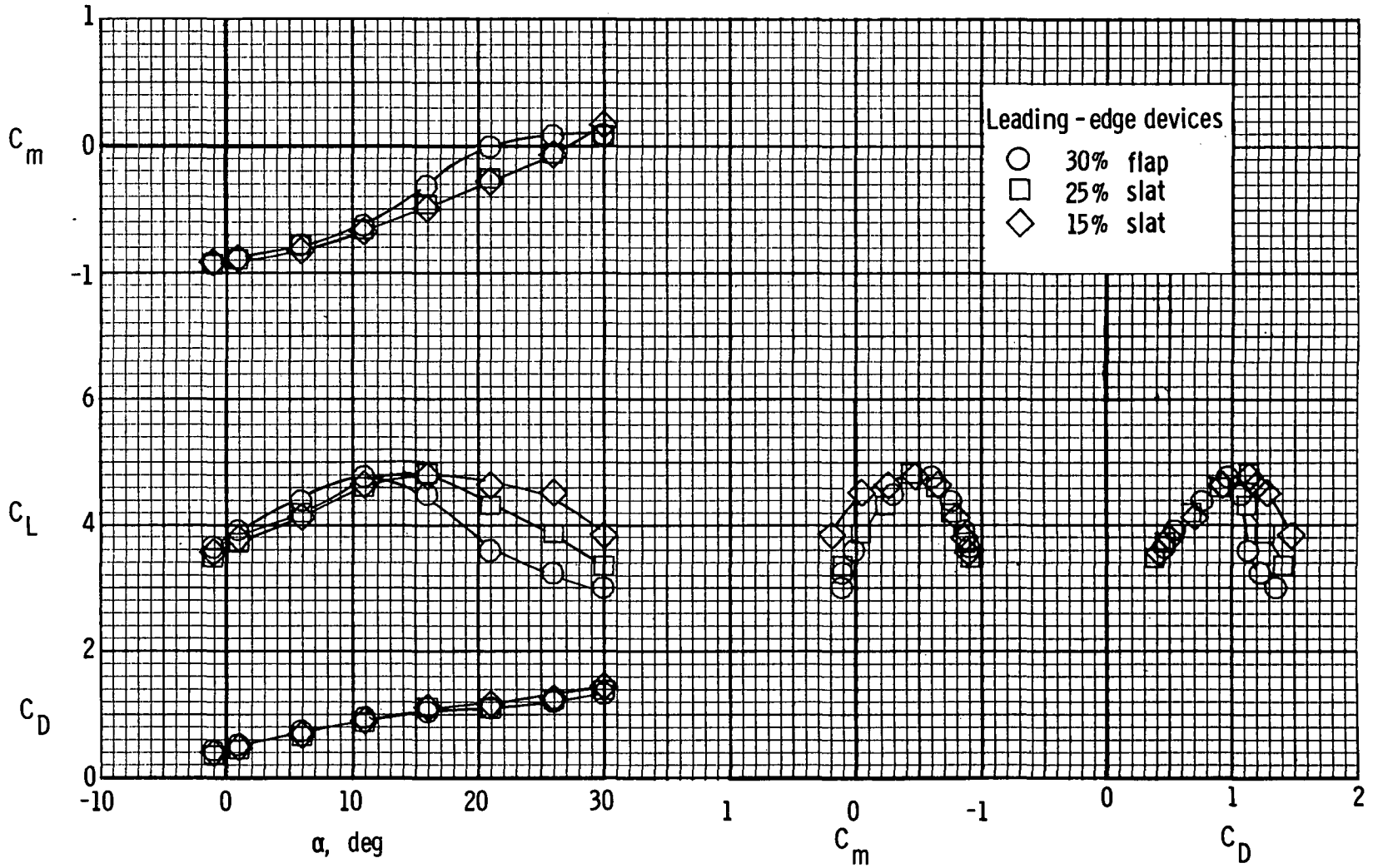

(c) $C_\mu = 0.97$; $R = 1.36 \times 10^6$.

Figure 15.- Continued.

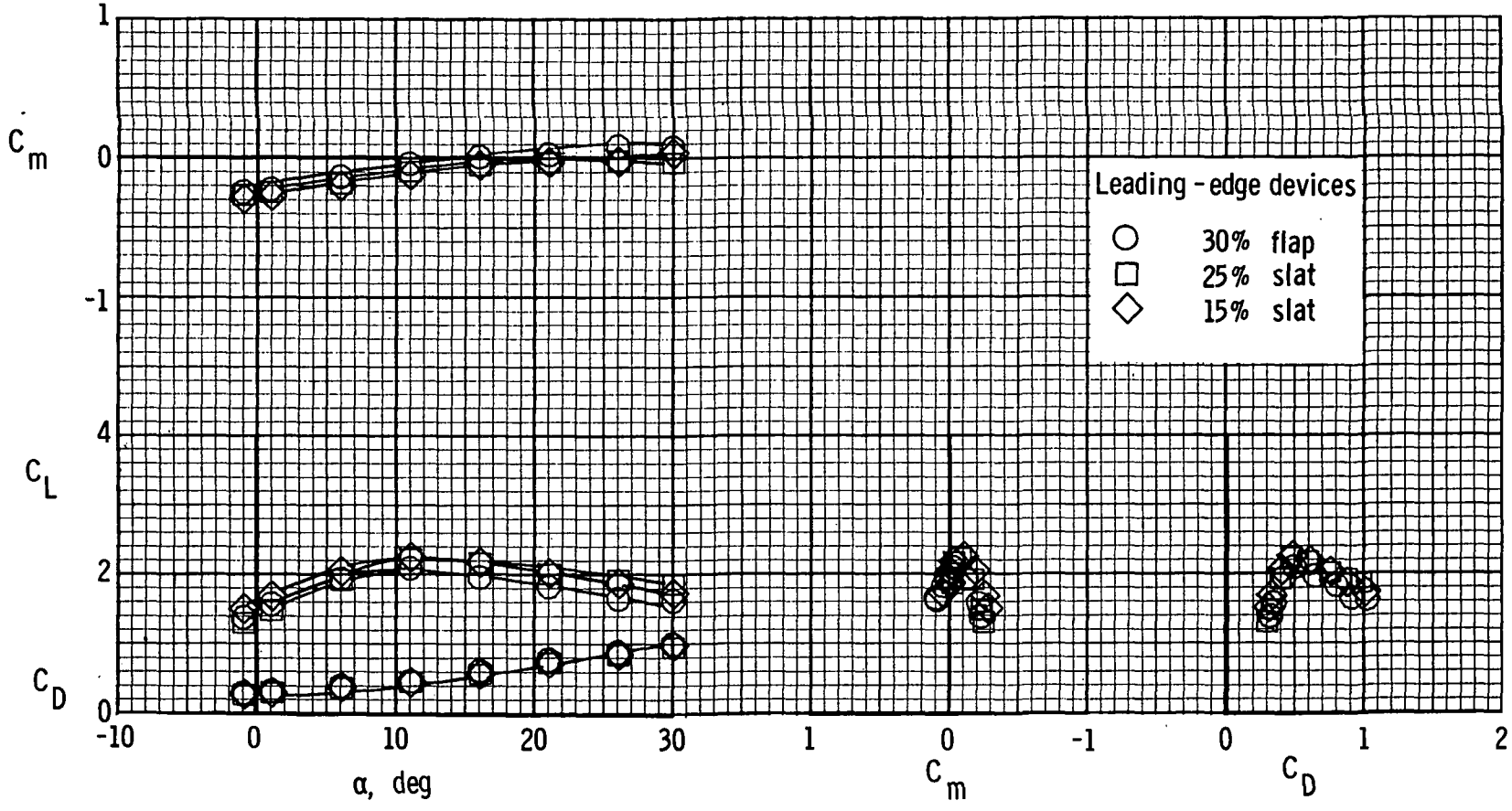

(d) $C_\mu = 0$; $R = 1.36 \times 10^6$.

Figure 15.- Concluded.

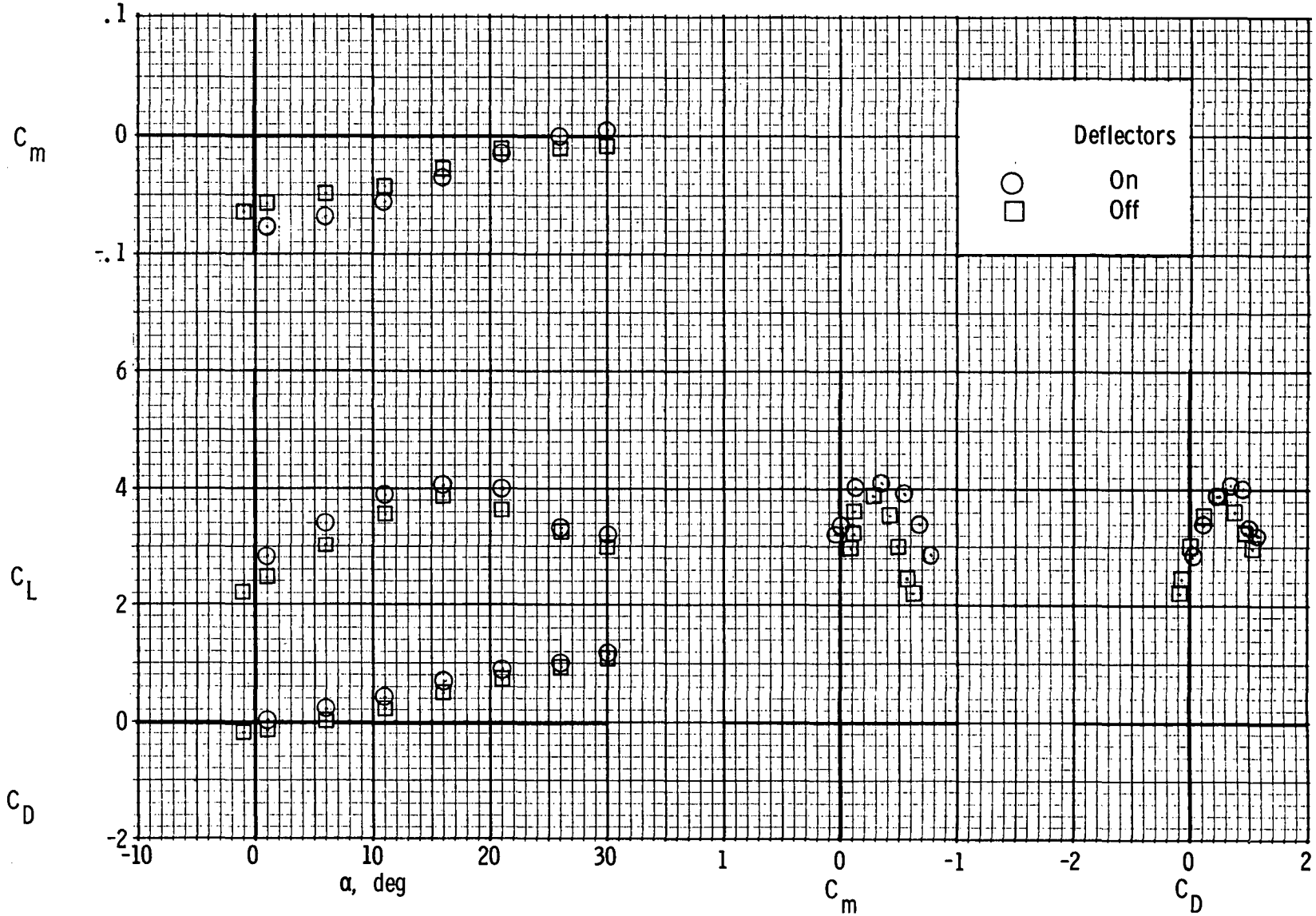

Figure 16.- Effect of thrust deflector on longitudinal characteristics of model. $\delta_{f1}/\delta_{f2} = 20^o/40^o$; $C_\mu = 0.97$; $R = 1.36 \times 10^6$; 30-percent leading-edge flap.

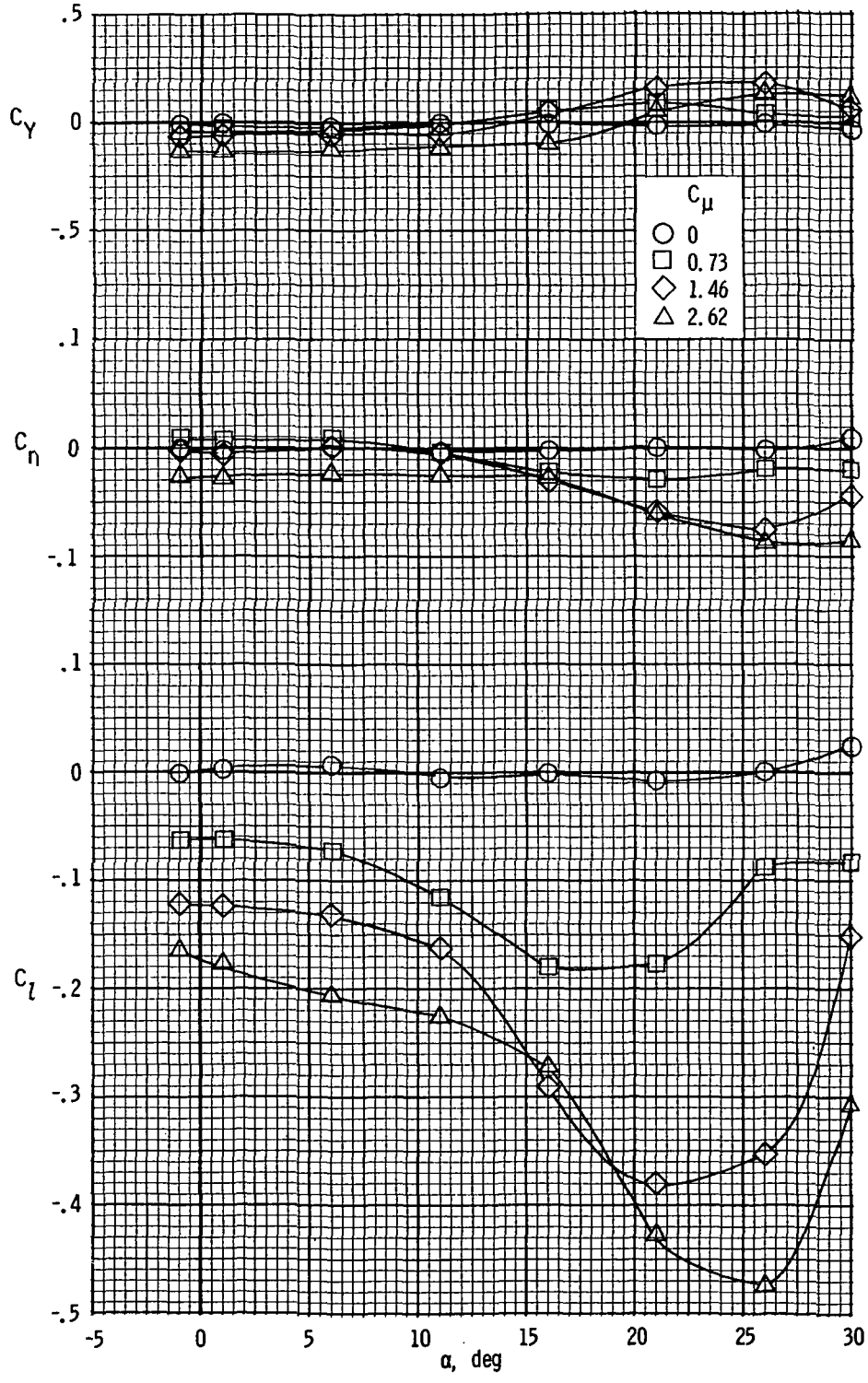

(a) Lateral characteristics. $R = 0.47 \times 10^6$.

Figure 17.- Longitudinal and lateral characteristics of model with left outboard engine not operating. 30-percent leading-edge flap; $\delta_{f1}/\delta_{f2} = 30^o/60^o$.

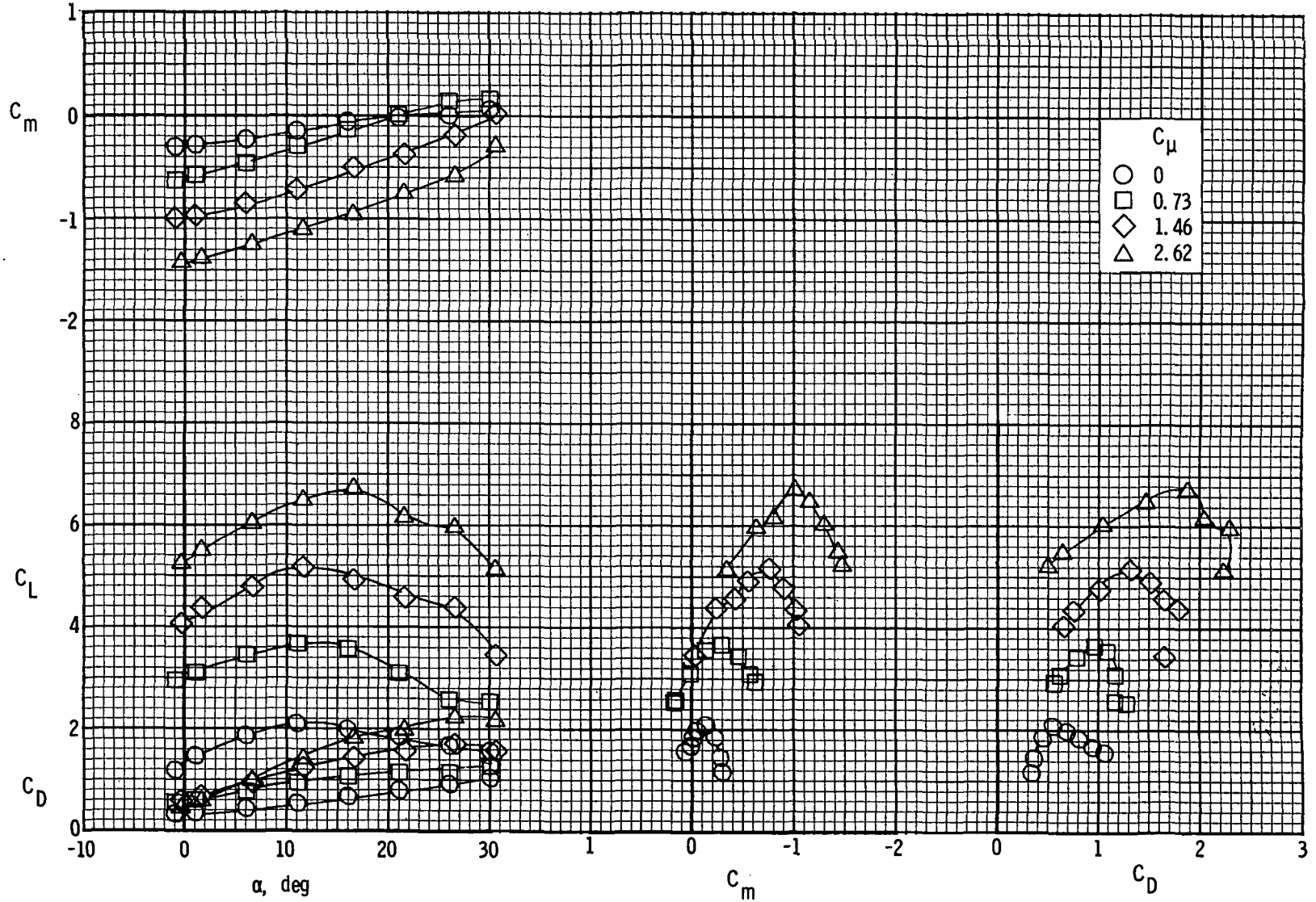

(b) Longitudinal characteristics. $R = 0.47 \times 10^6$.

Figure 17.- Continued.

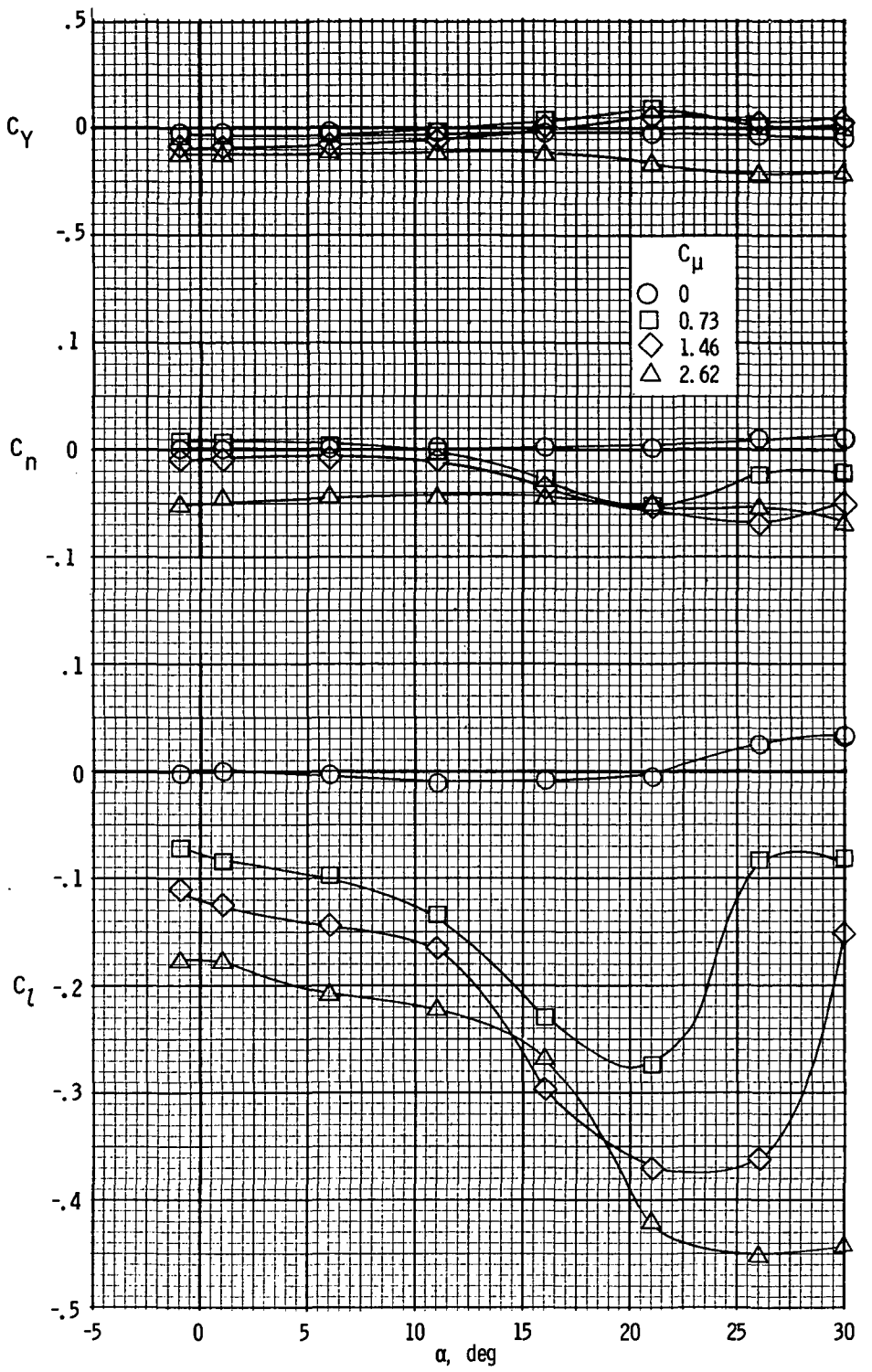

(c) Lateral characteristics. $R = 0.73 \times 10^6$.

Figure 17.- Continued.

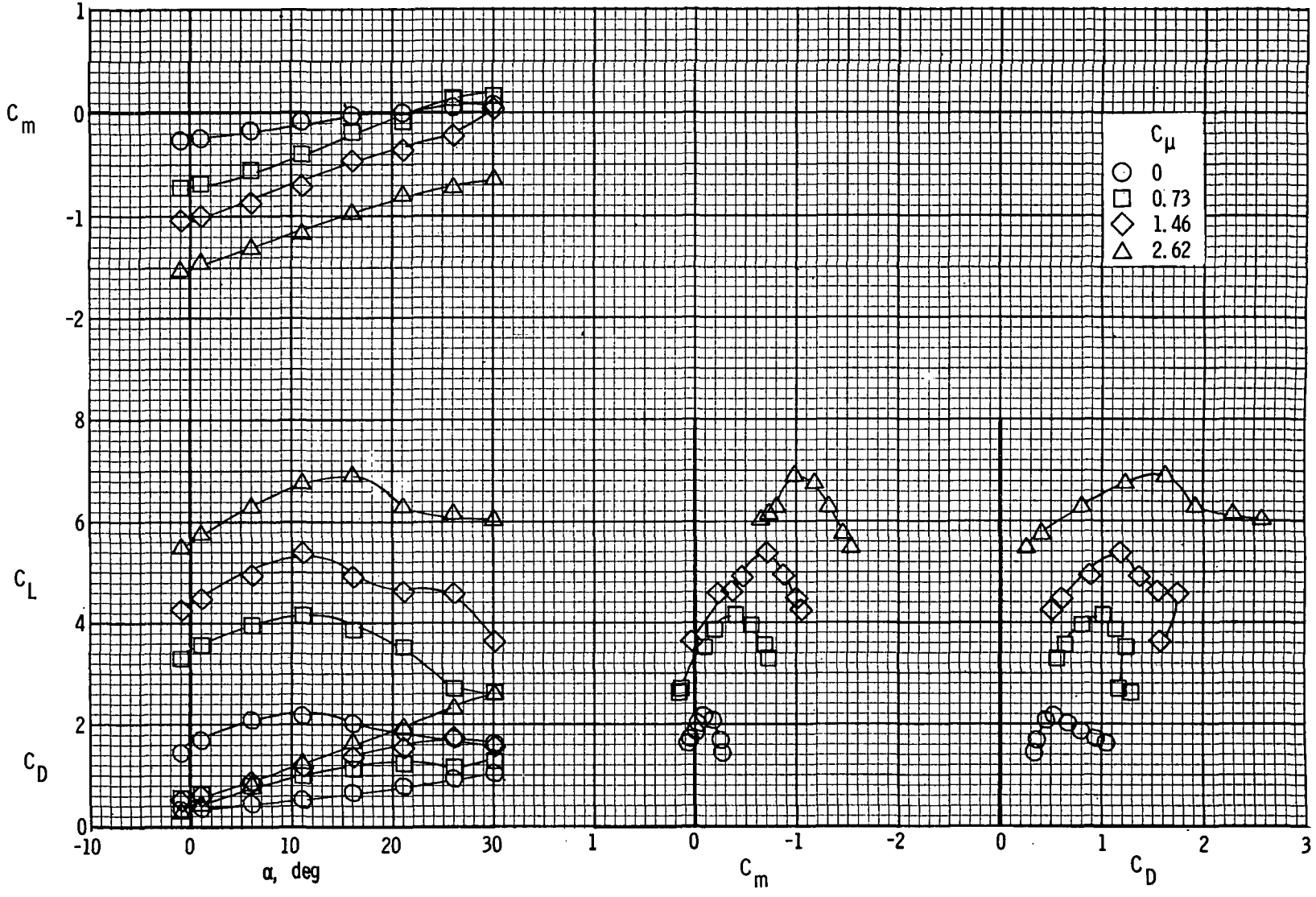

(d) Longitudinal characteristics. $R = 0.73 \times 10^6$.

Figure 17.- Continued.

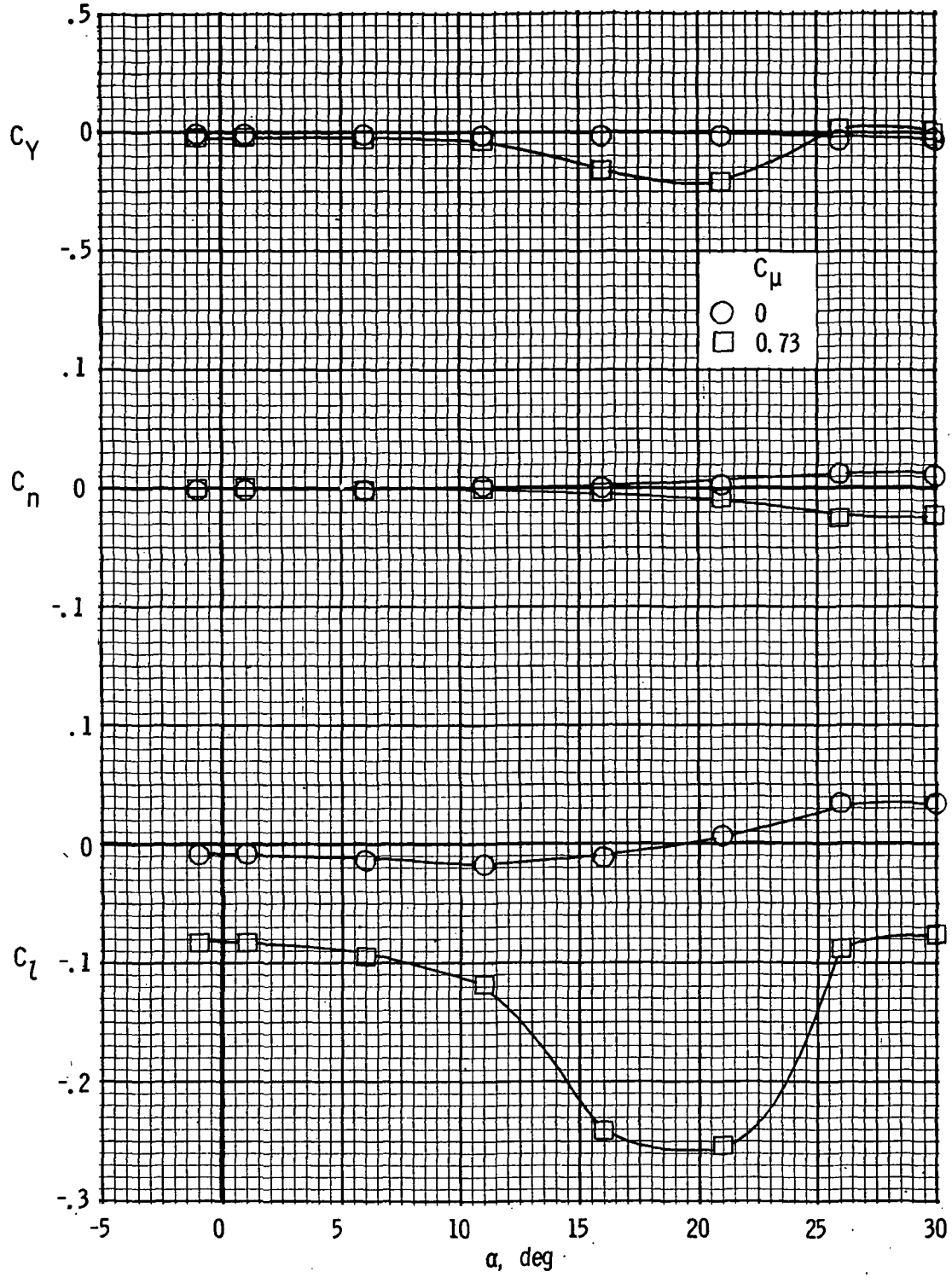

(e) Lateral characteristics. $R = 1.03 \times 10^6$.

Figure 17.- Continued.

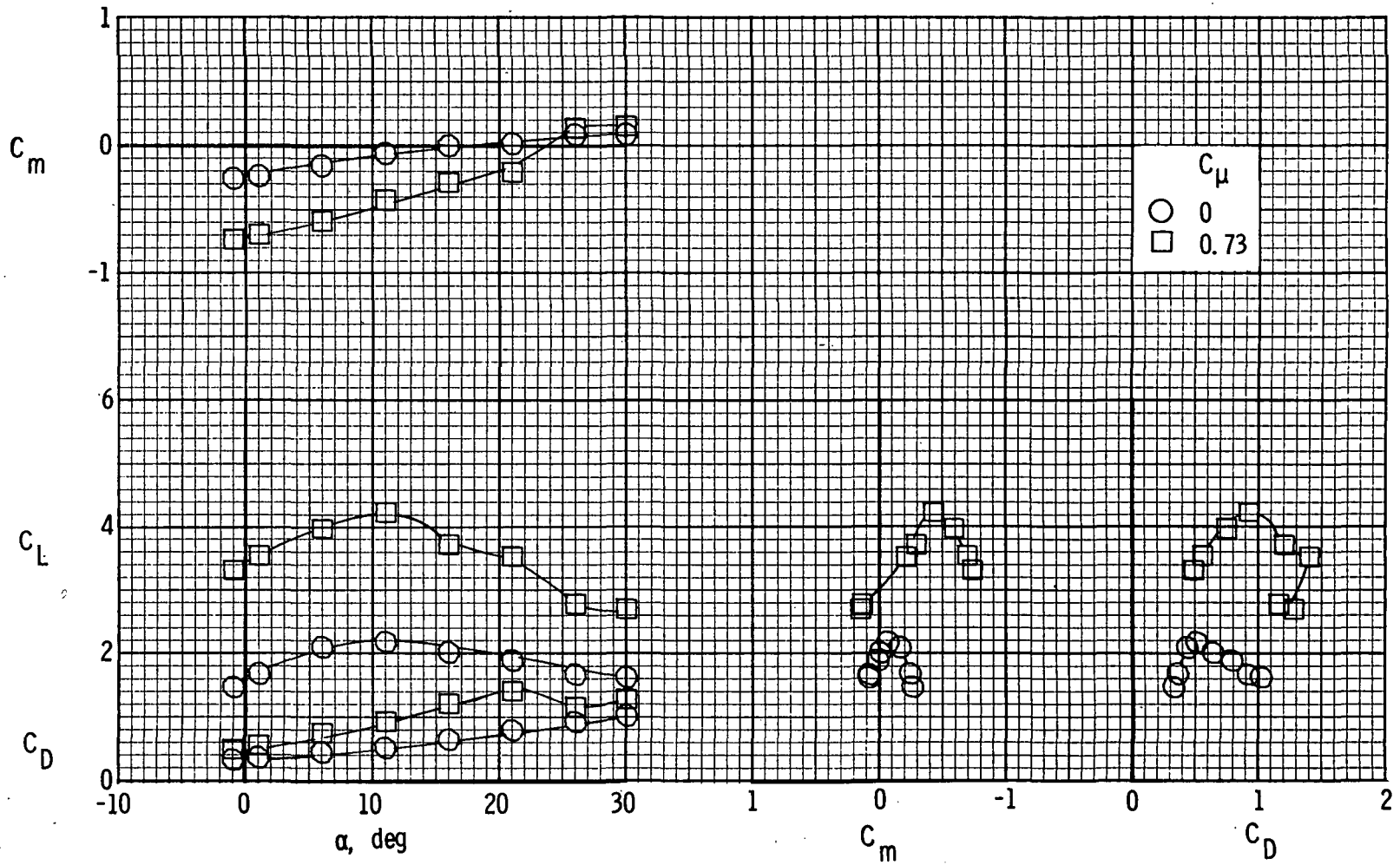

(f) Longitudinal characteristics. $R = 1.03 \times 10^6$.

Figure 17.- Continued.

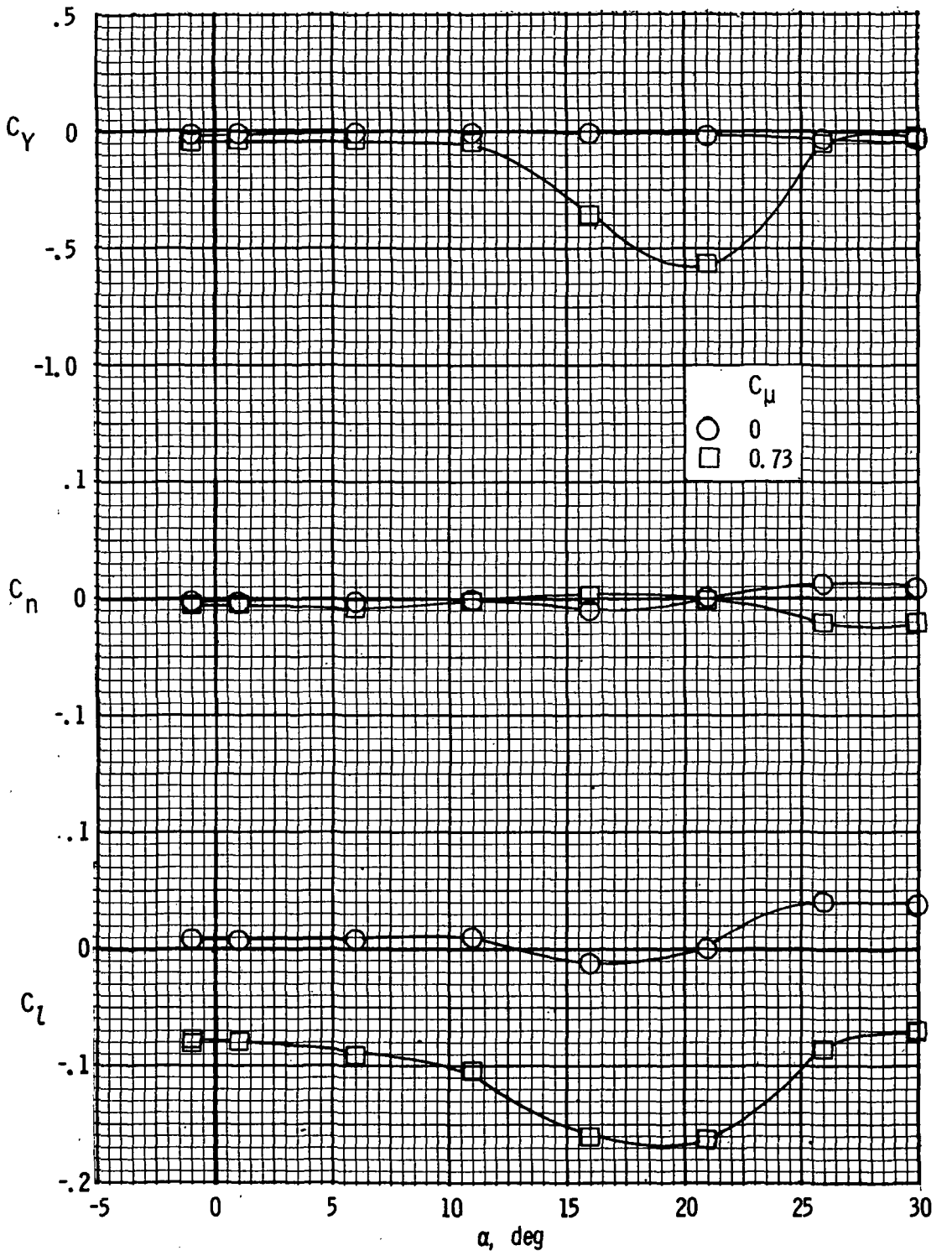

(g) Lateral characteristics. $R = 1.36 \times 10^6$.

Figure 17.- Continued.

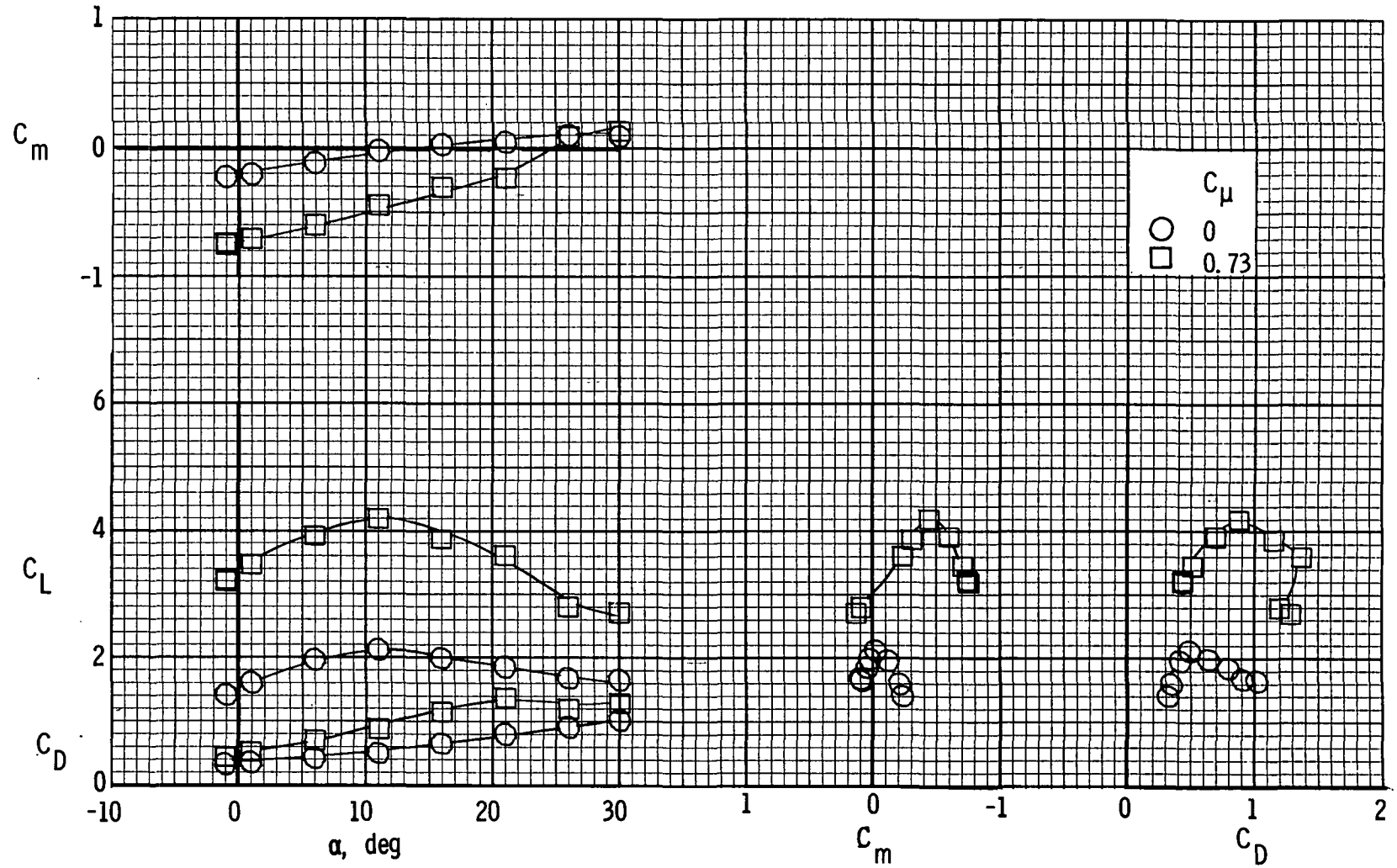

(h) Longitudinal characteristics. $R = 1.36 \times 10^6$.

Figure 17.- Concluded.

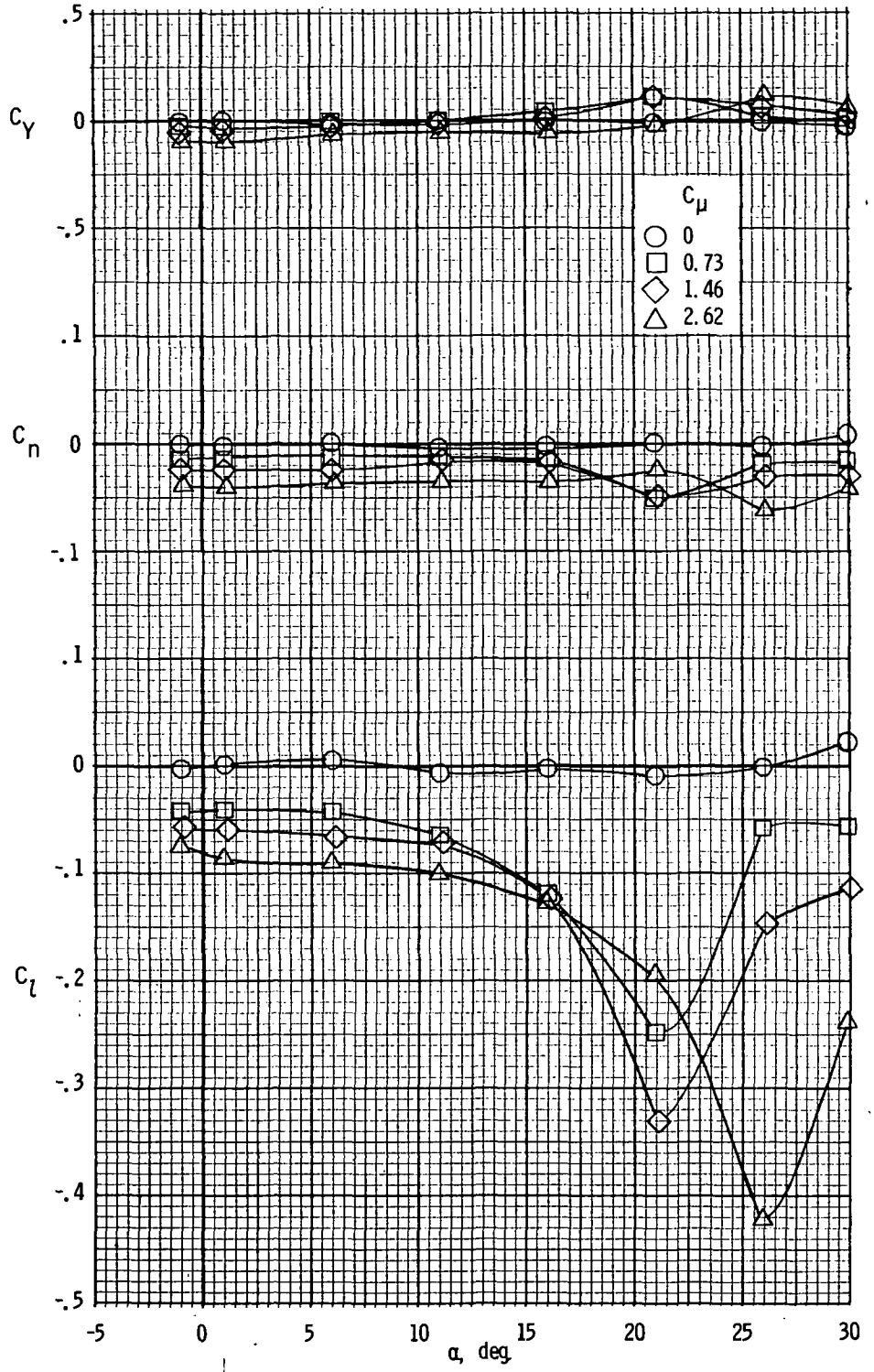

(a) Lateral characteristics. $R = 0.47 \times 10^6$.

Figure 18.- Longitudinal and lateral characteristics of model with left inboard engine not operating. 30-percent leading-edge flap; $\delta_{f1}/\delta_{f2} = 30^o/60^o$.

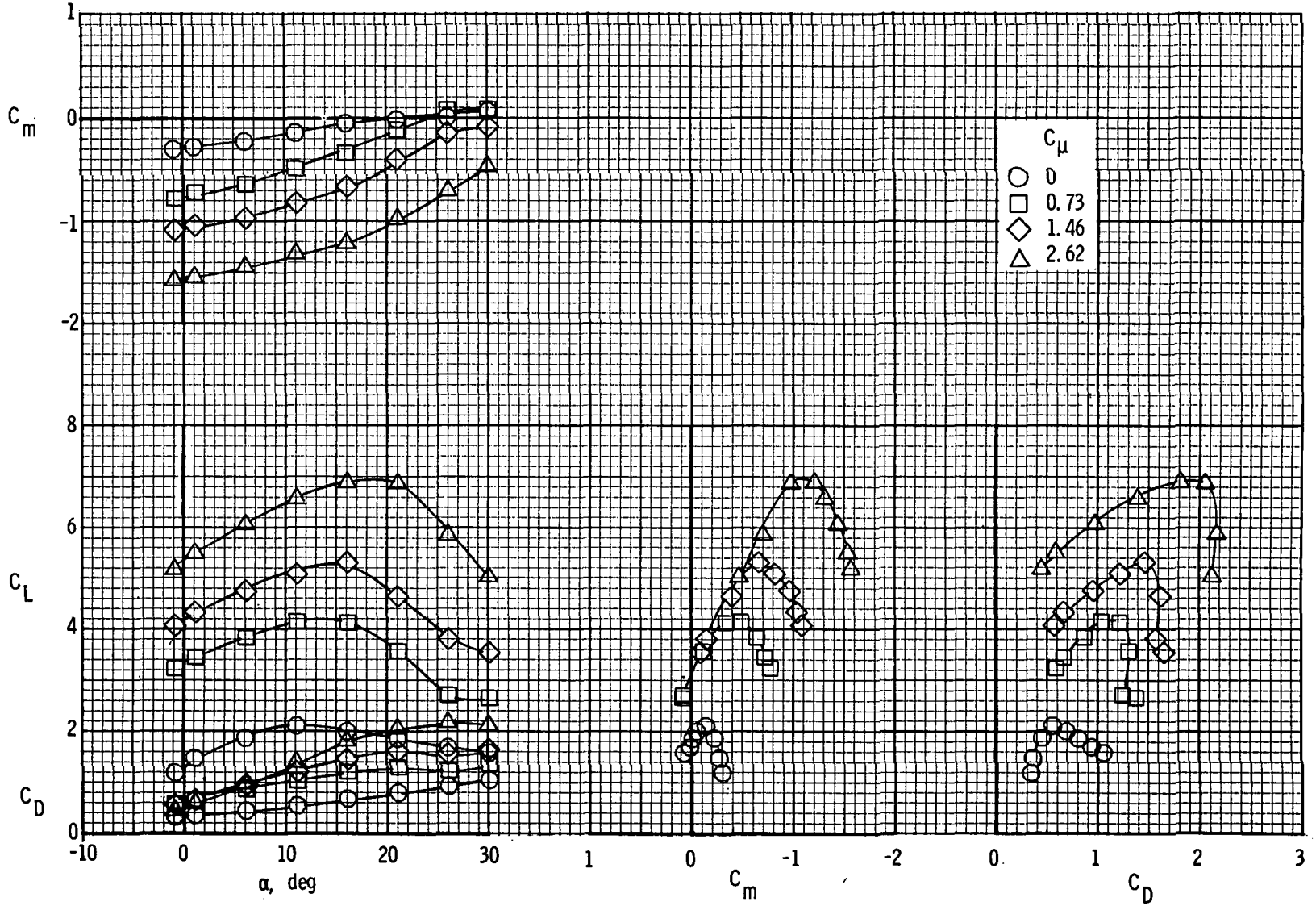

(b) Longitudinal characteristics. $R = 0.47 \times 10^6$.

Figure 18.- Continued.

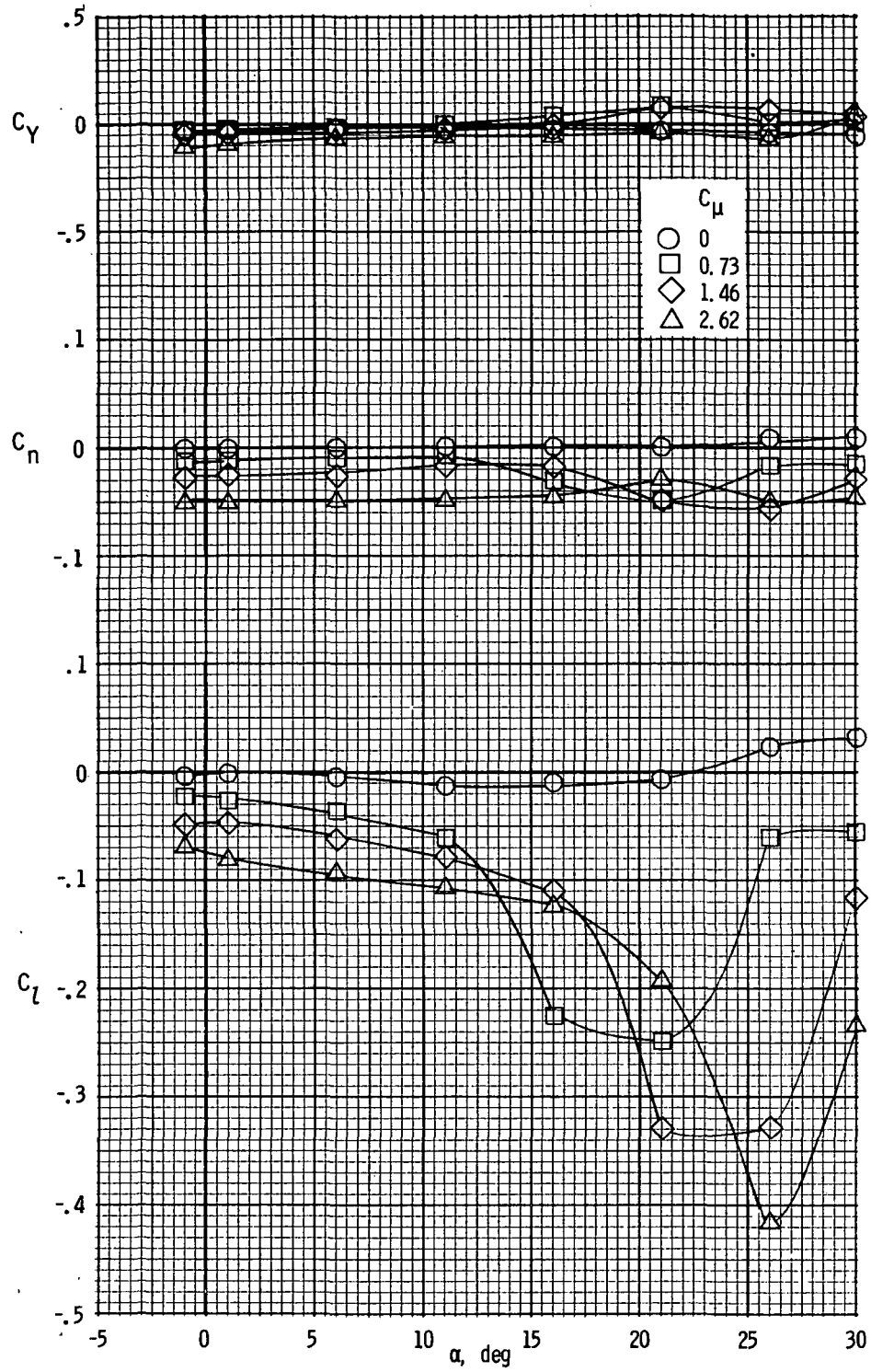

(c) Lateral characteristics. $R = 0.73 \times 10^6$.

Figure 18.- Continued.

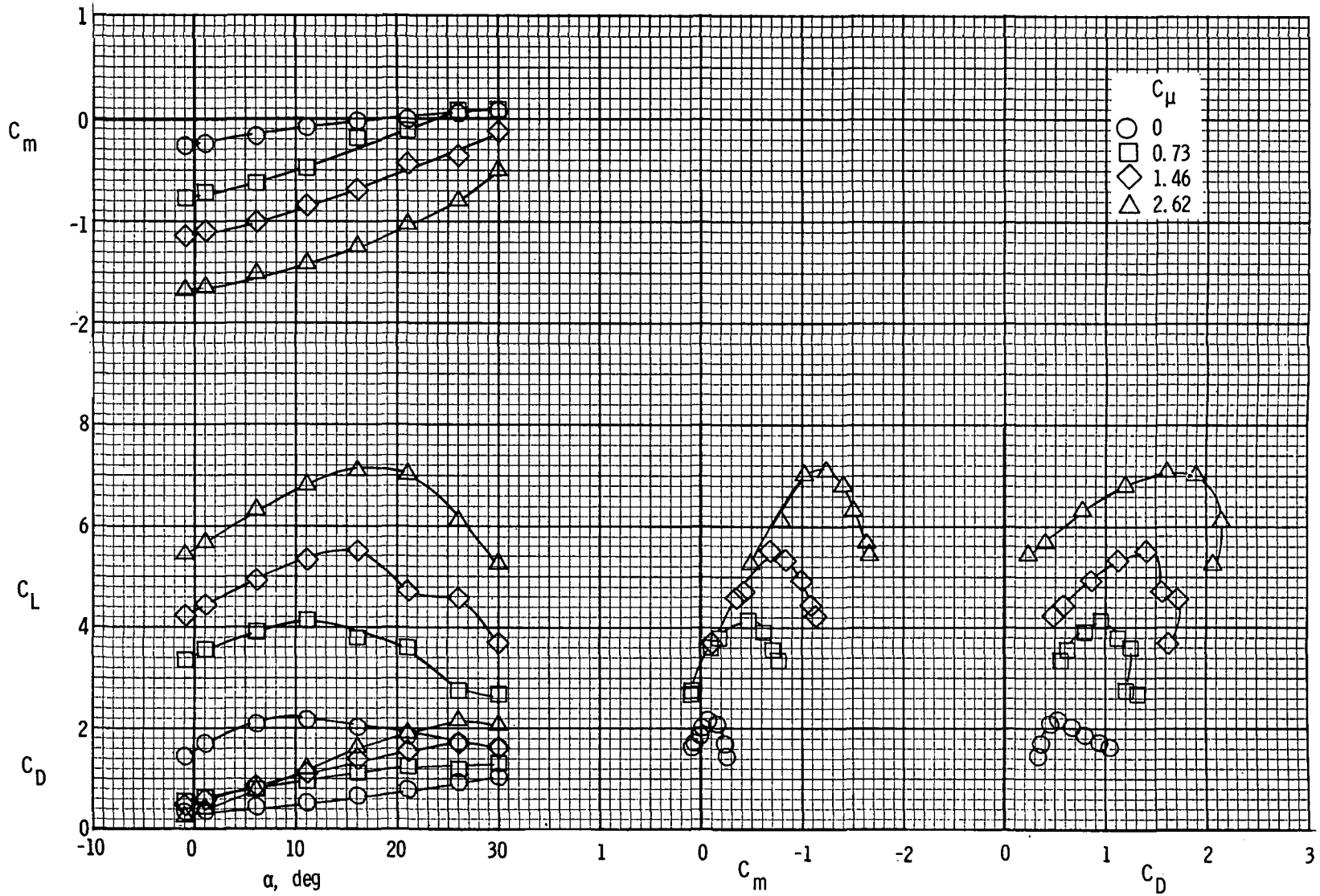

(d) Longitudinal characteristics. $R = 0.73 \times 10^6$.

Figure 18.- Continued.

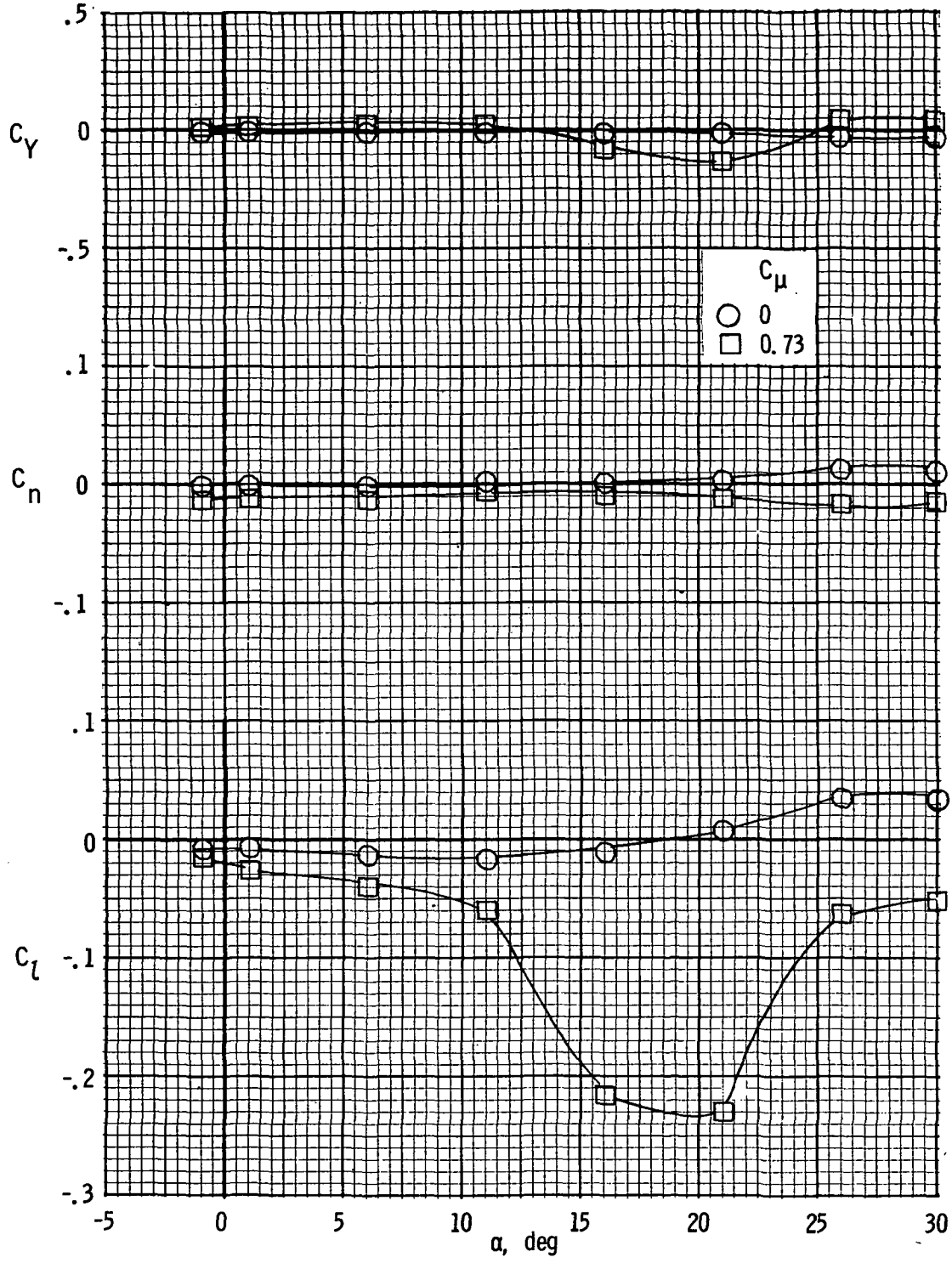

(e) Lateral characteristics. $R = 1.03 \times 10^6$.

Figure 18.- Continued.

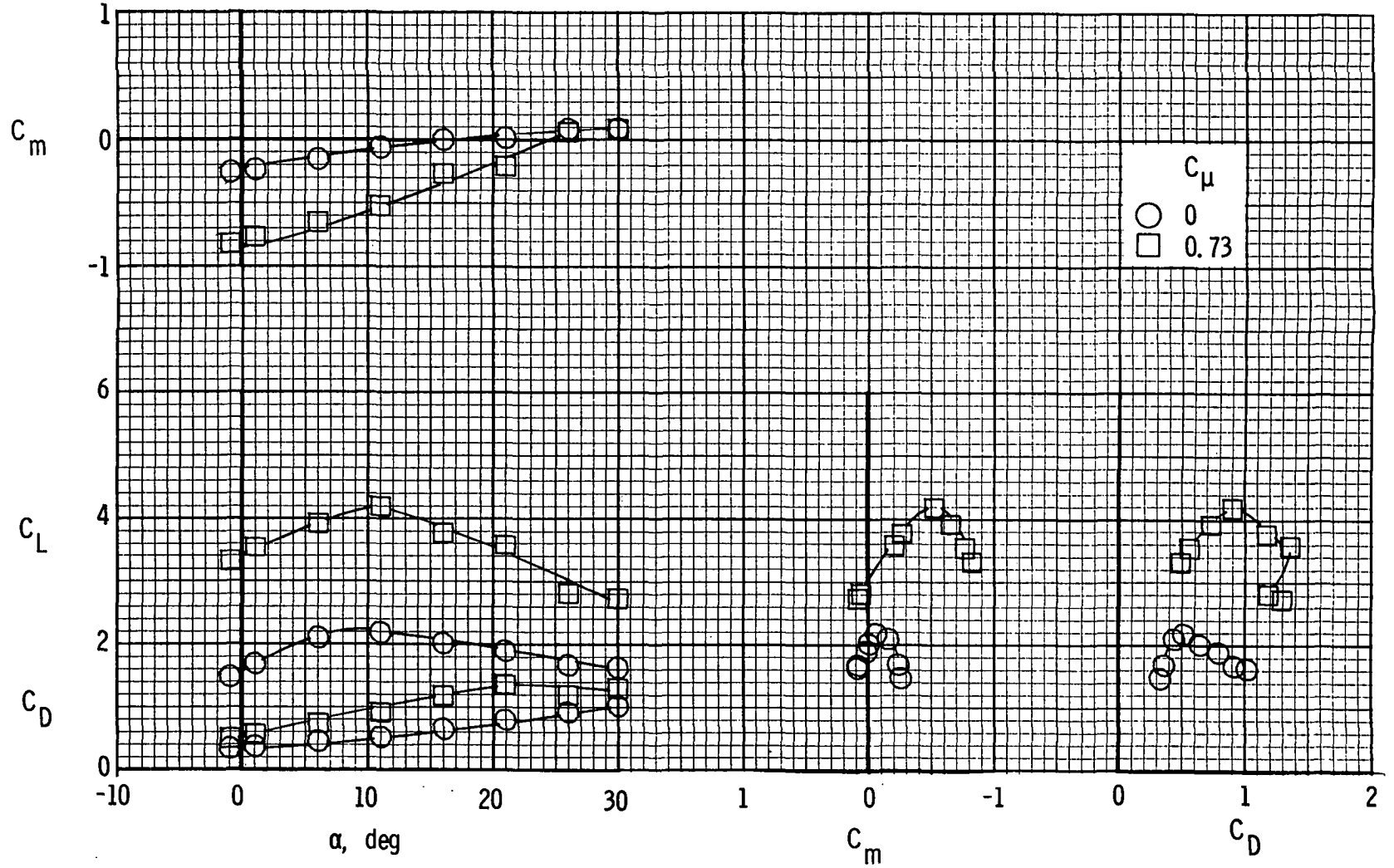

(f) Longitudinal characteristics. $R = 1.03 \times 10^6$.

Figure 18.- Continued.

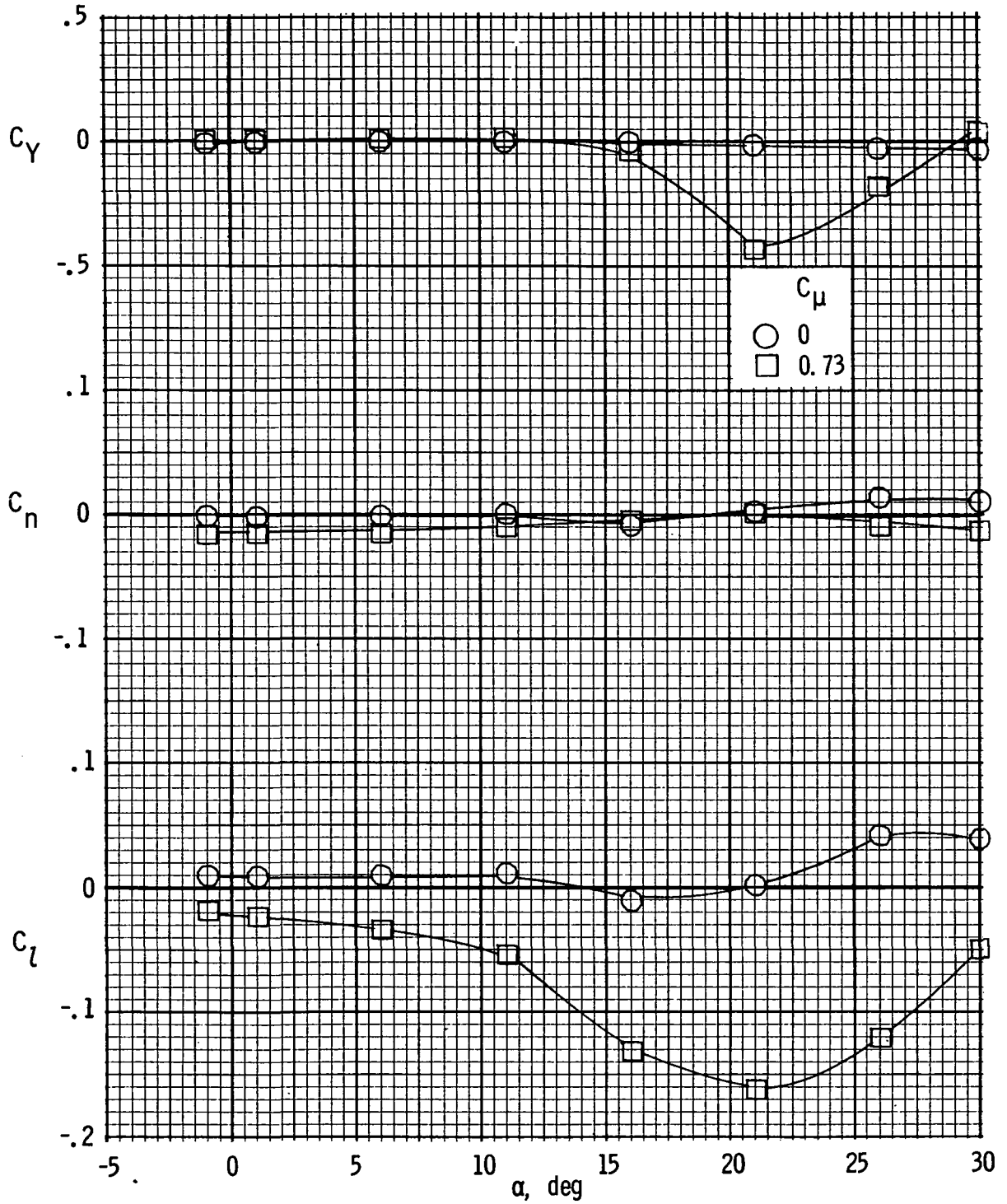

(g) Lateral characteristics. $R = 1.36 \times 10^6$.

Figure 18.- Continued.

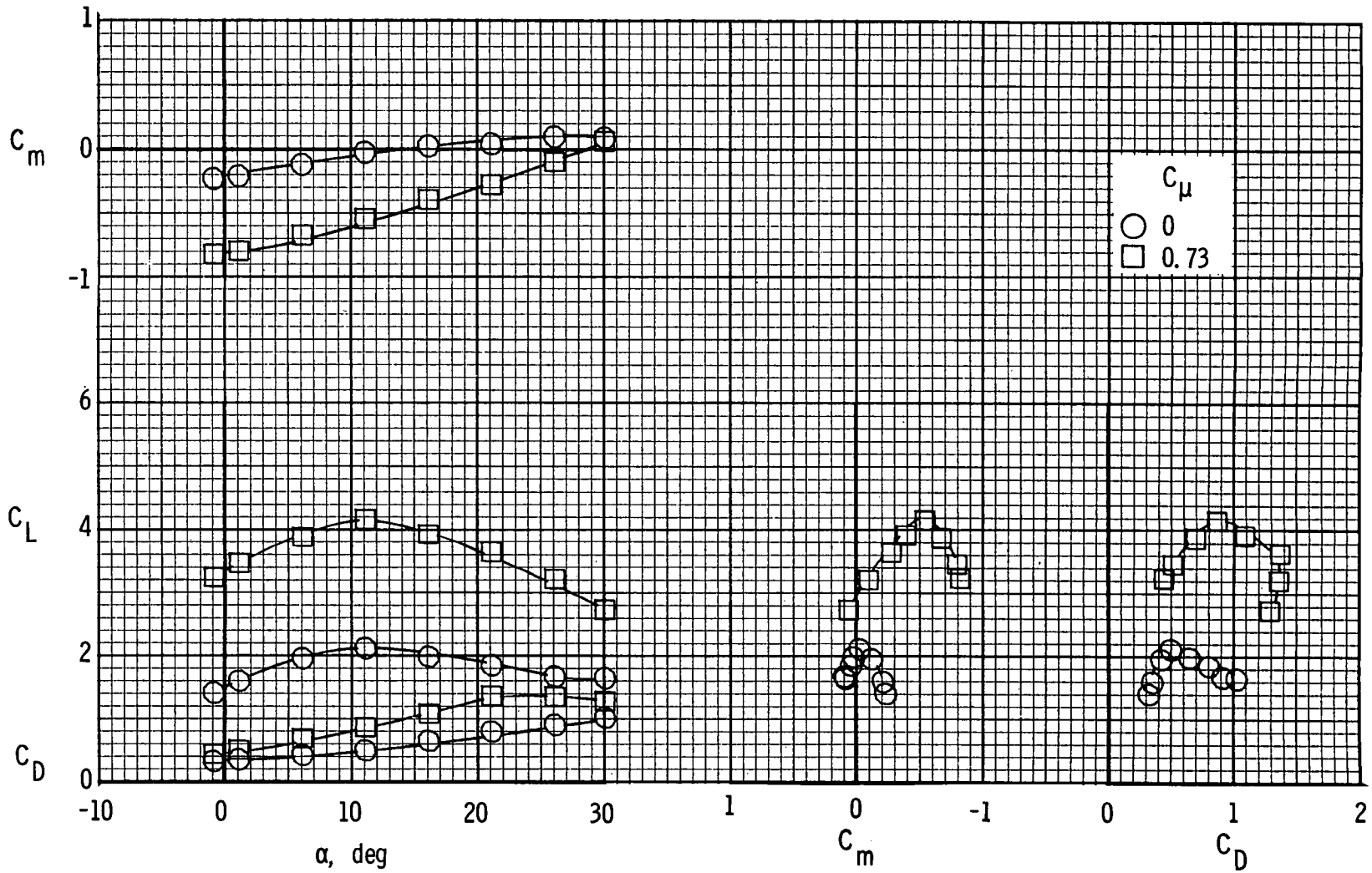

(h) Longitudinal characteristics. $R = 1.36 \times 10^6$.

Figure 18.- Concluded.

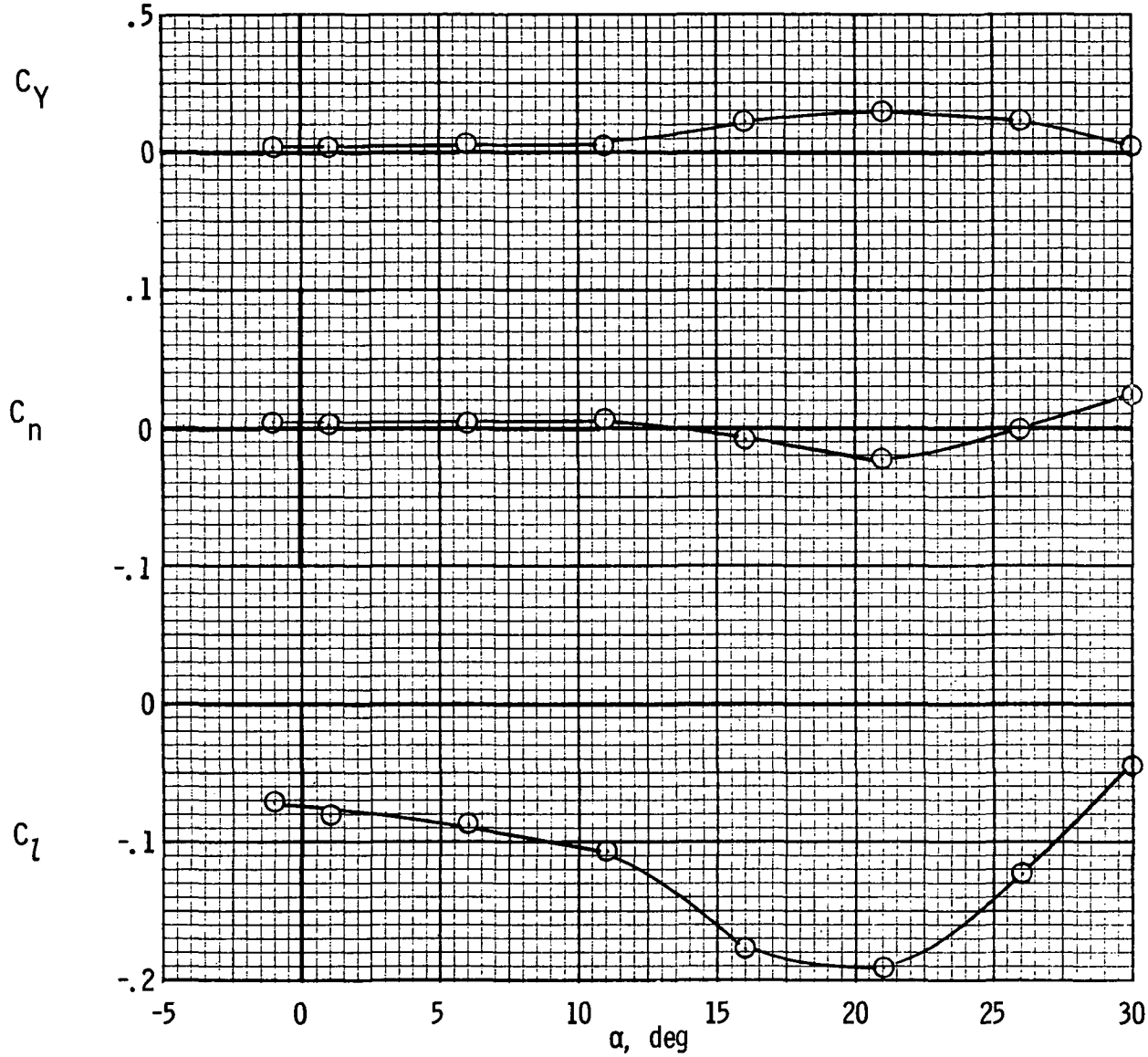

(a) Lateral characteristics. $R = 0.47 \times 10^6$.

Figure 19.- Longitudinal and lateral characteristics with left outboard engine not operating. $\delta_{f1}/\delta_{f2} = 30^o/60^o$; 25-percent leading-edge slat; $C_\mu = 0.73$.

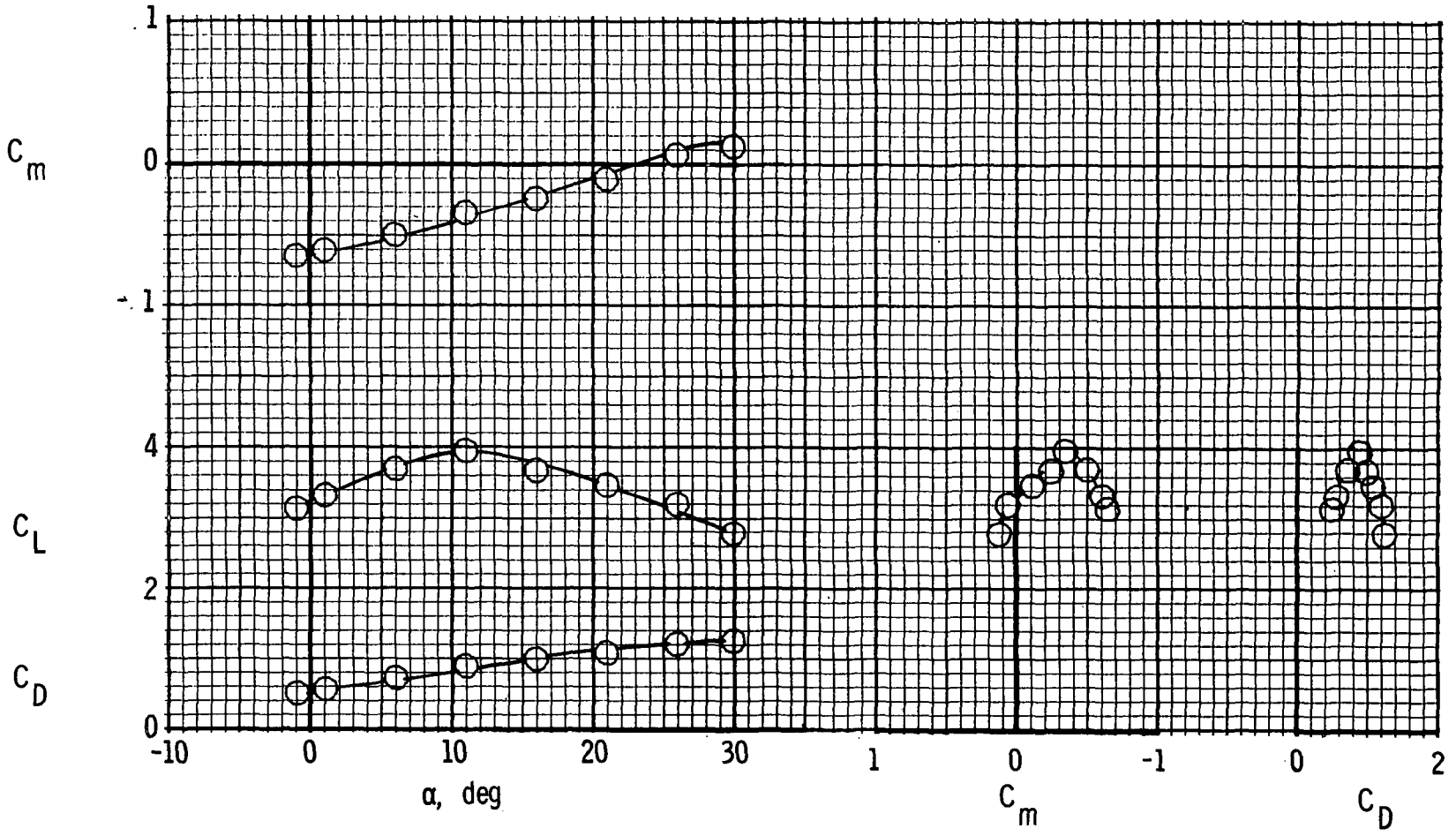

(b) Longitudinal characteristics. $R = 0.47 \times 10^6$.

Figure 19.- Continued.

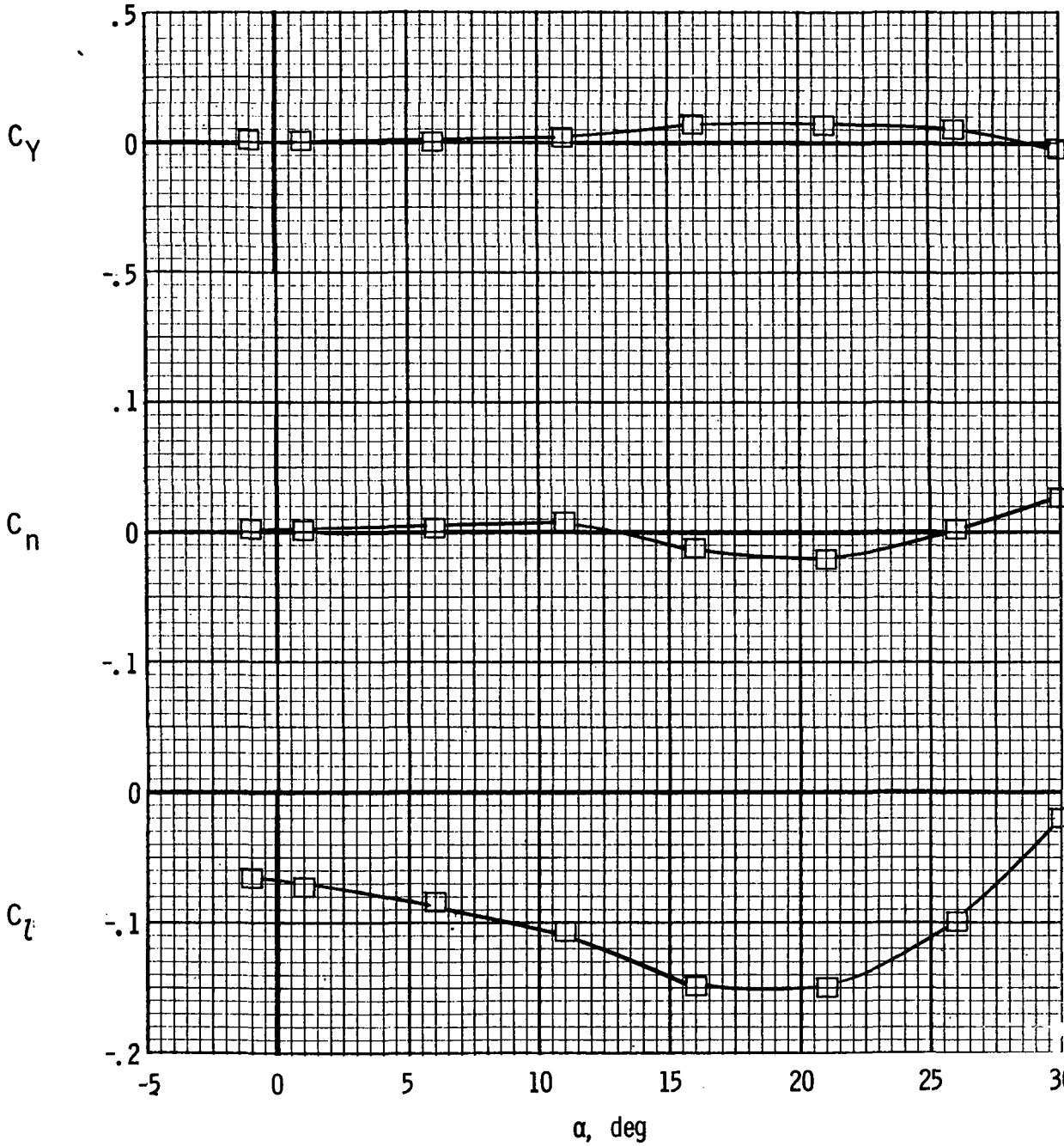

(c) Lateral characteristics. $R = 0.73 \times 10^6$.

Figure 19.- Continued.

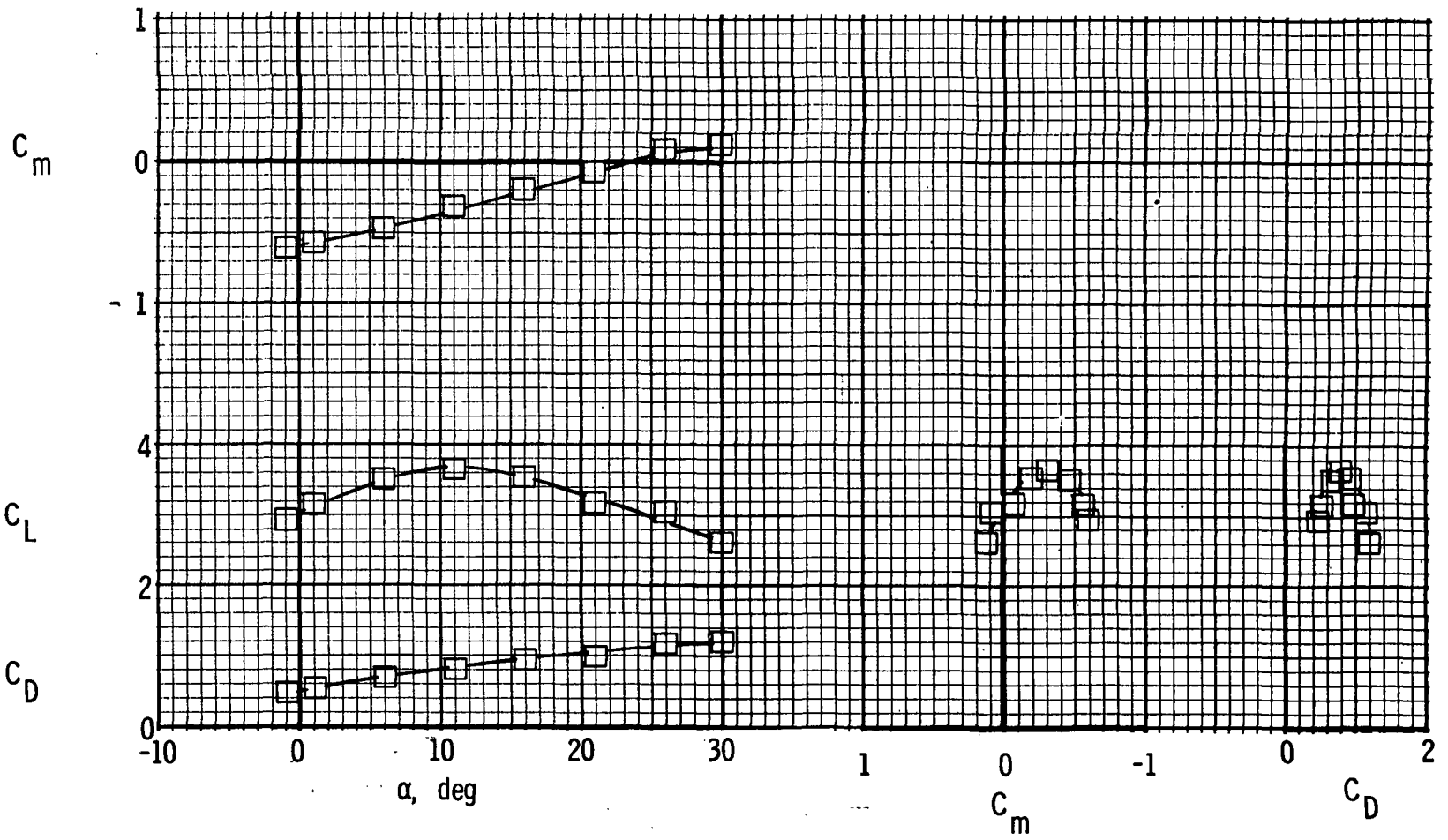

(d) Longitudinal characteristics. $R = 0.73 \times 10^6$.

Figure 19.- Continued.

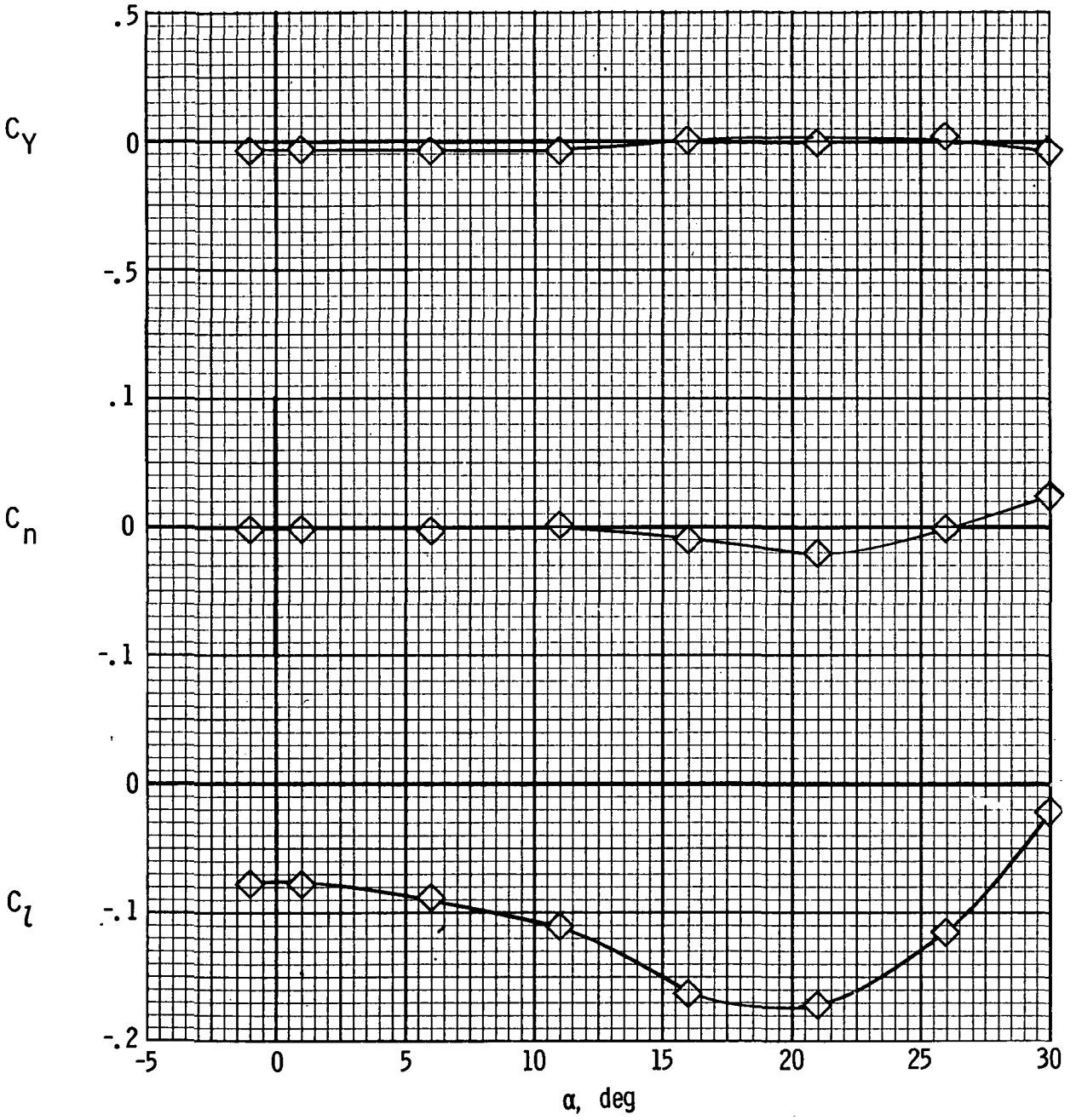

(e) Lateral characteristics. $R = 1.03 \times 10^6$.

Figure 19.- Continued.

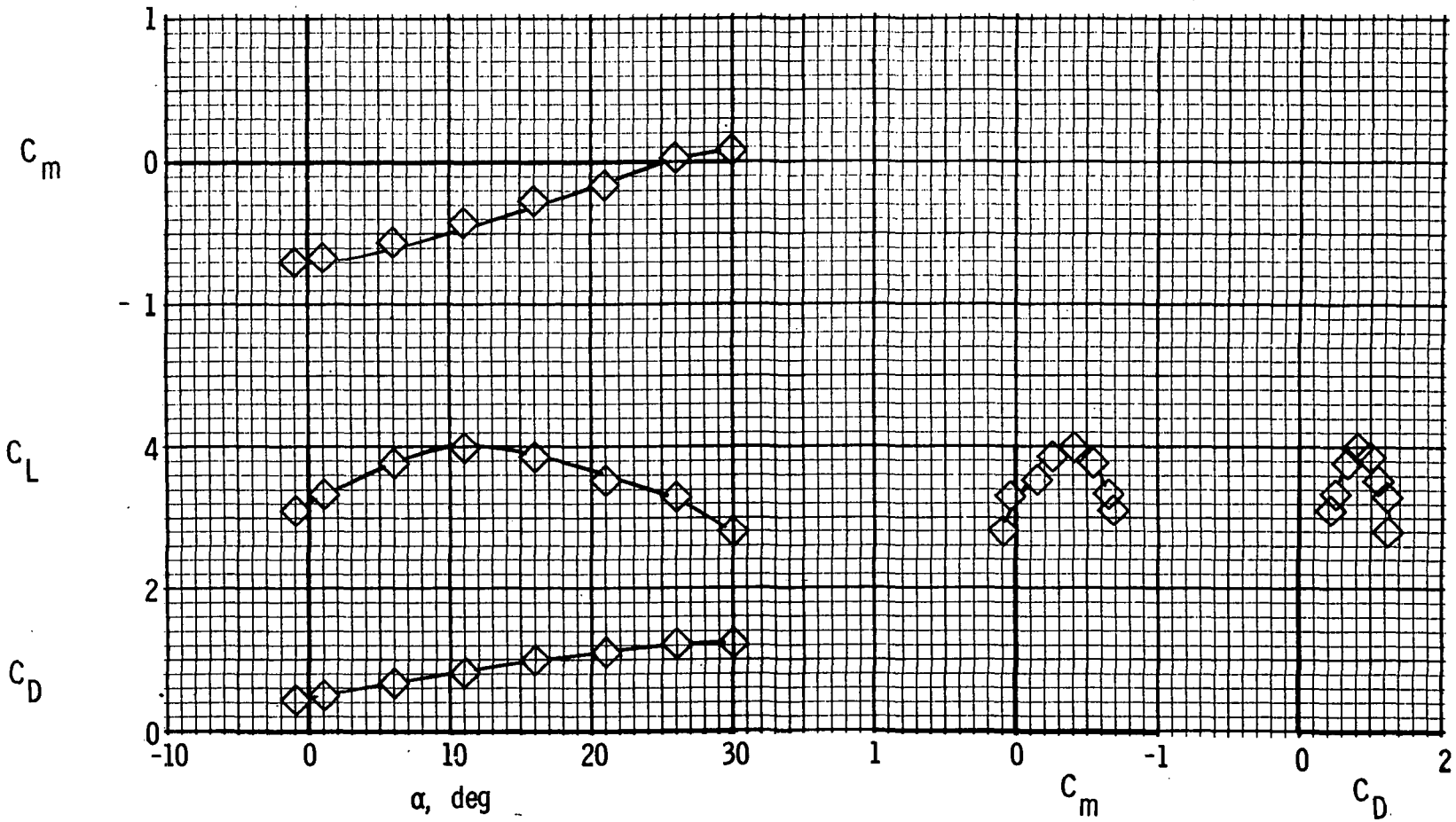

(f) Longitudinal characteristics. $R = 1.03 \times 10^6$.

Figure 19.- Continued.

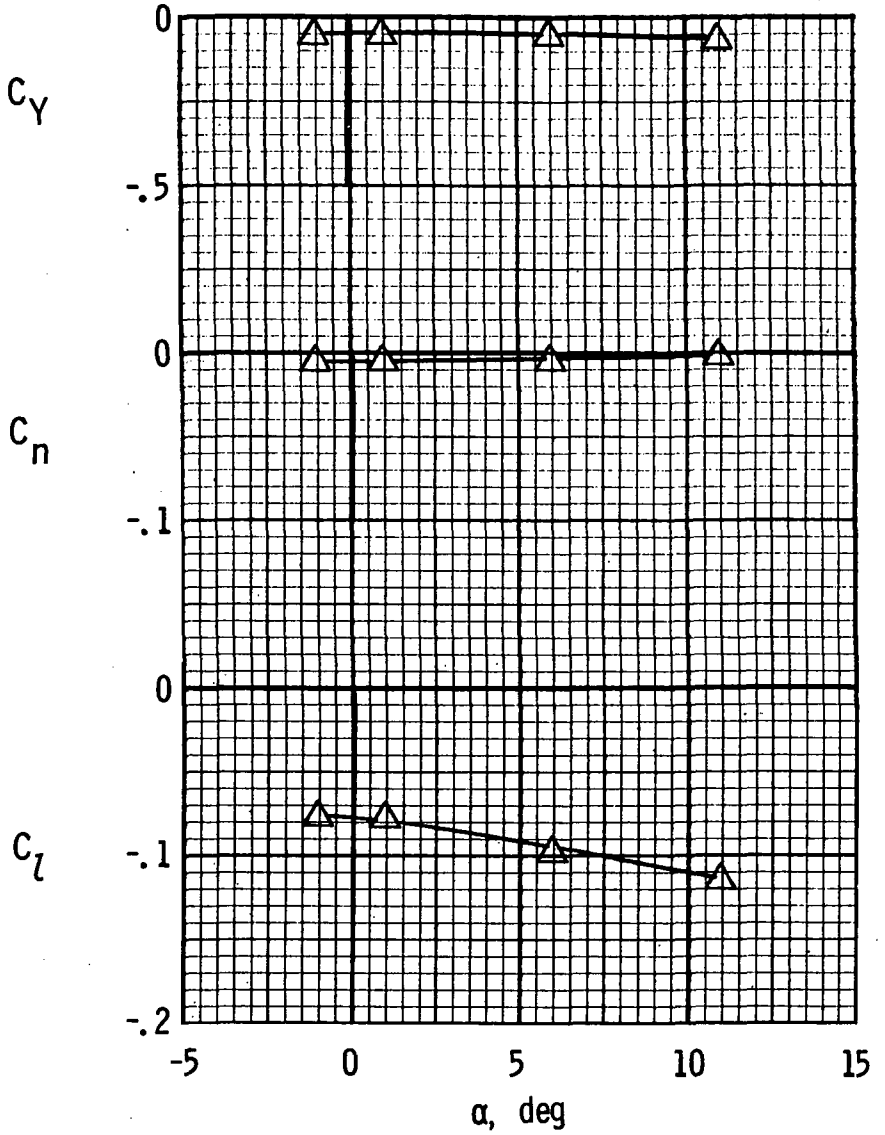

(g) Lateral characteristics. $R = 1.36 \times 10^6$.

Figure 19.- Continued.

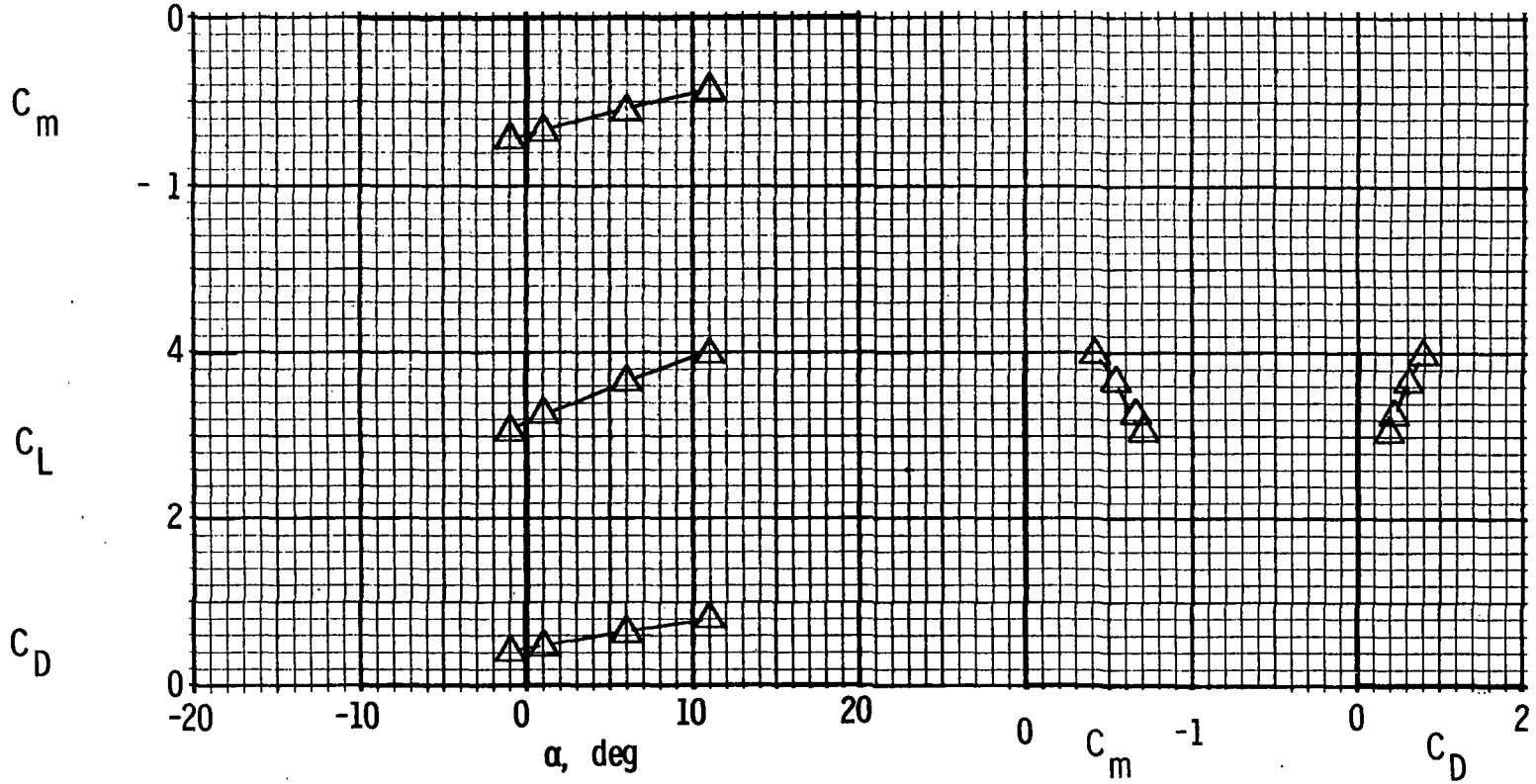

(h) Longitudinal characteristics. $R = 1.36 \times 10^6$.

Figure 19.- Concluded.

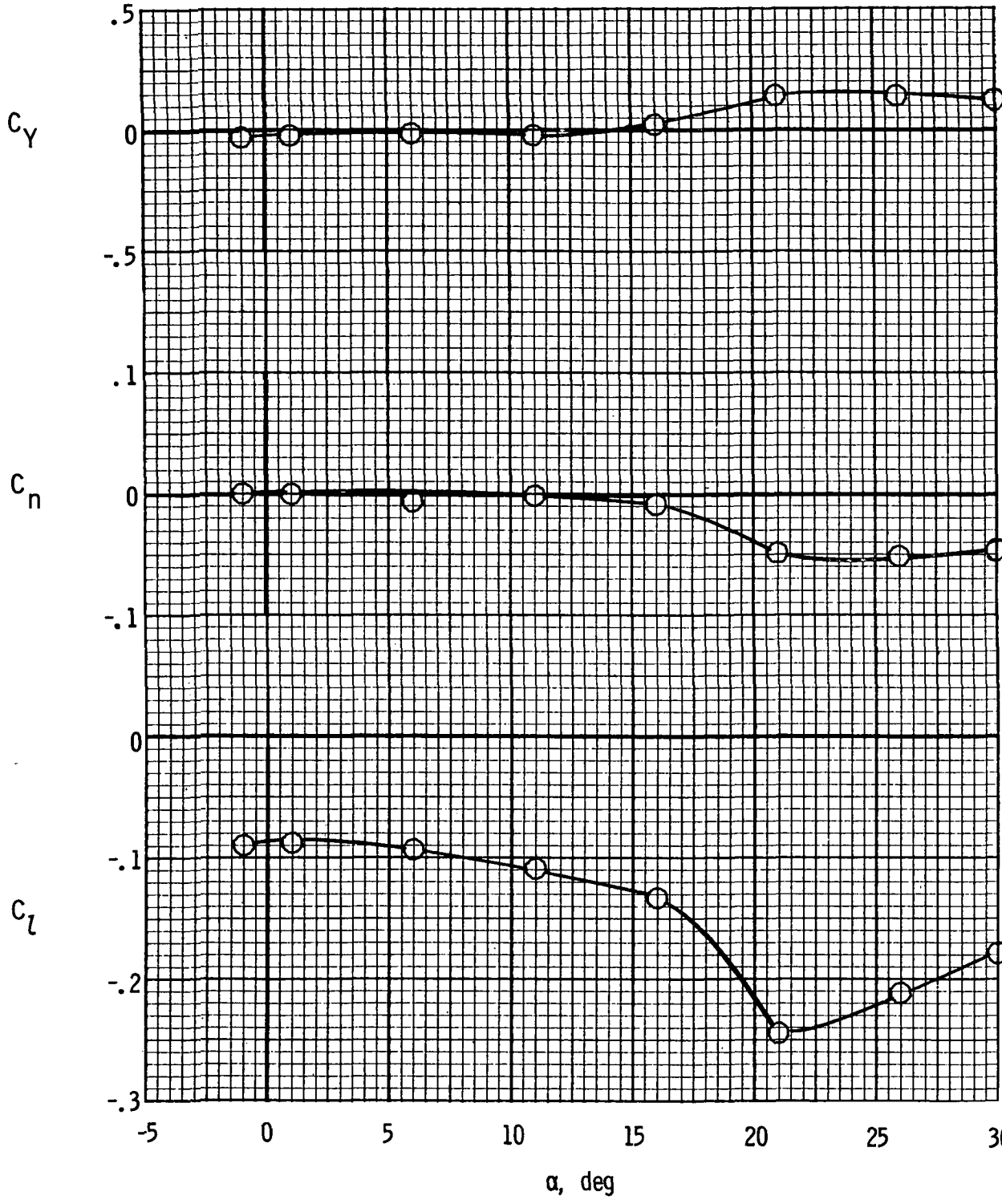

(a) Lateral characteristics. $R = 0.47 \times 10^6$.

Figure 20.- Longitudinal and lateral characteristics with left outboard engine not operating. $\delta_{f1}/\delta_{f2} = 30^o/60^o$; 15-percent leading-edge slat; $C_\mu = 0.73$.

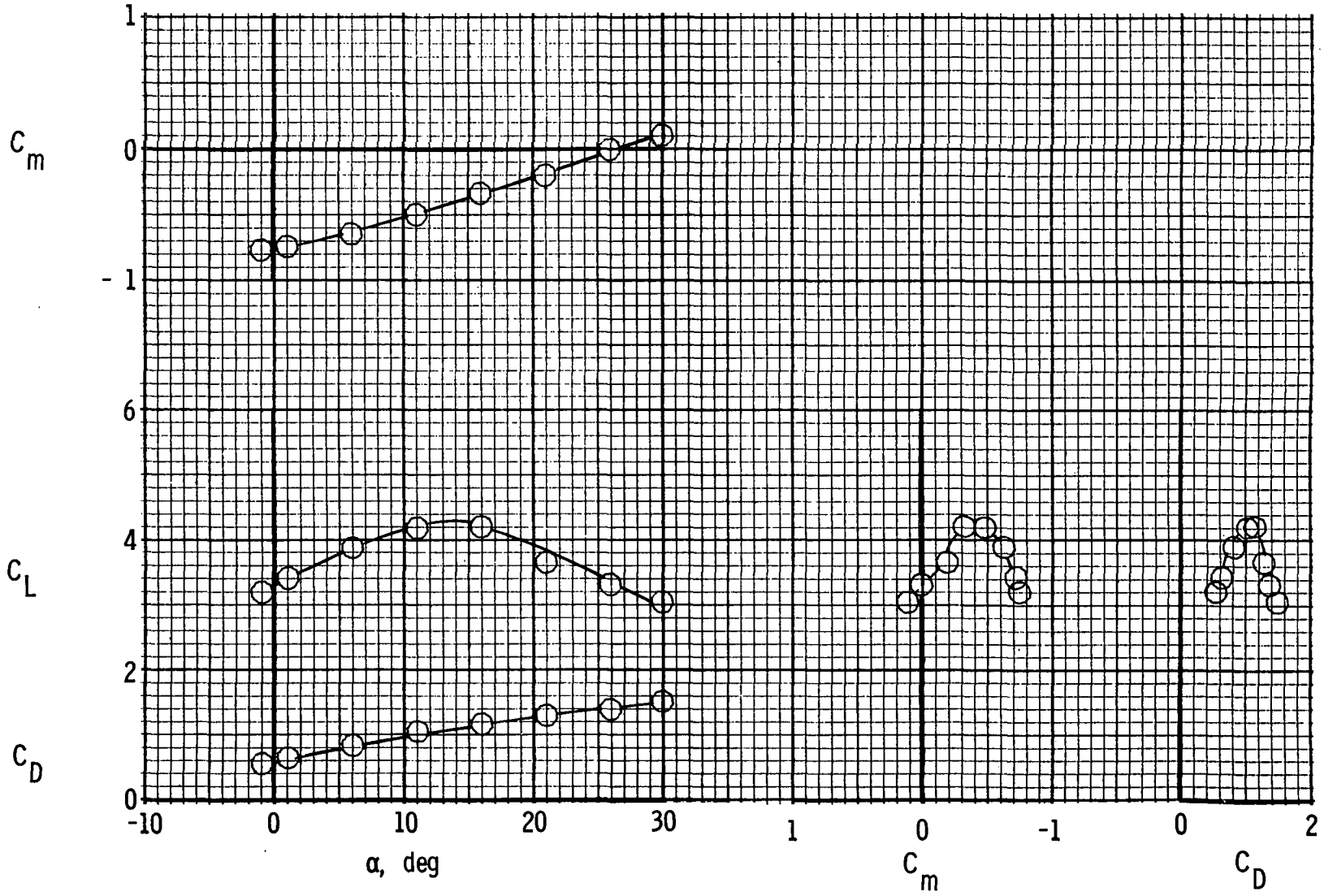

(b) Longitudinal characteristics. $R = 0.47 \times 10^6$.

Figure 20.- Continued.

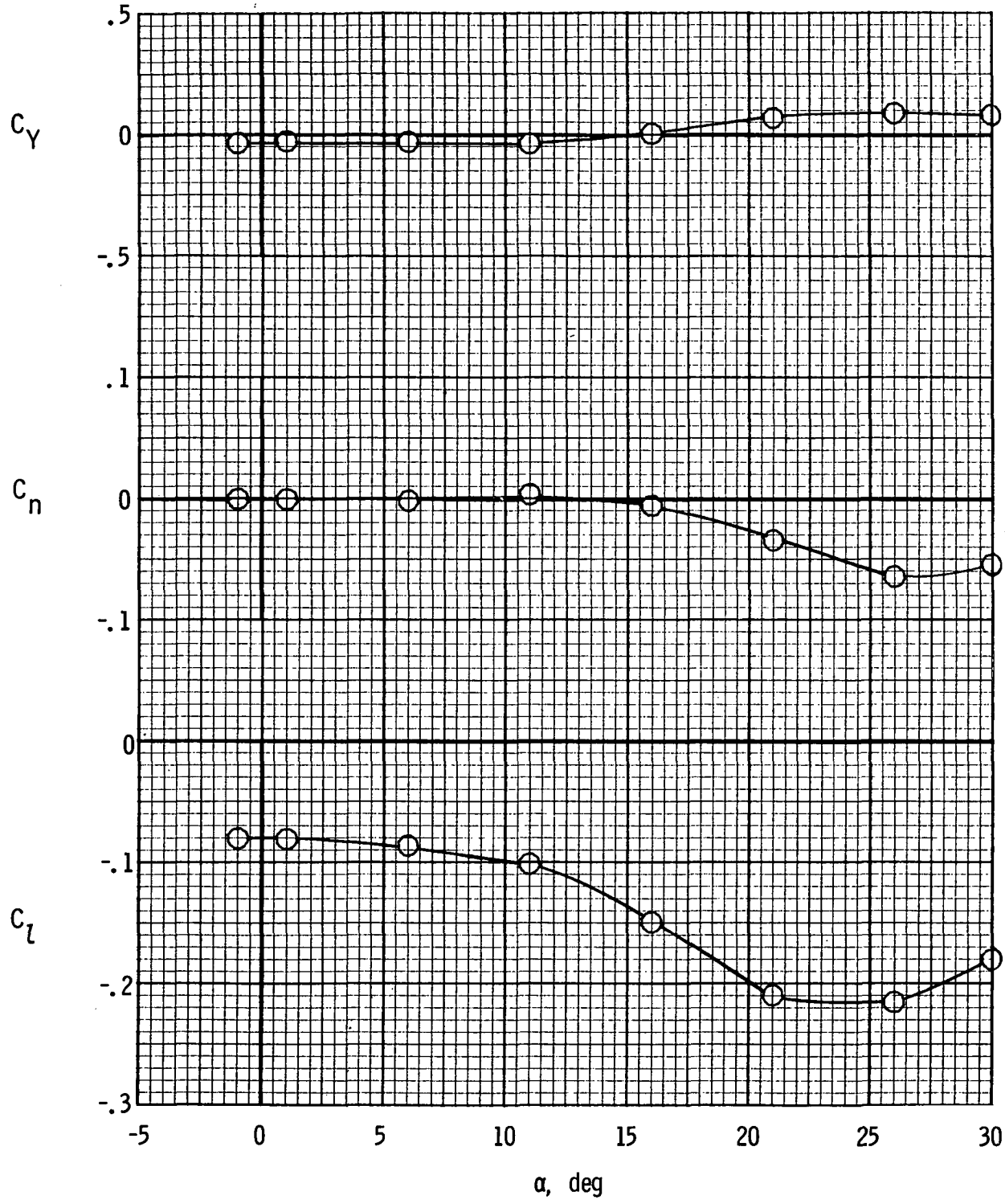

(c) Lateral characteristics. $R = 0.73 \times 10^6$.

Figure 20.- Continued.

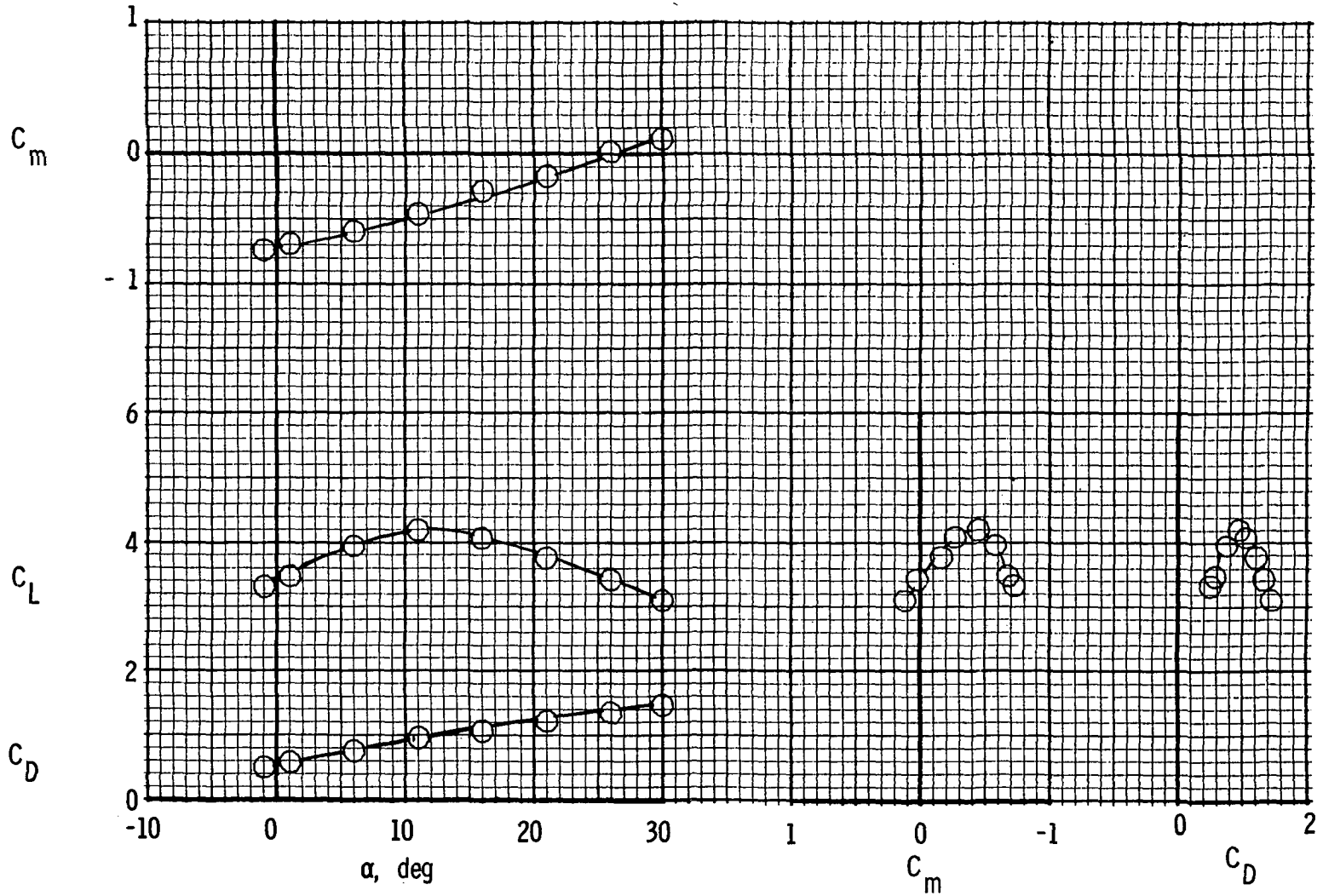

(d) Longitudinal characteristics. $R = 0.73 \times 10^6$.

Figure 20.- Continued.

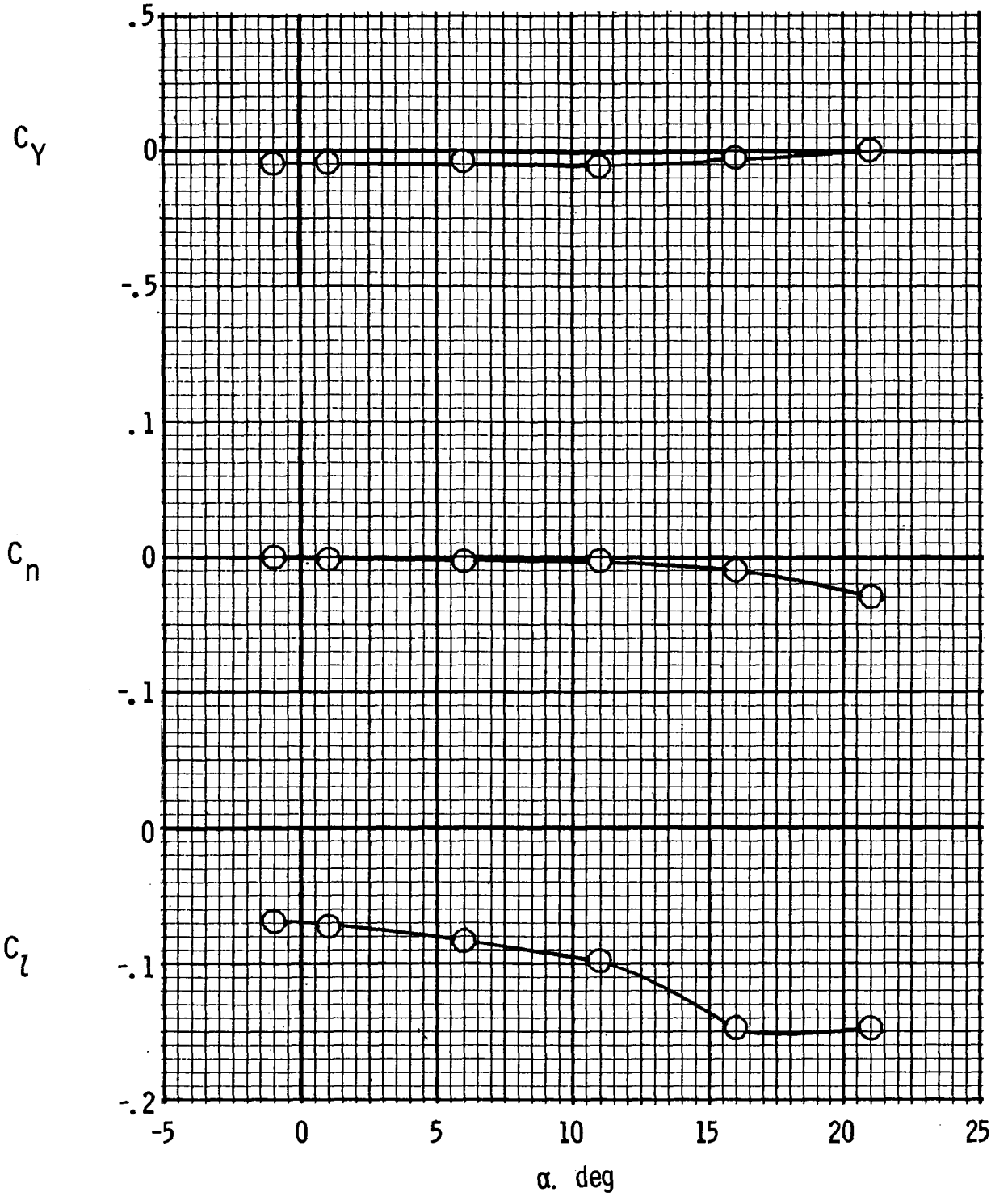

(e) Lateral characteristics. $R = 1.03 \times 10^6$.

Figure 20.- Continued.

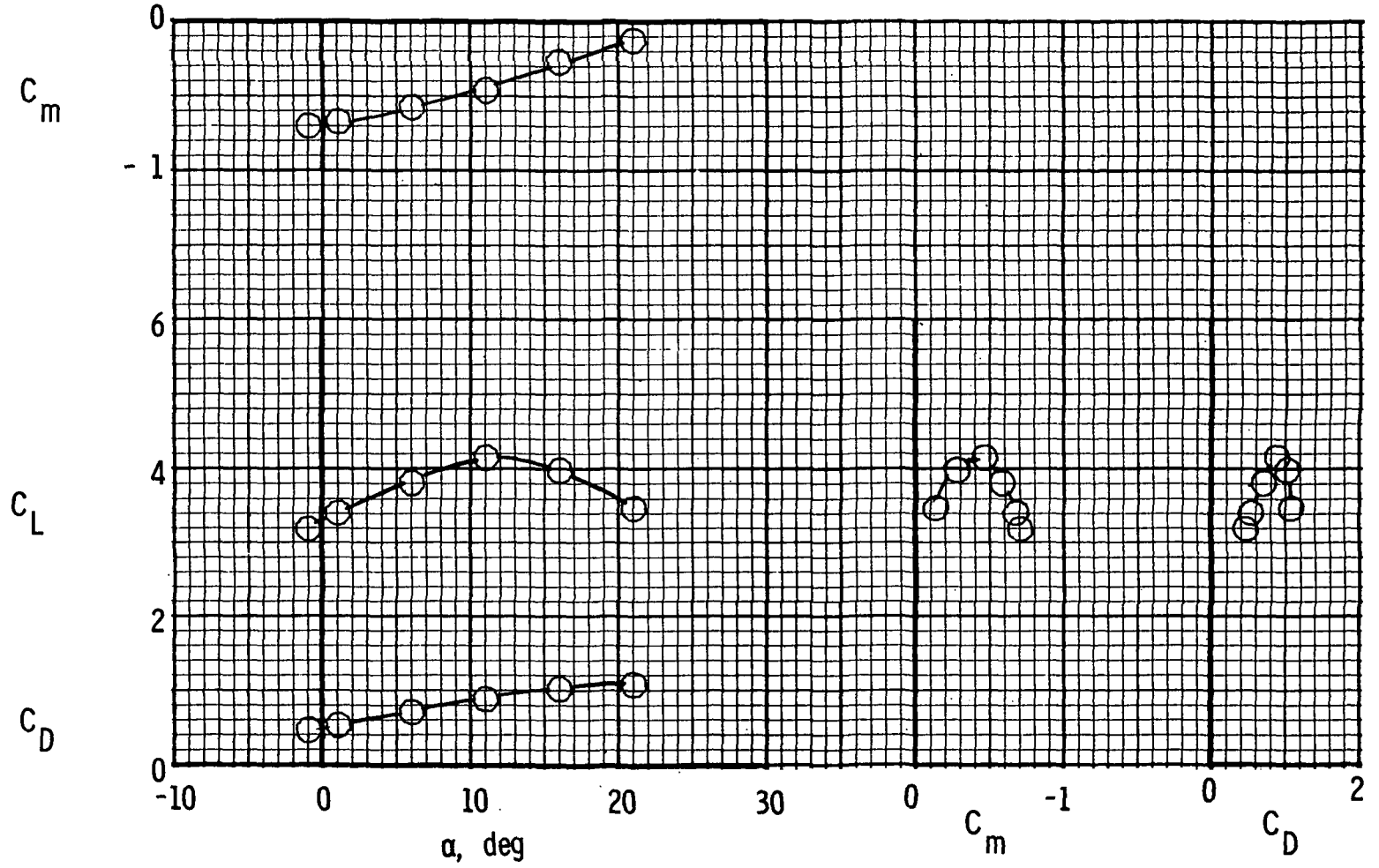

(f) Longitudinal characteristics. $R = 1.03 \times 10^6$.

Figure 20.- Continued.

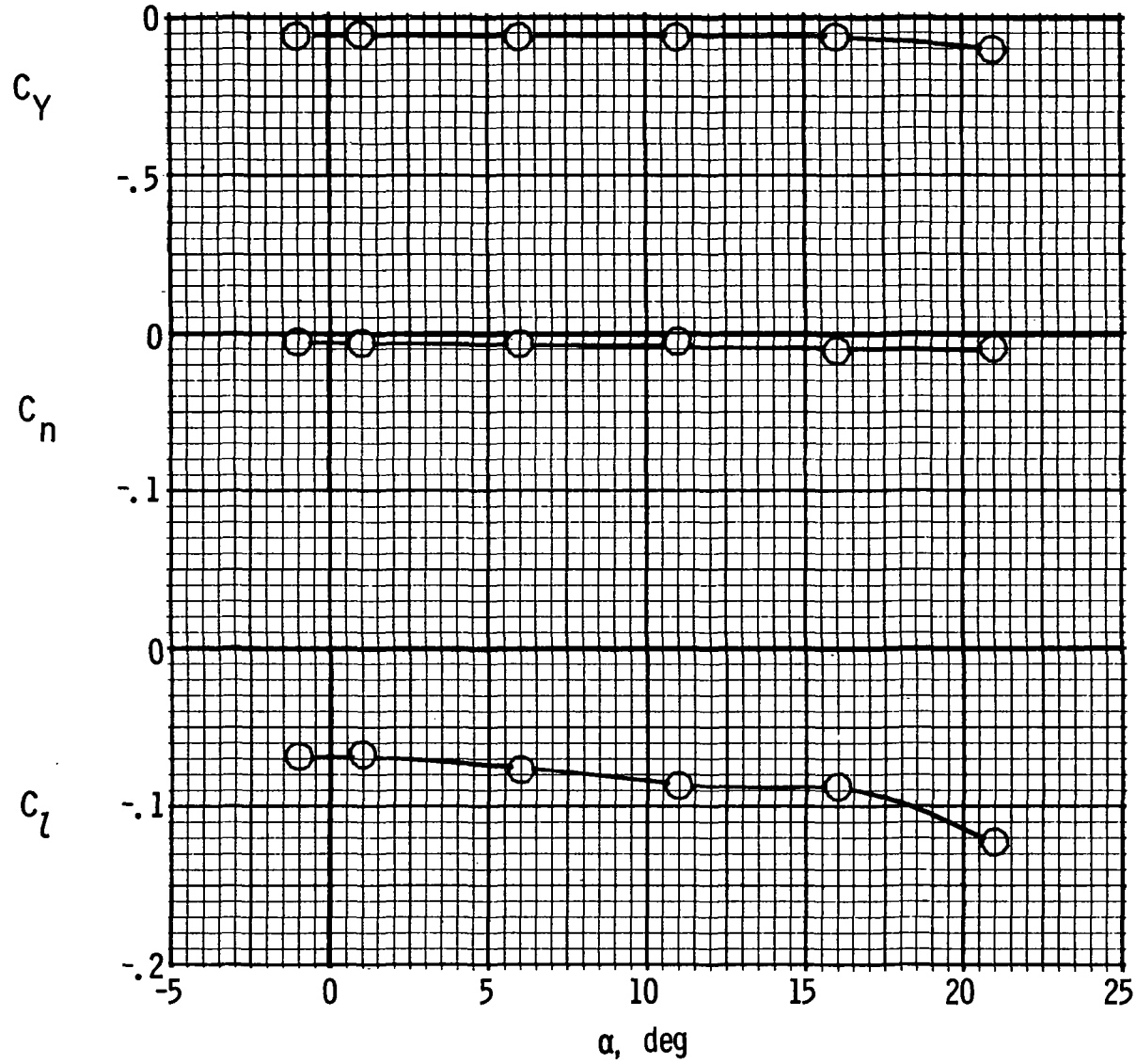

(g) Lateral characteristics. $R = 1.36 \times 10^6$.

Figure 20.- Continued.

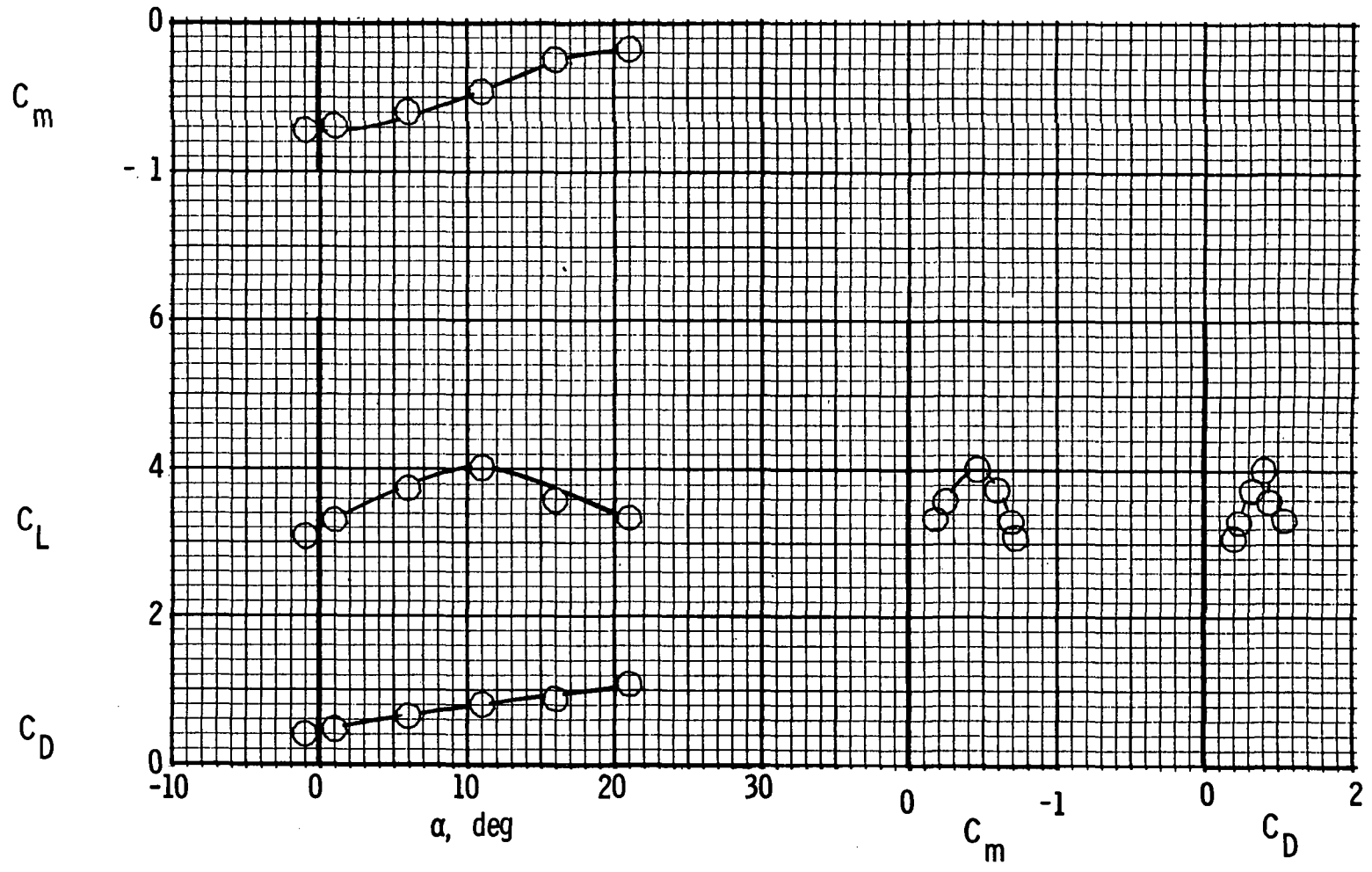

(h) Longitudinal characteristics. $R = 1.36 \times 10^6$.

Figure 20.- Concluded.

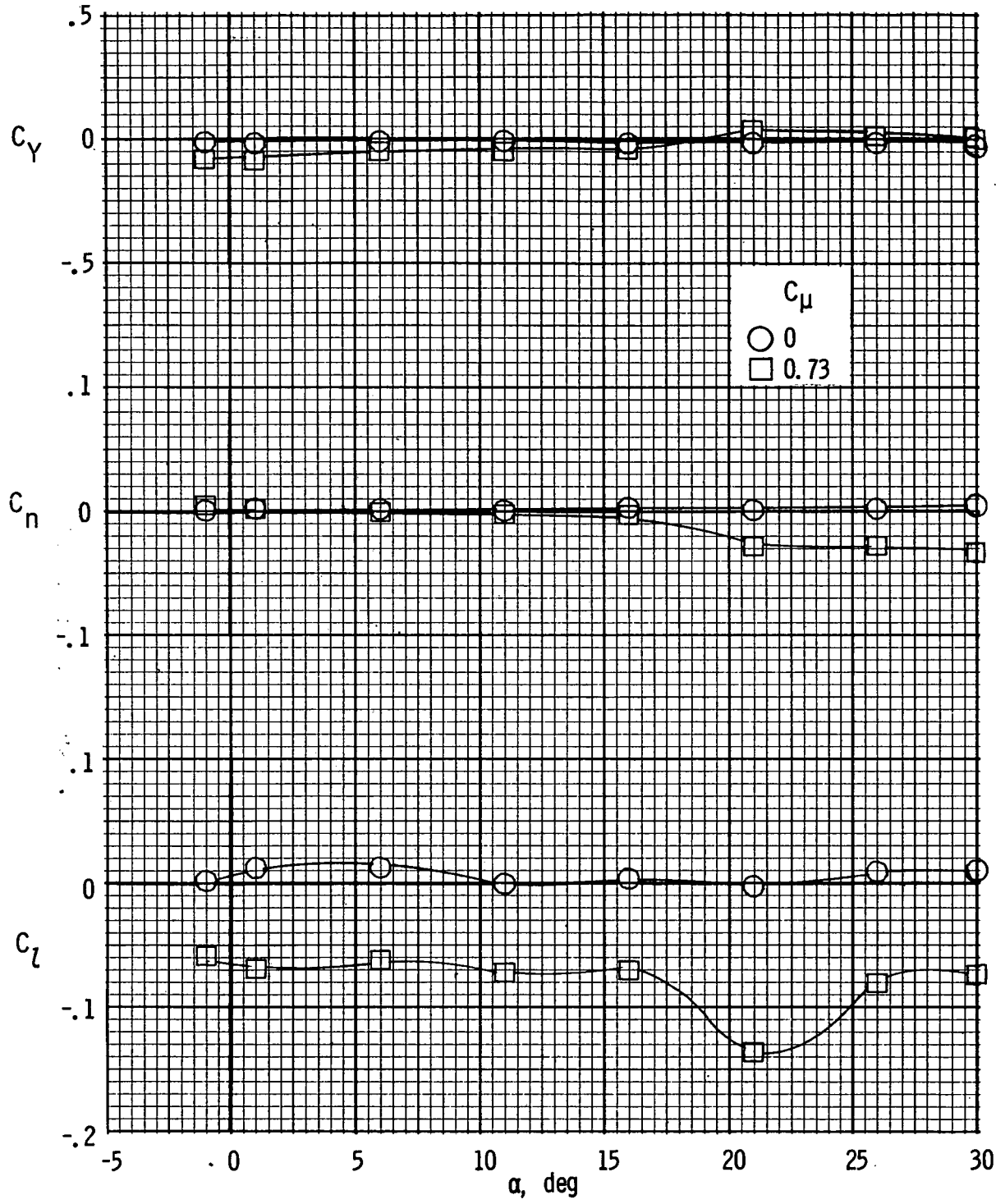

(a) Lateral characteristics. $R = 0.47 \times 10^6$.

Figure 21.- Longitudinal and lateral characteristics of model with left outboard engine not operating. 30-percent leading-edge flap; $\delta_{f1}/\delta_{f2} = 20^o/40^o$.

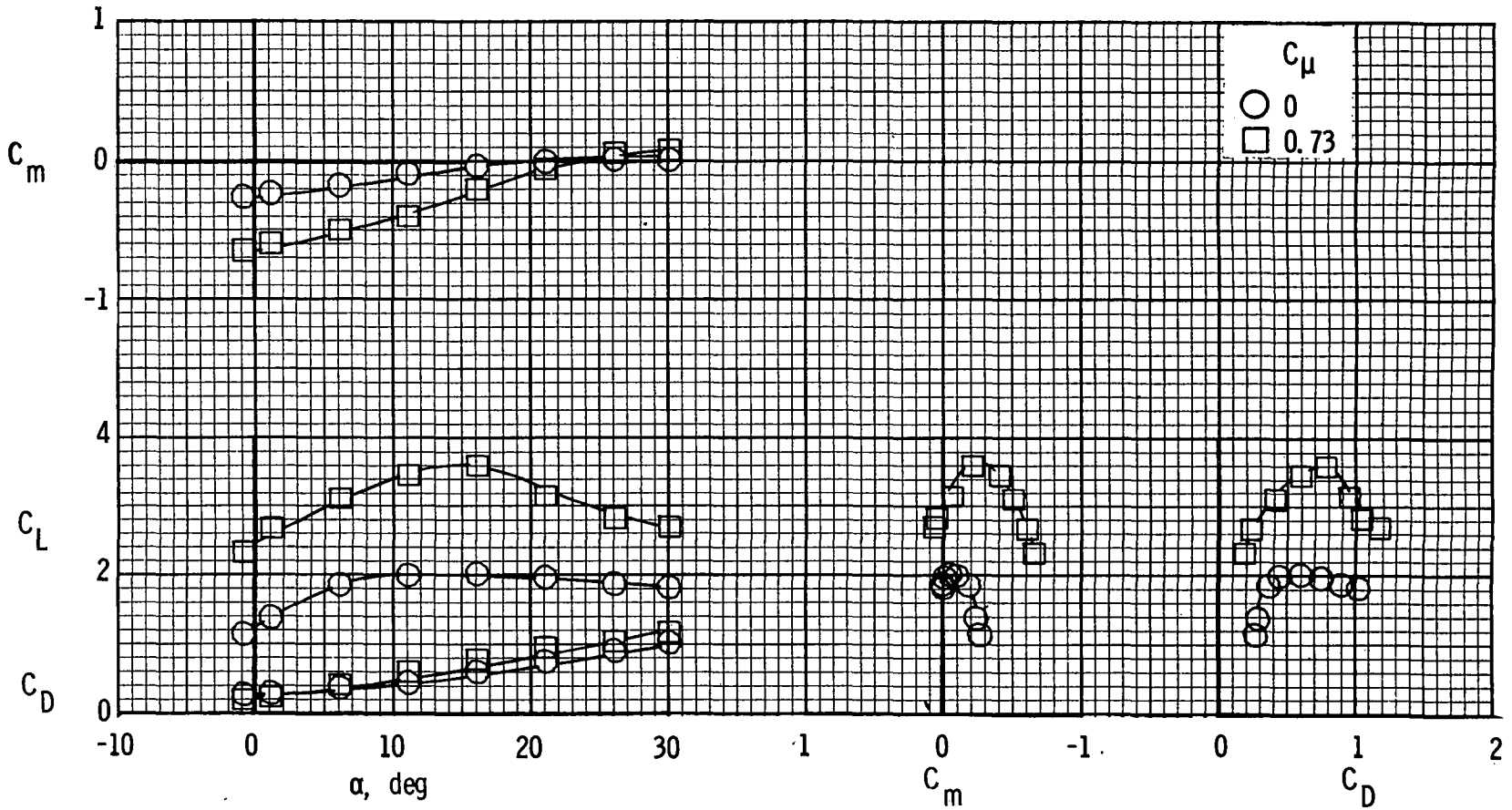

(b) Longitudinal characteristics. $R = 0.47 \times 10^6$.

Figure 21.- Continued.

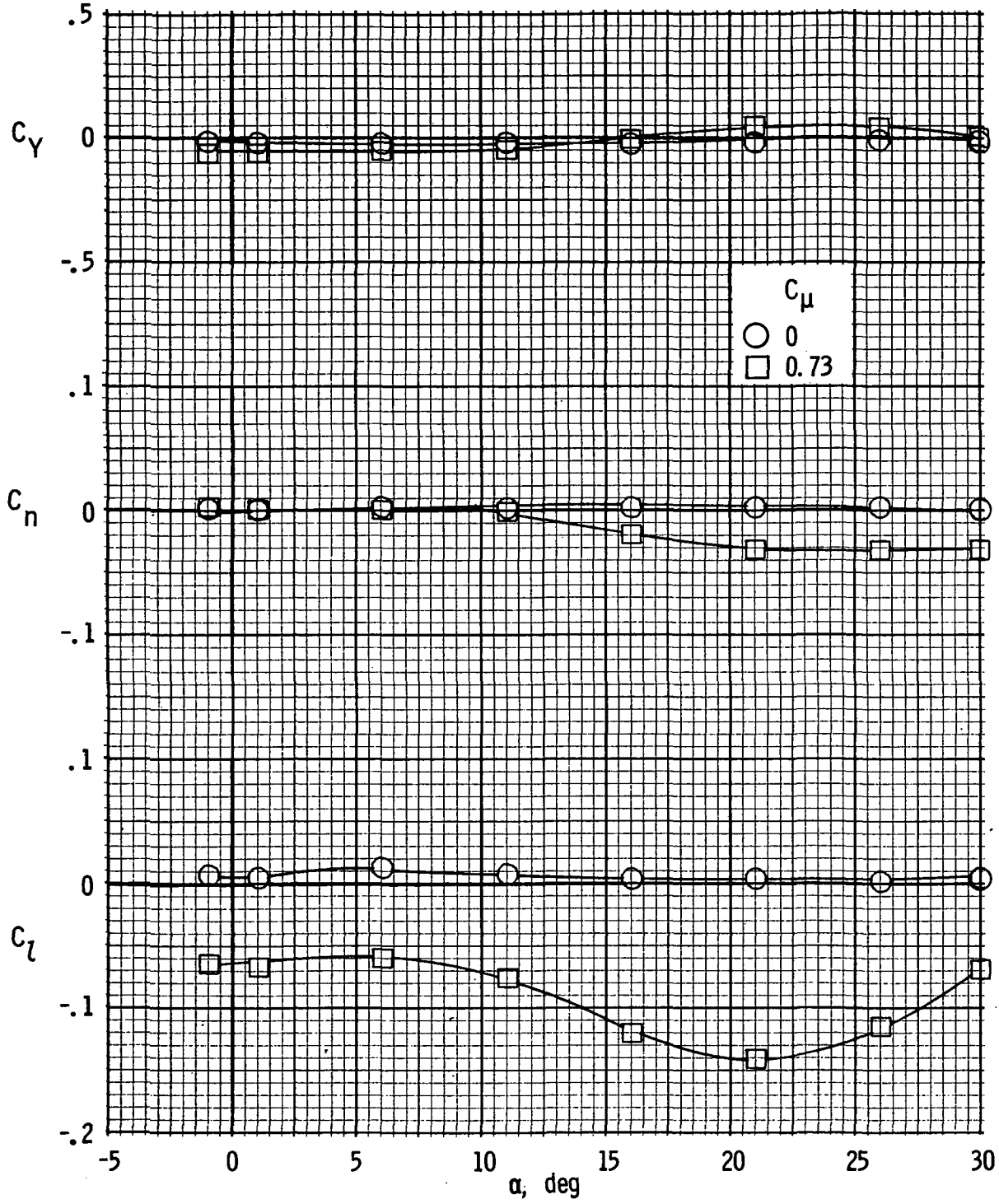

(c) Lateral characteristics. $R = 0.73 \times 10^6$.

Figure 21.- Continued.

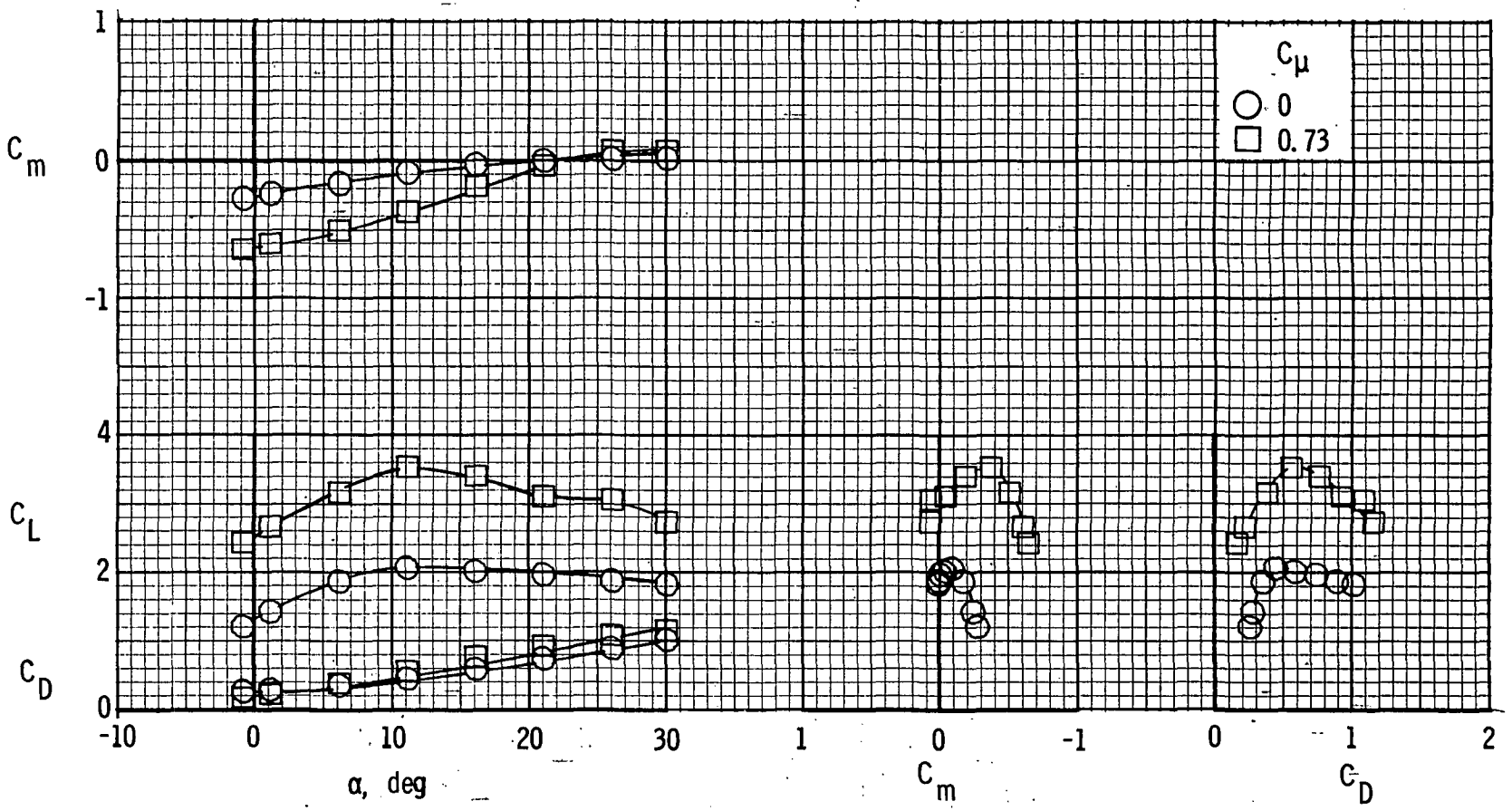

(d) Longitudinal characteristics. $R = 0.73 \times 10^6$.

Figure 21.- Continued.

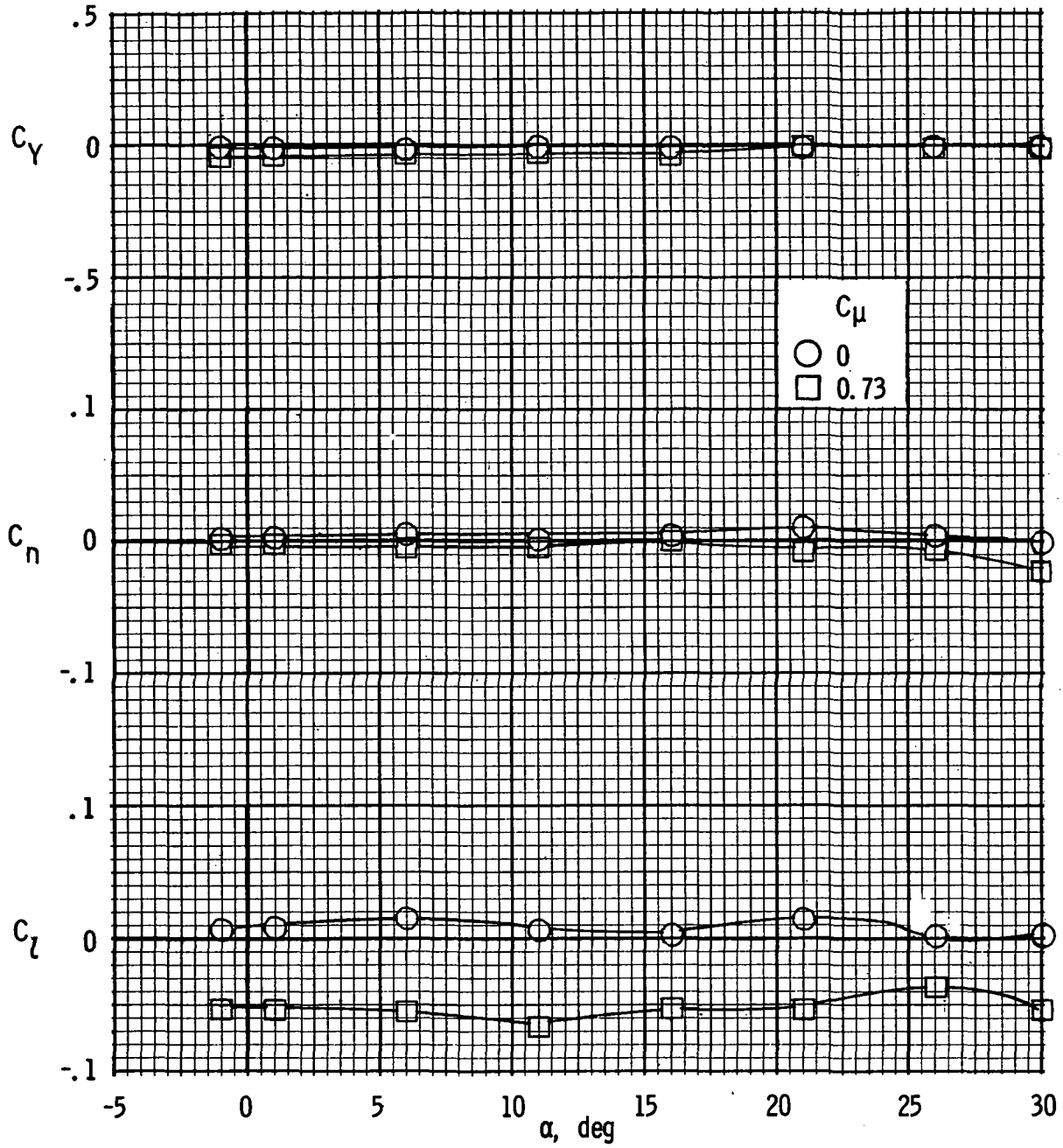

(e) Lateral characteristics. $R = 1.03 \times 10^6$.

Figure 21.- Continued.

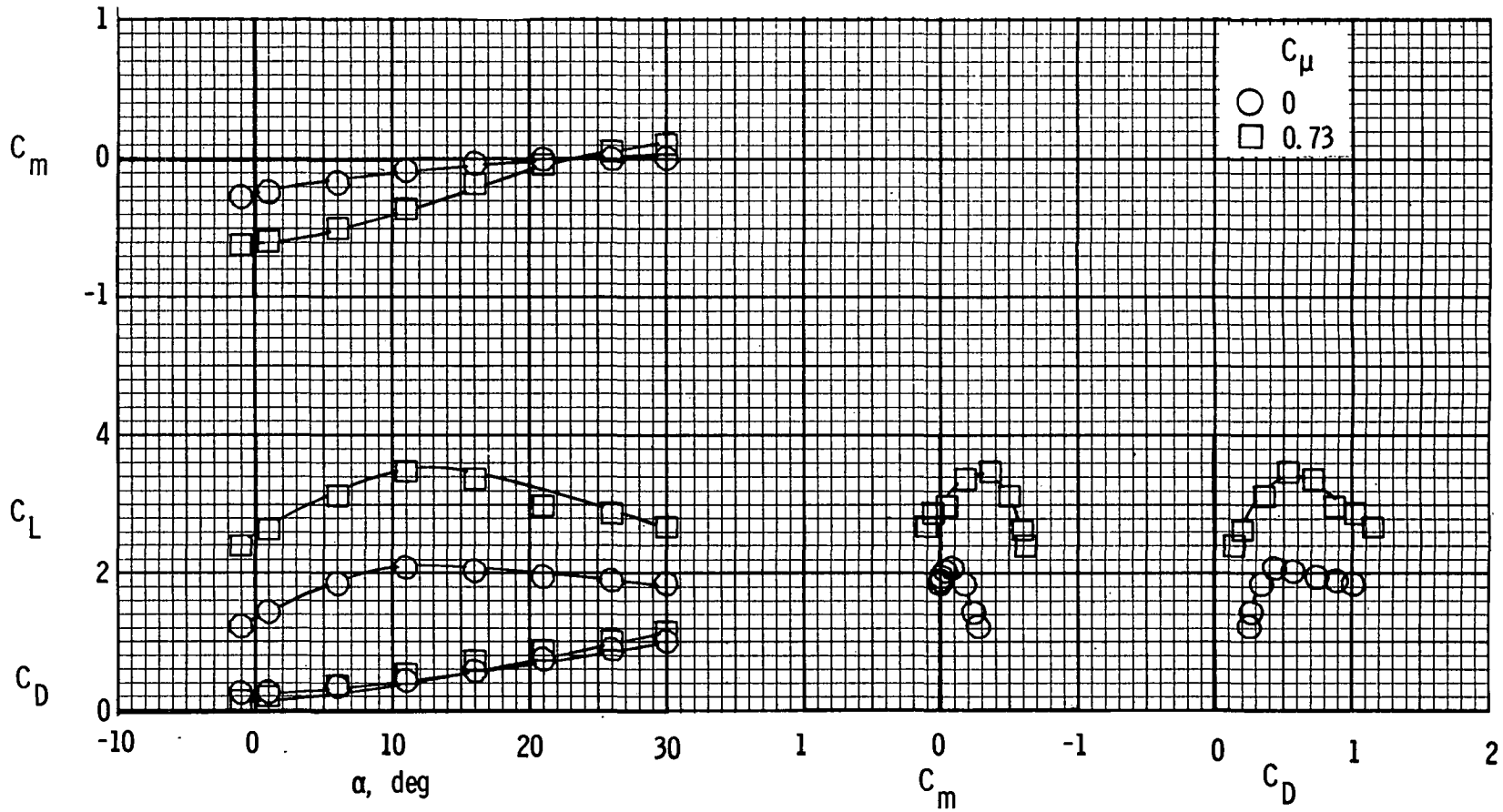

(f) Longitudinal characteristics. $R = 1.03 \times 10^6$.

Figure 21.- Continued.

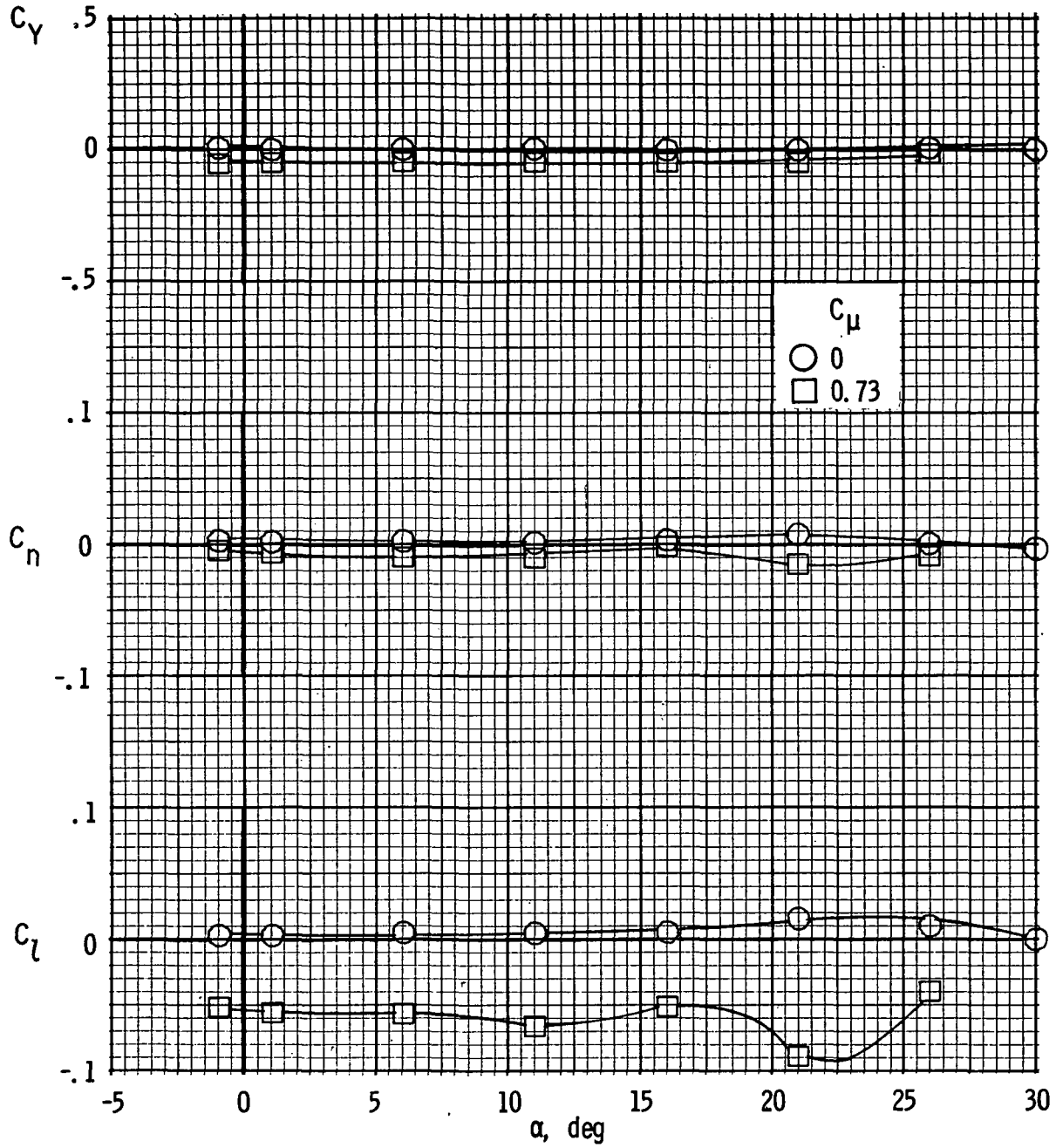

(g) Lateral characteristics. $R = 1.36 \times 10^6$.

Figure 21.- Continued.

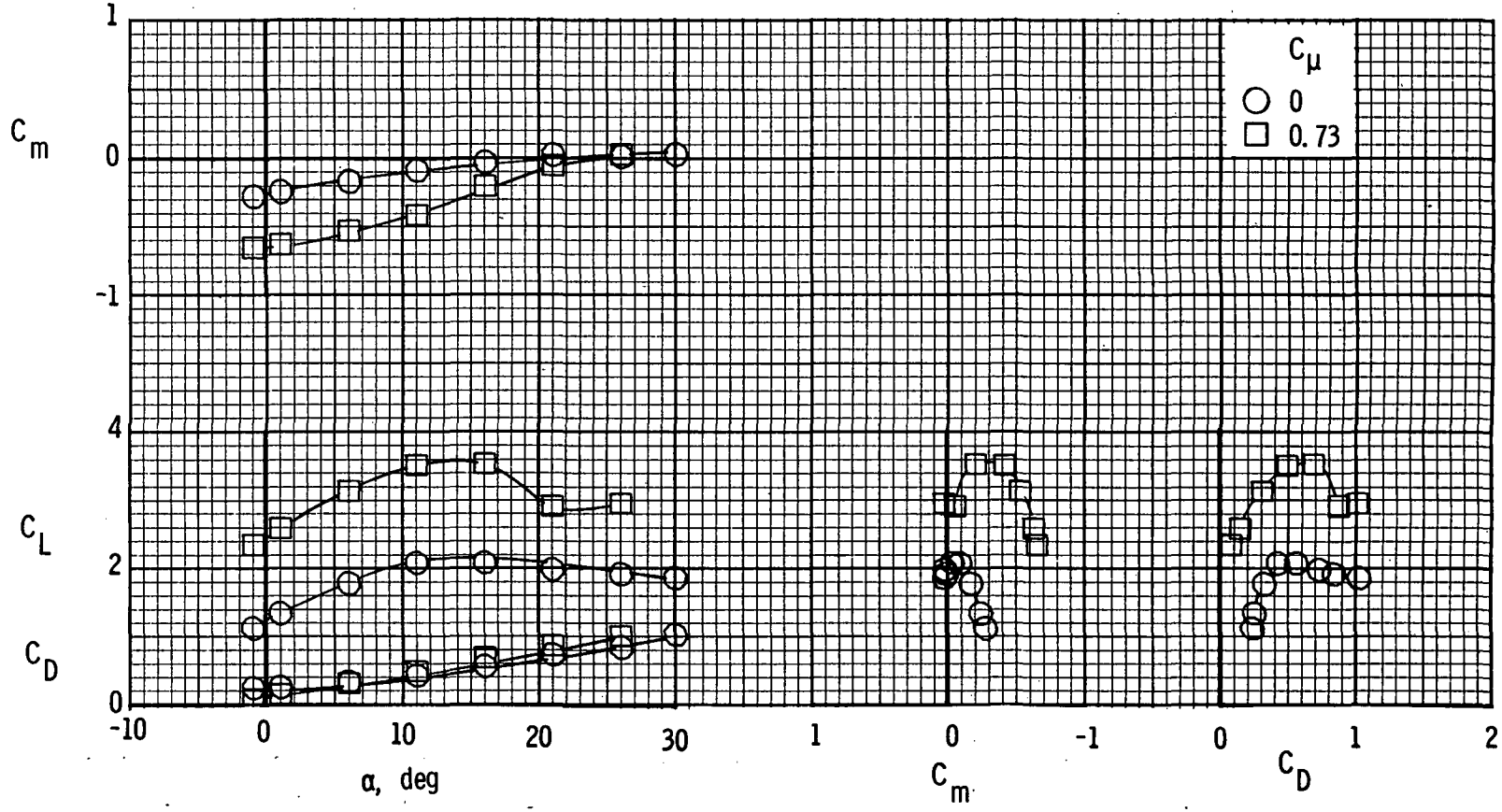

(h) Longitudinal characteristics. $R = 1.36 \times 10^6$.

Figure 21.- Concluded.

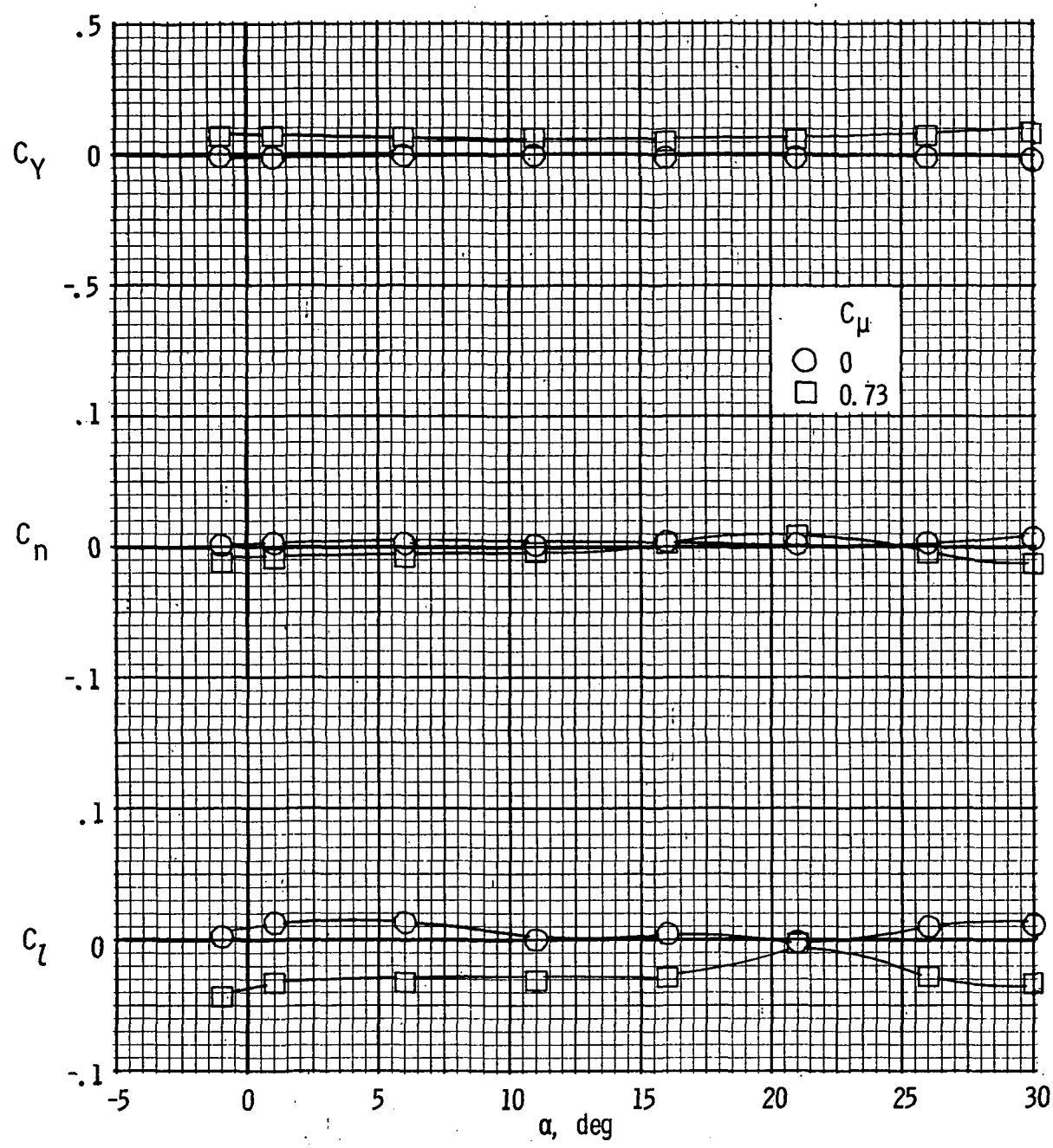

(a) Lateral characteristics. $R = 0.47 \times 10^6$.

Figure 22.- Longitudinal and lateral characteristics of model with left inboard engine not operating. 30-percent leading-edge flap; $\delta_{f1}/\delta_{f2} = 20^o/40^o$.

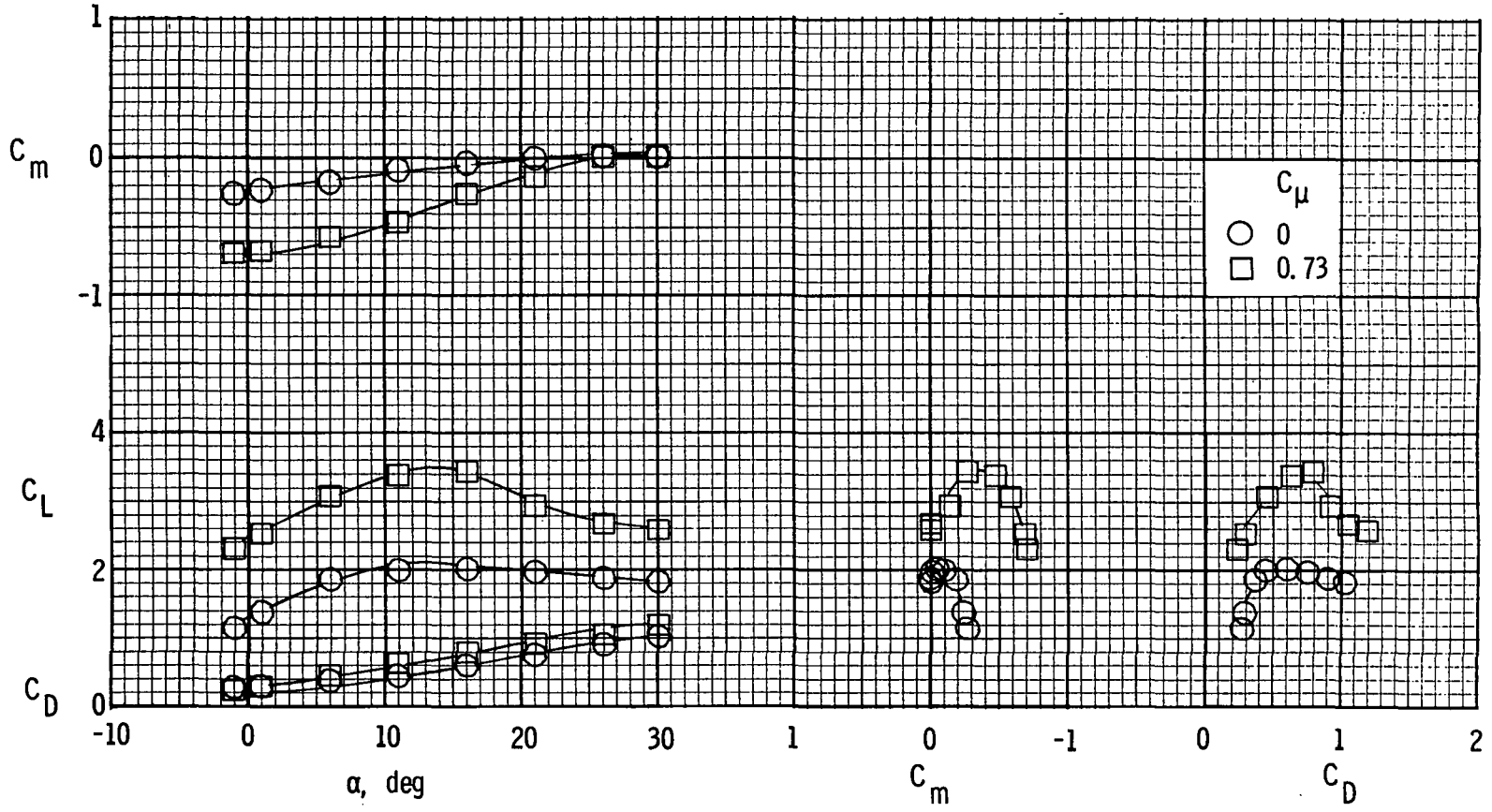

(b) Longitudinal characteristics. $R = 0.47 \times 10^6$.

Figure 22.- Continued.

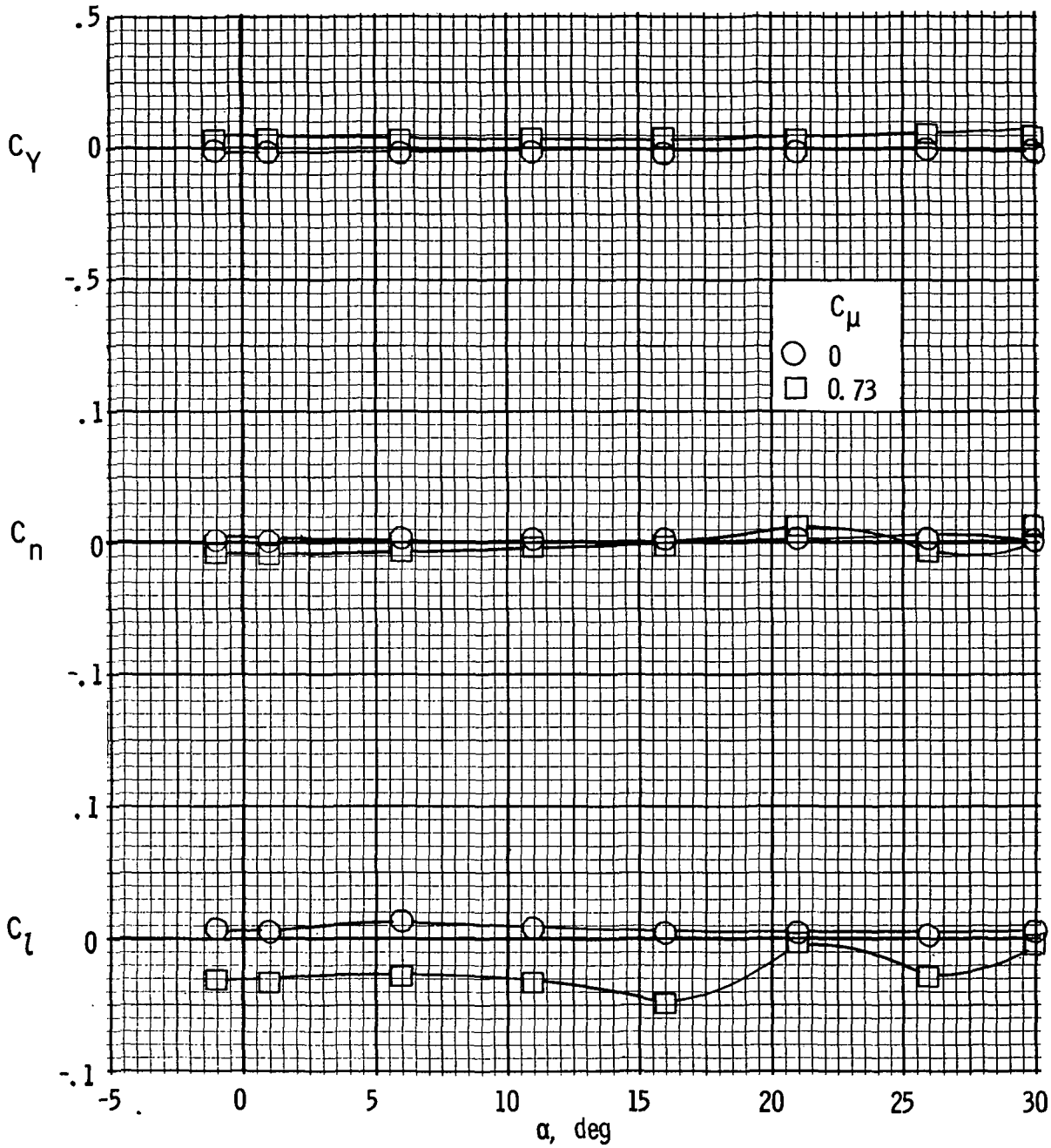

(c) Lateral characteristics. $R = 0.73 \times 10^6$.

Figure 22.- Continued.

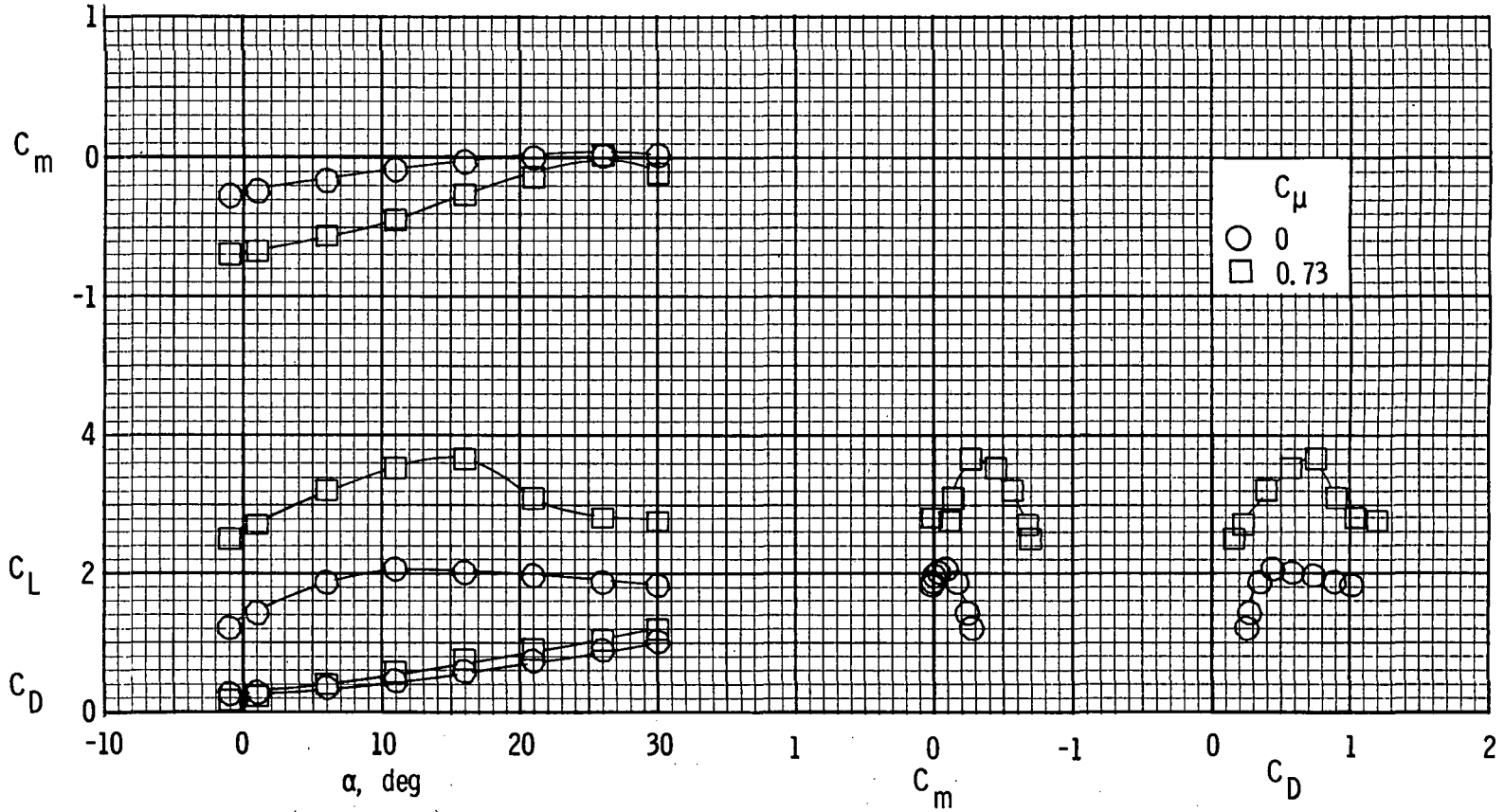

(d) Longitudinal characteristics. $R = 0.73 \times 10^6$.

Figure 22.- Continued.

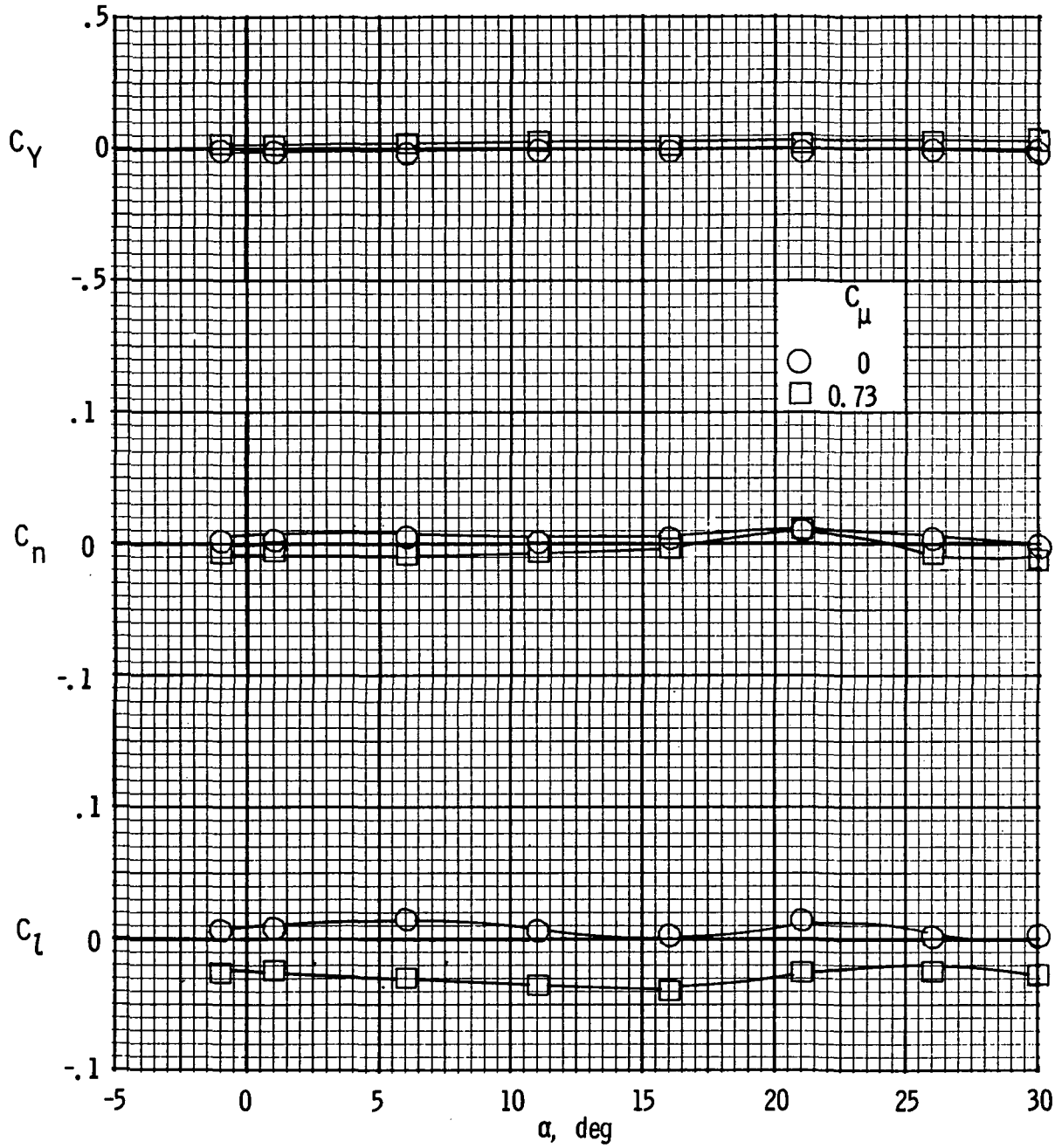

(e) Lateral characteristics. $R = 1.03 \times 10^6$.

Figure 22.- Continued.

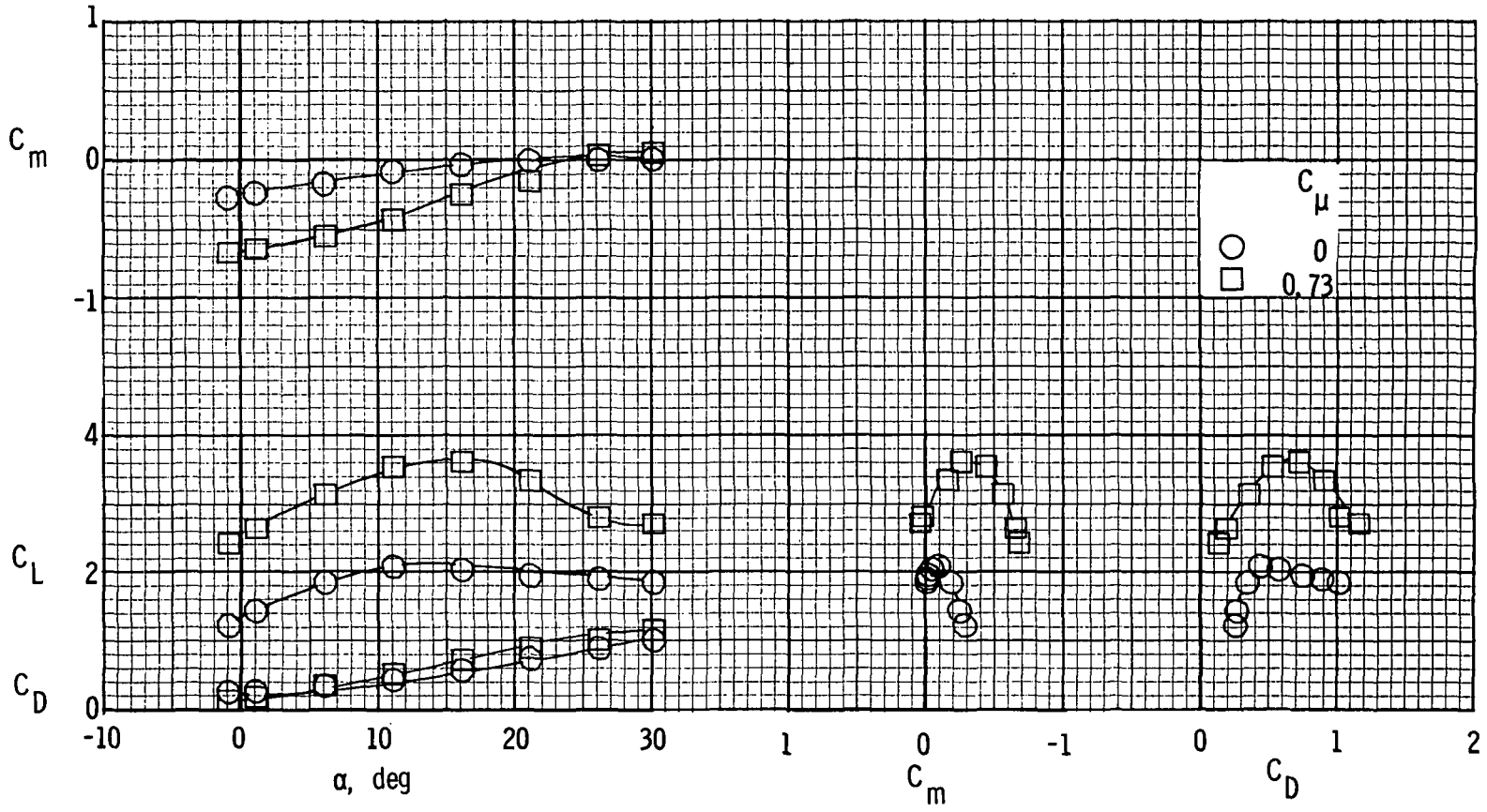

(f) Longitudinal characteristics. $R = 1.03 \times 10^6$.

Figure 22.- Continued.

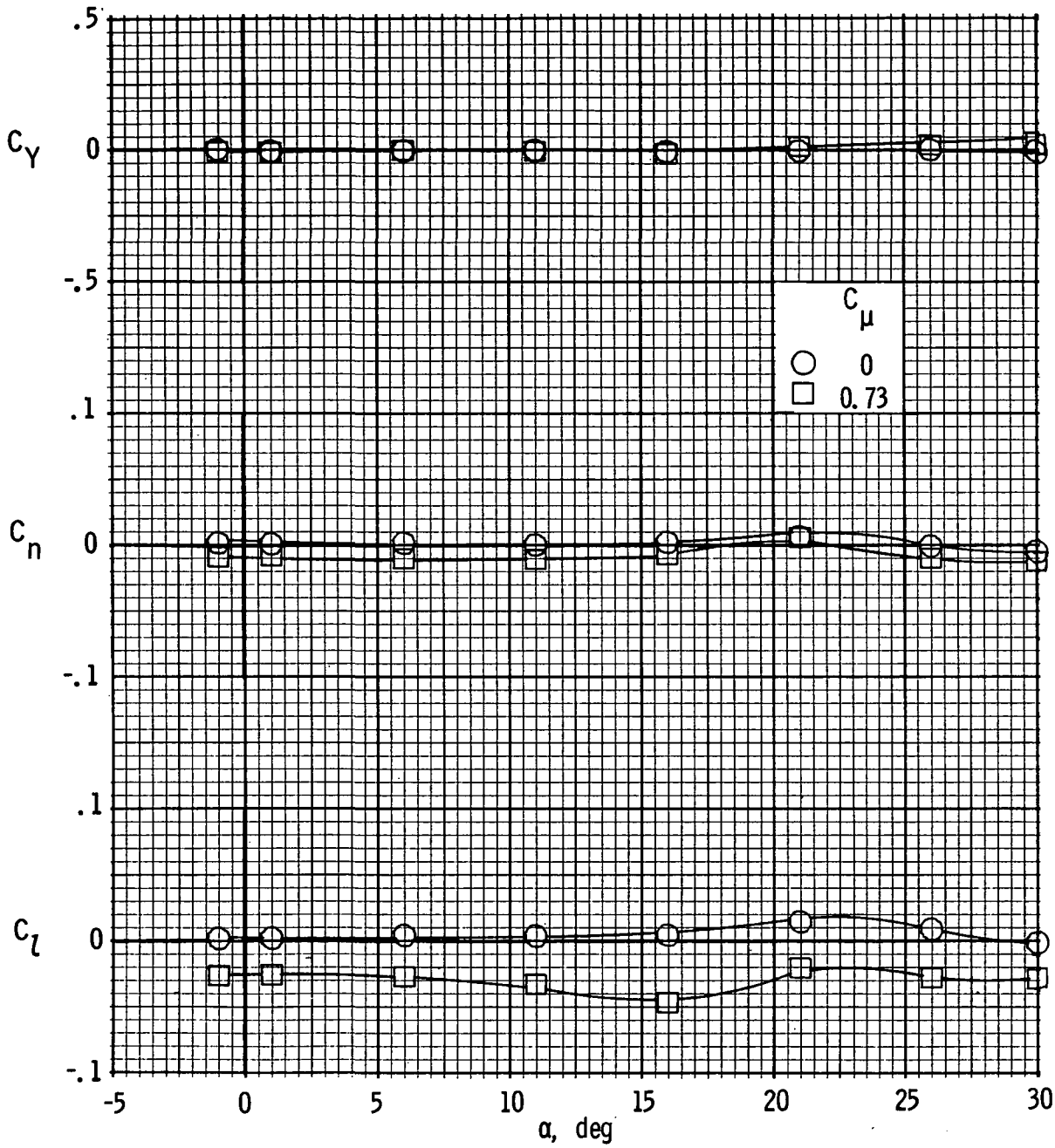

(g) Lateral characteristics. $R = 1.36 \times 10^6$.

Figure 22.- Continued.

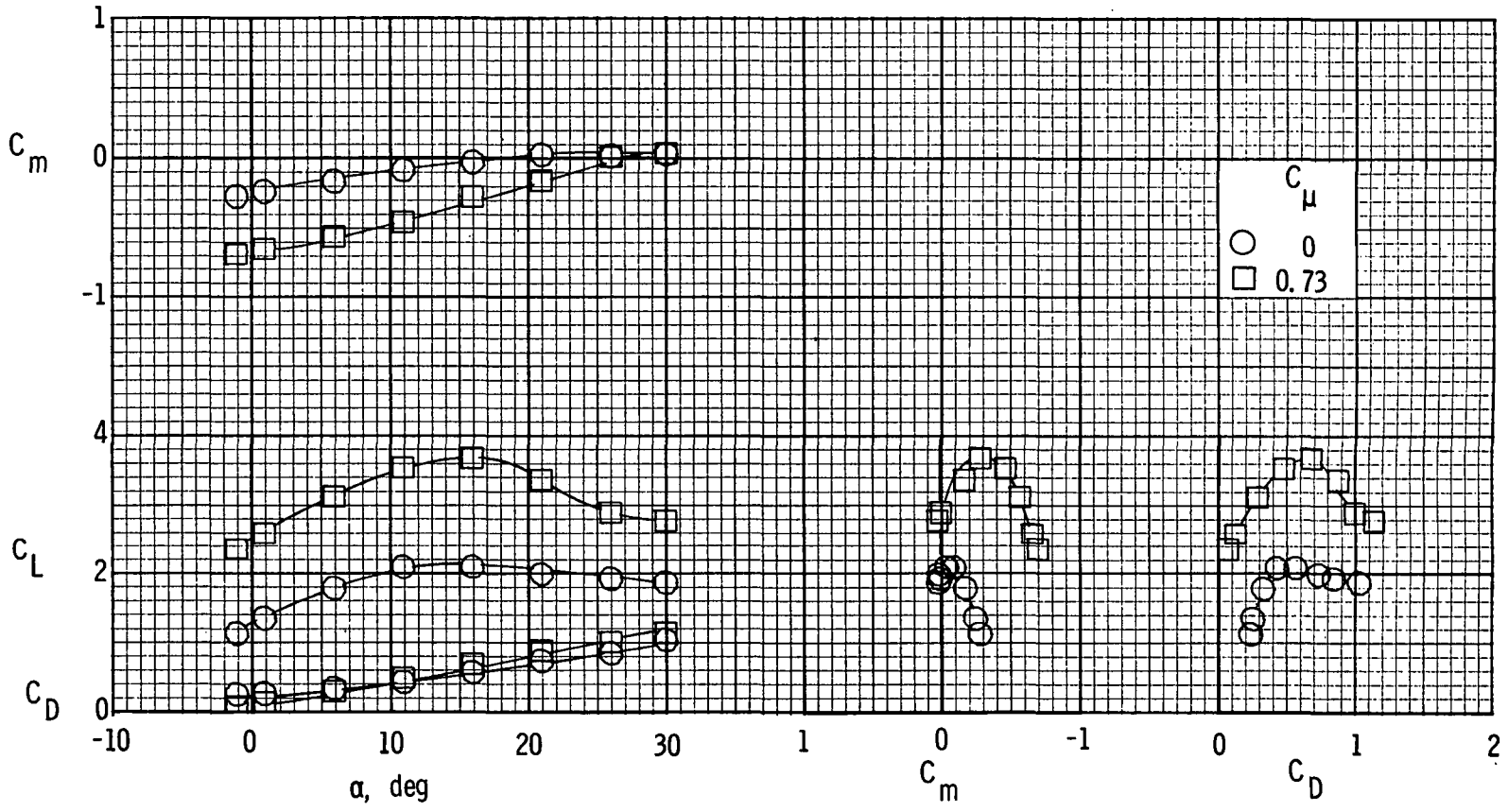

(h) Longitudinal characteristics. $R = 1.36 \times 10^6$.

Figure 22.- Concluded.

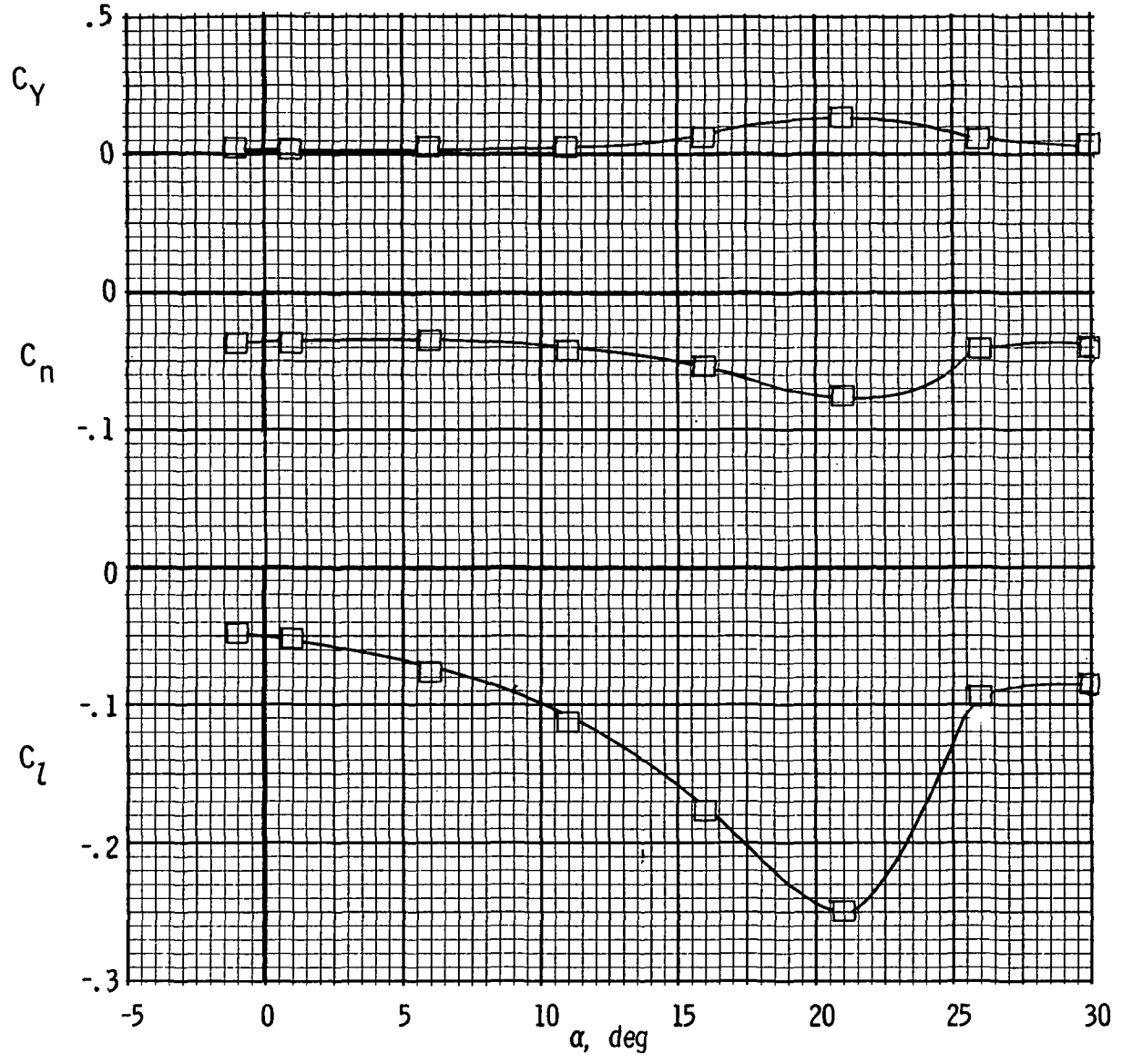

(a) Lateral characteristics. $R = 0.47 \times 10^6$; $C_\mu = 0.73$.

Figure 23.- Longitudinal and lateral characteristics of model with left outboard engine not operating and differential flap settings. 30-percent leading-edge flap; $\left(\delta_{f1}/\delta_{f2}\right)_R = 30^o/50^o$; $\left(\delta_{f1}/\delta_{f2}\right)_L = 30^o/70^o$.

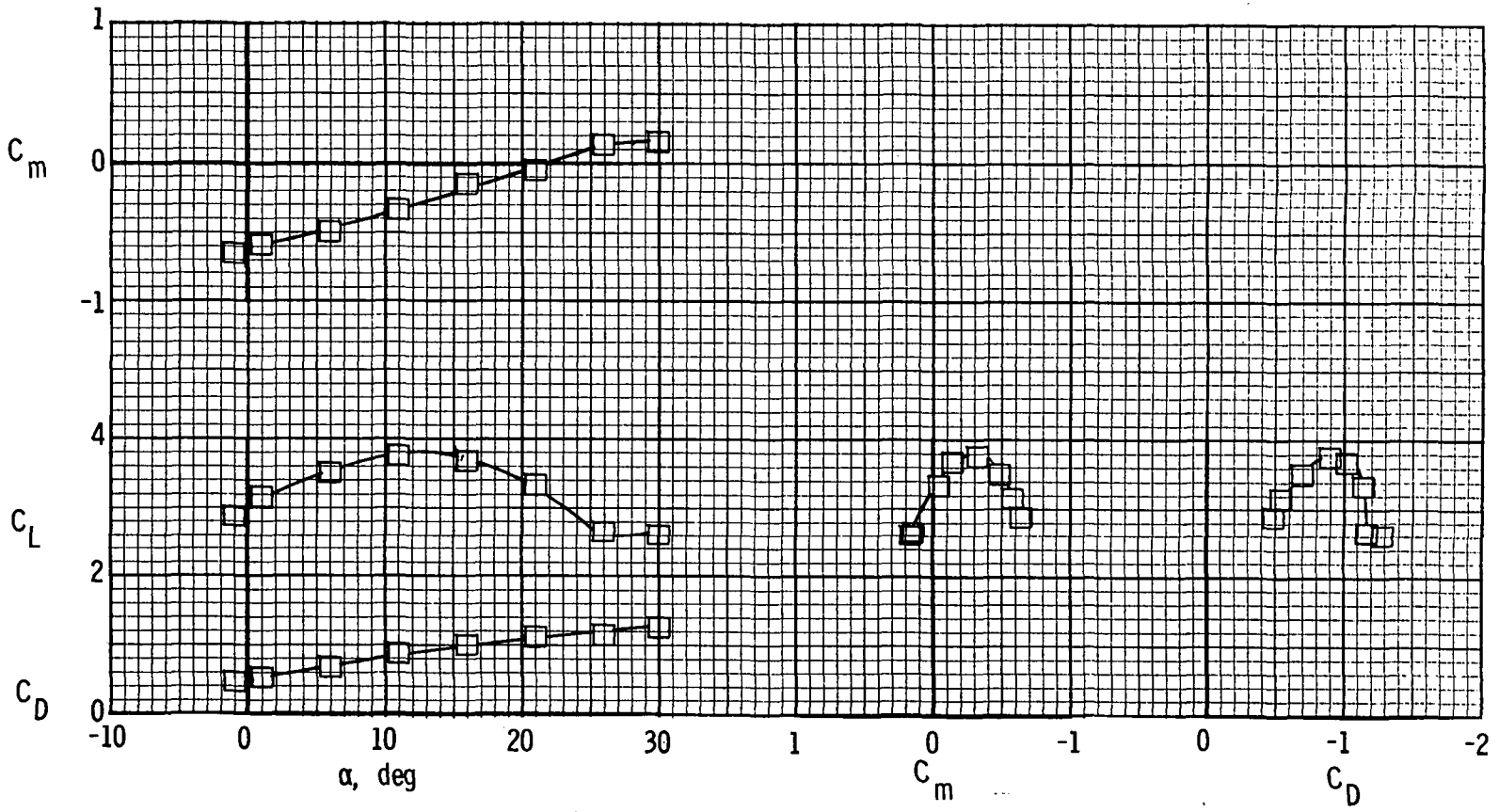

(b) Longitudinal characteristics. $R = 0.47 \times 10^6$; $C_\mu = 0.73$.

Figure 23.- Continued.

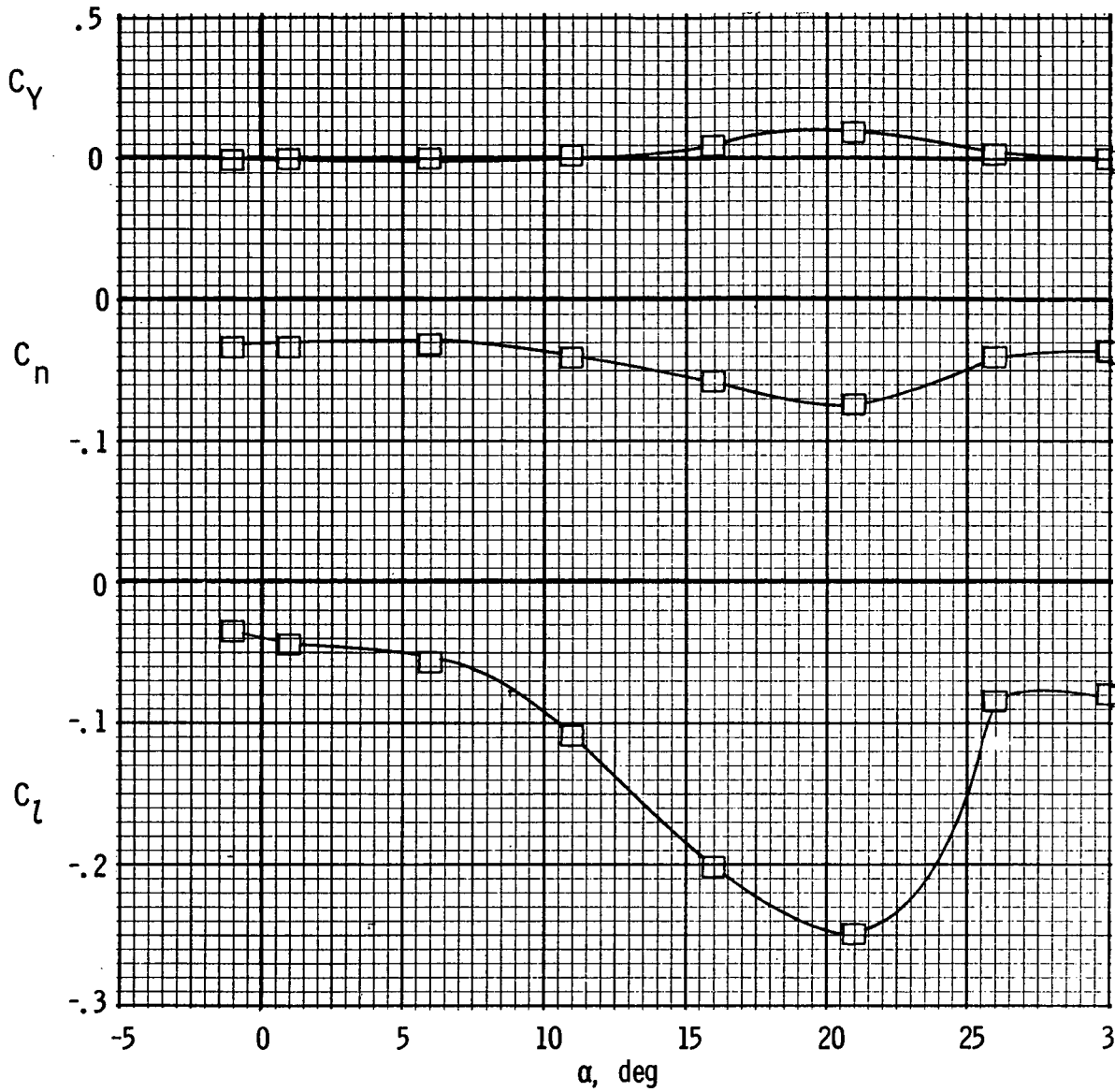

(c) Lateral characteristics. $R = 0.73 \times 10^6$; $C_\mu = 0.73$.

Figure 23.- Continued.

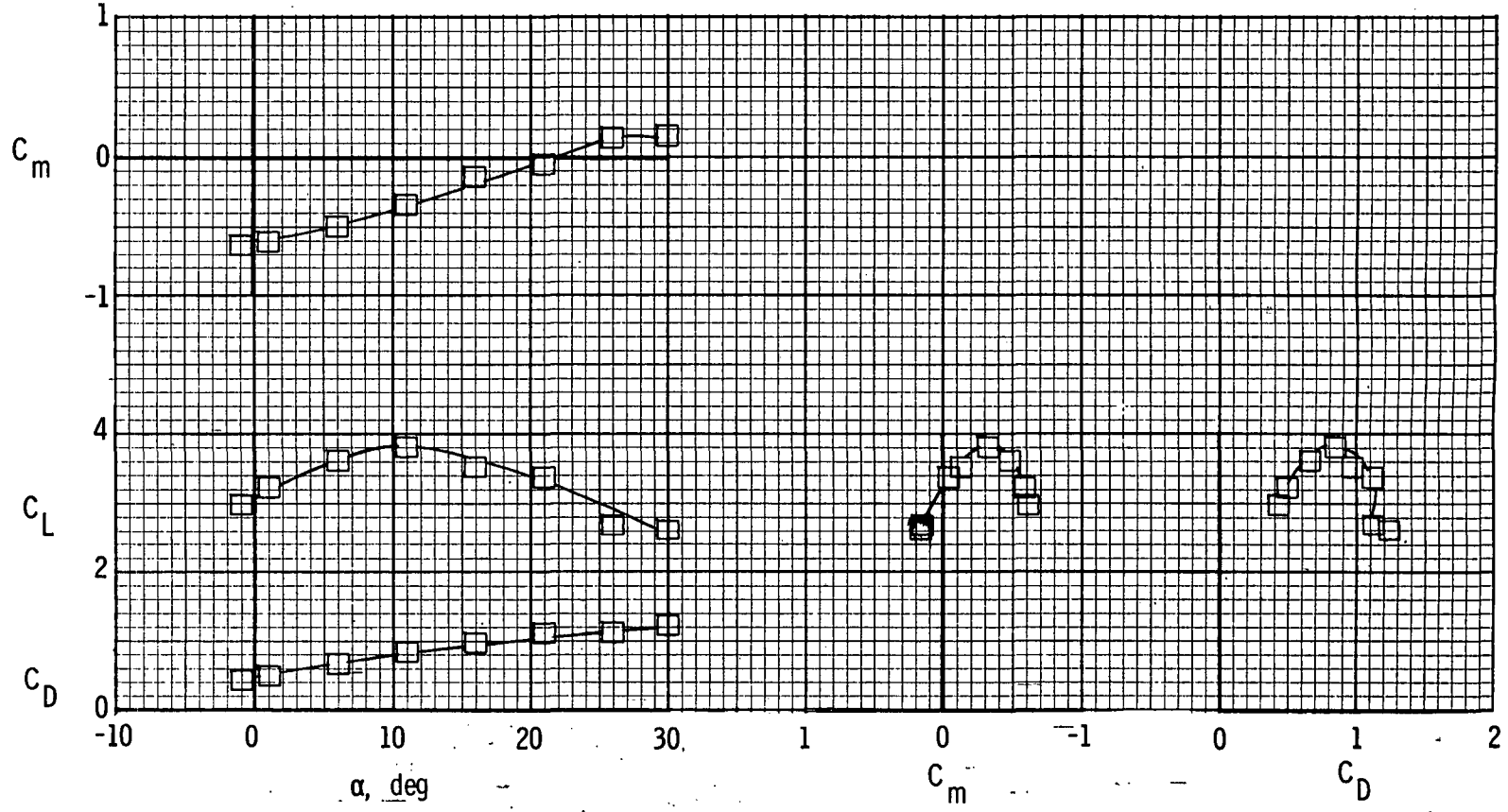

(d) Longitudinal characteristics. $R = 0.73 \times 10^6$; $C_\mu = 0.73$.

Figure 23.- Continued.

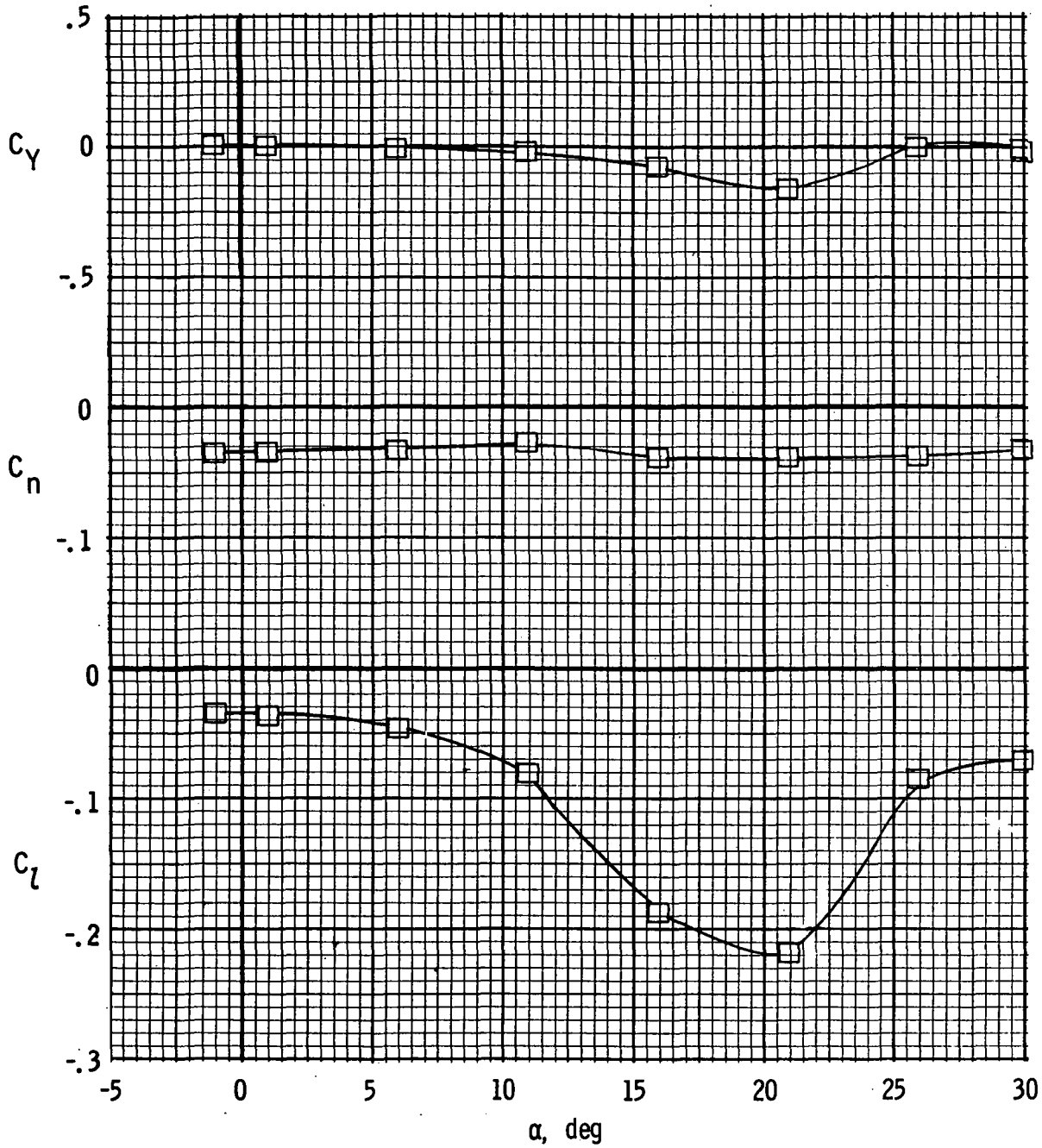

(e) Lateral characteristics. $R = 1.03 \times 10^6$; $C_\mu = 0.73$.

Figure 23.- Continued.

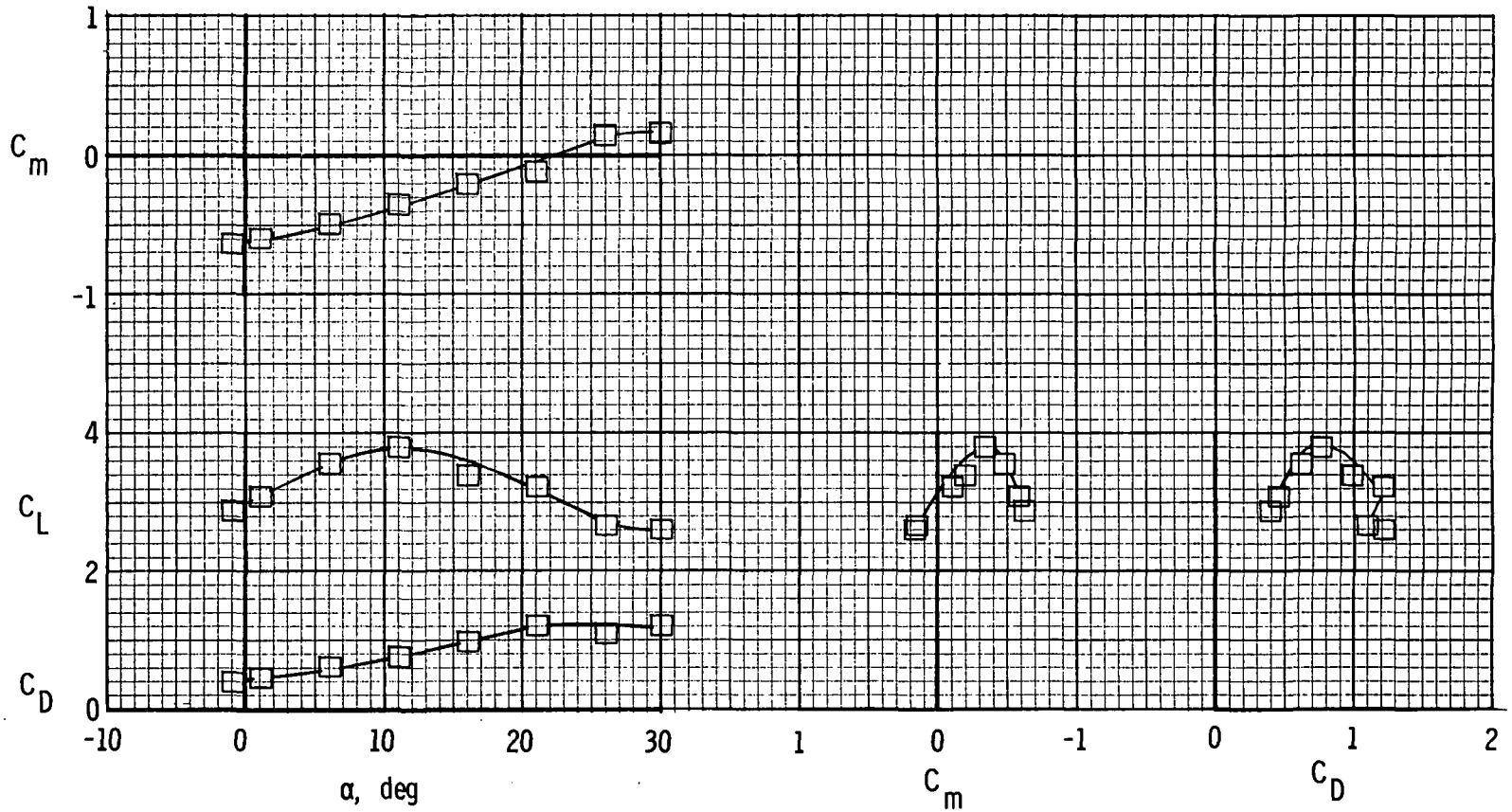

(f) Longitudinal characteristics. $R = 1.03 \times 10^6$; $C_\mu = 0.73$.

Figure 23.- Continued.

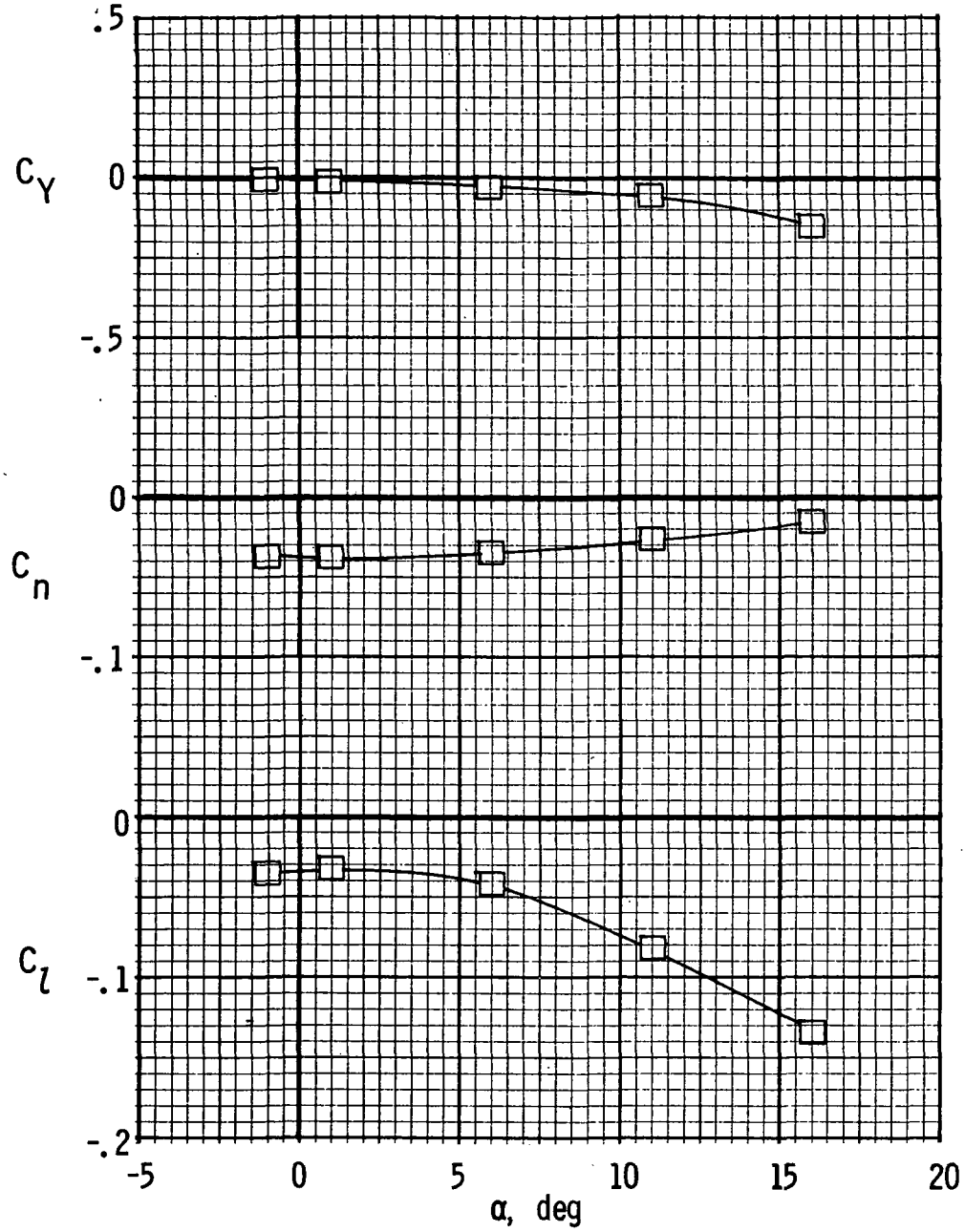

(g) Lateral characteristics. $R = 1.36 \times 10^6$; $C_\mu = 0.73$.

Figure 23.- Continued.

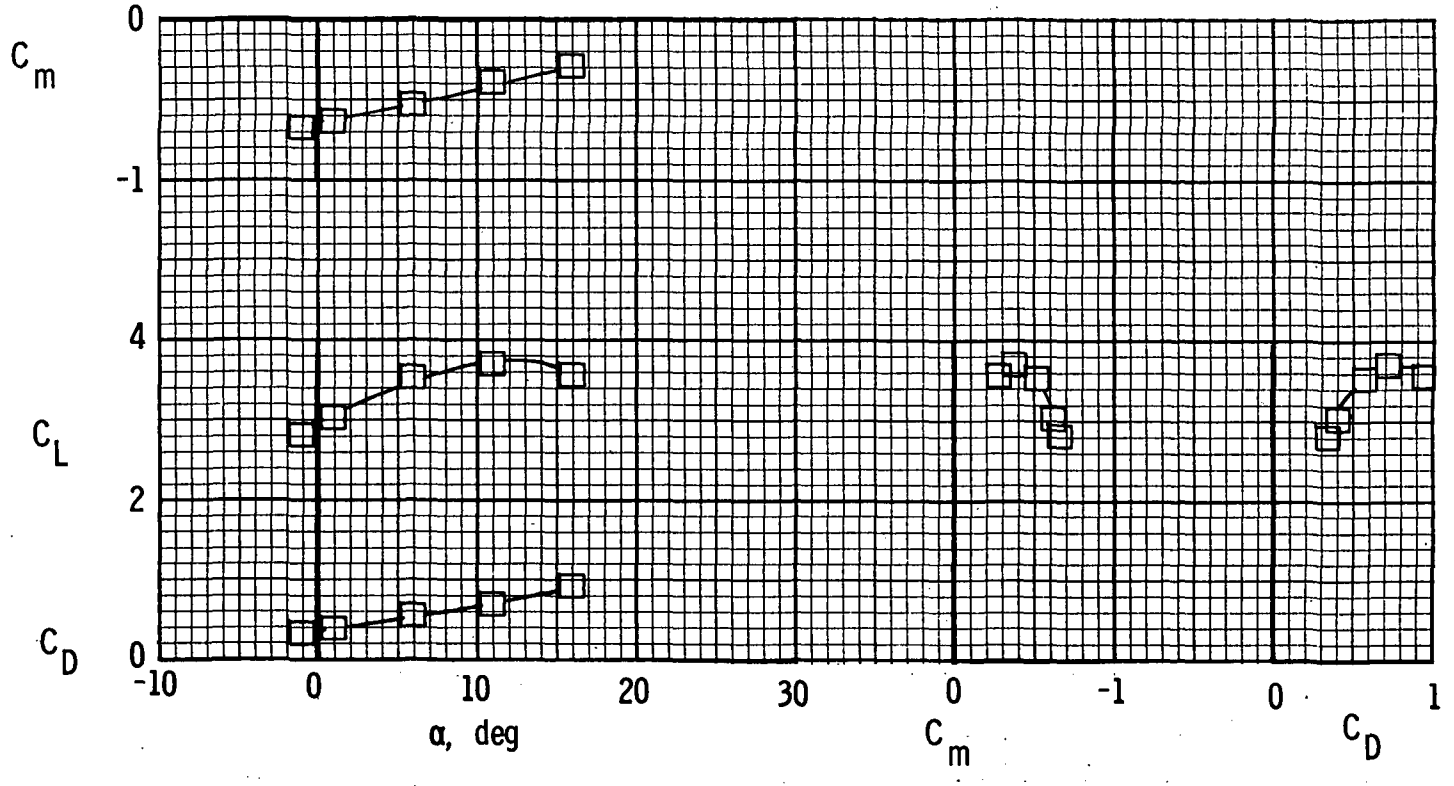

(h) Longitudinal characteristics. $R = 1.36 \times 10^6$; $C_\mu = 0.73$.

Figure 23.- Concluded.

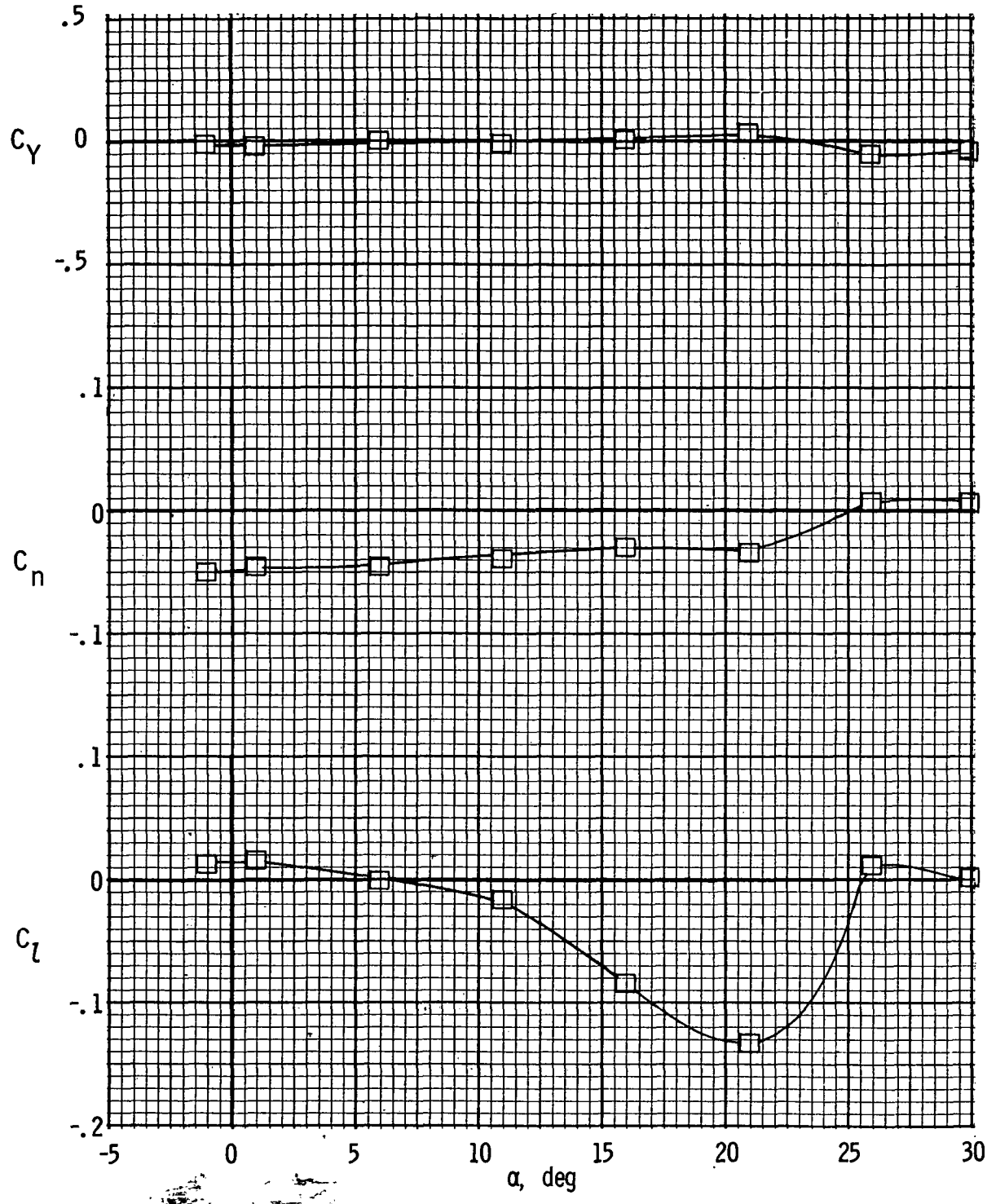

(a) Lateral characteristics. $R = 0.47 \times 10^6$; $C_\mu = 0.73$.

Figure 24.- Longitudinal and lateral characteristics of model with left inboard engine not operating and differential flap settings. 30-percent leading-edge flap; $(\delta_{f1}/\delta_{f2})_R = 30^o/50^o$; $(\delta_{f1}/\delta_{f2})_L = 30^o/70^o$.

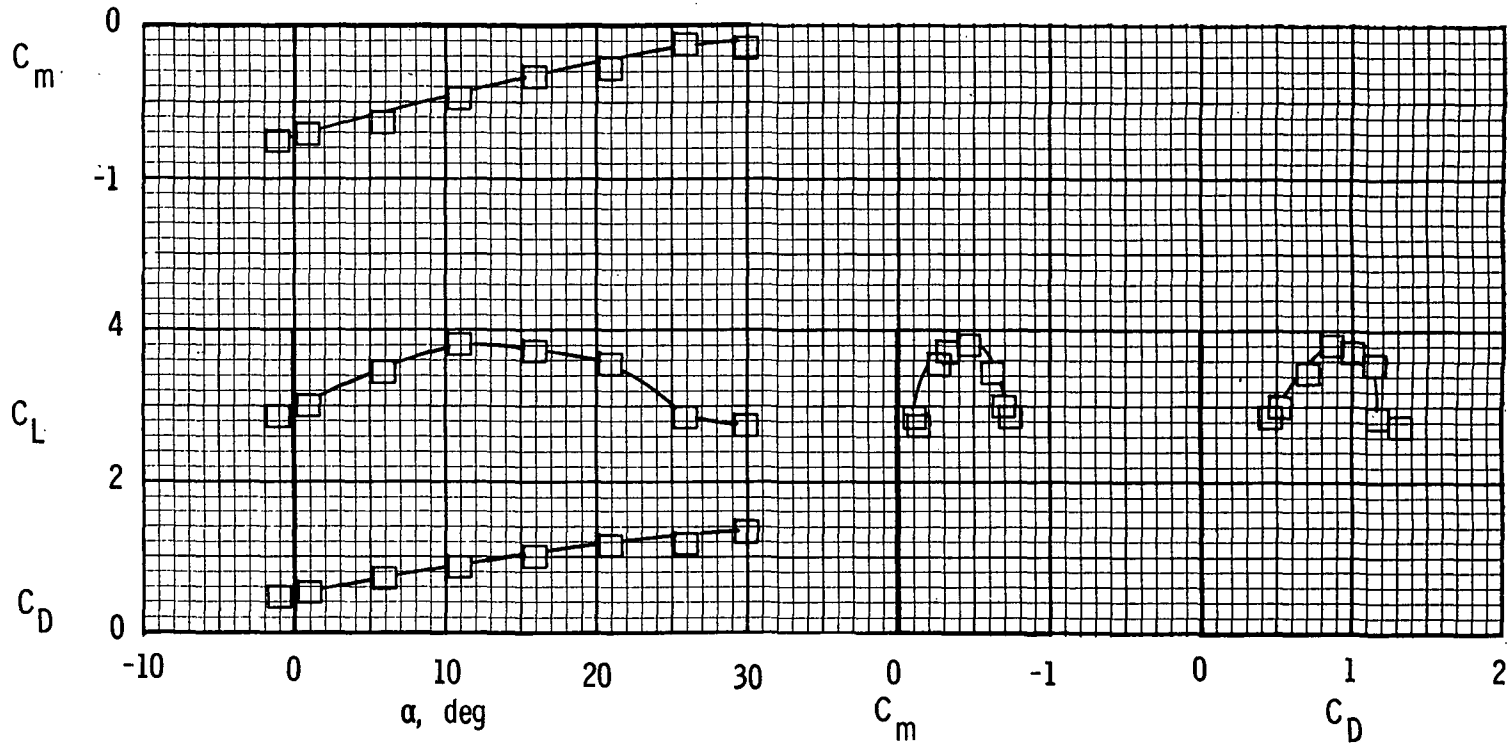

(b) Longitudinal characteristics. $R = 0.47 \times 10^6$; $C_\mu = 0.73$.

Figure 24.- Continued.

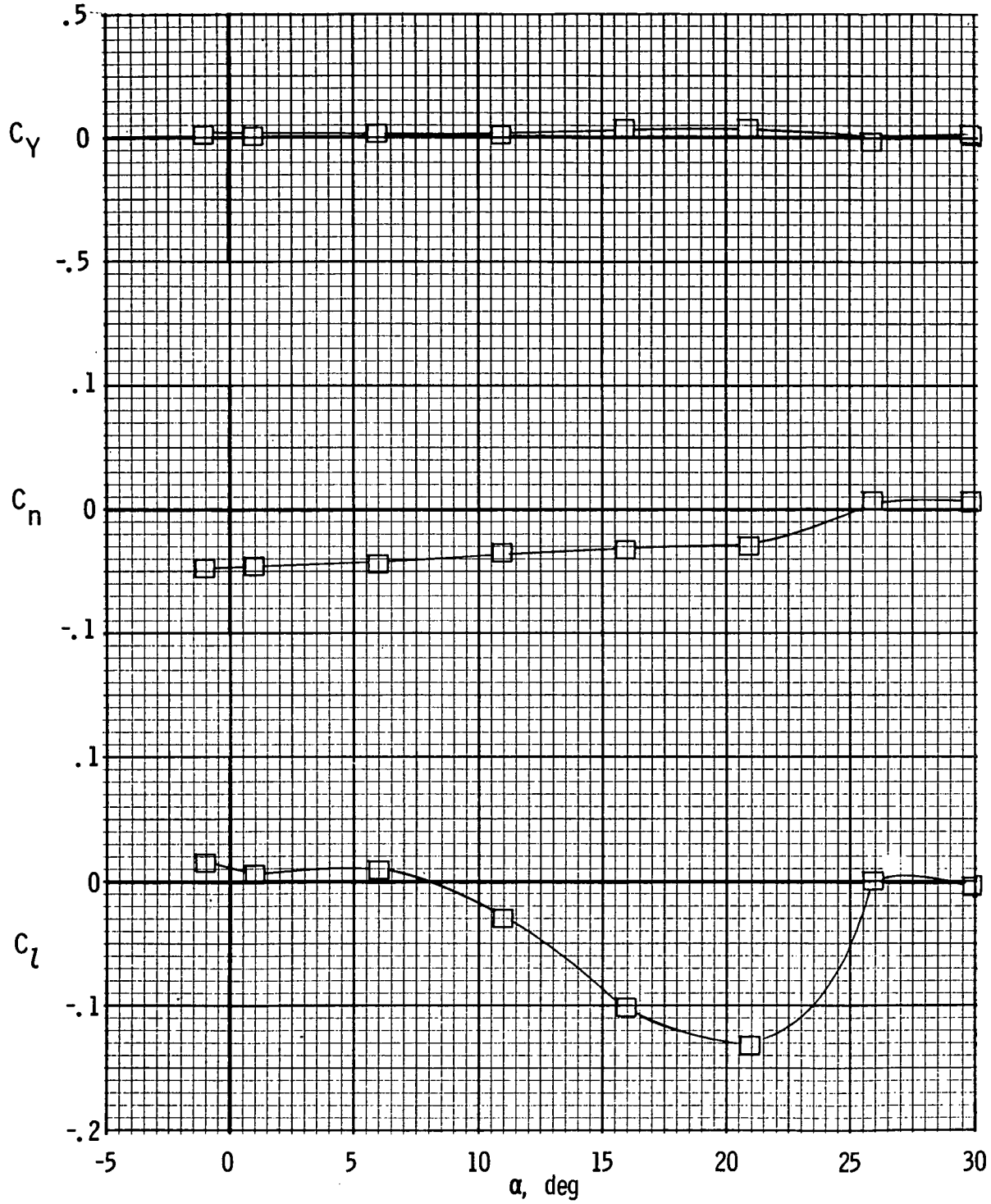

(c) Lateral characteristics. $R = 0.73 \times 10^6$; $C_\mu = 0.73$.

Figure 24.- Continued.

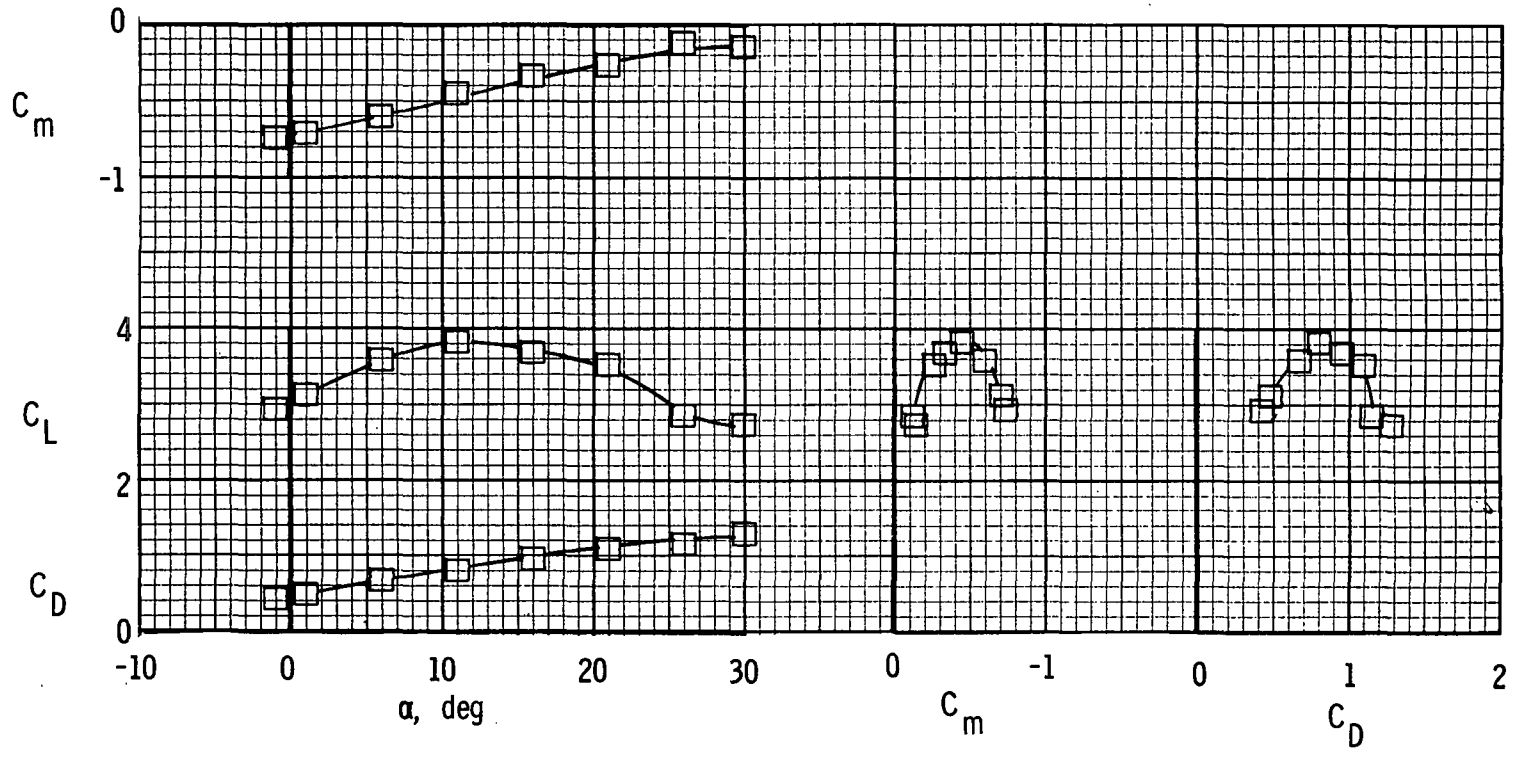

(d) Longitudinal characteristics. $R = 0.73 \times 10^6$; $C_\mu = 0.73$.

Figure 24.- Continued.

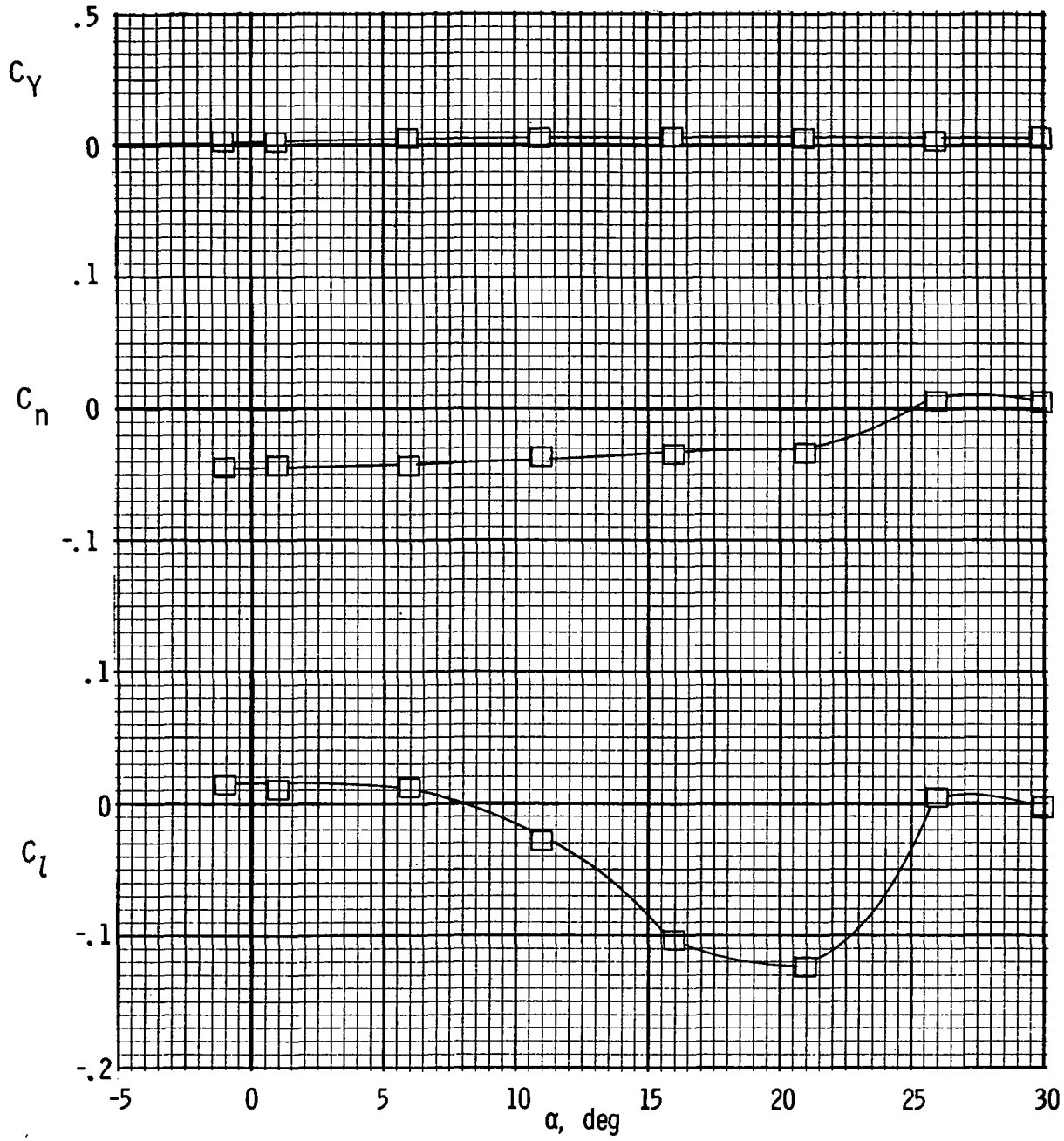

(e) Lateral characteristics. $R = 1.03 \times 10^6$; $C_\mu = 0.73$.

Figure 24.- Continued.

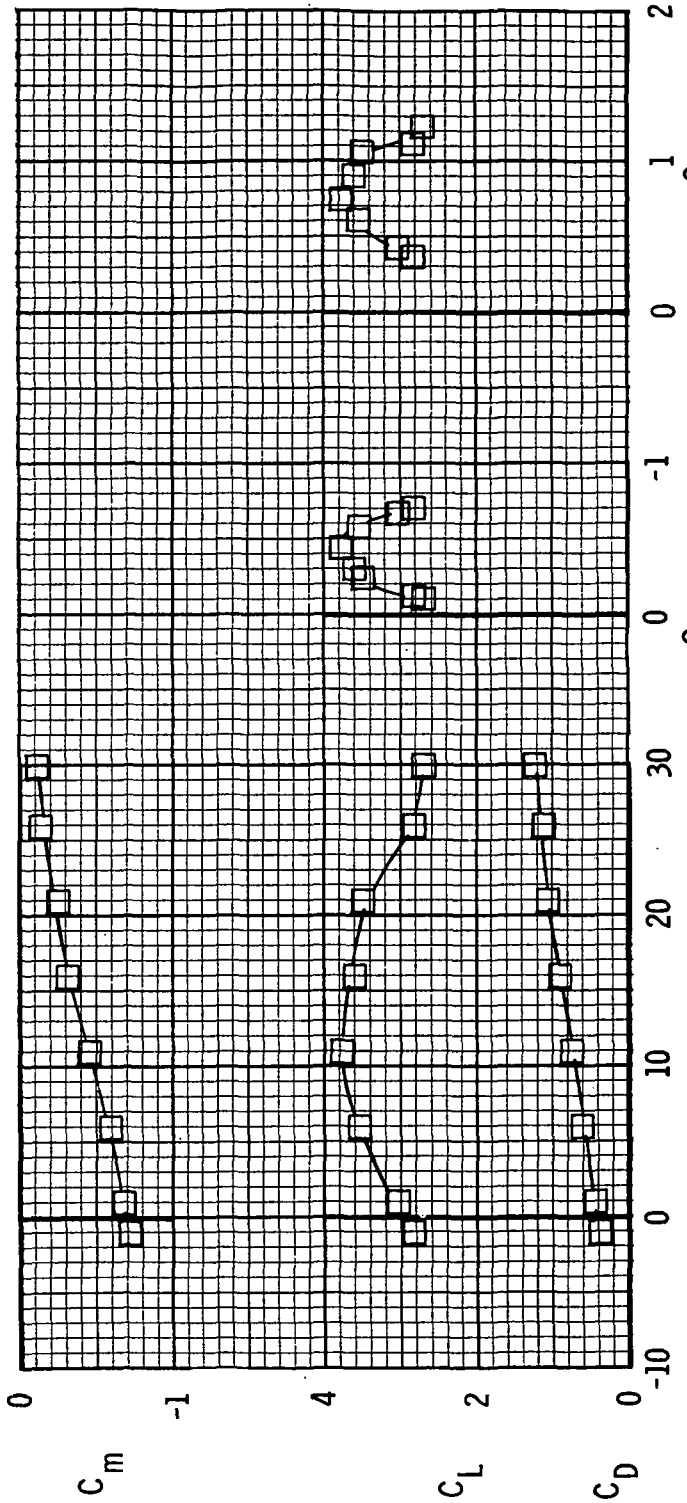

(f) Longitudinal characteristics. $R = 1.03 \times 10^6$; $C_\mu = 0.73$.

Figure 24.- Concluded.

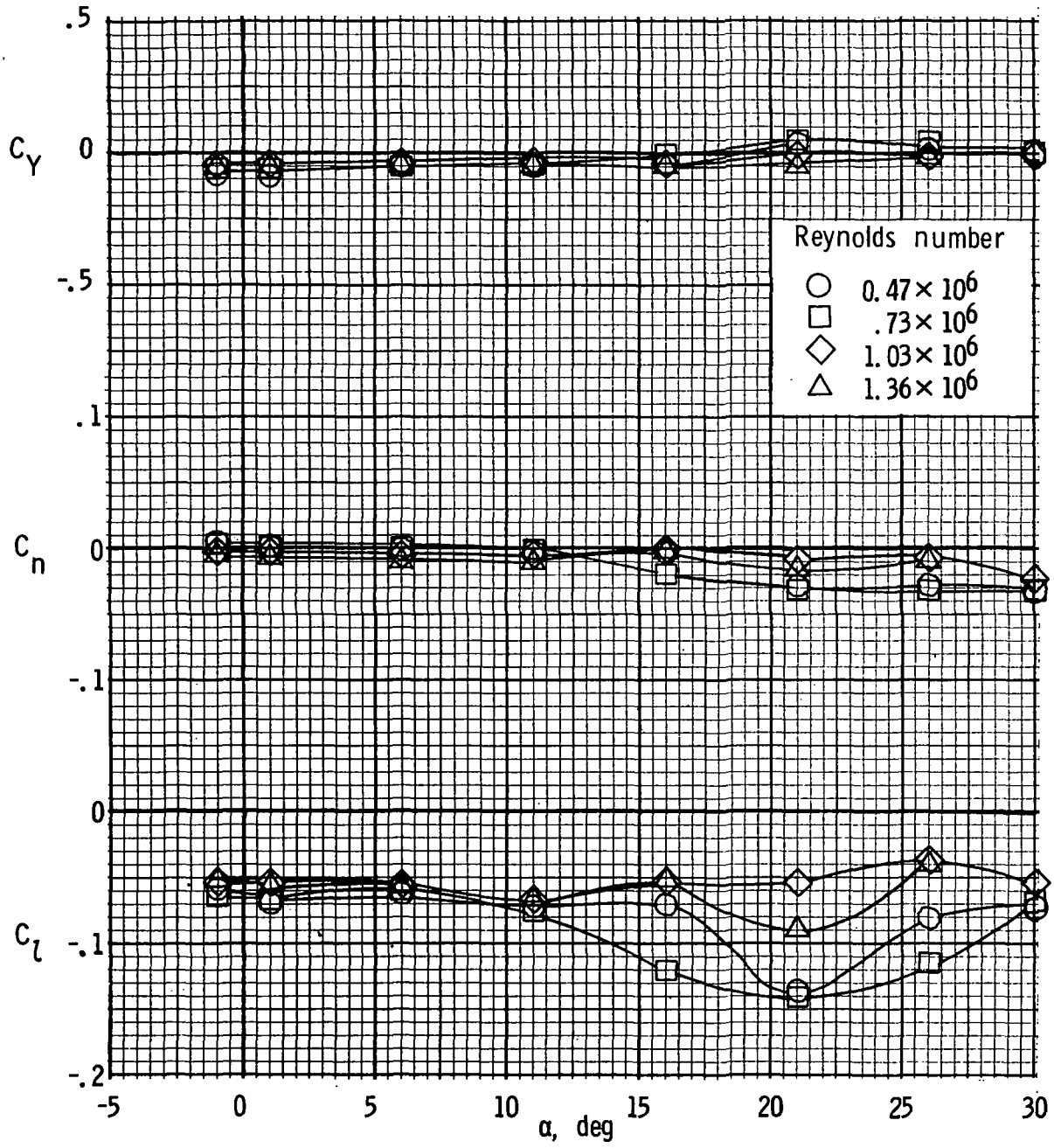

(a) Lateral characteristics.

Figure 25.- Effect of Reynolds number on longitudinal and lateral characteristics with left outboard engine not operating. 30-percent leading-edge flap; $\delta_{f1}/\delta_{f2} = 20^o/40^o$; $C_\mu = 0.73$.

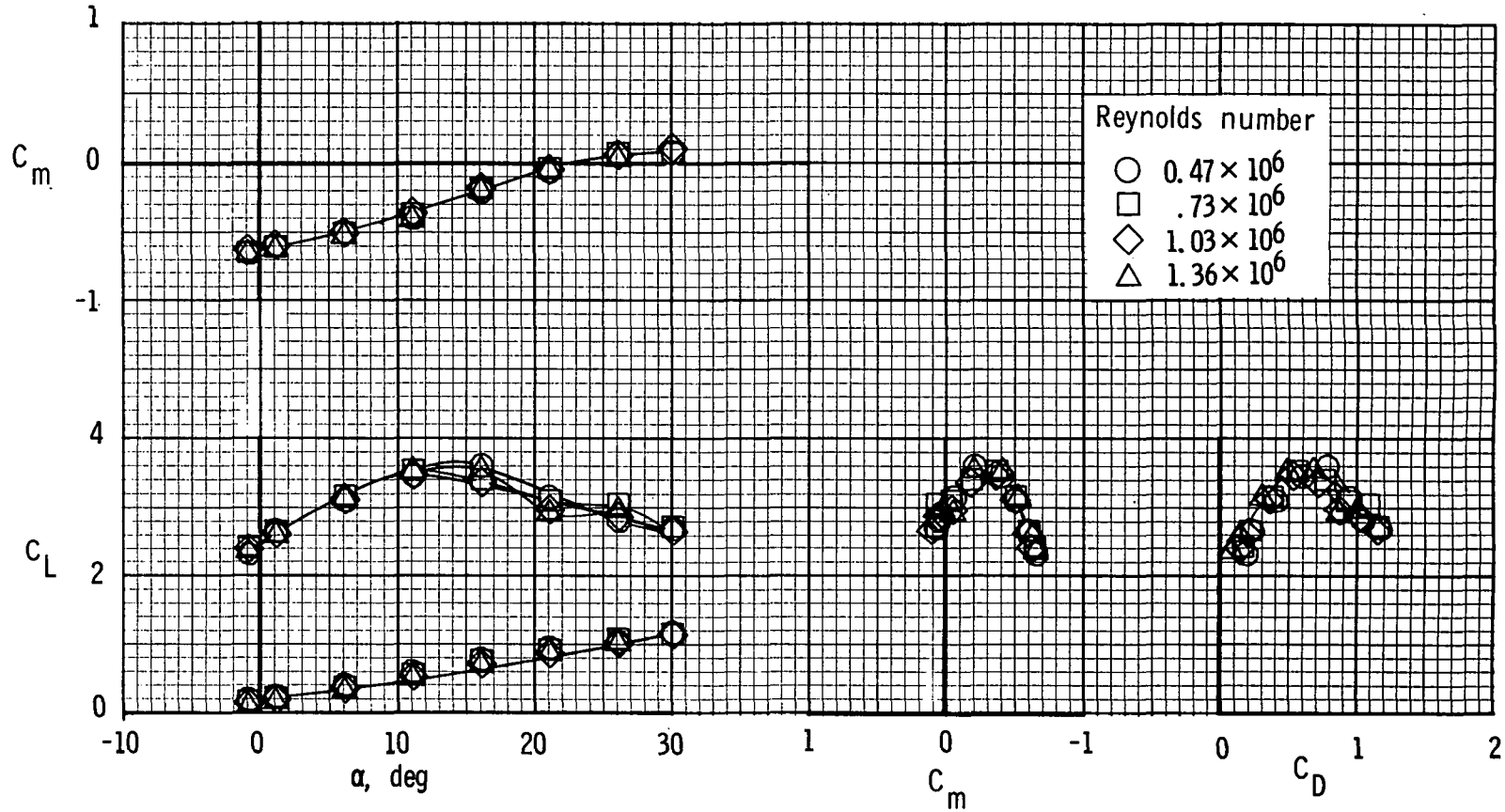

(b) Longitudinal characteristics.

Figure 25.- Concluded.

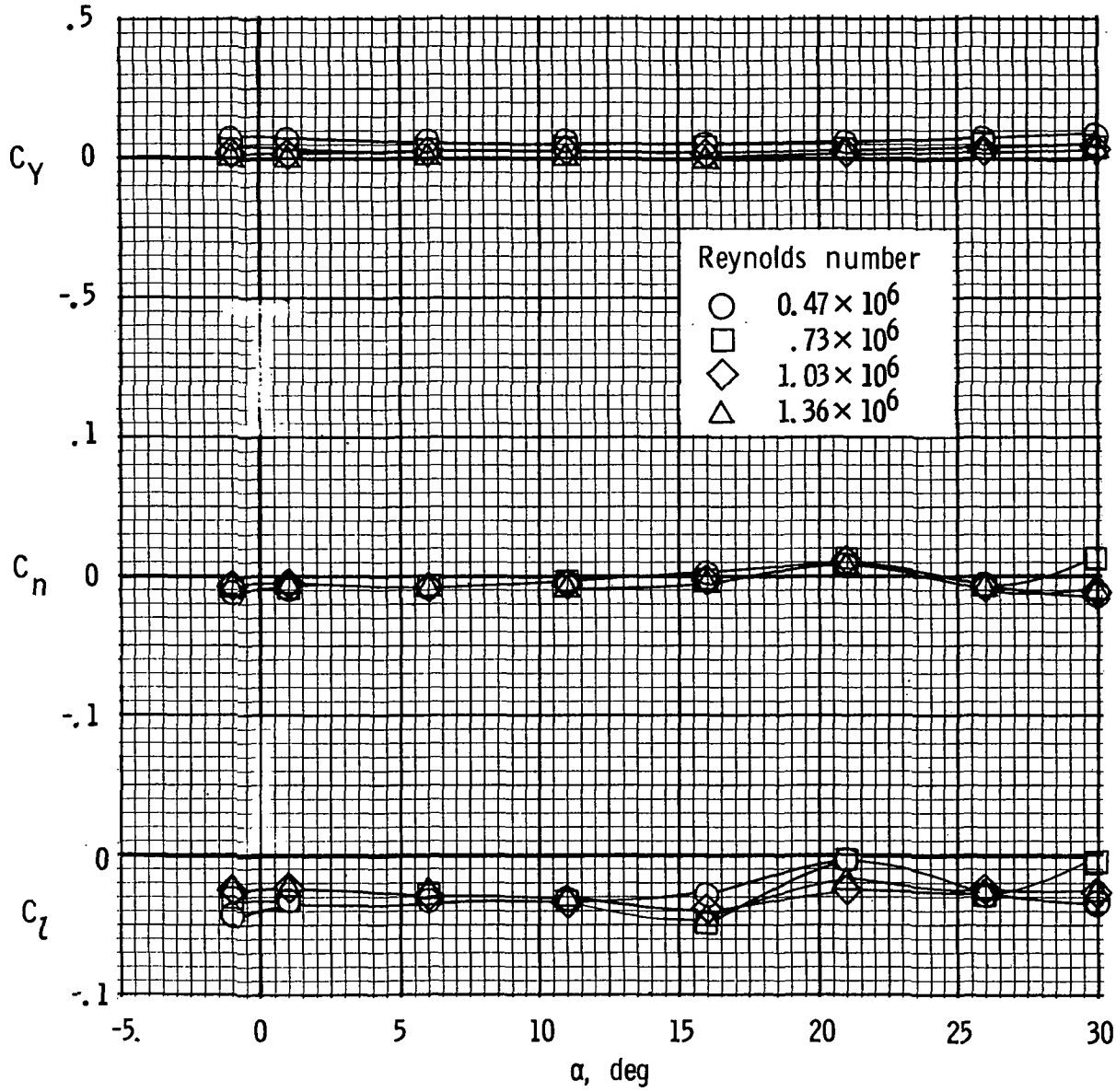

(a) Lateral characteristics.

Figure 26.- Effect of Reynolds number on longitudinal and lateral characteristics with left inboard engine not operating. 30-percent leading-edge flap; $\delta_{f1}/\delta_{f2} = 20^o/40^o$; $C_\mu = 0.73$.

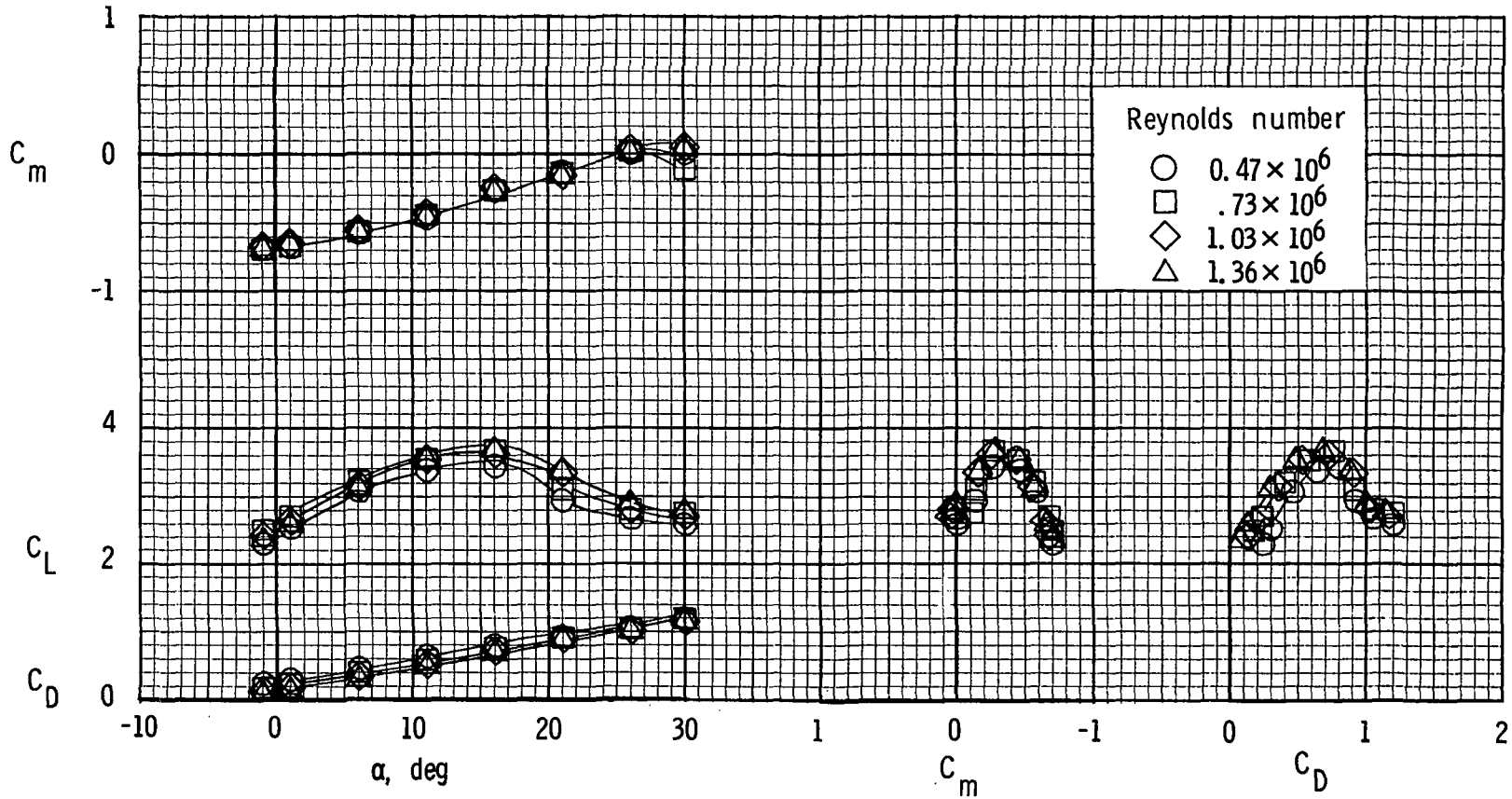

(b) Longitudinal characteristics.

Figure 26.- Concluded.

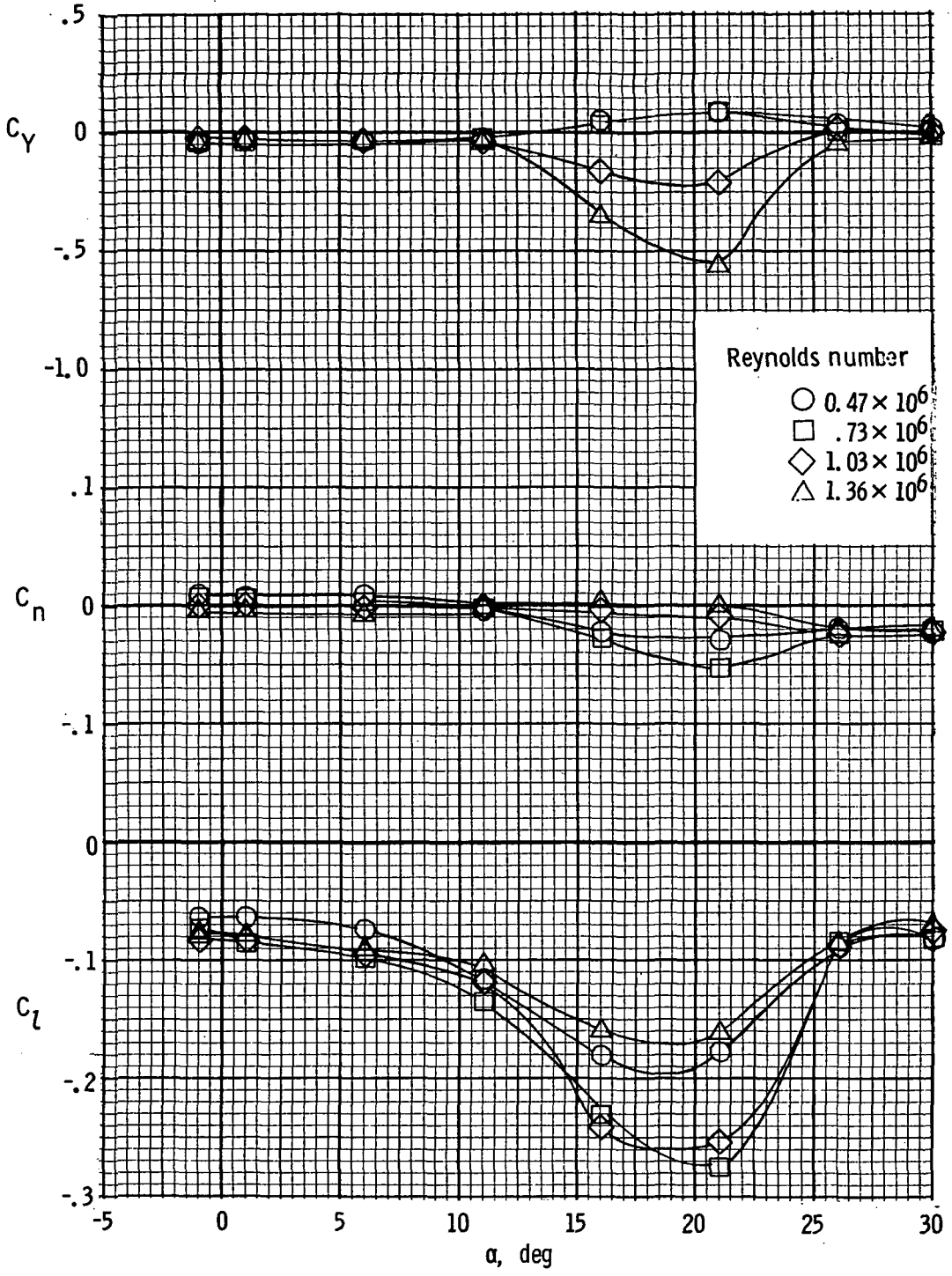

(a) Lateral characteristics. $C_\mu = 0.73$.

Figure 27.- Effect of Reynolds number on longitudinal and lateral characteristics with left outboard engine not operating. 30-percent leading-edge flap; $\delta_{f1}/\delta_{f2} = 30^o/60^o$.

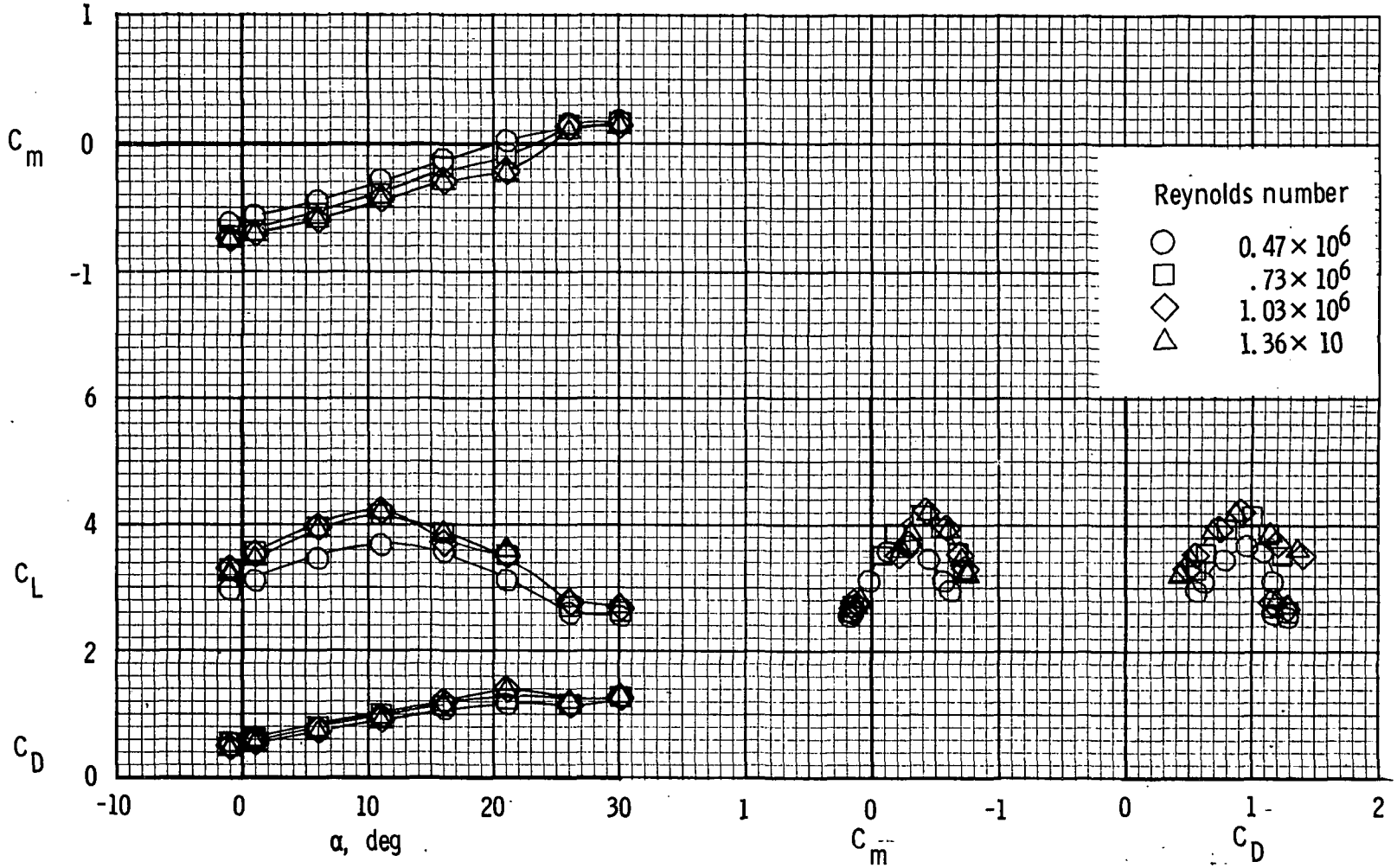

(b) Longitudinal characteristics. $C_\mu = 0.73$.

Figure 27.- Continued.

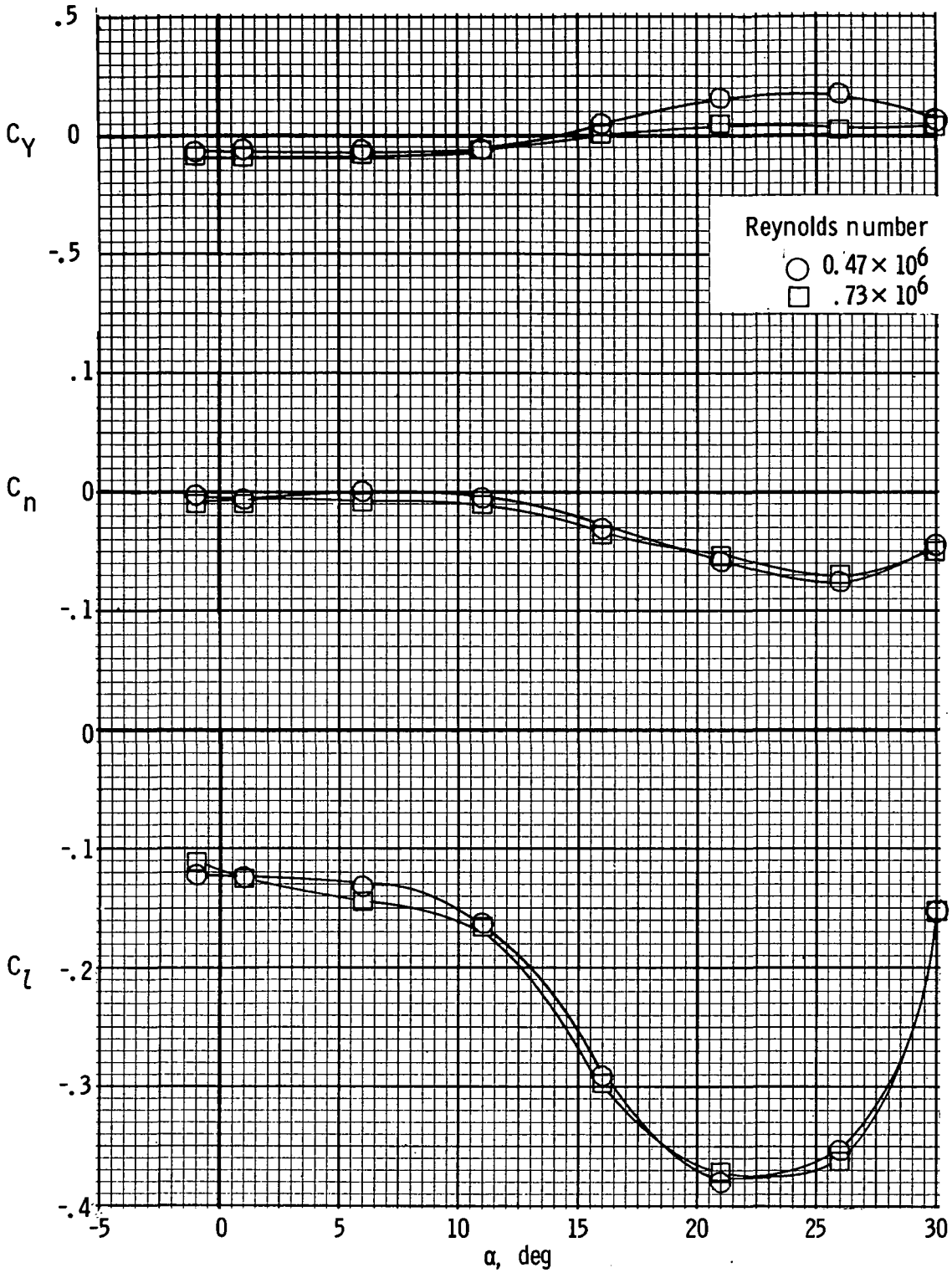

(c) Lateral characteristics. $C_\mu = 1.46$.

Figure 27.- Continued.

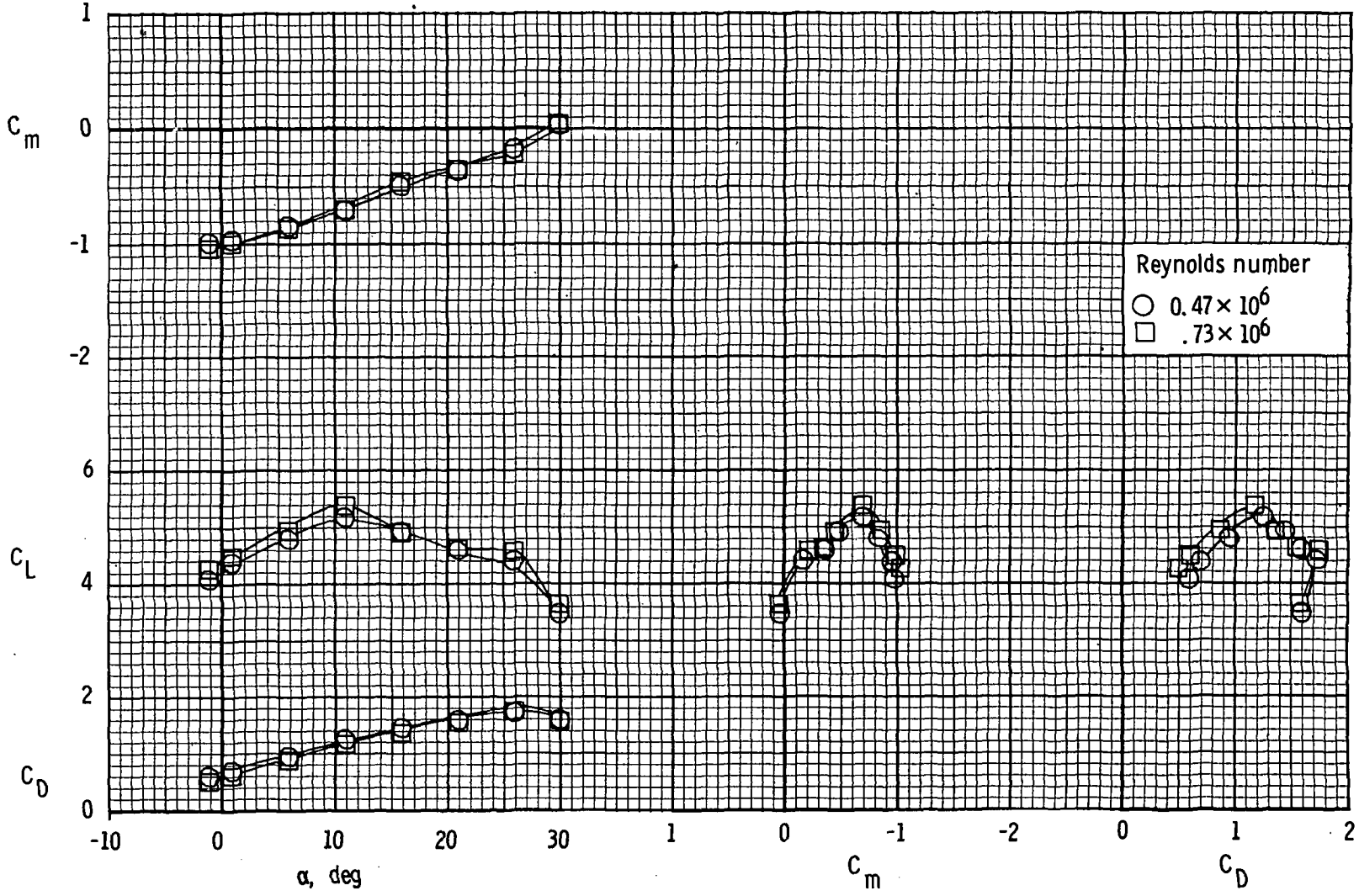

(d) Longitudinal characteristics. C_μ = 1.46.

Figure 27.- Continued.

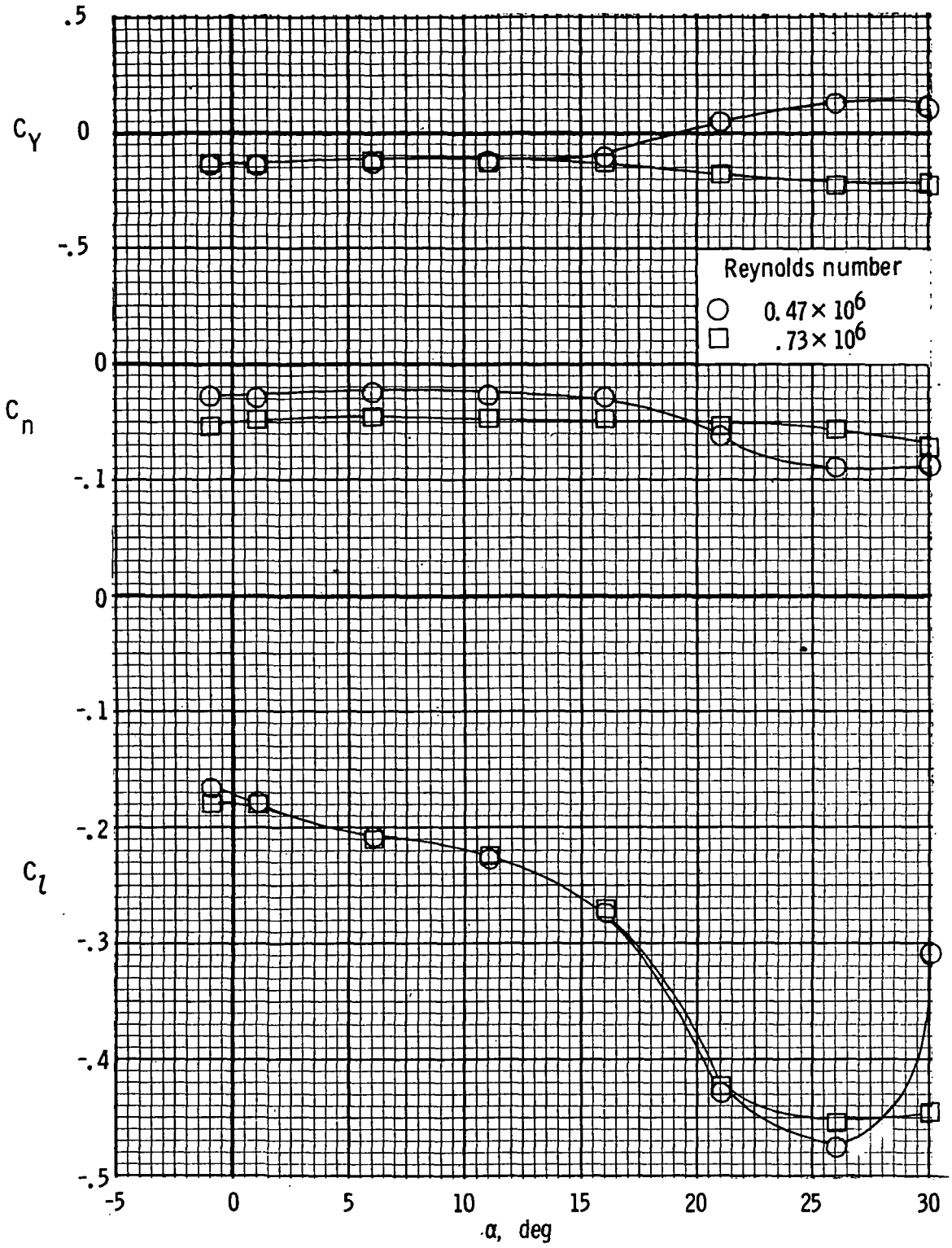

(e) Lateral characteristics. $C_\mu = 2.62$.

Figure 27.- Continued.

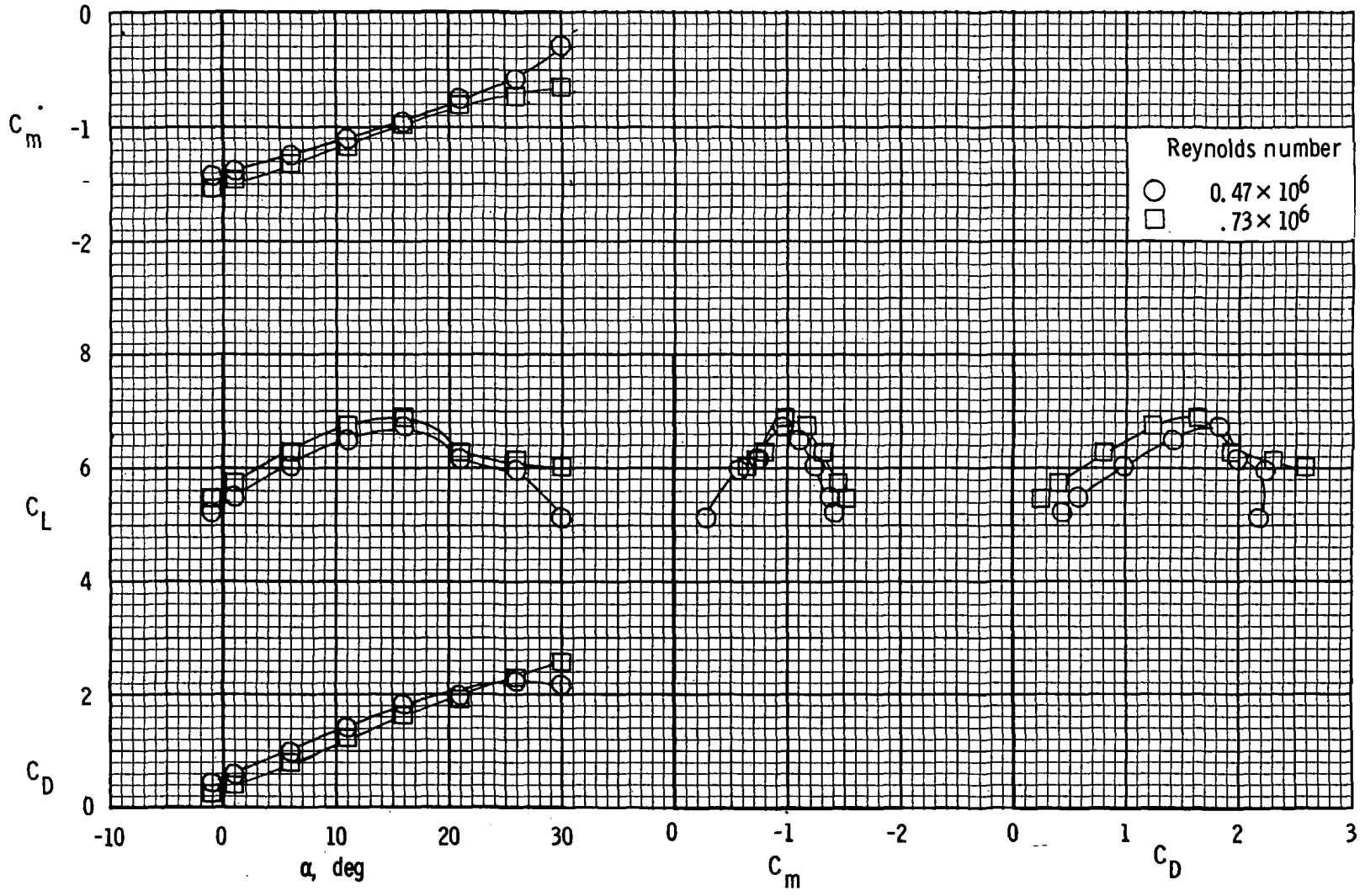

(f) Longitudinal characteristics. $C_\mu = 2.62$.

Figure 27.- Concluded.

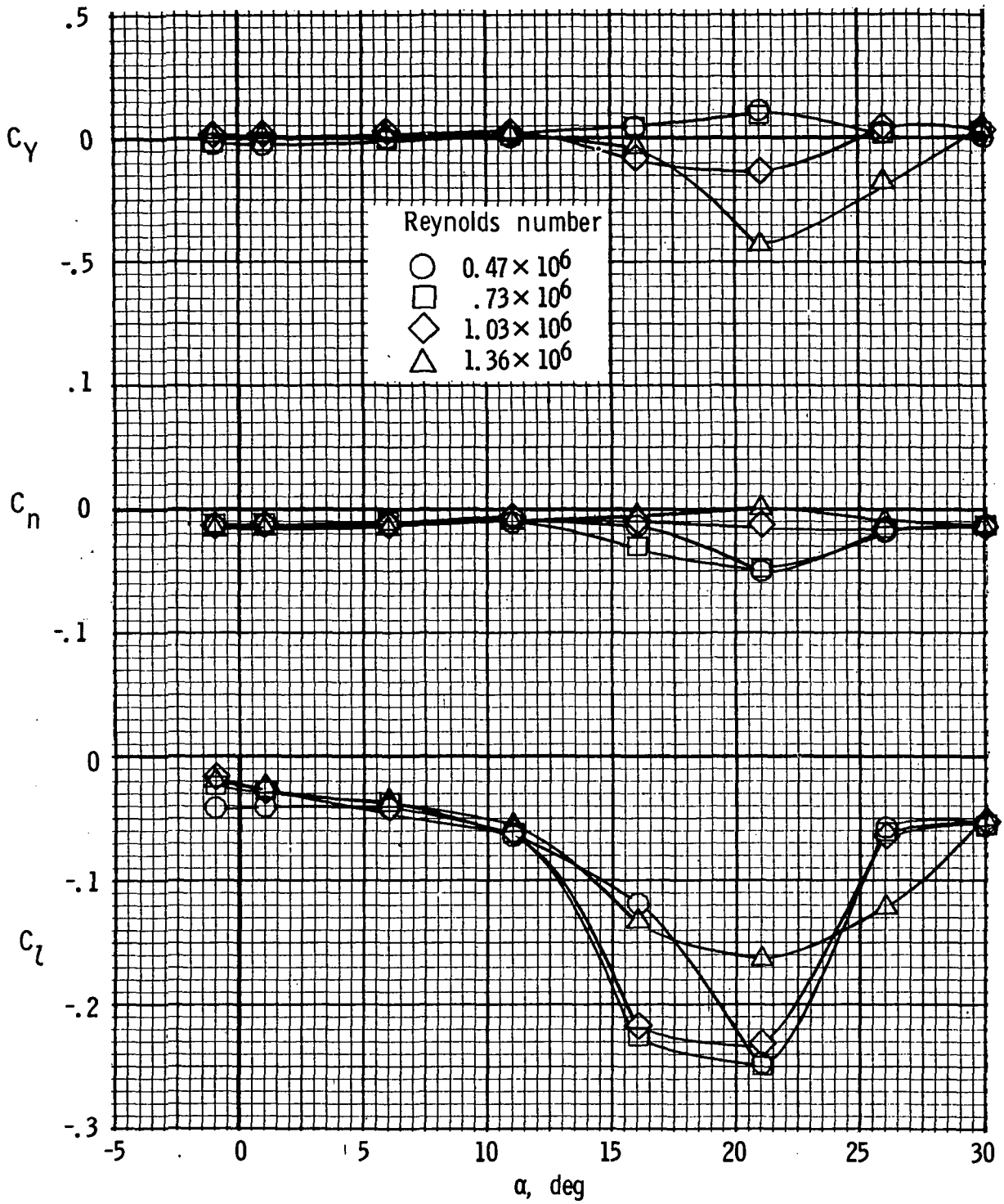

(a) Lateral characteristics. $C_\mu = 0.73$.

Figure 28.- Effect of Reynolds number on longitudinal and lateral characteristics with left inboard engine not operating. 30-percent leading-edge flap; $\delta_{f1}/\delta_{f2} = 30^o/60^o$.

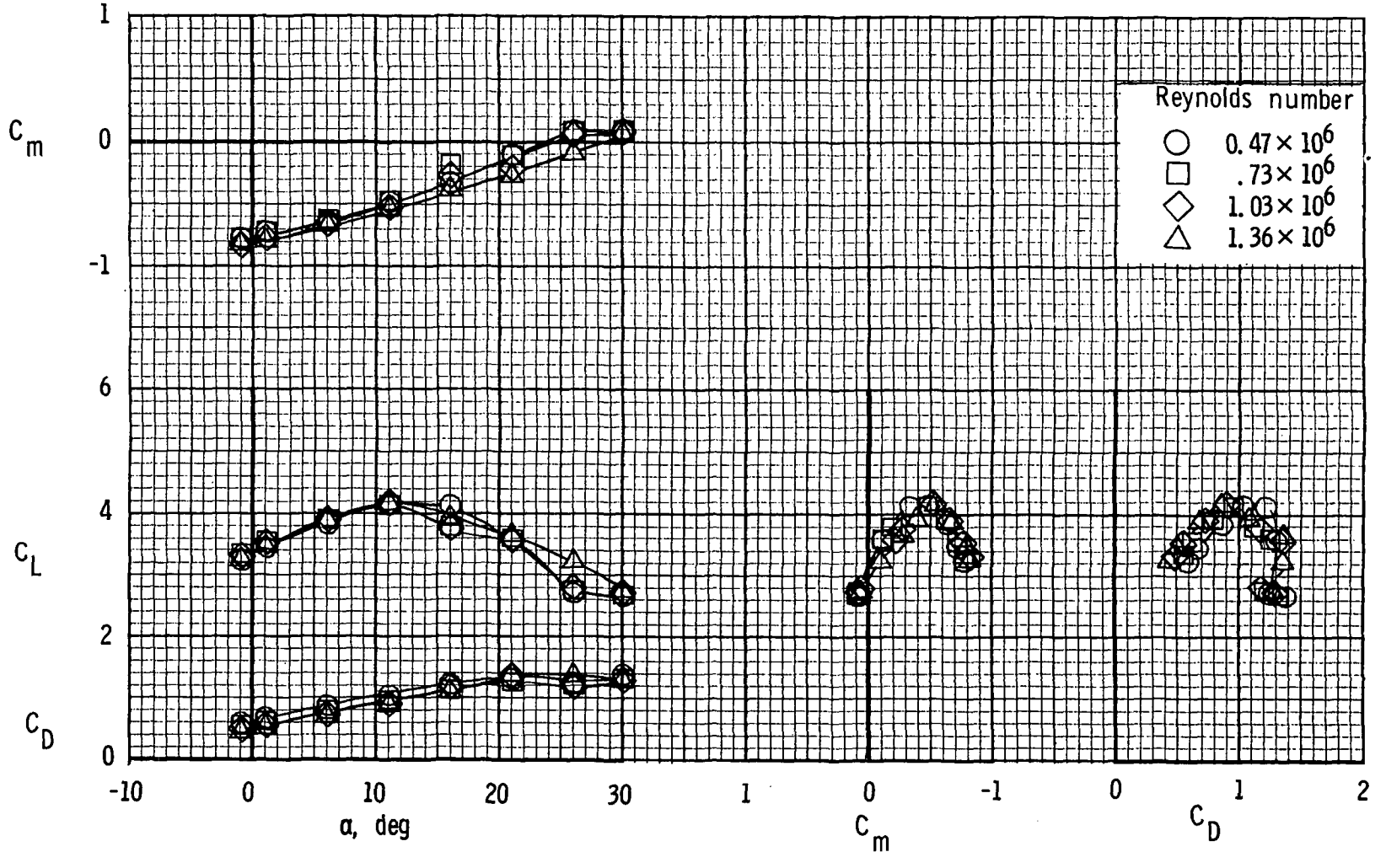

(b) Longitudinal characteristics. $C_\mu = 0.73$.

Figure 28.- Continued.

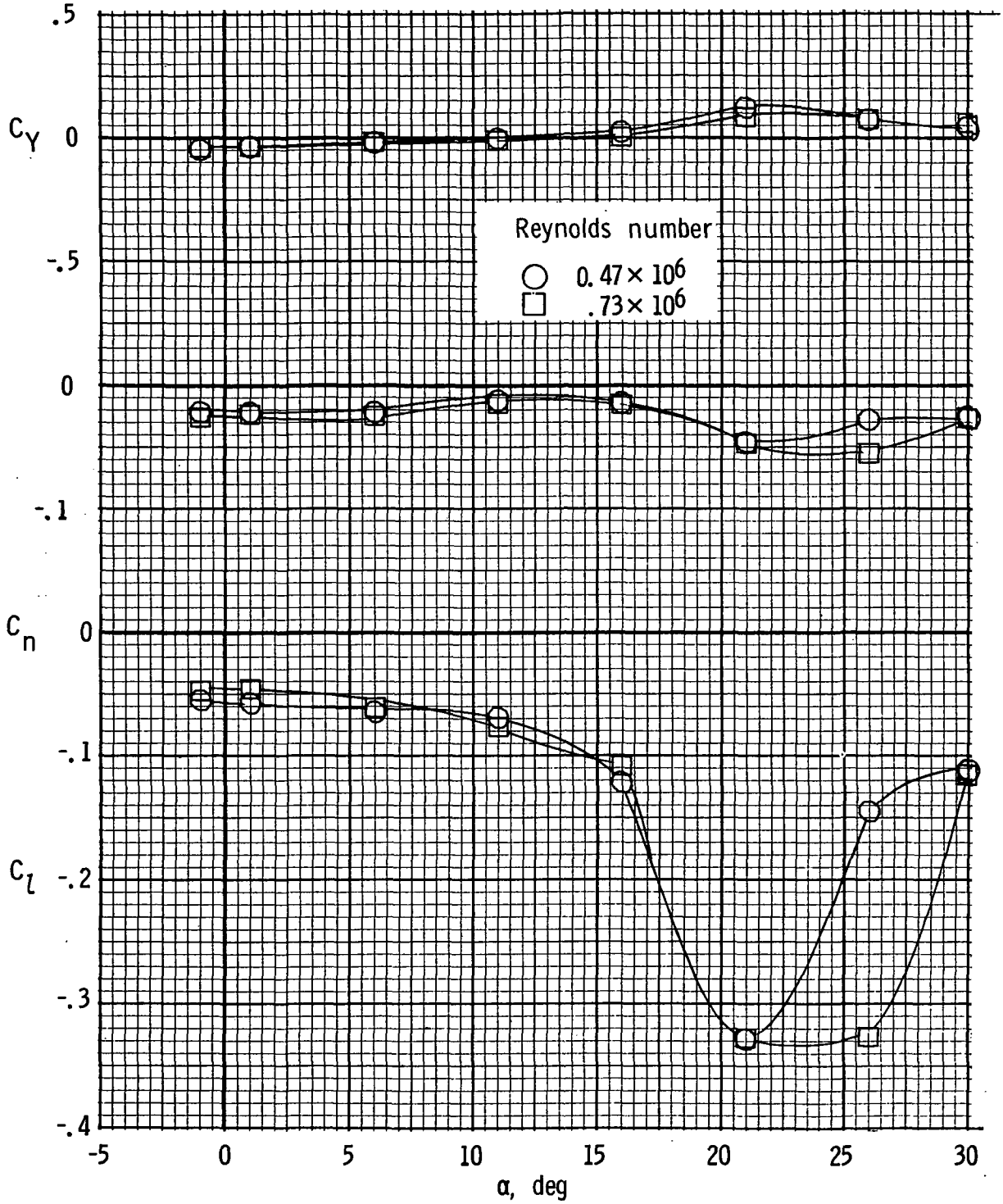

(c) Lateral characteristics. C_μ = 1.46.

Figure 28.- Continued.

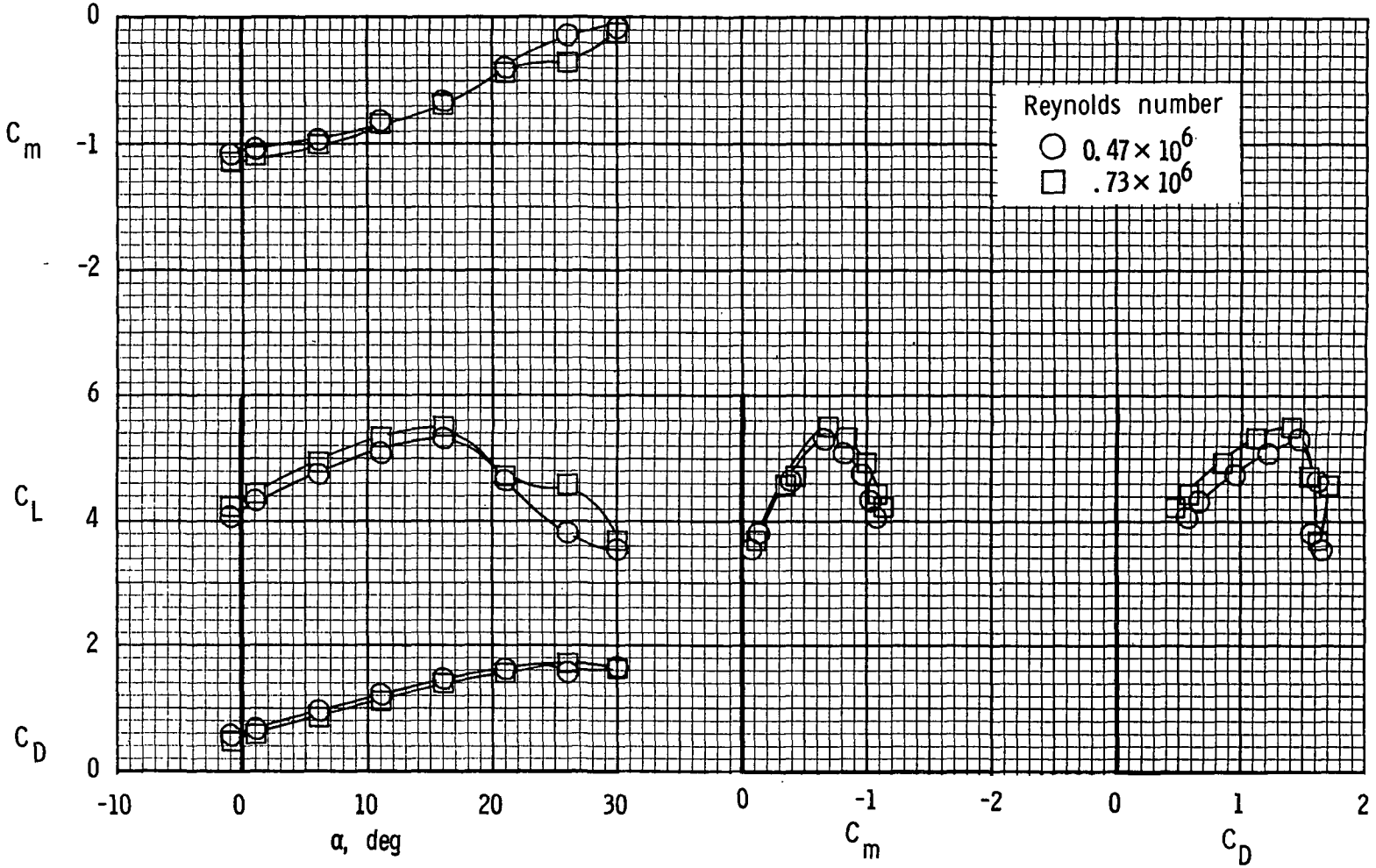

(d) Longitudinal characteristics. $C_\mu = 1.46$.

Figure 28.- Continued.

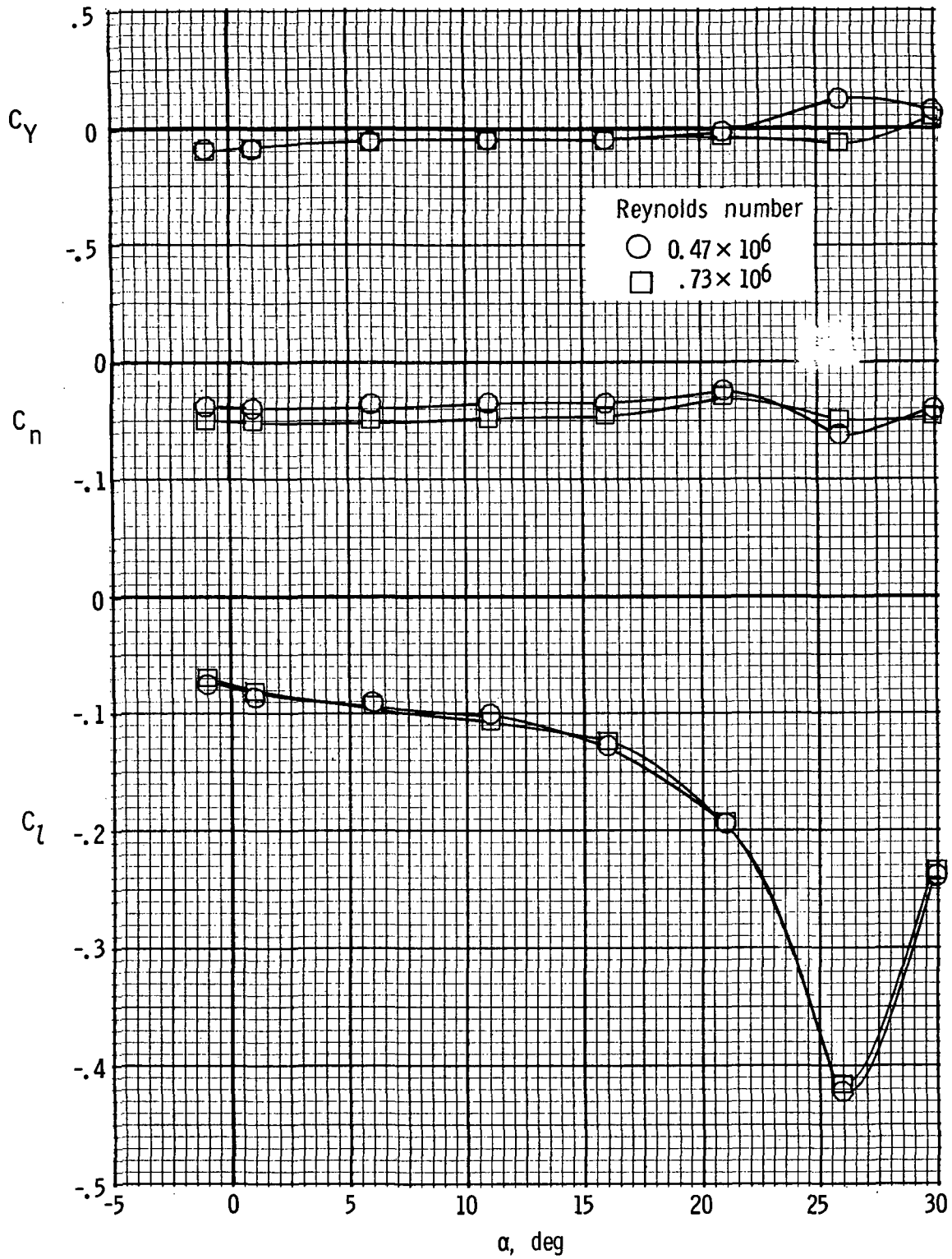

(e) Lateral characteristics. $C_\mu = 2.62$.

Figure 28.- Continued.

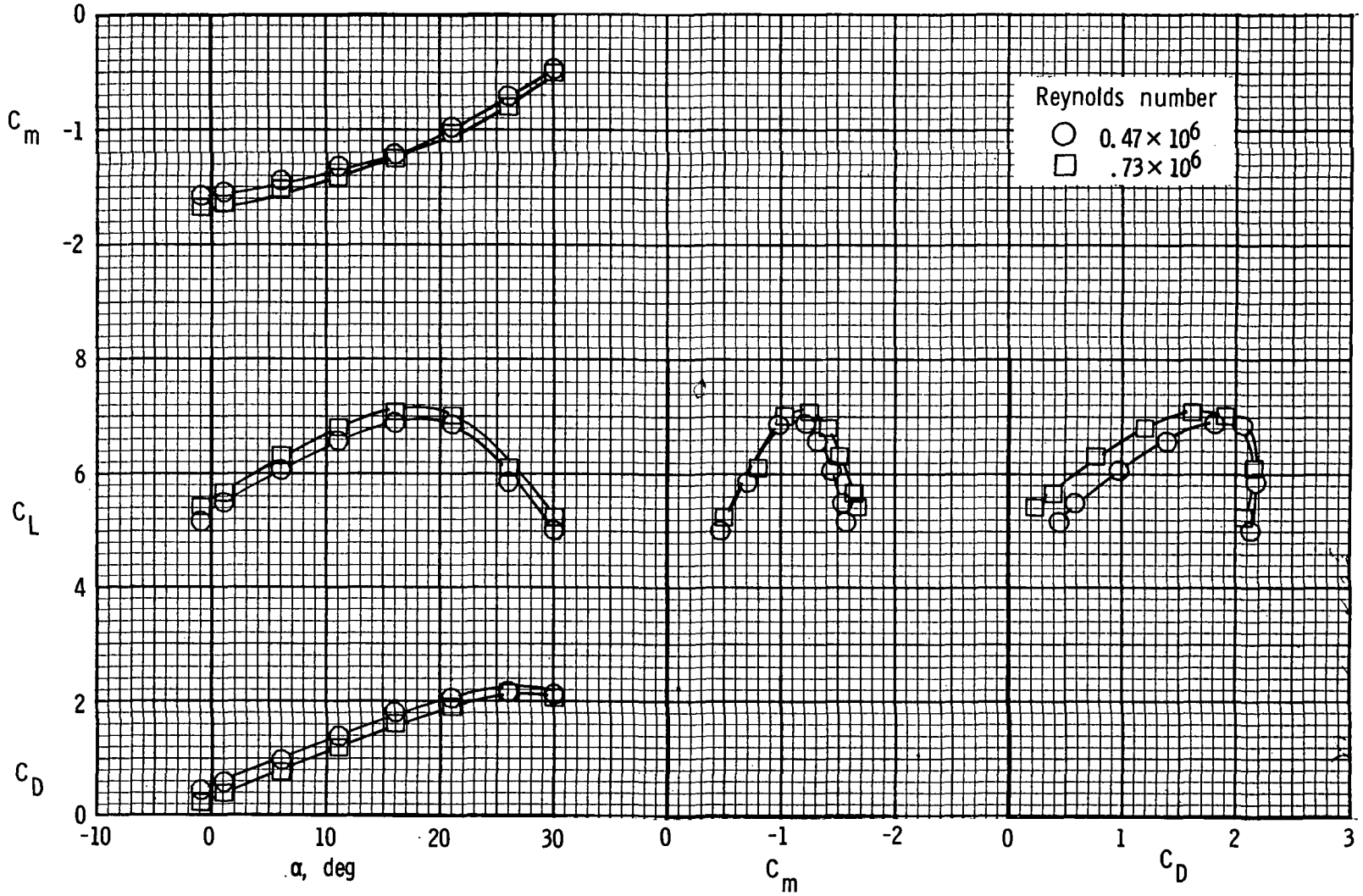

(f) Longitudinal characteristics. $C_\mu = 2.62$.

Figure 28.- Concluded.

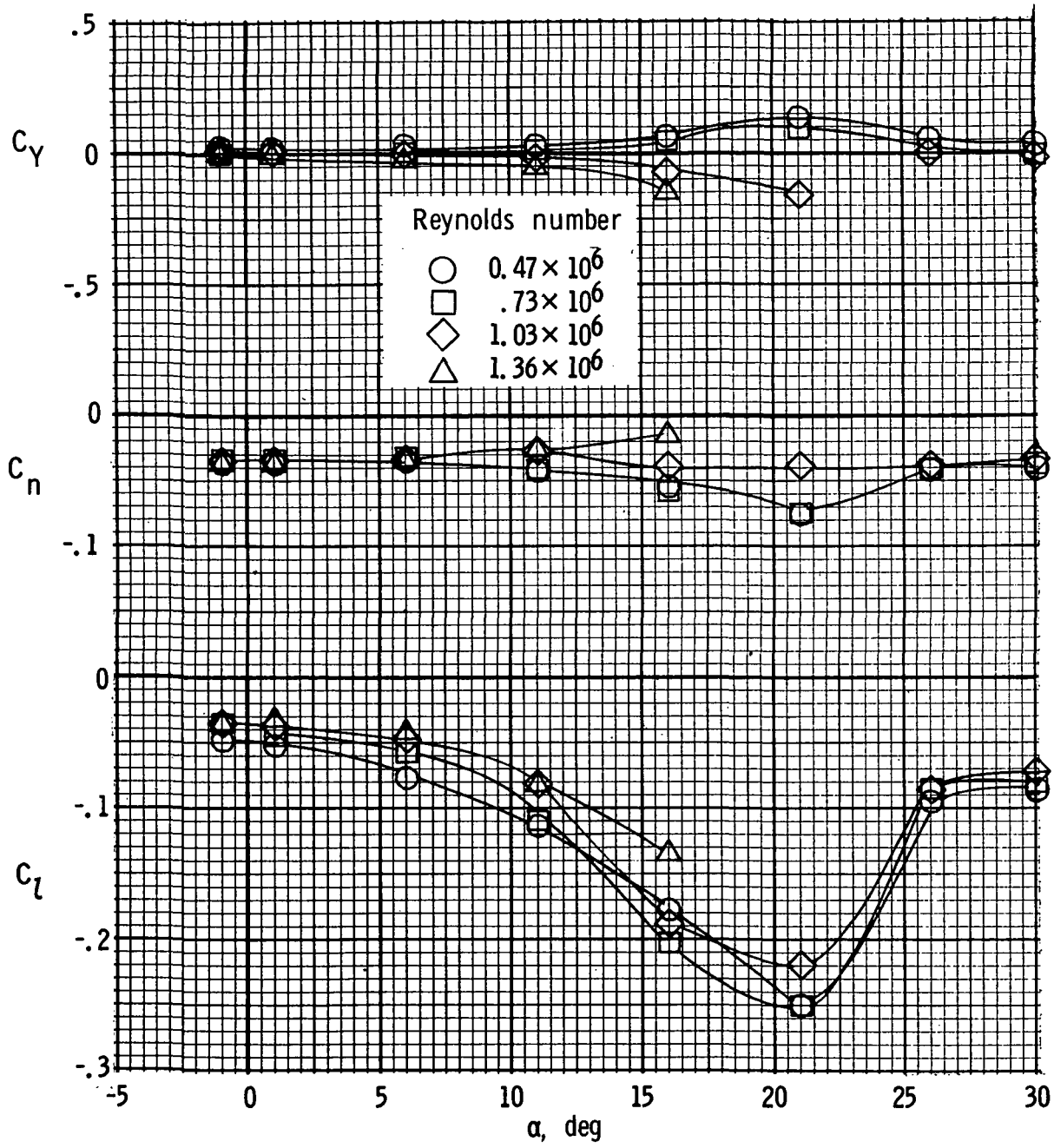

(a) Lateral characteristics.

Figure 29.- Effect of Reynolds number on longitudinal and lateral characteristics with left outboard engine not operating and differential flap settings. 30-percent leading-edge flap; $\left(\delta_{f1}/\delta_{f2}\right)_R = 30^o/50^o$; $\left(\delta_{f1}/\delta_{f2}\right)_L = 30^o/70^o$; $C_\mu = 0.73$.

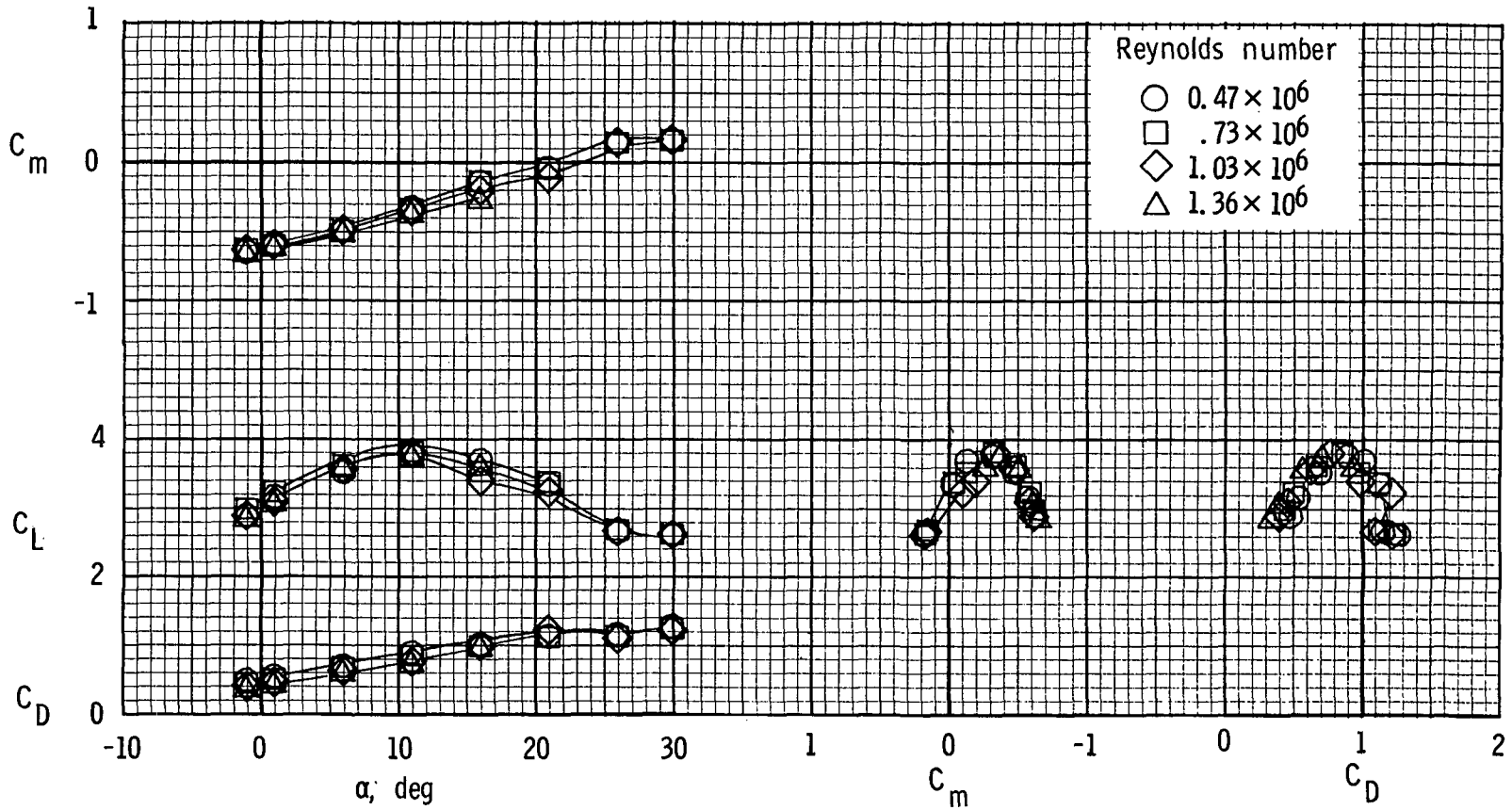

(b) Longitudinal characteristics.

Figure 29.- Concluded.

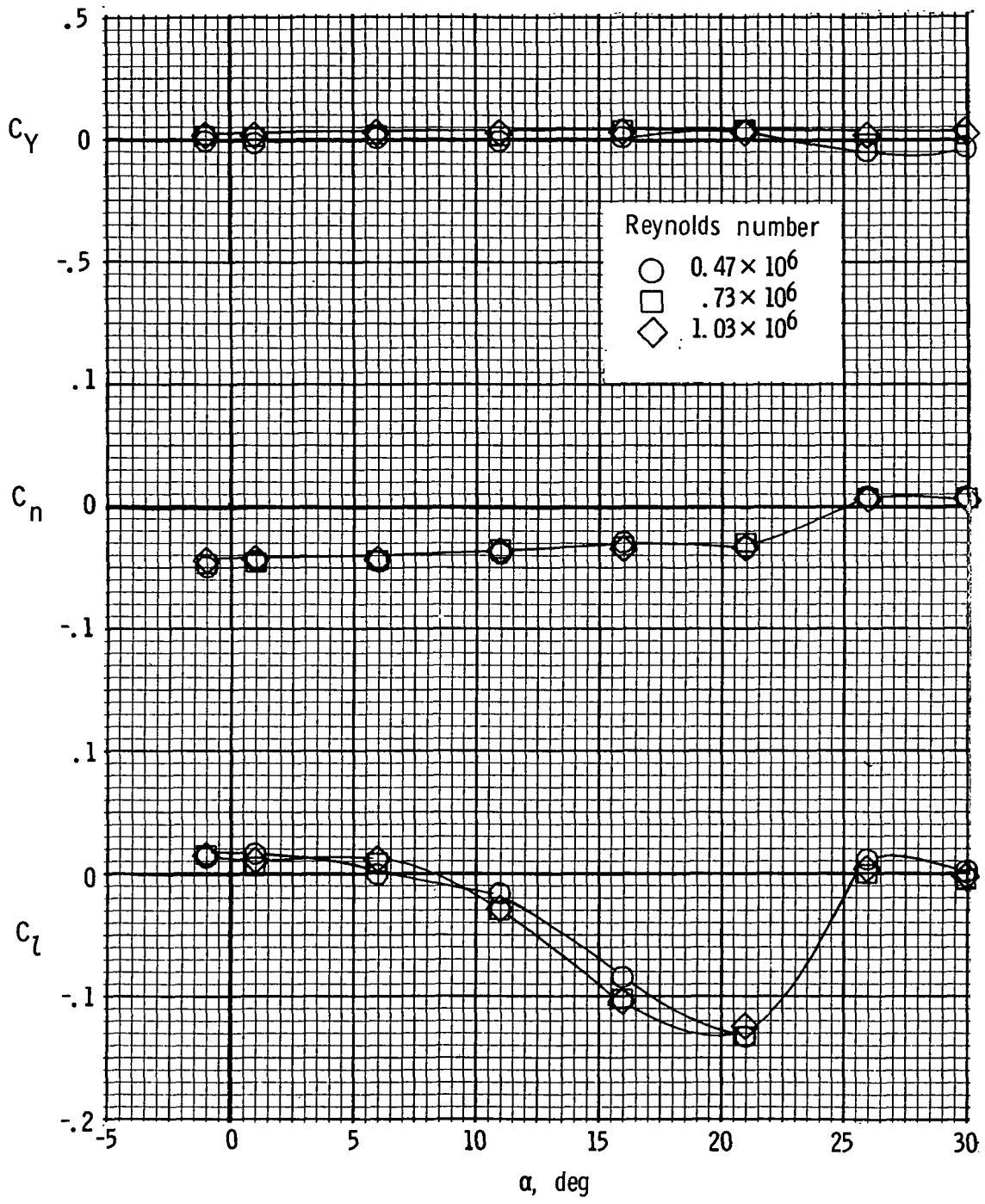

(a) Lateral characteristics.

Figure 30.- Effect of Reynolds number on longitudinal and lateral characteristics with left inboard engine not operating and differential flap settings. 30-percent leading-edge flap; $\left(\delta_{f1}/\delta_{f2}\right)_R = 30^o/50^o$; $\left(\delta_{f1}/\delta_{f2}\right)_L = 30^o/70^o$; $C_\mu = 0.73$.

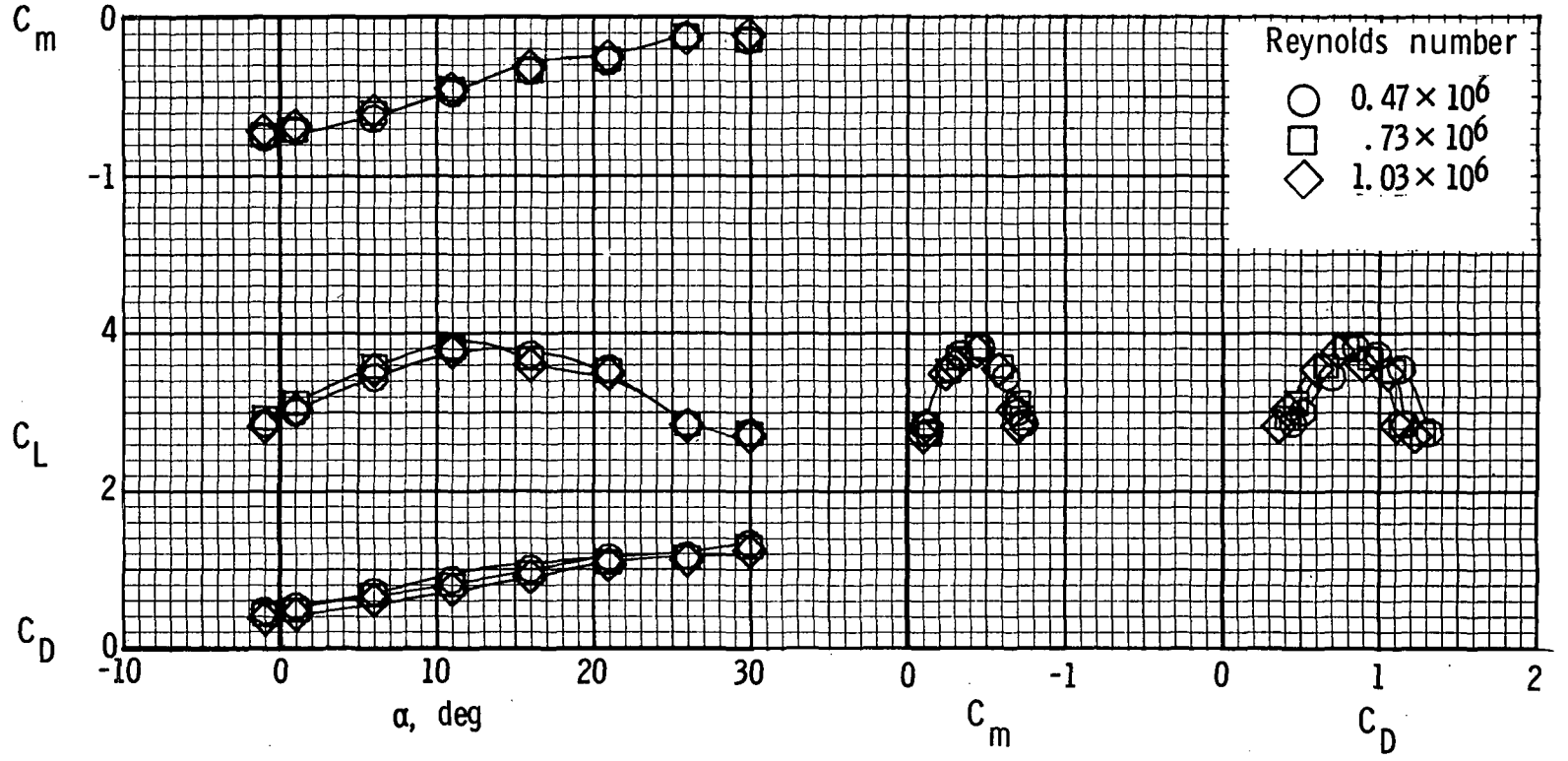

(b) Longitudinal characteristics.

Figure 30.- Concluded.

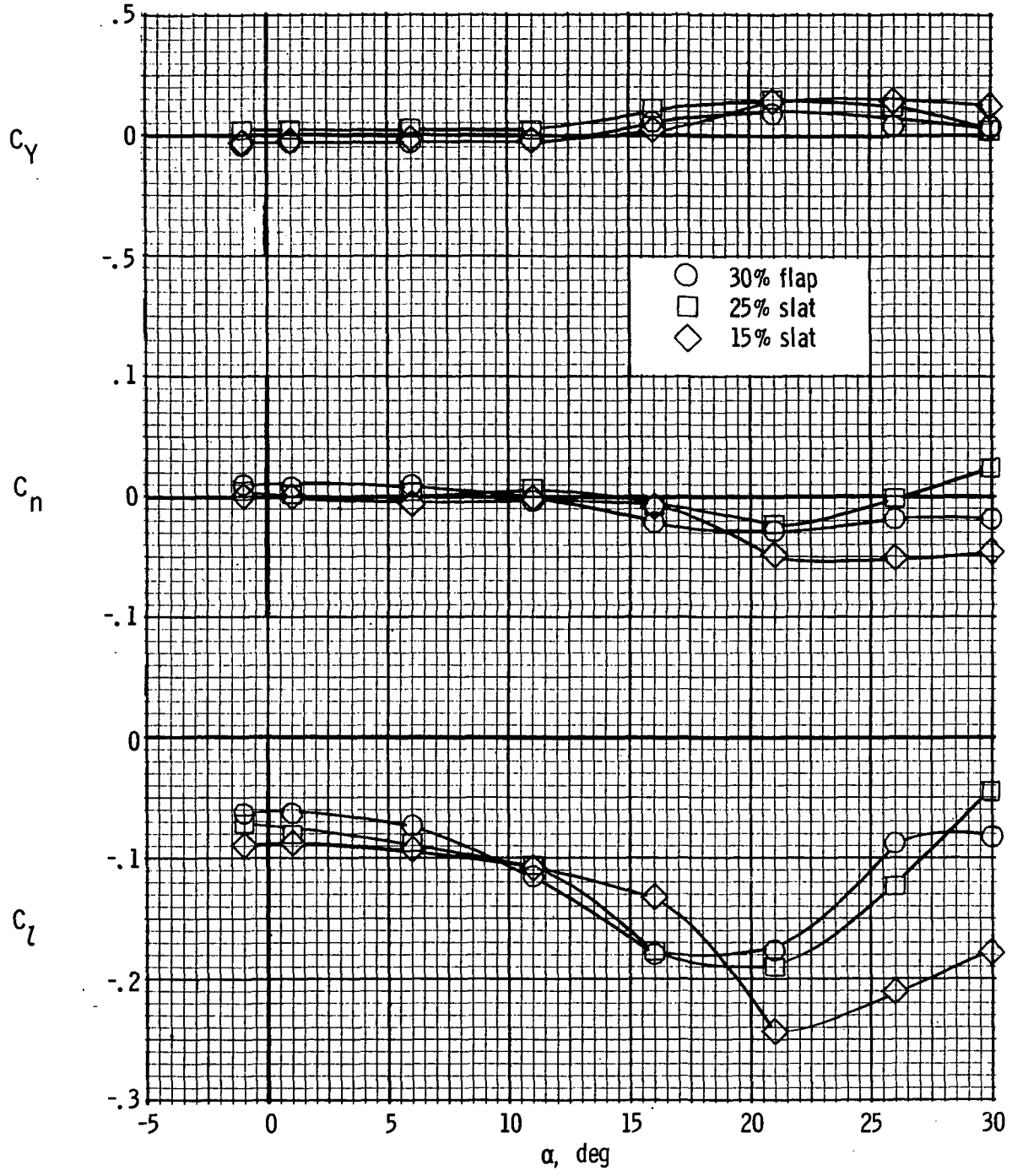

(a) Lateral characteristics. $R = 0.47 \times 10^6$.

Figure 31.- Effect of leading-edge devices on longitudinal and lateral characteristics with left outboard engine not operating. $\delta_{f1}/\delta_{f2} = 30^o/60^o$; $C_\mu = 0.73$.

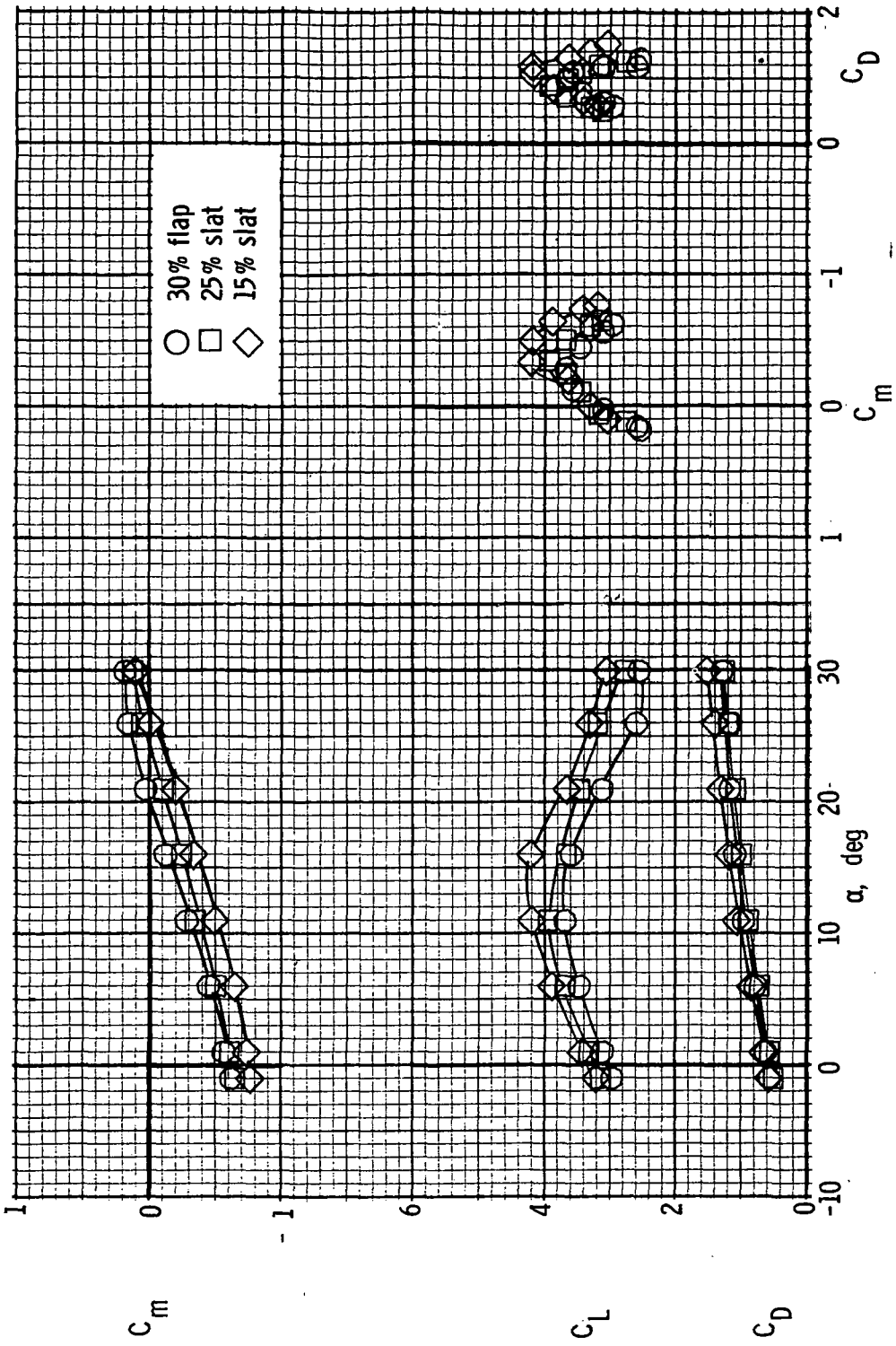

(b) Longitudinal characteristics. $R = 0.47 \times 10^6$.

Figure 31.- Continued.

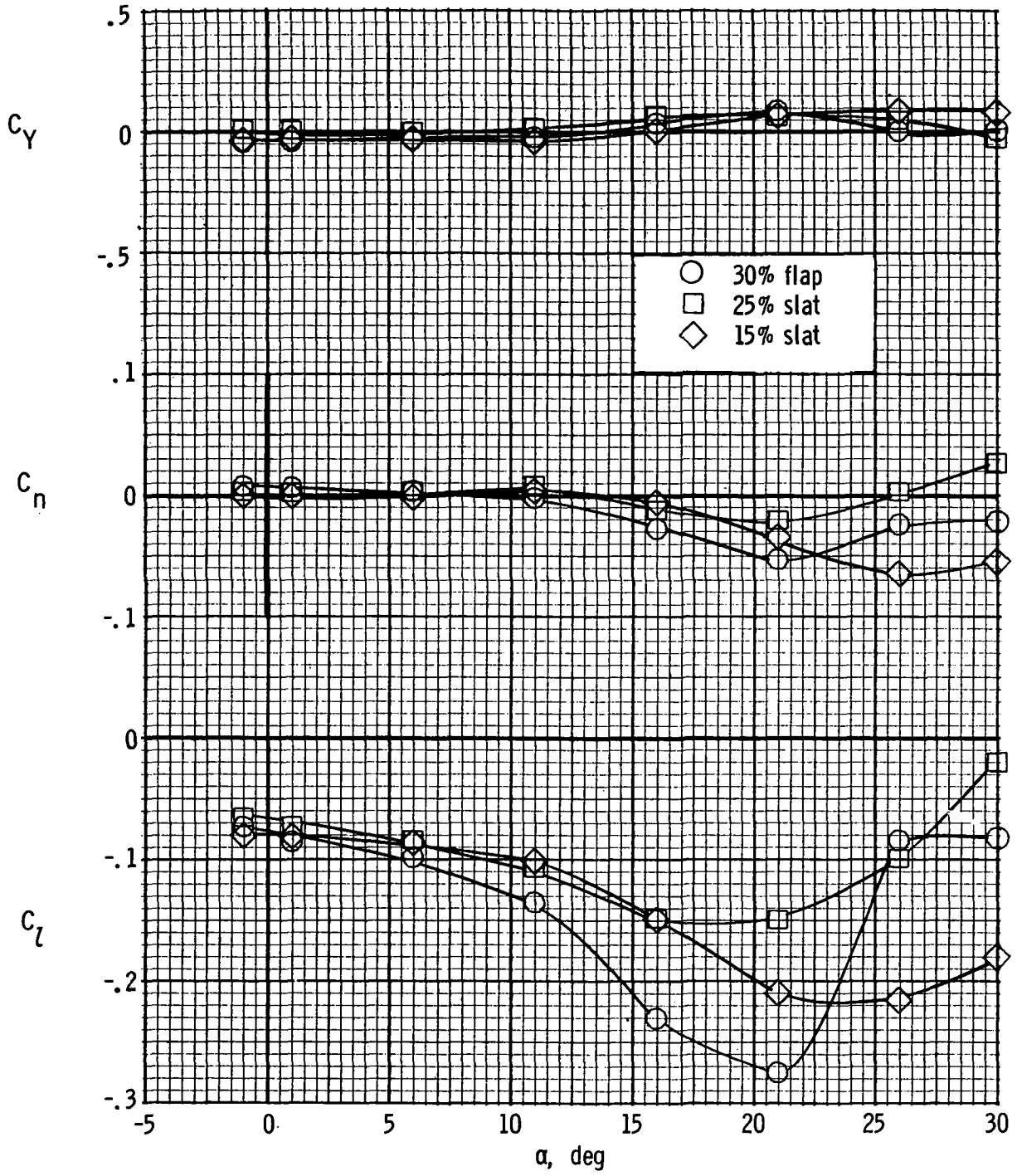

(c) Lateral characteristics. $R = 0.73 \times 10^6$.

Figure 31.- Continued.

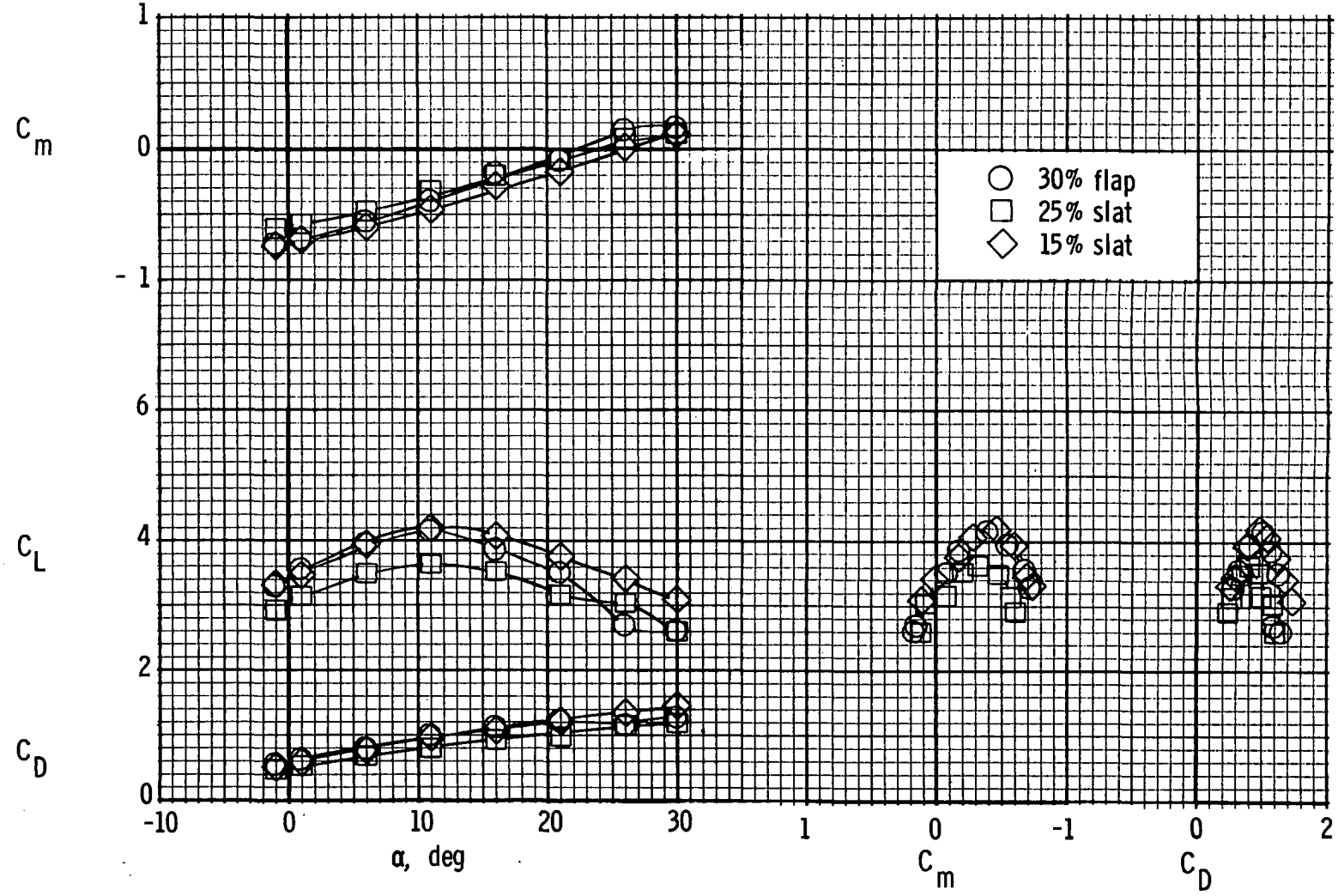

(d) Longitudinal characteristics. $R = 0.73 \times 10^6$.

Figure 31.- Continued.

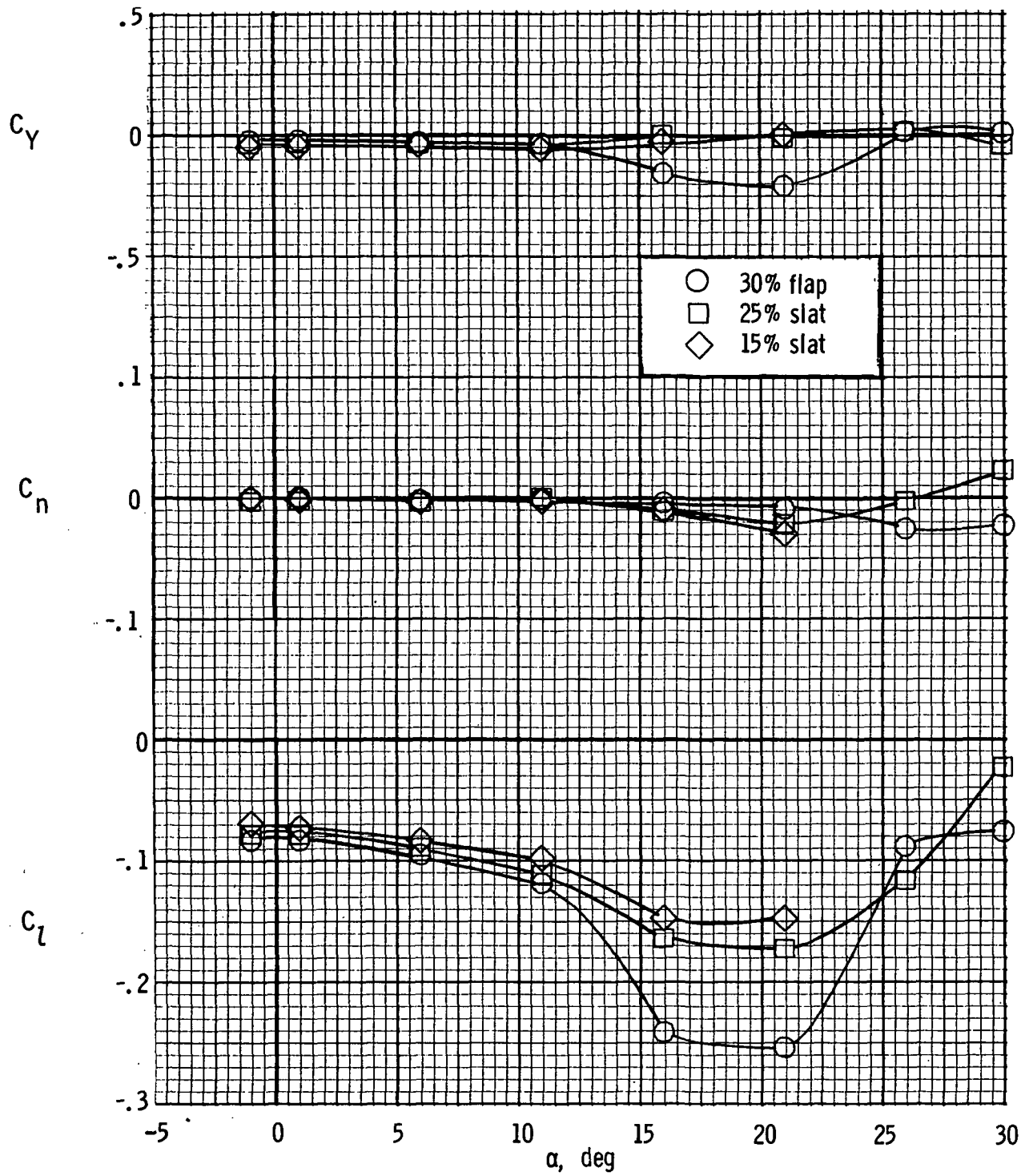

(e) Lateral characteristics. $R = 1.03 \times 10^6$.

Figure 31.- Continued.

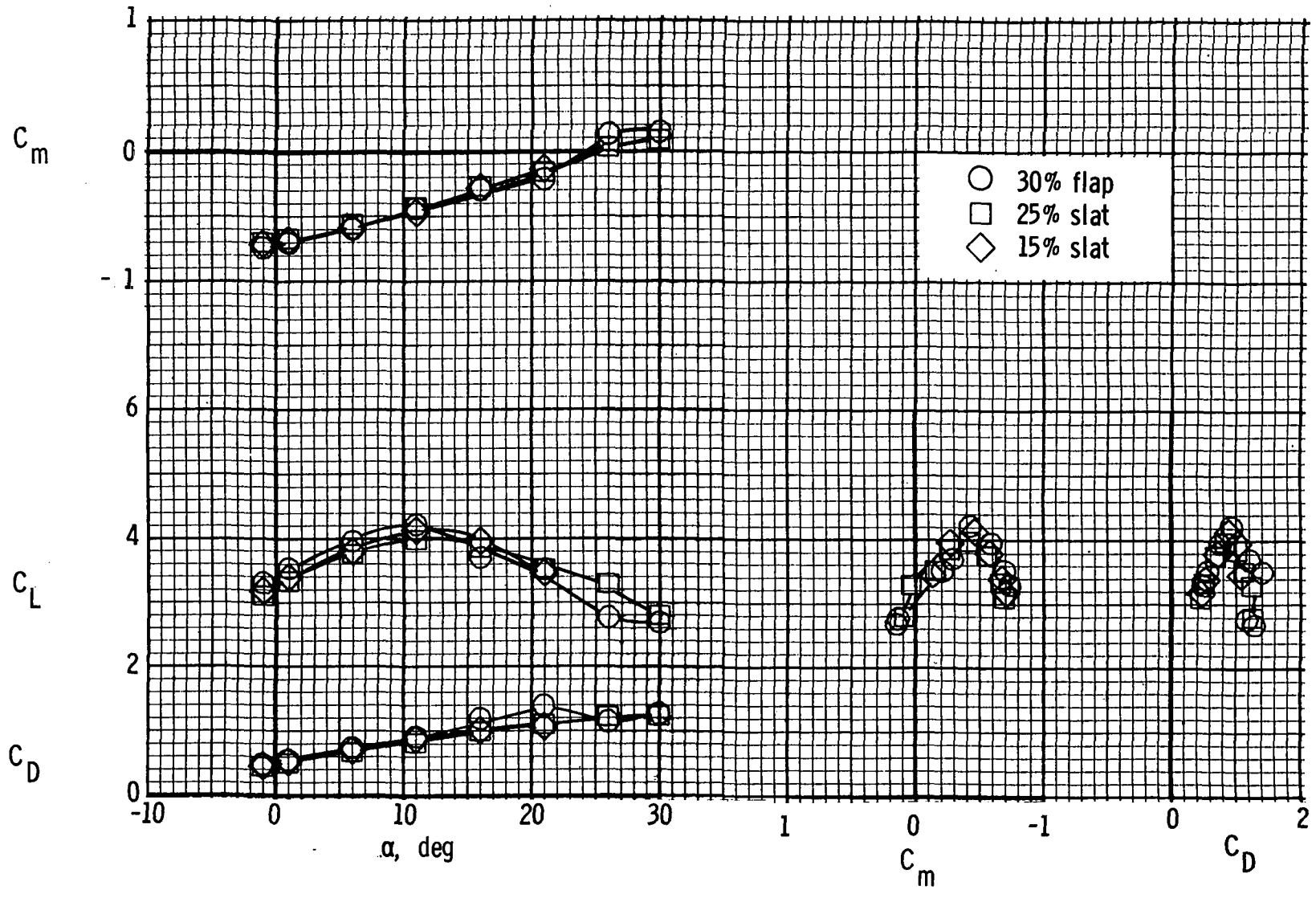

(f) Longitudinal characteristics. $R = 1.03 \times 10^6$.

Figure 31.- Continued.

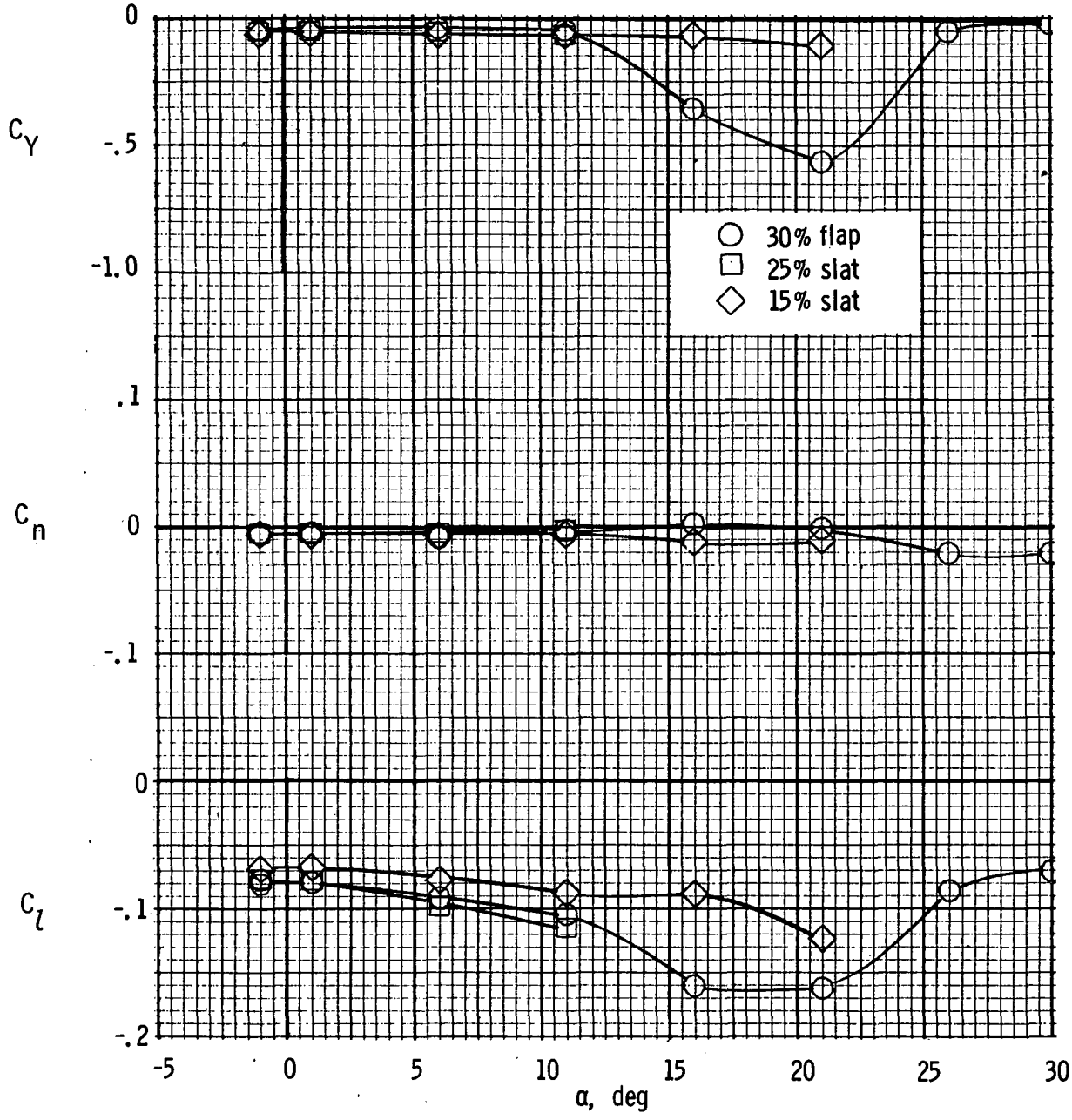

(g) Lateral characteristics. $R = 1.36 \times 10^6$.

Figure 31.- Continued.

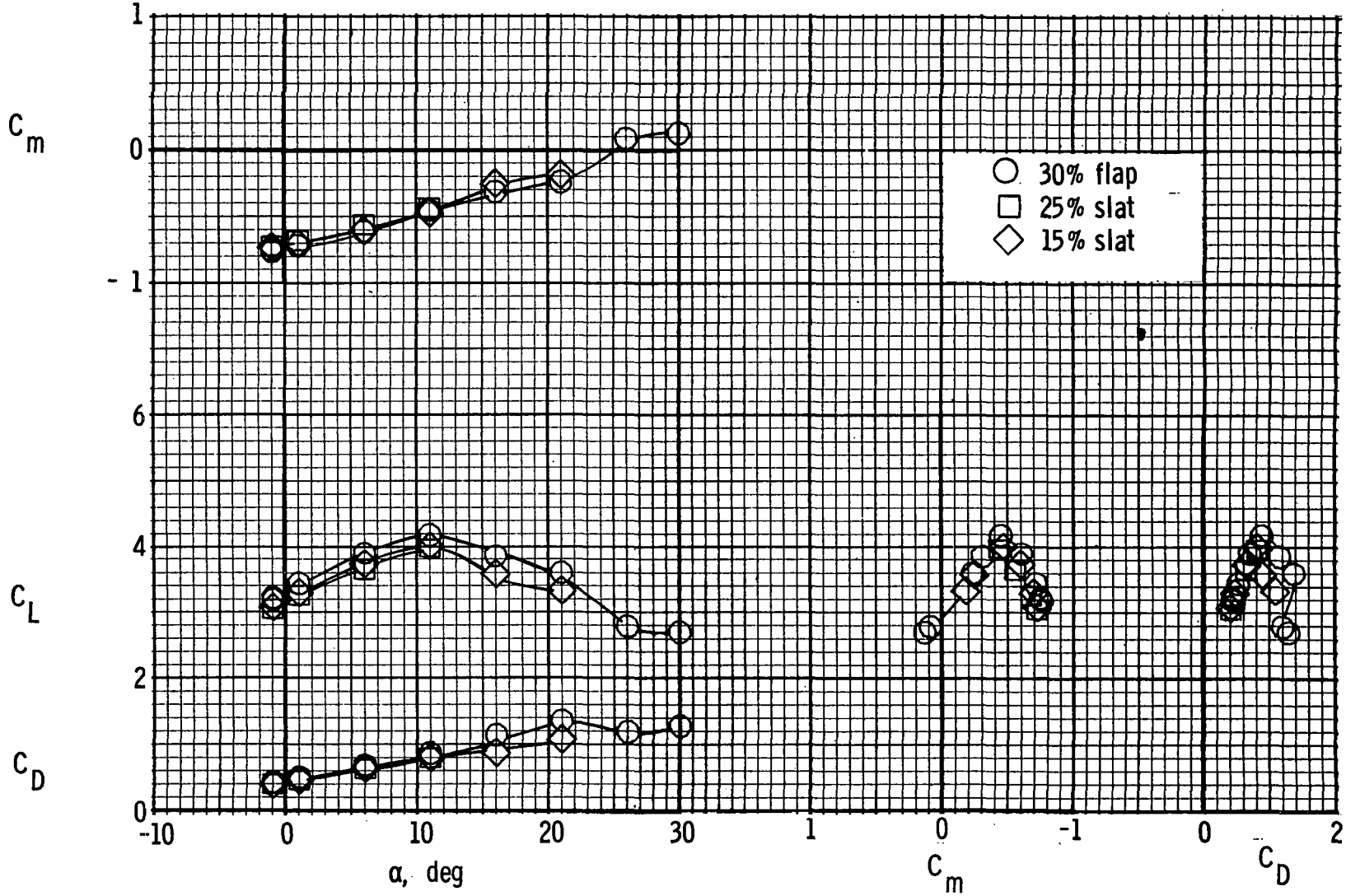

(h) Longitudinal characteristics. $R = 1.36 \times 10^6$.

Figure 31.- Concluded.

*U.S. GOVERNMENT PRINTING OFFICE: 1973-739-151/7

"The aeronautical and space activities of the United States shall be conducted so as to contribute . . . to the expansion of human knowledge of phenomena in the atmosphere and space. The Administration shall provide for the widest practicable and appropriate dissemination of information concerning its activities and the results thereof."

—NATIONAL AERONAUTICS AND SPACE ACT OF 1958

NASA SCIENTIFIC AND TECHNICAL PUBLICATIONS

TECHNICAL REPORTS: Scientific and technical information considered important, complete, and a lasting contribution to existing knowledge.

TECHNICAL NOTES: Information less broad in scope but nevertheless of importance as a contribution to existing knowledge.

TECHNICAL MEMORANDUMS: Information receiving limited distribution because of preliminary data, security classification, or other reasons. Also includes conference proceedings with either limited or unlimited distribution.

CONTRACTOR REPORTS: Scientific and technical information generated under a NASA contract or grant and considered an important contribution to existing knowledge.

TECHNICAL TRANSLATIONS: Information published in a foreign language considered to merit NASA distribution in English.

SPECIAL PUBLICATIONS: Information derived from or of value to NASA activities. Publications include final reports of major projects, monographs, data compilations, handbooks, sourcebooks, and special bibliographies.

TECHNOLOGY UTILIZATION PUBLICATIONS: Information on technology used by NASA that may be of particular interest in commercial and other non-aerospace applications. Publications include Tech Briefs, Technology Utilization Reports and Technology Surveys.

Details on the availability of these publications may be obtained from:

SCIENTIFIC AND TECHNICAL INFORMATION OFFICE

NATIONAL AERONAUTICS AND SPACE ADMINISTRATION

Washington, D.C. 20546